Molecular Markers of Pancreatic β-cell Death

Ryan Farr

Supervisor: Associate Professor Anandwardhan Hardikar

Auxiliary Supervisor: Professor Alicia Jenkins

A thesis submitted in fulfilment of the requirements
for the degree of Doctor of Philosophy (Medicine)

April 2017

NHMRC Clinical Trials Centre

Sydney Medical School

The University of Sydney

THE UNIVERSITY OF SYDNEY

Statement of Originality

This is to certify that to the best of my knowledge, the content of this thesis is my own work. This thesis has not been submitted for any other degree or used for any other purpose.

I certify that the intellectual content of this thesis is the product of my own work and that all the assistance received in preparing this thesis and sources have been acknowledged.

Signature

Name Ryan James Farr

Date 23/04/2017

Abstract

Loss of insulin-producing β-cells is central to the development of Type 1 diabetes (T1D). Currently, we lack diagnostic tools to quantitate this β-cell loss.

Non-protein coding RNAs called microRNAs (miRNAs/miRs) play an important role in islet development and function. Recent detection of miRNAs in peripheral circulation, has renewed interest in microRNA biomarkers of diabetes. Comparably, circulating insulin cell-free (cf)DNA has been proposed as a direct biomarker of β-cell death. DNA methylation studies have identified specific sites within DNA that are unmethylated in β-cells but methylated in other cell types, thus providing a handle to discriminate between cfDNA from β-/non-β-cells.

Previous research carried out in the Hardikar lab identified a signature of 20 miRNAs (the 'RAPID' signature) with potential as a biomarker of β-cell death. The RAPID signature was revised to accommodate other microRNAs finally constituting a panel of 50 microRNAs (PREDICT T1D panel). An analysis of these 50 miRNAs, as well as insulin cfDNA in serum/plasma from individuals before, during and after clinical diagnosis of T1D is presented.

Human islet cell death assays using sodium nitroprusside exposure identified a subset of 27 miRNAs and insulin cfDNA associated with islet cell stress/death. Non-obese diabetic mice (N=32) were found to have elevated candidate miRNAs prior to immune infiltration and glycaemic dysfunction. This trend was also noted in the human progression to T1D; 26 miRNAs were elevated in (N=19) high-risk individuals and those at diagnosis (N=199) but decreased within 6-weeks after diagnosis. Furthermore, candidate miRNAs exhibited differential abundance with disease duration, residual C-peptide, and microvascular complications in 180 subjects with prolonged T1D. At diagnosis, miRNAs and cfDNA associated with GAD

autoantibody titres (N=167 P-values range from 0.044 to <0.0001) and HbA1c levels (N=187, P-values range from 0.047 to 0.00095).

Such biomarkers may inform medical researchers as to how to predict the development of T1D, monitor response to interventions such as islet transplantation, vaccines & drugs aiming to retard β-cell loss. In basic research, such an assay may help to select treatments to block β-cell death and guide the development of new treatments to lessen the burden of diabetes.

Table of Contents

List of Figures and Tables

Chapter 1:

Chapter 2:

Chapter 3:

Chapter 4:

Chapter 5:

Chapter 6:

Supplementary Chapter 1:

Supplementary Chapter 2:

Peer-Reviewed Publications

Original Research

1. Farr R.J., Januszewski A.J., Joglekar, M.V., Liang H., McAulley A.K., Hewitt A.W., Thomas H.E., Loudovaris T., Kay T.W., Jenkins A., and Hardikar, A.A., A comparative analysis of high-throughput platforms for validation of a circulating microRNA signature in diabetic retinopathy. **Scientific Reports**, 2015. 5: p.10375.

Methodology

2. Wong W., Farr R.J., Joglekar M.V., Hardikar A.A., TaqMan-based approaches to detect the abundance of circulating microRNAs. **Journal of Visualized Experiments**, 2015 (98). URL: http://www.jove.com/video/52586/probe-based-real-time-pcr-approaches-for-quantitative-measurement
3. Hardikar A.A., Farr, R.J., and Joglekar, M.V., Circulating microRNAs: Understanding the limits for quantitative measurement by real-time PCR. **Journal of the American Heart Association**, 2014. 3(1): p.e000792.

Reviews

4. Farr R.J., Taylor C.J., Satoor S.N., Williams M.D., and Joglekar M.V., From Cradle to the Grave: Tissue-specific microRNA signatures in detecting clinical progression of diabetes. **Non-coding RNAs in Endocrinology**, 2013: p.16-27.
5. Farr R.J., Joglekar M.V., Taylor C.J., and Hardikar A.A., Circulating non-coding RNAs as biomarkers of β-cell death in diabetes. **Pediatric Endocrinology Reviews**, 2013. 11(1): p.14-20.

Book Chapter

1. Farr R.J., Joglekar M.V., Hardikar, A.A. Circulating MicroRNAs in Diabetes Progression: Discovery, Validation, and Research Translation. In: Circulating microRNAs in Disease Diagnostics and their Potential Biological Relevance, ed. Igaz P., **EXS**, 2015. 106: p. 215-244.

Scholarships and Awards

Scholarships

2014 - 2016	Juvenile Diabetes Research Foundation (JDRF) Top-Up Scholarship
2013	National Heath and Medical Research Council Clinical Trials Centre Top-Up Scholarship
2013 - 2016	Australian Postgraduate Award

Travel Grants

2016	European Association for the Study of Diabetes (EASD) Travel Grant
2015	JDRF Travel Grant (declined due to acceptance of another grant)
2015	European Association for the Study of Diabetes (EASD) Travel Grant
2014	JDRF Travel Grant
2014, 2015 & 2016	Postgraduate Research Support Scheme Award
2014, 2015 & 2016	Australian Diabetes Society (ADS) Travel Grant

Awards/Prizes

2016	Australian Diabetes Educators Association Annual Scientific Meeting Basic Science Best Poster Award.
2015	ADS Pincus Taft Young Investigator Award Finalist

2015	Oral Presentation Award, Islet Society and Australian Islet Study Group Joint Annual Meeting
2014	Life Technologies Publication Award

Authorship Attribution Statement

Chapter 1 of this thesis contains material published previously. Section 1.4.2 contains material from a review publication, Farr R.J. et al (2013) ncRNA Endocrinol. Sections 1.4.1, 1.4.3 and 1.5.2 contain material from a book chapter, Farr R.J. et al (2016) EXS. As first author of both of these publications, I researched and compiled the majority of the information and wrote the first draft. All figures within this chapter are appropriately referenced/acknowledged.

Chapter 2 of this thesis is published as Farr R.J. et al. Sci Rep (2015). As first author on this paper, I prepared the majority of the samples, carried out the bulk of the data generation on the ViiA7 and OpenArray platforms, completed the initial data analysis and wrote the first draft. Dr. Andrzej Januszewski (NHMRC Clinical Trials Centre (CTC), University of Sydney) generated radar plots on the data and carried out further statistical analysis. Dr. Mugdha Joglekar (NHMRC CTC) isolated the RNA and analysed some of the samples on the qPCR platforms. Prof. Alicia Jenkins (CTC, University of Sydney, then at SVI Melbourne), Dr Andrzej Januszewski (CTC, University of Sydney, previously at SVI Melbourne), Dr Helena Liang (CERA, Melbourne), Dr. Annie McAulley (CERA, Melbourne) and A/Prof Alex Hewitt (CERA, Melbourne) obtained written informed consent, recruited and clinically characterised non-diabetic controls and Type 1 diabetic subjects with and without vascular complications. . The CERA team or Prof. Jenkins along with Dr. Virginia Cotta (O'Brien Institute, Melbourne), collected blood samples and isolated plasma as per the SOPs from Hardikar lab, then at the O'Brian Institute, Melboune. A/Professor Helen Thomas, Dr Tom Loudovaris and Professor Tom Kay (St. Vincent's Institute, Melbourne) obtained written informed consent (through Red Cross) and provided human cadaveric islets/pancreas that were consented for research use and were spare/excess/available for the study. A/Professor Anandwardhan Hardikar (NHMRC,

CTC) obtained all the required ethics and biosafety approvals, planned the study design, analysed all results and wrote/revised the manuscript to its final publication.

Permission to include the published material following due acknowledgement has been granted by the corresponding author.

Signature

Name Ryan James Farr Date 23/04/2017

As supervisor for the candidate's research project upon which this thesis is based, I can confirm that the authorship attribution statements above are correct.

Signature 

Name Anandwardhan A. Hardikar

Date 23/04/2017

Conference Presentations

- Farr R.J. Joglekar M.V., Akil A., Januszewski A., Taylor C.J., Cotta V., Craig M., Jenkins A., and Hardikar A.A. *Molecular markers of β-cell mortality*. European Association for the Study of Diabetes 52nd Annual Meeting (Oral presentation). September 2016. Munich, Germany.

- Farr R.J., Joglekar M.V., Akil A., Januszewski A., Taylor C.J., Cotta V., Craig M., Jenkins A., and Hardikar A.A. *Molecular markers of β-cell mortality*. Australian Diabetes Society – Australian Diabetes Educators Association Annual Scientific Meeting (ADS Basic Science Poster Award session). August 2016. Gold Coast, Australia

- Farr R.J., Joglekar M.V., Akil A., Januszewski A., Taylor C.J., Cotta V., Craig M., Jenkins A., and Hardikar A.A. *Predicting islet cell death using miRNAs: small molecules giving big insights*. European Association for the Study of Diabetes 51st Annual Meeting (Moderated poster presentation). September 2015. Stockholm, Sweden.

- Farr R.J., Joglekar M.V., Akil A., Januszewski A., Taylor C.J., Cotta V., Craig M., Jenkins A., and Hardikar A.A. *Predicting islet cell death using miRNAs: small molecules giving big insights*. Australian Diabetes Society – Australian Diabetes Educators Association Annual Scientific Meeting (Oral presentation, ADS Pincus Taft Young Investigator Award Finalist). August 2015. Adelaide.

- Farr R.J., Joglekar M.V., Akil A., Januszewski A., Taylor C.J., Cotta V., Craig M., Jenkins A., and Hardikar A.A. *Small molecules with big potential: discovery, validation and research translation of circulating microRNA biomarkers*. Islet Society and Australian Islet Study Group Joint Meeting (Oral presentation). July 2015. Sydney.

- Farr R.J., Joglekar M.V., Taylor C.J., Januszewski A., Akil A., Cotta V., Craig M., Jenkins A., Hardikar A.A. *Analysis of the RAPID Signature in a Longitudinal Cohort at High Risk of Type 1 Diabetes.* Australian Diabetes Society – Australian Diabetes Educators

Association Annual Scientific Meeting (Poster presentation, abstract 212). August 2014. Melbourne.

- Farr R.J., Wong W., Joglekar M.V., Taylor C.J., Satoor S.N., Januszewski A., Akil A., Cotta V., Craig M., Jenkins A., Hardikar A.A. *Pancreatic non-coding RNAs: from cradle to grave*. Bosch Institute Facilities User Group Meeting (Invited oral presentation). May 2014. Sydney

- Farr R.J., Joglekar M.V., Taylor C.J., Januszewski A., Akil A., Cotta V., Craig M., Jenkins A., Hardikar A.A. *Pancreatic islet-specific ncRNAs: from cradle to grave*. Genetic Solutions World Tour (Oral presentation). May 2014. Sydney.

- Farr R.J., Joglekar M.V., Taylor C.J., Januszewski A., Akil A., Cotta V., Craig M., Jenkins A., Hardikar A.A., *Pancreatic islet-specific ncRNAs: from cradle to grave*. Genetic Solutions World Tour (Oral presentation). May 2014. Brisbane.

- Farr R.J., Joglekar M.V., and Hardikar A.A. *Comparing High-throughput qPCR Technologies for miRNA Diagnostics: Does Size Matter?* Australian Diabetes Society – Australian Diabetes Educators Association Annual Scientific Meeting (*Poster Presentation, Abstract 255*). August 2013. Sydney.

- Farr R.J., Joglekar M.V., and Hardikar A.A. *Comparing High-throughput qPCR Technologies for miRNA Diagnostics: Does Size Matter?* Australian Islet Study Group Meeting (*Poster Presentation*). August 2013. Sydney.

Abbreviations

Ago2	Argonaute 2
ANOVA	Analysis of variance
ath-miR	*Arabidopsis thaliana* microRNA
BGL	Blood glucose level
BSA	Bovine serum albumin
CD	Cluster of differentiation
cDNA	Complementary DNA
cfDNA	Cell-free DNA
Cre	Cre-recombinase
CRT	Cycle relative threshold
CT	Cycle threshold
CV	Coefficient of variation
Cx	Complications
DA	Dynamic Array
ddPCR	Digital droplet PCR
DGCR8	DiGeorge syndrome critical region gene 8
DNA	Deoxyribonucleic acid
DPBS	Dulbecco's phosphate buffered saline
DR	Diabetic retinopathy
dsRNA	Double-stranded RNA
EDTA	Ethylenediaminetetraacetic acid
ELISA	Enzyme linked immunosorbent assay
eN	Embryonic day N
E-T1D	Established Type 1 diabetes
GADA	Glutamic acid decarboxylase autoantibody
GCG	Glucagon
H&E	Haematoxylin and eosin
HbA1c	Haemoglobin A1c
Hes1	Hairy enhancer of split 1
HLA	Human leukocyte antigen
hr	Hour/s
hrINFα	Human recombinant interferon-α
IA-2	Islet autoantigen-2
IAA	Insulin autoantibody
IFNα	Interferon-α
INS/*Ins*	Insulin
IPA	Isopropyl alcohol
IQR	Interquartile range
LADA	Latent autoimmune diabetes in adults
LB	Luria Bertani (agar/broth)
M *Ins* cfDNA	Methylated insulin cfDNA
MHC	Major histocompatibility complex
min	Minute/s
miRNA/miR	MicroRNA
MODY	Maturity onset diabetes of the young
mRNA	Messenger RNA
ncRNA	Non-coding RNA
NDR	No diabetic retinopathy
NDSS	National Diabetes Services Scheme
ND-T1D	Newly diagnosed Type 1 diabetes
NeuroD1	Neurogenic differentiation factor 1
Ngn3	Neurogenin 3
NGS	Next generations sequencing
NO	Nitric oxide
OA	OpenArray
PA	Pre-amplification
PBMCs	Peripheral blood mononuclear cells
PCR	Polymerase chain reaction
Pdx1	Pancreatic and duodenal homebox 1
PFA	Paraformaldehyde

PI	Propidium idodide
poly(A)	Polyadenine
Pre-miRNA	Precursor microRNA
Pri-miRNA	Primary microRNA
qPCR	Quantitative PCR
RIP	Rat insulin promoter
RISC	RNA induced silencing complex
RNA	Ribonucleic acid
RT	Reverse transcription
rxn	Reaction
SD	Standard deviation
sec	Second/s
SEM	Standard error of the mean
snoRNA	Small nucleolar RNA
SNP	Sodium nitroprusside
ssRNA	Single-stranded RNA
STZ	Streptozotocin
T1D	Type 1 diabetes
T2D	Type 2 diabetes mellitus
TLDA	TaqMan Low Density Array
UM *Ins* cfDNA	Unmethylated insulin cfDNA
UTR	Untranslated region
wga	Weeks of gestational age
wk	Week/s
ZnT8A	Zinc transporter 8 autoantibody

Gene names are designated by an italicised mnemonic: *Ins* for insulin. The protein product of the gene is capitalised without italics: INS. MicroRNAs are denoted with “miR-” prior to their designated number: miR-199a. If the species of origin is any other than human, a three letter prefix is added detailing the species, such as “cel” for *Caenorhabditis elegans*: cel-miR-54. To differentiate between the 5’ and 3’ arms of the pre-miRNA that the mature miRNA originates from, a “-5p” or “-3p” is appended to the name of the miRNA: cel-miR-54-3p.

Dedication

This body of work is dedicated to my son, Lachlan. Born of a father with T1D, this thesis may end up being more than just a book on a dusty bookshelf. I hope that my small contribution can leave a better world for you.

"Nothing in life is to be feared, it is only to be understood. Now is the time to understand more, so that we may fear less."

Marie Curie (1867-1934)

Acknowledgments

Any significant scientific project cannot be completed alone; support, collaboration and mentoring are integral components of success. I am unbelievably lucky to have been part of the team at the NHMRC Clinical Trials Centre. Everybody, whether they are researchers, clinicians, or biostatisticians (or, frequently, a combination of the three), were always ready to lend their expertise and give advice. Some, however, deserve a special mention.

First and foremost, a big thank you to my supervisor, A/Prof Anand Hardikar. Your unerring support and mentorship drew the best from me; I would not have been able to achieve so much without you. Over the past four years, you have helped me to develop into a better researcher and a better person.

To my co-supervisor, Prof. Alicia Jenkins, thank you for your continuous support and advice. Your warm and welcoming personality has made it a pleasure to work at the CTC.

To Dr. Mugdha Joglekar, thank you for always being a kind and patient teacher, despite my mistakes. I have learnt so much over the past four years; you have shown me the kind of Postdoc I hope to become.

To Dr. Andrzej Januszewski, thank you for helping me through the complexities of statistical analysis and your patience when I didn't always grasp the concepts. You always brought such laughter and joy to my time at the CTC; you made "pushing the boundaries of science" fun.

To Wilson Wong, my fellow PhD survivor, thank you for going on this journey with me. It is easier to go through when you don’t do it alone, and I am very grateful that I had you to bounce ideas off, vent my frustrations, and have a laugh. Your friendship has meant a lot over the past four years and I hope it continues.

Last, but by no means least, a big thank you to all of my friends and family that supported me through this journey. To my wife, Leah, who was there during the highs and lows, and who nodded politely while I vented about things she had no idea about. To my son, Lachlan, who has been a continual source of joy in my life. To my dad, who always believed in me and pushed me to do my best. To my mum, who has always supported me. To my sister, Samantha, who is an inspiration and a friend. Thank you.

1. Introduction

1.1. History of Type 1 Diabetes Mellitus (T1D)

Type 1 diabetes mellitus (T1D) has captured the attention of physicians for more than three millennia. This condition presented with frequent urination, weight loss, and excessive thirst, and was invariably fatal until the early 1920s. The earliest records of T1D can be traced back to 1500 B.C.E in ancient Egypt, where it is described in the Ebers Papyrus as a rare disorder that resulted in "too great emptying of the urine". Indian physicians around the same time noted that the urine had a sweet taste that attracted flies and ants, and so they named the condition "madhumeha" or "honey urine". The term diabetes has been used since 230 B.C.E. and was derived from the Greek "diabainein", which means "to pass through", a reference to the excessive urination of those afflicted. Aretaeus of Cappadocia, a Greek physician who lived between 80 and 130 B.C.E. distinguished diabetes mellitus (mellitus being Latin for "honeyed" or "sweet") and the unrelated disorder diabetes insipidus, which also results in excessive urination, but not hyperglycaemia. He wrote:

> *"Diabetes is a dreadful affliction, not very frequent among men, being a melting down of flesh and limbs to urine. The patients never stop making water and the flow is incessant, like the opening of the aqueducts. Life is short, unpleasant and painful, thirst unquenchable, drinking excessive and disproportionate to the large quantity of urine, for yet more urine is passed … If for a while they abstain from drinking their mouths become parched and their bodies dry; the viscera seem scorched up, the patients are affected by nausea, restlessness and a burning thirst, and within a short time they expire." (1)*

Sushruta and Charaka, two Indian physicians, were the first to note the differences between what is now considered Type 1 and 2 diabetes (fifth century C.E.). They observed that thinner individuals with diabetes developed the disorder at a younger age and subsequently survived for a shorter amount of time than heavier individuals with diabetes. It wasn't until 1776 that British physiologist Matthew Dobson identified that the sweetness of diabetic urine was caused by elevations in sugar content. He further described the 'sweetness of serum' in patients with diabetes and thus identified hyperglycaemia (2).

Despite the centuries of interest in T1D, the prognosis for individuals was universally bleak until the discovery of insulin in the early 20th century. Numerous important advances were made in the 19th century that subsequently led to this discovery. In 1889 Minkowski and von Mering found that complete pancreatectomy in dogs resulted in diabetes, while ligation of the pancreatic duct caused digestive issues in dogs but did not culminate in diabetes. Furthermore, in 1893 French scientist Edouard Hedon identified that grafting a small piece of the pancreas under the skin after pancreatectomy protected animals from developing diabetes. Upon the removal of the graft, symptomatic diabetes began immediately; a finding mirrored by Minkowski (1). This supported the idea that the pancreatic secretion within the body were central to the pathogenesis of T1D. A young Canadian surgeon, Frederick Banting, had the idea to isolate the internal pancreatic secretions by ligating the pancreatic ducts in dogs, and then waiting until the exocrine pancreas degenerated to minimise the contamination of digestive secretions. He approached John J.R. Mcleod, a professor at the University of Toronto, who gave him limited laboratory space, dogs, and a medical student research assistant (Charles Best) to conduct his investigations. In July 1921, Banting and Best were successful in harvesting the atrophied canine pancreases, grinding them up, and straining out the subsequent solution. They injected this extract into the vein of a

pancreatectomised dog and found that its condition greatly improved. Subsequent experiments yielded similar dramatic improvements in diabetic dogs, and so the pair then repeated these using different pancreatic extractions and administration routes (3). By January 1922, Banting and Best, with collaboration from biochemist Collip, were ready to inject this extract into patients with T1D. The first patient, Leonard Thompson, was a 14-year old then being treated at Toronto General Hospital. After injection, the patient's blood glucose dropped from 520 to 120 mg/dl during the following 24 hours. Thompson continued to receive subcutaneous insulin treatment that enabled him to live until succumbing to pneumonia at age 27. The discovery of insulin, and the subsequent large-scale manufacture of the substance by the Eli Lilly Company, finally removed the death-sentence that had always come with the diagnosis of T1D. Ted Ryder, one of the first children to receive the treatment after Thompson, was the greatest example of this; he lived until 76 years of age, dying in 1993.

Banting and McLeod were awarded the 1923 Nobel Prize for Medicine for the discovery of insulin and shared their prize with Best and Collip. Today, because of the availability of exogenous insulin therapy there are children and adults with T1D in every country, an estimated 40 million people. With access to insulin and related diabetes care a long and full life is possible for many, albeit with daily challenges of balancing exogenous insulin doses, meals and exercise, monitoring glucose levels and the challenges of avoiding (or dealing with) the chronic complications of diabetes related to eye, renal, nerve and cardiovasculature (4).

There is much recent and ongoing research to prevent or at least delay the onset of T1D (5) and to preserve as much β-cell function as possible. Even low level residual C-peptide levels are associated with better glucose control, lower risk of diabetic ketoacidosis and severe

hypoglycaemia and lower risk of chronic complications (6). This thesis explores and provides tools that can facilitate such research.

1.2. Current Impact of T1D

Type 1 diabetes is a multi-faceted disorder characterised by immune-mediated destruction of insulin producing pancreatic β-cells thought to arise in genetically susceptible individuals following an 'environmental' trigger. Patients typically present acutely with days to weeks of hyperglycaemia, polyuria, polyphagia, and polydipsia, and require immediate intervention with exogenous insulin to maintain normal blood glucose levels and reverse or prevent life-threatening diabetic ketoacidosis (DKA). This β-cell destruction culminates from a complex interplay between host genetics, immunity and environmental factors. Although T1D is often seen as a pancreas-specific disorder, the dysregulation of glucose homeostasis impacts upon a wide range of tissues. Individuals with T1D can develop numerous complications that stem from poor glucose control, including retinopathy, nephropathy, neuropathy and micro- and macrovascular events (4). Indeed, studies have concluded that people with T1D are at least two-fold more likely to have a cardiovascular event (7), and experience less favourable outcomes following an acute coronary event (8).

Type 1 diabetes is one of the most common chronic diseases in children, with a mean age of onset of approximately 12 years, although diabetes onset can occur at any age. In Australia, the incidence of T1D equates to 11 cases per 100,000, with slightly more males diagnosed than females (12 versus 9 per 100,000 respectively) (9). As of the 31st of March 2016, there were 117,319 people with T1D registered with the National Diabetes Services Scheme (NDSS), representing approximately 10% of Australian people with diabetes (10). Globally, both the incidence and prevalence of T1D is rising, although there is a large degree of heterogeneity in the incidence and prevalence of this currently incurable disease between countries (4). Regardless, T1D places an enormous physical, social and financial burden on the individual,

their family, the healthcare system and society. The T1D-associated costs amount to 14.4-14.9 billion annually in the U.S.A. alone (11; 12). In Australia, the annual cost of T1D to the healthcare system is 570 million dollars (13)., whilst that of the more common Type 2 diabetes (T2D) which affects over 1 million Australians is 6 billion dollars (14).

1.3. Progression of T1D

Once T1D is clinically diagnosed, individuals have lost a substantial proportion of their insulin producing β-cells. It is often cited that 80-95% of β-cells are destroyed prior to clinical diagnosis; however, some studies have reported that this figure may be highly variable and dependent on other factors, such as age of onset (4; 15-17). Post-mortem studies of people with Type 1 diabetes have demonstrated residual insulin producing cells (16; 17) even after many years of diabetes. This β-cell death occurs gradually, over months to years, with no overt symptoms and apparent normoglycaemia (Figure 1-1). Research continues towards identifying a plethora of endogenous and exogenous factors that may affect the incidence of T1D (see 1.3.1 and 1.3.2). The natural history of T1D, first proposed by Eisenbarth in 1986 (18), has had several iterations to reflect this continuous increase in knowledge. Although the loss of β-cells, which may be due to cell death or to dormancy, appears to occur in a generally linear fashion, there is evidence that the pancreas is capable of regeneration and so an individual's functional β-cell mass may show fluctuations over time (Figure 1-1). Although pancreatic regeneration has been demonstrated in diabetic mouse models (19), we are yet to understand mechanisms that will enable/facilitate us to reverse the β-cell loss seen in humans after T1D diagnosis.

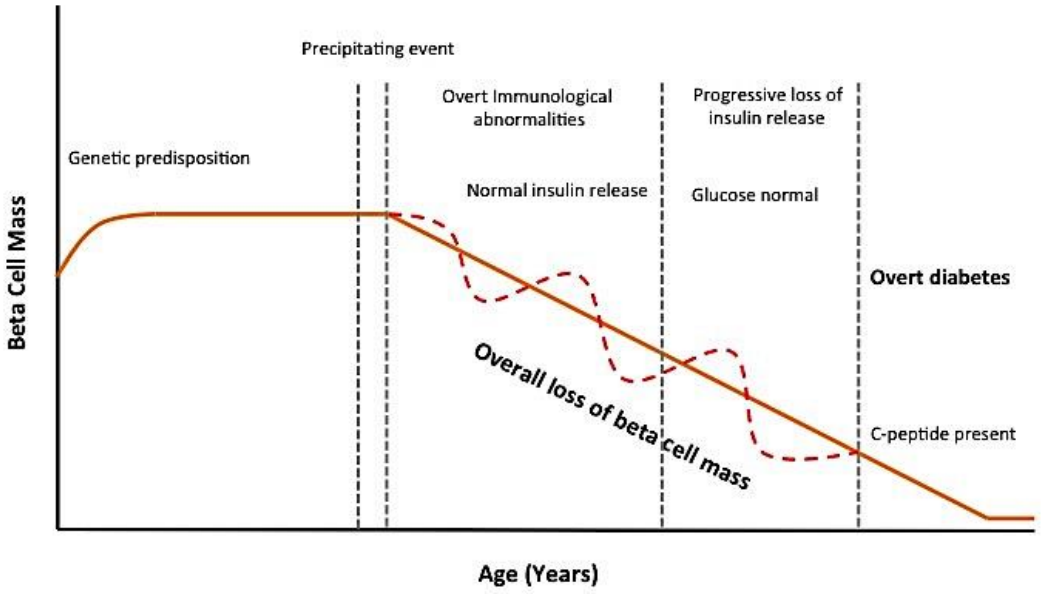

Figure 1-1. Natural history of Type 1 diabetes

Schematic representation of β-cell loss during the progression to T1D. A precipitating event causes the gradual, and potentially fluctuating, loss of β-cell mass. The individual presents with no overt clinical symptoms, including normal glucose control, until the majority of the β-cell mass is lost. After the clinical diagnosis of T1D, C-peptide is often still detected.

Atkinson et al (2014) (20).

Recent studies have further shown that although individuals diagnosed with T1D have a marked reduction in insulin, they are not always completely devoid of the hormone. C-peptide is cleaved from the proinsulin molecule and secreted in equimolar amounts with mature insulin, and hence can be used as a marker of endogenously produced insulin (as C-peptide is absent in pharmacologically produced insulin). Indeed, Davis and colleagues identified that almost one in three patients demonstrated detectable circulating C-peptide (21). This correlated with a subsequent finding that pancreatic tissue from people with T1D had residual insulin-containing islets, irrespective of disease duration (16).

1.3.1. Genetic Risk Factors

As stated earlier, T1D is a complex disorder, and this is reflected in its polygenic and multifactorial nature. With reference to the genetic component, there are over 40 loci that have been associated with either susceptibility or resistance to the condition (22). The human leukocyte antigen (*HLA*) region, located on chromosome 6, stands out as having the greatest influence on T1D. This region spans approximately 4 megabases, contains over 200 genes, and is subject to extreme polymorphism (23). This association was initially identified in 1973 by Singal and Blajchman (24), with many subsequent studies attempting to tease out loci or haplotypes that exhibit the strongest association for progression to T1D (25). Intriguingly, not all haplotypes pose a high T1D risk, some are even seen to be protective (26), with reported odds ratios ranging from 0.02 to >11 (27). The principle of linkage disequilibrium (alleles that are inherited together more often than would be expected by random chance) underlies the observation that a given *HLA* allele is often found in a limited number of haplotype combinations (23). As the name suggests, the classical HLA genes encode for cell-surface proteins that are involved in the capture and presentation of antigens to the T-cell receptor. These proteins are also known as the major histocompatibility complexes (*MHC*). Furthermore, these molecules (especially MHC Class I) have an important involvement in the immune-mediated destruction of β-cells.

Many of the other genes that have been identified with T1D risk also interact with various aspects of the immune system, including some that lie within the *HLA* region (these are often referred to as HLA class III, although they do not code for the classical HLA proteins). Tumour necrosis factor-α (*TFN-α*) – in particular single nucleotide polymorphisms (SNPs) found in the promoter region – has been the subject of numerous investigations, often with conflicting conclusions (28; 29). *TNF-α* also demonstrates linkage disequilibrium with the *HLA* DR3

haplotype, which may explain the genetic association with T1D (28). Furthermore, MHC class I chain-related gene A (*MIC-A*), cytotoxic T-lymphocyte-associated protein 4 (*CTLA*), protein tyrosine phosphatase non-receptor type 22 (*PTPN22*), and genes involved in the complement system have been investigated for T1D association (30-33).

Early investigations also highlighted an association between T1D and polymorphisms in regions flanking the insulin gene (34). Three different classes were described, depending on the number of tandem repeats in the allele. Class I (associated with T1D susceptibility) was shown to result in a reduction of insulin transcription and translation within the thymus, which may lead to a reduction in central immune tolerance to insulin (35; 36). This hypothesis correlates with subsequent studies that highlighted insulin as the major autoantigen in precipitating T1D (37; 38).

Genetic susceptibility is still seen as a predisposing factor for the development of T1D, however, it is no longer seen as the central pathogenic cause of the disease. This is due, in part, to the realisation that genetic influences, or even an increase of progeny from T1D mothers, cannot fully explain the global rise in T1D incidence (39). Intriguingly, the rise in T1D prevalence has been associated with greatest increases in people with low to moderate risk genotypes, not high risk genotypes (40).

1.3.2. Environmental Risk Factors

There are numerous environmental factors that have been linked with the incidence of T1D, with viruses, bacteria, diets (particularly during early childhood), and vitamin D deficiency /its associated pathways, receiving the most attention (41-43). A lower incidence of T1D in babies born by normal vaginal delivery (vs caesarean section) (44) and the hygiene hypothesis, which implicates a cleaner environment early in life and a less challenged immune system and

greater risk of autoimmune diseases (45), suggest important roles of body's microbiome, which may modulate immune system development, in the first couple of years of life. So far these associations have been unsuccessful in confirming the underlying cause or precipitating events in the progression into T1D. As we currently lack tools needed to accurately quantify β-cell death, it is difficult to monitor the death of insulin-producing cells in response to any of the potential risk factors listed above. The characterisation of a biomarker signature of β-cell death would aid in the identification of factor(s) that could precipitate the loss of an individual's β-cell mass and thus progress into clinical T1D. It would also help monitor the efficacy of potential therapeutic agents, such as in the many current (and likely future) trials, to prevent or retard T1D (as outlined at www.trialnet.org).

1.3.3. Autoimmunity and T1D

Type 1 diabetes results from the selective destruction of the insulin-producing β-cells by the host immune system. CD8+ T cells are the main immune cells involved in directly killing β-cells via exocytosis of granules containing perforin and granzymes (46) as well as in a death receptor-dependent manner (47). Although T-cells are responsible for the majority of the immune-mediated cell death seen in the progression to T1D, additional leukocytes, such as CD20+ B-cells and antigen-presenting cells, also play a role (48).

A recent study conducted by Leete and colleagues has highlighted the role of CD20+ B-cells in the development of insulitis (infiltration of immune cells into the pancreatic islets) in T1D patients (16). The investigators identified profound heterogeneity in the numbers of B-cells that infiltrated T1D islets. When they stratified the patients into $CD20^{High}$ and $CD20^{Low}$ groups, they found that individuals diagnosed before the age of 7 years were uniformly $CD20^{High}$, while those diagnosed after 13 years of age were always $CD20^{Low}$ (16). This corresponded to an

increase in residual insulin containing islets (determined through insulin staining), and points to CD20+ B-cells as an indicator of differentially aggressive immune infiltration in T1D (16).

A common characteristic of T1D is the presence of auto-antibodies against islet specific antigens. Greater than 90% of individuals with T1D are positive for one or more antibodies targeting insulin (insulin autoantibody, IAA), glutamic acid decarboxylase (GADA), islet autoantigen-2 (IA-2), or zinc transporter 8 (ZnT8A). These antibodies can appear during infancy (peaking between 9 months and 2 years of age) and are often present prior to clinical diagnosis of T1D (49).Heterogeneity of autoantibodies in people with T1D from different ethnic groups (50) is well known as well as the possible decline in their levels after T1D onset.

1.3.4. Prediction of T1D Progression

Currently, we lack the tools to accurately predict the progression into T1D. The lack of overt clinical symptoms prior to glycaemic dysfunction means that measurement of an individual's blood glucose is the main tool used to identify and diagnose T1D. While this tool is incredibly important in the confirmation of T1D diagnosis and application of exogenous insulin, it only detects individuals at the tail end of T1D progression (Figure 1-1). Many potential therapies for T1D, such as immune suppression (51; 52), are unable to make a meaningful impact once clinical symptoms are present, reflecting the loss of more than 70 to 80% of functional islet β-cell mass. Identification and monitoring of individuals currently undergoing non-symptomatic β-cell death is of utmost importance, as early interventions may delay the onset of clinical T1D and the often life-threatening complications that arise from it.

There has been significant interest in other markers of T1D risk, however many other approaches have been unsuccessful in easily identifying and monitoring those individuals that

will progress into clinical T1D. Several approaches have estimated an individual's risk for developing T1D, usually based upon genetic or immunological parameters.

Genetic links based on family history. Previous studies have found that a child with a first degree relative affected by T1D has a higher risk of developing it themselves (~5% versus 0.4% in the normal population). Further stratification is possible depending on the relationship of the affected family member (3, 7 or 8% risk is their mother, father or sibling had T1D respectively). If the child has two affected first-degree relatives their risk increases significantly to 20%, and it increases even further to 36% if they have an identical twin with T1D (53; 54). Furthermore, an individual's risk may be further affected by their underlying HLA genotype (55).

Islet autoantibodies have also been scrutinised for their predictive value. The presence of a single antibody only confers a marginal increase in T1D risk, regardless of family T1D history. Indeed, only 5% of individuals positive for one islet autoantibody progress to clinical T1D (56). This may be a symptom of non-specific antibody binding, and so affinity testing may be required to increase the sensitivity of this test. The associated risk increases significantly if the individual undergoes seroconversion for two or more islet autoantibodies, but varies widely depending on the antibodies present (57). IAA and IA-2 are associated with the highest risk of T1D (57). Interestingly, the age of seroconversion seems to associate with the rate of progression to T1D (58; 59). Both age of seroconversion and IAA antibody titres, but not GADA or IA-2 titres, have been shown to be determinants of the age of T1D diagnosis (59). Unfortunately, antibody positivity can be transient in individuals without a genetic risk, and this may obfuscate the findings interpreted from a single islet autoantibody result (60).

Glucose and insulin kinetics. Other approaches, mainly used in a research setting, include the monitoring of glucose and insulin responses to an oral or IV glucose tolerance test as the normal phases of insulin release alter and subtle hyperglycaemia occurs prior to clinical T1D onset (61). These changes are likely later in the progression to T1D.

Currently, we lack the tools to accurately quantify the β-cell death that occurs after these precipitating factors. The development of a refined biomarker signature of β-cell death would allow us to 1) estimate the risk and timeframe of a child or adult progressing to T1D, 2) stratify individuals at risk of developing T1D, 3) monitor the rejection of islet transplants, which are now available for clinical use in a subset of T1D adults (62) and 4) monitor responses to interventions in trials, such as related to vaccines, immunomodulatory therapy and diet/lifestyle interventions.

1.4. MicroRNAs (miRNAs)

It was once thought that as organisms became increasingly complex, the number of protein-coding genes increase accordingly. People theorised that if yeast had genomes containing approximately 6,000 protein-coding genes, then humans must have significantly more, with estimates as high as 2 million (63). In recent years, due largely to the Human Genome Project, this figure has identified to just over 20,000 protein-coding genes, intriguingly around half the number of genes in the rice plant genome. Conversely, it has been demonstrated that the amount of non-coding DNA increases with an organism's complexity (64), indicating that regulatory agents produced from the non-coding part of the genome contribute largely to an organisms developmental and functional processes.

Non-coding (nc)RNAs were first found to regulate gene expression in 1993 by Lee and colleagues (65); since then varying classes of these molecules have been characterised, with many found to be highly conserved among different species. MicroRNAs (miRNAs/miRs) are one such subset of ncRNAs and are the most abundant small RNAs in animals, with 2588 mature sequences described in humans (miRBase release 21, June 2014) (66). These 18-22 nucleotide molecules post-transcriptionally regulate endogenous gene expression, and as each miRNA is predicted to have multiple potential target messenger RNAs (mRNAs), they could potentially regulate up to 30% of the protein-coding genes within the human genome (67). The expression of a single gene can be modulated by multiple miRNAs and a single microRNA can target multiple genes (68) thereby increasing the complexity in understanding the mechanisms through which microRNAs can fine-tune gene expression.

1.4.1. Biogenesis and Function

The biogenesis of miRNAs involves multistage post-transcriptional processing of primary miRNA (pri-miRNA) transcripts, which are large polycistronic precursor molecules with multiple stem-loop structures connected via single stranded RNA segments (69). Pri-miRNAs are transcribed by RNA polymerase II or III and contain poly(A) tails and cap structures (70). Within the nucleus, these molecules are processed by the Microprocessor complex, which includes the RNAse III enzyme Drosha and the RNA binding protein Pasha (or DiGeorge syndrome critical region gene 8, DGCR8), to produce stem-loop precursor miRNAs (pre-miRNAs) approximately 70 nucleotides in length (71). Pasha first interacts with the ssRNA segments of the pri-miRNA and guides Drosha to a stem-loop structure. Drosha then cleaves the dsRNA ~11bp from the ssRNA-dsRNA junction, leaving a short 3' overhang (72). Additional proteins, such as the helicases p68 and p72, have also been shown assist the Microprocessor complex cleave pri-miRNAs (73).

The subsequent pre-miRNA molecule is exported out of the nucleus by exportin 5, which recognises the dsRNA stem (minihelix structure) and the 3' overhang (74). Once in the cytoplasm, Dicer, another RNAse III enzyme, cleaves the pre-miRNA near the terminal hairpin loop, generating mature dsRNA miRNAs (75). Dicer is a highly conserved protein, found in almost all eukaryotes; indeed, many organisms contain more than one Dicer homologue that each perform distinct roles. Dicer also associates with additional proteins, including Trbp (TAR RNA binding protein), PRKRA (protein activator of interferon induced protein kinase EIF2AK2) and Hsp90 (heat shock protein 90), which aid in forming the RNA-induced Silencing Complex (RISC) (76). RISC is a ribonucleoprotein complex that carries out the post-transcriptional silencing of the mRNA identified by the miRNA (76). Hsp90 is particularly important for RISC formation as it is predicted to mediate the conformation change required to allow entry of

the miRNA into RISC (76). Once incorporated into RISC, one strand of the miRNA is retained (active strand), while the other is removed (passenger strand). This strand selection is thought to be based on the thermodynamic characteristics of the miRNA; the strand with the weakest binding at the 5' terminal often becomes the active strand (76). It was initially thought that the passenger strand was degraded and did not participate in mRNA silencing; however, recent reports have confirmed that both of the strands are often detected at comparable levels and that the passenger strand may also be incorporated into a different RISC with distinct or overlapping targets (77). Therefore, the nomenclature has been changed from miR/miR*, where * designated the passenger strand, to -3p/-5p, reflecting which arm of the pre-miRNA contains the sequence (3'or 5') (66).

After strand selection, RISC uses the active miRNA strand to identify the target mRNA, usually through complementarity to the 3' untranslated region (UTR) of the mRNA. Although the first miRNA described, lin-4, demonstrated extensive complementarity with its target mRNA (78), many of the subsequent metazoan miRNA targets only show clear complementarity with the miRNA seed sequence (79). The seed sequence is comprised of 6-8 nucleotides on the 5' end of the miRNA (usually nucleotides 2-7 of the miRNA sequence) and is thought to guide the miRNA-mRNA interaction (79). However, some of these canonical sites (regions complementary to the miRNA seed site) have no apparent effect on mRNA abundance, increasing the difficulty in predicting miRNA target sites. Non-canonical sites (sites effective in downregulating gene expression but with non-perfect complementarity to the seed sequence) have been described but are considered relatively rare (79). If the target mRNA has perfect complementarity to the miRNA seed region, the slicer activity of Ago2 cleaves the target between nucleotides 10 and 11 (relative to the active strand) and initiates rapid degradation of the transcript (80). If the target is only partially complementary, as the majority of animal

miRNA targets seem to be, then RISC can either induce translational repression or guide the target to the 5'-to-3' mRNA decay pathway, where the transcript is deadenylated, decapped, and then ultimately degraded by the endogenous 5'-to-3' exonuclease 1 (Xrn1, reviewed in (81)).

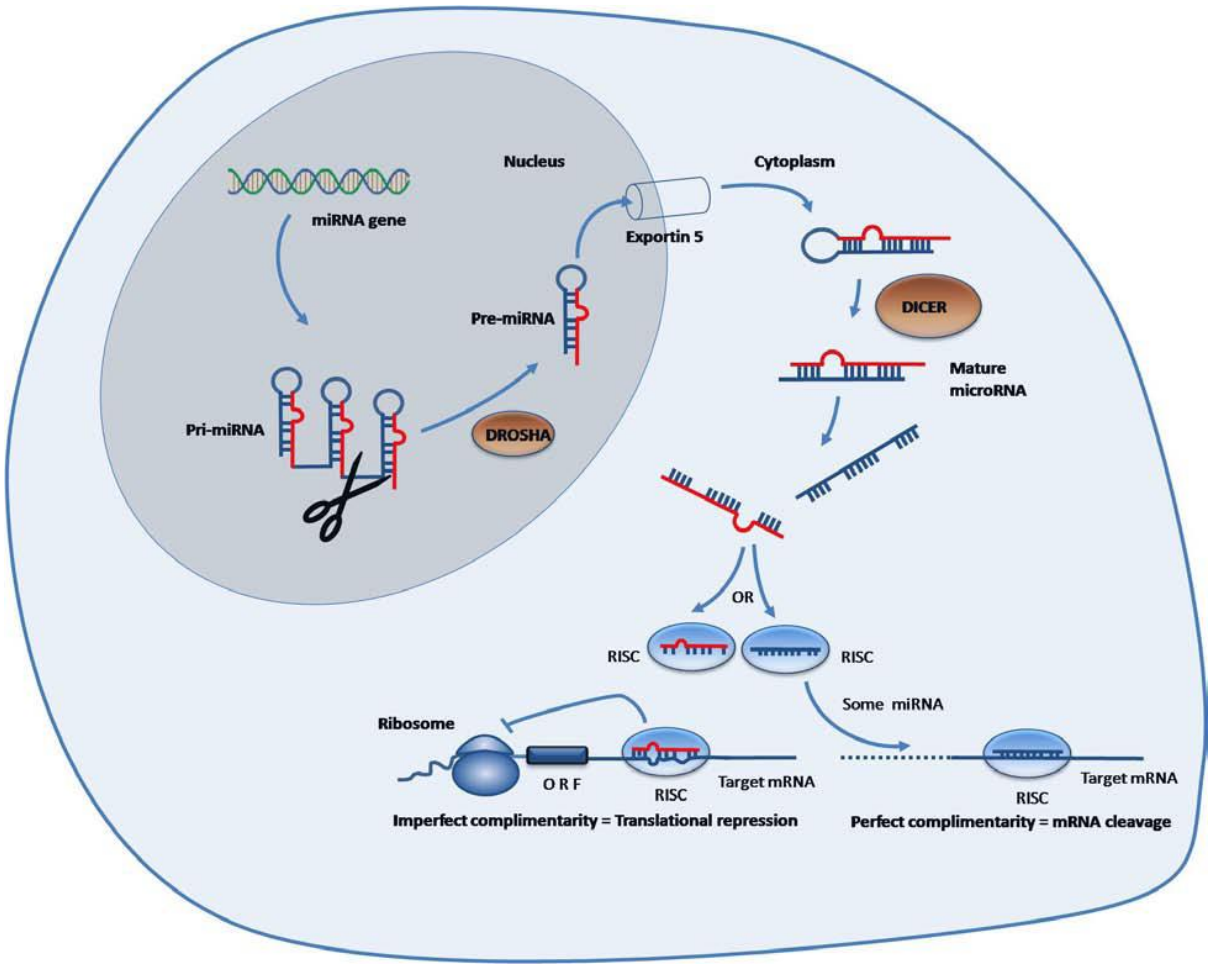

Figure 1-2. Biogenesis and function of microRNAs

A schematic depicting synthesis and function of miRNA. Mature miRNAs are synthesized in the nucleus as primary miRNAs and processed to precursor miRNAs by Drosha. These precursors are then transported outside the nucleus, where they are further truncated by Dicer into double stranded mature miRNAs. Single strands of mature miRs are incorporated into RISC, which then targets the gene transcripts. Based on the complementarity of the mRNA:miRNA, the target mRNA is either destroyed or translationally repressed.

Farr et al 2013 (82).

1.5. Role of MicroRNAs in Glucose Homeostasis and T1D

MicroRNAs are essential for normal cellular development and function. A plethora of studies (83-109) have identified numerous miRNAs that regulate several aspects of glucose homeostasis, including the development of the pancreas, insulin production and secretion, as well as insulin utilisation in peripheral tissues. The following sections discuss the currently known miRNAs that are critically involved in these processes. Table 1-A summarises the important miRNAs and their site specific roles.

Table 1-A. Important miRNAs involved in glucose homeostasis and T1D

MicroRNA	Site	Role	Reference/s
miR-375	Pancreatic islets	Pancreatic development, insulin secretion, glucose homeostasis	(96; 101; 102)
miR-7	Pancreatic islets	Pancreatic development, β-cell mass, insulin production	(83; 84; 96; 100)
miR-9	Pancreas	Pancreatic development	(96)
miR-376	Pancreas	Pancreatic development	(96)
miR-1	Skeletal muscle	Glucose homeostasis	(86; 89; 108)
miR-133a	Skeletal and cardiac muscle	Glucose homeostasis	(89; 93; 95; 106)
miR-206	Skeletal muscle	Glucose homeostasis	(89)
miR-222, -27a, -195, -103	Skeletal muscle	T2D (Goto Kakizaki rats)	(91; 92; 94)
miR-106b	Myotubes	Insulin resistance	(109)
miR-143	Adipocytes	Adipocyte differentiation, obesity, insulin resistance	(88; 97; 107)

miR-103	Adipocytes	Obesity, insulin resistance	(107)
miR-29a/b/c	Skeletal muscle, adipocytes, liver	Insulin resistance, T2D (Goto Kakizaki rats), gluconeogenesis	(91; 98)
miR-122	Liver	Hepatic glucose homeostasis, fatty acid and cholesterol synthesis	(87; 105)
miR-148a	Liver	Hepatic glucose homeostasis	(105)
miR-192	Liver	Hepatic glucose homeostasis	(105)
miR-194	Liver	Hepatic glucose homeostasis	(105)
miR-33a/b	Liver	Insulin signaling	(85)
miR-126	Liver	Insulin signaling	(104)
miR-223	Cardiac muscle	Glucose homeostasis	(99)
miR-208a	Cardiac muscle	Insulin sensitivity, glucose tolerance	(90)
miR-21	Pancreatic islets	Inflammation	(103)
miR-34a	Pancreatic islets	Inflammation, cytokine-mediated cell death	(103)
miR-146a	Pancreatic islets	Inflammation, cytokine-mediated cell death	(103)

1.5.1. Pancreas Development and Function

1.5.1.1. MicroRNA Regulation of Pancreas Development

Early studies attempted to investigate the role of miRNA-induced gene regulation upon embryonic development by creating Dicer-deficient mice models. As Dicer is crucial for the maturation of miRNAs, its removal caused an ablation of all miRNA functions. Unfortunately,

the results were inconclusive, as this loss of function appears to be lethal at e7.5 (110), however it underscored the importance of miRNAs in embryonic development. Lynn *et al* then conditionally deleted Dicer1 from the developing mouse pancreas via pancreatic and duodenal homeobox 1:Cre-recombinase (Pdx1:Cre)-mediated ablation, demonstrating that knockout mice suffered severe pancreatic agenesis and neonatal death (111). The authors noted that the gross endocrine defect was associated with increased levels of hairy enhancer of split 1 (Hes1) and a reduction is Hes1's target gene neurogenin3 (Ngn3). This association suggests that Hes1, and possibly other notch signalling genes could be actively targeted by miRNAs during early pancreatic development. A more recent study, utilising a Ngn3:Cre knockdown of Dicer, found morphological defects within the islets and noted a loss of hormone production (112). Once the mutant mice were born they quickly (within 2 weeks) developed diabetes.

Intriguingly, when Dicer is conditionally knocked out of β-cells, using a Cre-lox system under the control of the rat insulin promoter (RIP:Cre), no disruption of foetal or neonatal β-cell development was observed (113). The Dicer knockout mice did, however, demonstrate impaired insulin secretion, progressive hyperglycaemia and spontaneous development of diabetes later in life (113). Although the removal of Dicer indicates a general role for miRNAs in pancreatic development, several studies have implicated individual miRNAs in the regulation of important transcription factors (for a comprehensive review, please see (114)). As yet there are no known clinical case reports of defects in human pancreas development caused as a result of mutations/deletion in specific microRNAs

1.5.1.2. MicroRNA-375

MicroRNA-375 is central to the development and function of the endocrine pancreas. It was one of the first islet-specific miRNAs to be characterised (101) and has been the subject of numerous subsequent investigations. Initial experiments in zebrafish confirmed the central role of this miRNA in pancreatic development. Knockdown of miR-375 during embryological development, using morpholino oligonucleotides, caused abnormal migration and morphology of pancreatic islets (115). Interestingly, the zebrafish islets are intact for 24 hours post-fertilisation before developing overt abnormalities. This observation may indicate that miR-375 helps to maintain cellular identity. A subsequent study by Joglekar and colleagues found miR-375 to be robustly expressed during the development of human islets (96). The expression of pri-miR-375 was found to be within both β-cells and non-β-cells in the islet, and coincided with augmented insulin production and β-cell proliferation. Interestingly, using immune-FISH and single cell PCR technologies, Joglekar et al demonstrated that the expression of mature miR-375 was more restrictive to non-β-islet cells indicating that microRNA processing may be differentially regulated in β-cells versus non-β-cells.

A miR-375 knockout (375KO) mouse model has also been described (102). This deletion was shown to decrease the β-cell fraction, while increasing α-cells, circulating glucagon and gluconeogenesis. Indeed, the 375KO resulted in a 38% and 31% decrease in β-cell area at 3 and 10 weeks of age, respectively. Further investigation demonstrated that a number of genes involved in cellular proliferation were increased in the 375KO model (102). A luciferase plasmid construct containing the partial or complete 3’ UTR of some of the cell proliferation genes found that apoptosis-inducing factor, mitochondrion-associated 1 (Aifm1), RAS, dexamethasone-induced 1 (Rasd1), eukaryotic translation elongation factor 1 epsilon 1

(Eef1e1), Hu Antigen D (HuD) and cell adhesion molecule 1 (Cadm1) demonstrate reduced reporter expression in the presence of miR-375, indicating direct targeting of these transcripts (102). All of these targets are involved in the negative regulation of cellular growth, and so post-transcriptional regulation via miR-375 may help to increase proliferation both during foetal development and during metabolic stress. Intriguingly, the expression of two other genes, tyrosine hydroxylase (Th) and neuronatin (Nnat), was up-regulated despite the lack of a miR-375 motif within their 3' UTR (102). This suggests that miR-375 can indirectly regulate gene expression, widening its area of influence within the endocrine pancreas.

A recent study used human embryonic stem cells to analyse the dynamic expression of miRNAs during differentiation into insulin-producing cells (116). It identified some prominent pancreatic transcription factors, such as hepatic nuclear factor 1 β (Hnf1β), SRY-box 17 (Sox17), Gata binding protein 6 (Gata6) and paired box 6 (Pax6), had an inverse relationship with miR-375 expression, suggesting regulation by this miRNA. MicroRNA-375 overexpression experiments demonstrated a decrease in the pancreatic progenitor markers Hnf1β and Sox9 (116). Additionally, a recent study has linked miR-375 with the regulation of yes-associated protein 1 (Yap1), a transcriptional co-activator of the Hippo signalling pathway involved in the proliferation of pancreatic progenitor cells (117).

Another validated target of miR-375 is the protein kinase Pdk1 (118). Pdk1 is part of the PI 3-kinase signalling cascade (119), a pathway that can phosphorylate Pdx1, a major pancreatic transcription factor (120). Exposure of INS-1E cells or isolated rat islets to high glucose reduced the transcript abundance of miR-375 (and increased Pdk1). MicroRNA-375 is also increased (and Pdk1 decreased) in the islets of neonatal rats from mothers on a low protein diet, which

also show reduced β-cell mass and function (121). Together, this highlights that nutritional stimuli may affect miRNA expression, which is particularly relevant for pancreatic islets.

Islet specific expression of miR-375 is transcriptionally regulated by conserved promoter regions, cis-elements and enhancer boxes. The miR-375 gene is driven by an upstream TATA-box containing promoter in both α- (122) and β-cells (123). This promoter region contains potential binding sites for several pancreatic transcription factors, including Hnf1, Hnf6, Ap1, Insm1, Xfd3 and Ptf1 (123). Additionally, the enhancer boxes are required for complete transcriptional activity of pre-miR-375, indicating that this miRNA may be regulated by basic helix-loop-helix transcription factors, such as Ngn3 and NeuroD1 (123). Chromatin immunoprecipitation experiments have also shown that Pdx1, along with NeuroD1, interact with conserved regions (labelled proximal promoter and distal enhancer binding regions) surrounding the miR-375 gene (124). Together, this data suggests that miR-375 is involved in a complex regulatory network throughout the development and function of the endocrine pancreas.

1.5.1.3. MicroRNA-7

MicroRNA-7, like miR-375 discussed above, has been identified as a major islet miRNA (83), and increases in expression during the development of the endocrine pancreas in humans (84; 96). *In situ* hybridisation experiments identified that miR-7 expression during development was predominantly within the epithelial region of the pancreas (84). Moreover, the maximum expression of miR-7 seen during development (14-18 weeks of gestational age) coincides with the rapid increase of pancreatic endocrine hormones (84). Knockdown of miR-7 in early mouse embryos (e10.5) using an ultrasound-guided intrauterine injection of antisense miR-7 morpholino oligonucleotides directly into the foetal heart reduced the number of β-cells,

down-regulated insulin production and caused glucose intolerance in the progeny (100). *In vitro* inhibition of miR-7 in isolated pancreatic buds causes the death of developing insulin producing cells, reinforcing the crucial role of this miRNA in the development of the endocrine pancreas (100).

MicroRNA target prediction has identified that the pancreatic transcription factor Pax6 has three potential miR-7 target sites, two of which have been functionally validated (125). One of these is conserved among humans, pigs, rodents, frogs and fish, while the other is restricted to primates (125). Luciferase reporter assays containing the 3' UTR of Pax6 have confirmed that it is indeed a target of miR-7 (125; 126). The interaction of miR-7 and Pax6 seems to affect the differentiation of endocrine precursors; overexpression of miR-7 reduces both α- and β-cells but increases ε-cells, whereas inhibition results in the inverse (126).

Due to the established importance of miR-7 within the endocrine pancreas, researchers have investigated its transcriptional regulation. There are two conserved E-box elements within the miR-7 promoter region, allowing transactivation via Ngn3 and its downstream transcription factor NeuroD1 (127).

1.5.1.4. Other Important MicroRNAs During Pancreas Development

Although the discovery of novel microRNAs continues at a brisk pace, the identification and validation of their targets remains a more arduous process. Additional miRNAs have demonstrated expression patterns during foetal pancreatic development but their specific targets during this process still elude us. Joglekar and colleagues have previously identified miR-7, miR-9, miR-375 and miR-376 expression during human pancreatic development (96). Further investigations into the miRNAs expressed during development and their specific roles will help to elucidate the intricate regulatory mechanism within this process.

1.5.2. Insulin Target Tissues

Glucose homeostasis requires an appropriate balance between the release of insulin from pancreatic β-cells and the sensitivity of the target tissues to the action of insulin. Insulin sensitivity of peripheral tissues such as adipose tissue, skeletal muscle and liver is directly influenced by the expression of certain miRNAs.

1.5.2.1. Skeletal muscle

Muscle tissue, the primary site of glucose uptake, accounts for approximately 75% of insulin-dependent glucose removal from the plasma (128). MicroRNA-1, -133 and -206, which are also called as myomiRs due to their muscle-specific expression, regulate muscle proliferation and differentiation (8; 9). Gene targets of miR-1 and miR-133a are involved in glucose homeostasis. MicroRNA-133 has been shown to alter expression of insulin like growth factor-1 receptor (IGF-R1) in developing skeletal muscle (95) as well as the glucose transporter GLUT4 by inhibiting expression of the Krüppel-like transcription factor KLF15 (93). MicroRNA-1 also targets insulin like growth factor 1 (IGF-1), blocking the capacity of glucose induced IGF-1 to cause mitochondrial dysfunction, cytochrome-c release and apoptosis in cardiomyocytes (108). Both IGF-1 and IGF-R1 were shown to be targets of miR-1 in c2c12 myoblasts; interestingly, this study also determined that IGF-1 is able to regulate the expression of miR-1 via the transcription factor FoxO3a (86).

Studies have examined the expression of miRNAs in skeletal muscle from Goto Kakizaki rats (91; 92; 94), a model of insulin resistance and diabetes (129). Different miRNAs, including miR-222, miR-27a, miR-195, and miR-103 are altered in type 2 diabetes. A recent study also suggests a role of miR-106b in mitochondrial dysfunction and insulin resistance of c2c12 myotubes (10; 109). MicroRNA-106b regulates mitochondrial function by targeting mitofusin-

2 and also controls skeletal muscle insulin sensitivity. A study carried out in 2009 examined the expression levels of miRNA in the skeletal muscle of healthy individuals before and after a 3 hour euglycemic-hyperinsulinemic clamp (89). Out of 216 miRNAs expressed in skeletal muscle, 39 were found to be down-regulated by insulin, including the muscle specific miRNAs miR-1, miR-133a and miR-206. This down-regulation of miR-1/miR-133a by insulin was shown to be mediated by the transcription factors sterol regulatory element binding protein (SREBP)-1c and myocyte enhancer factor 2c (mEF2c). The effect of insulin on miR-1 and miR-133a was altered in the skeletal muscle of type 2 diabetic individuals; however, levels of these miRNAs in the absence of insulin were not altered compared to healthy individuals. Another study by Gallagher *et al* (130) examined mRNA and miRNA changes in skeletal muscle of healthy (non-diabetic) individuals and those with impaired glucose tolerance or T2D. Of 172 miRNAs expressed in skeletal muscle, 61 were altered in individuals with T2D with a subset also found to be altered in individuals who had impaired glucose tolerance (130) suggesting that some expression changes occur before the onset of diabetes.

1.5.2.2. Adipose tissue

In adipose tissue, insulin stimulates lipogenesis, the conversion of blood glucose into fatty acids for efficient energy storage. MicroRNAs are demonstrated to be important in adipocyte lineage commitment, differentiation and proliferation. MicroRNA-143 has been shown to be involved in adipocyte differentiation both in vivo and in vitro (88; 107). Overexpression of miR-143 and miR-103 in pre-adipocytes leads to an increase in the expression of adipogenesis markers and triglyceride accumulation. Interestingly, both miR-143 and miR-103 are downregulated in adipocytes from ob/ob mice which are insulin resistant and obese (107). MicroR-143 overexpressing mice demonstrate impaired insulin sensitivity, while miR-143

knock out animals do not develop obesity symptoms (21; 97). This indicates that miR-143 is one of the regulators of obesity and diabetes.

The miR-29 family (miR-29a, b and c) have been shown to be upregulated in both the skeletal muscle and adipose tissue of diabetic Goto Kakizaki rats (91). The upregulation of miR-29a and miR-29b could be reproduced *in vitro* when 3T3-L1 adipocytes were incubated in the presence of high glucose and insulin. Indeed, overexpression of miR-29 in the same cell type decreased insulin-stimulated glucose uptake (91). These results suggest that miR-29 may be involved in mechanisms leading to insulin resistance in type 2 diabetes.

1.5.2.3. Liver

Selective deletion of the miRNA processing enzyme Dicer1 in the liver early after birth leads to mild hyperglycaemia in the fed state and in severe hypoglycaemia in the fasting state due to depletion of glycogen stores (105). The expression levels of four microRNAs that are highly enriched in the liver, miR-122, miR-148a, miR-192 and miR-194, were found to be decreased in Dicer null hepatocytes indicating that these miRNAs are important for hepatic glucose homeostasis. MicroRNA-122 is the most abundant miRNA in the liver, with copy numbers reaching 50,000-82,000 per average mouse liver cell, and 135,000 per primary human hepatocyte (131). In mice, inhibition of miR-122 leads to a decrease in hepatic fatty acid and cholesterol synthesis along with a reduction in plasma cholesterol (87). Inhibition of miR-122 in a mouse model of diet-induced obesity also led to a reduction in plasma cholesterol concentrations. These results suggest that miR-122 inhibition may be of therapeutic benefit in lowering plasma cholesterol levels. The expression levels of miRNAs in liver have been examined in animal models of diabetes (92; 132-134), however, their precise role in regulation of liver function are not yet determined. In vitro, a number of microRNAs have been shown to

inhibit the expression of insulin receptor substrates (IRS). MicroRNA-33a/b inhibits the expression of IRS-2 in cultured hepatic cells reducing the activation of insulin signalling pathways including AKT and ERK (85). IRS-1 has been shown to be down-regulated by miR-126 in the hepatic cancer cell line SK-Hep-1 (104). MicroRNA-145 has also been shown to down-regulate IRS-1 in human colon cancer cells but it is unclear whether this is also the case in the liver (135). Recently, the effect of the miR-29 family on the liver of diabetic mice has been explored (98). Overexpression of these miRNAs, through adenovirus vectors, leads to improved fasting glucose and insulin tolerance in diet-induced obese mice. It is thought that this effect is a direct result of lowering hepatic gluconeogenesis via the decrease of PGc-1α and G6Pase protein levels.

1.5.2.4. Cardiac Muscle

Cardiac muscle, and muscle tissue in general, is a major site of glucose uptake. Therefore, many of the cardiac-specific miRNAs impact upon this process. MicroRNA-133, as discussed under the 'skeletal muscle' section (above), is seen to negatively regulate the expression of GLUT4, a major glucose transporter in cardiac muscle (106). Indeed, when miR-133 is overexpressed in cardiomyocytes it lowers GLUT4 expression and the associated insulin-induced glucose uptake (93). Conversely, miR-223 has been shown to increase the levels of GLUT4 within cardiomyocytes (99). A cardiac-specific miRNA, miR-208a, has recently been demonstrated to impact upon energy homeostasis in mice by down regulating the expression of mED13, a component of the mediator complex (90). Inactivation of miR-208a, either by pharmacological means or the generation of miR-208a-/- mice, confers resistance to high-fat diet induced obesity and improves glucose tolerance and insulin sensitivity. Additionally, miR-208a-/- mice are resistant to cardiac stress-induced remodelling (136). Further miRNAs, such

as miR-378 (137), have been theorised to regulate energy homeostasis within cardiac cells, although more work is needed to validate the potential targets.

1.5.3. MicroRNA Expression in Type 1 Diabetes

In T1D, β-cells undergo immunologic-mediated destruction. Few studies have investigated the response of miRNA expression within islets during this cellular stress. When MIN6 cells and human pancreatic islets are exposed to proinflammatory cytokines, such as IL-1β and TNF-α, the expression of miR-21, miR-34a and miR-146a is increased within thse cells (103). This increase was also observed within the islets of NOD mice undergoing pre-diabetic insulitis (103). Knockdown of miR-34a and miR-146a conferred protection against cytokine-mediated apoptosis to MIN6 cells, indicating a role for these miRNAs in the immune destruction of β-cells (103).

1.6. Circulating MicroRNAs

MicroRNAs have been extensively investigated as biomarkers in both research and clinical settings for a variety of diseases, including diabetes (82; 138; 139) and cancer (140). This is due to the fact that miRNAs are easily detected within the peripheral circulation and their abundance is seen to change with many pathophysiological states. It has also been reported that miRNA abundance does not vary significantly when challenged with multiple freeze-thaw cycles or exceedingly high or low pH levels (141), making them ideal biomarker candidates. Clinical usage of these molecules as indicators of disease status or stage would allow monitoring, early intervention and therapeutic stratification for patients. In terms of diabetes, miRNA biomarkers would provide multi-faceted benefits, such as in i) quantifying the level of islet cell death in type 1 diabetes (T1D) and islet transplant recepients; ii) identification of individuals at high-risk of developing diabetes prior to its clinical onset; and iii) allow monitoring of treatment efficacy for potential early intervention therapies for high-T1D-risk individuals; iv) monitoring the progression of established diabetes; and v) assessing systemic damage in tissues to predict progression of diabetic complications.

How does one identify potential circulating miRNA biomarkers for diabetes progression? Due to the systemic nature of diabetes and its complications, miRNAs may be released from several tissues in response to cellular stress, injury, or death (Figure 1-3). Special attention should be placed on the pancreas due to its central role in this disease; however, it is important to note that in a dynamic *in vivo* system, other tissues may contribute to the overall biomarker signature. The death of β-cells during diabetes causes a release of the cellular contents, including β-cell enriched miRNAs, into the extracellular milieu, which may be detectable in circulation.

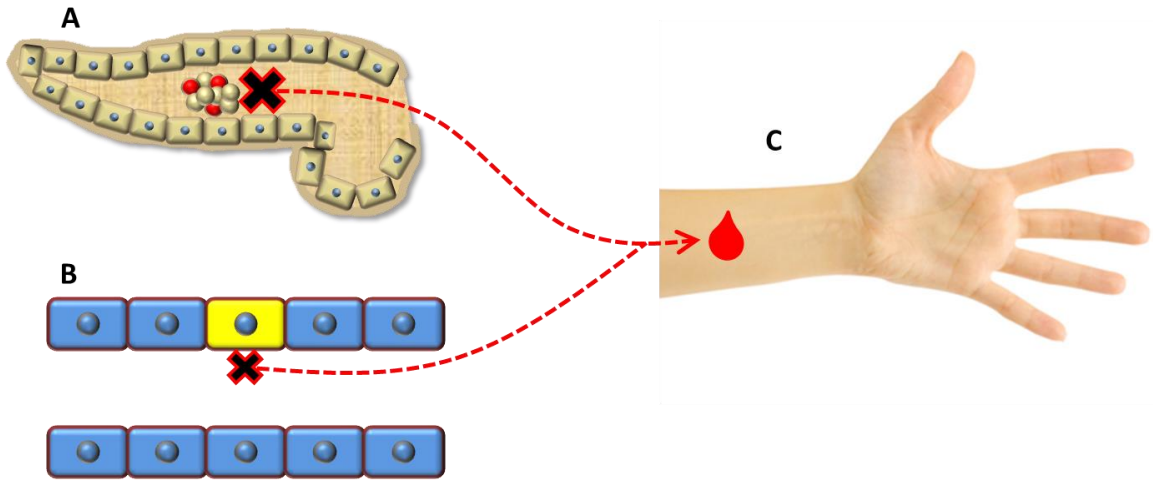

Figure 1-3. Theoretical model of a microRNA-based biomarker signature.

A) Cellular death of pancreatic islets release enriched miRNAs into circulation. B) Cellular stress or injury in blood vessels or other tissues may also release miRNAs into circulation. C) Released miRNAs are detectable within peripheral circulation via routine phlebotomy. Farr et al 2015. (114)

1.6.1. Stability

How miRNAs enter the circulation, and why they are not readily degraded by the abundant endogenous nucleases, is a point of much recent interest. Many investigations into circulating miRNAs utilise plasma as the sample of choice, however plasma contains a large number of endogenous RNases (142). Indeed, when naked miRNAs from *Caenorhabditis elegans* are spiked into plasma samples prior to protein denaturation they are quickly degraded (within 2 mins), whereas endogenous miRNAs are unperturbed (140). This indicates that endogenous miRNAs are protected from degradation within circulation.

There are at present multiple mechanisms to explain the presence and stability of miRNAs within circulation. Firstly, miRNAs could be passively leaked from damaged cells during tissue injury or oncogenesis (141). This possibility can neatly explain the presence of miRNAs within circulation, but not why they are robustly protected from degradation. Membranous vesicles,

such as microvesicles (143) or apoptotic bodies (144), have been found to harbour miRNAs and protect them from damage. Microvesicle-associated miRNAs have been demonstrated to comprise the majority of miRNAs found within plasma (145). Furthermore, data has shown that these miRNA microvesicles are a mediator of cell signalling (143; 144). MicroRNAs have also been found complexed with proteins (146) and lipoproteins (147), which may hide the miRNAs from endogenous nucleases. Figure 1-4 outlines the major forms of miRNA transfer.

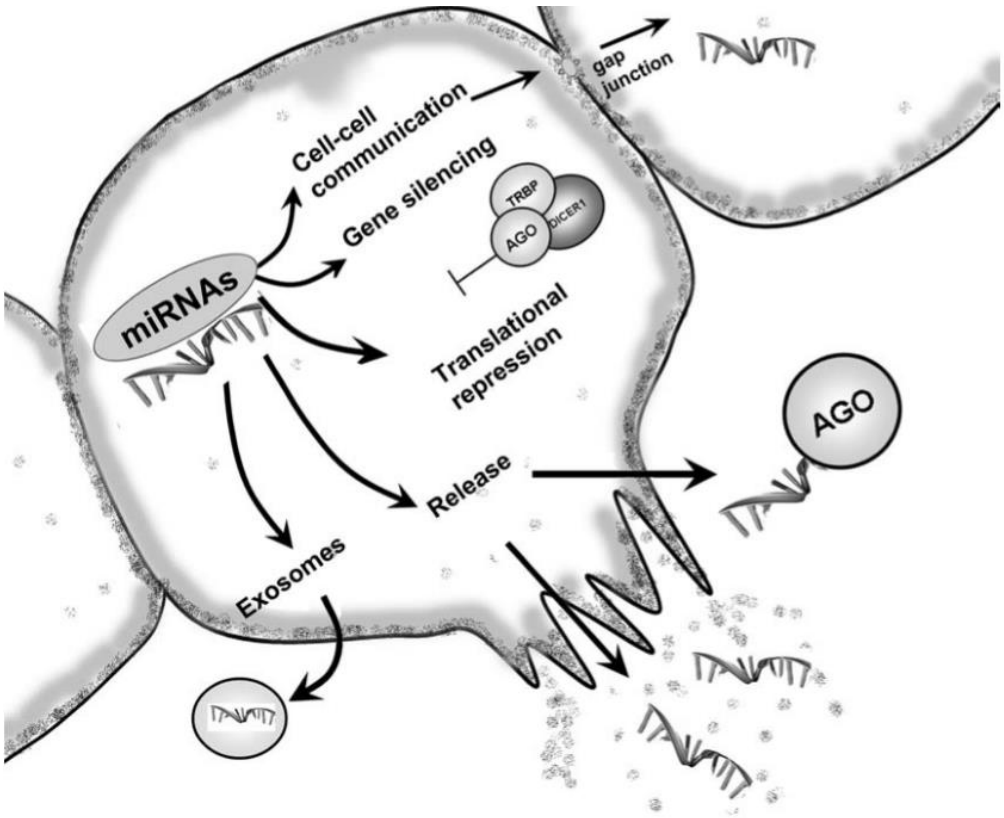

Figure 1-4. MicroRNA transfer

A schematic representing the modes of miRNA transfer. Cellular miRNAs can travel via gap-junctions or exosome-mediated transfer to surrounding cells. MicroRNAs that are released from damaged cells (ruptured cell membrane above) can be detected in body fluids, including in the peripheral circulation, where they are known to be fairly stable due to their resistance to endogenous nucleases.

Farr et al 2013 (138)

1.6.2. Circulating MicroRNAs in T1D

MicroRNAs are intriguing transcripts; they are incredibly diverse and yet many are highly conserved across species. They represent the largest class of small RNAs within animals and impact upon a staggering amount of different cellular processes. Their discovery reshaped our knowledge of how varying genomes resulted in increased complexity without an ever-increasing number of protein coding genes. In recent years, miRNAs have grown from post-transcriptional regulators to biomarkers of disease (138-140). Their release and stability in peripheral circulation has created the potential to develop minimally-invasive tests (requiring a blood or other biofluid sample) to predict the onset of diabetes and track its progression within an individual. Although previous studies have identified some miRNAs that are differentially expressed in individuals with diabetes, there has not been a validated signature for the progression of diabetes and its complications.

To date, there have been few investigations into the circulating miRNAs within individuals with T1D (148-154). So far most of the studies have had a candidate approach, identifying one or more miRNAs as increased or decreased within circulation (described below). To develop a biomarker signature that can accurately detect the progression of diabetes, there is a need to identify a combination of miRNAs that best reflect the natural progression of the disease. The sections below outline the miRNAs that have been found to be differentially expressed within T1D circulation and are summarised in Table 1-B.

The first study, by Sebastiani and colleagues in 2011, identified an increase in the expression of miR-326 in the peripheral blood lymphocytes of patients with T1D currently undergoing islet autoimmunity (152). This implicates this miRNA as a marker or effector of the immune destruction seen in T1D, however, the study was quite small (19 individuals) and did not

compare levels with non-diabetic individuals. Another study that investigated miRNAs from peripheral blood mononuclear cells (PBMCs) in T1D patients found that miR-21a and miR-93 were downregulated when compared to controls, however no associated with autoimmunity was found (150). Furthermore, a recently published small study found that miR-146a expression in PBMCs was decreased in individuals with T1D (154). Interestingly, the authors found that the decreased miR-146a expression significantly correlated with high serum GAD autoantibody titres, indicating that this miRNA may be a marker of ongoing islet autoimmunity (154). The changes seen in these studies, however, are not truly representative of circulating miRNAs, but rather mobile cell-associated miRNAs.

In 2012, Nielsen and colleagues published a study that found 12 miRNAs (miR-152, miR-30a-5p, miR-181a, miR-24, miR-148a, miR-210, miR-27a, miR-29a, miR-26a, miR-27b, miR-25, and miR-200a) had a significantly increased abundance within the serum of two groups of individuals with T1D compared to matched controls (148). This was the first study that analysed cell-free circulating miRNAs in T1D patients. Interestingly, the authors found that miR-25 had a negative correlation with residual β-cell function as assessed by stimulated C-peptide, but a positive correlation with HbA1c levels (148). Another study found that T1D patients had increased levels of miR-21 and miR-210 within their plasma and urine, when compared to age and gender matched controls (149). Additionally, the study found that urinary miR-126 was decreased in T1D individuals and negatively correlated with the patient's concurrent HbA1c level (149). A recent study has investigated select miRNAs in the circulation of subjects with pre-diabetes, T2D, T1D, and latent autoimmune diabetes in adults (LADA), and compared them with non-diabetic control subjects (153). LADA is a late onset form of T1D, which can often be mistaken for T2D initially, and whilst initially being able to be managed with lifestyle and oral glucose control agents, progresses to needing exogenous

insulin (155). The investigators found that miR-148a, miR-21, miR-24, and miR-375 were elevated in the circulation of T1D individuals (153). Unfortunately, this study, like many before it, rely on investigating select candidates within small sample numbers (T1D; N=16) and so may possibly miss out on some of the key/important circulating miRNA biomarkers of diabetes progression.

A recent study conducted by Samandari and colleagues assessed circulating miRNAs within 123 individuals with newly-diagnosed T1D to identify whether they reflected measurements of β-cell function (151). Using a discovery approach, six miRNAs, miR-24-3p, miR-146a-5p, miR-194-5p, miR-197-3p, miR-301a-3p, and miR-375, at 3 months were found to correlate with residual β-cell function at 6-12 months. Interestingly, an increase in the circulatory abundance of these miRNAs corresponded to higher stimulated C-peptide and lower insulin dose adjusted HbA1c. In the validation cohort, only miR-197-3p abundance at 3 months significantly predicted stimulated C-peptide at 12 months. These findings indicate that circulating miRNAs could also assist in the prediction of clinical outcomes after diagnosis.

Table 1-B. Circulating miRNAs in T1D

Author (year)	miRNA/s	Observation	Reference
Sebastiani (2011)	miR-326	Increased in PBMCs from T1D patients	(152)
Nielsen (2012)	miR-152, -30a-5p, -181a, -24, -148a, -210, -27a, -29a, -26a, -27b, -25, -200a	Increased in T1D circulation	(148)
Salaz-perez (2013)	miR-21a, -93	Decreased in T1D PBMCs	(150)
Osipova (2014)	miR-21, -210	Increased in T1D plasma and urine	(149)
Yang (2015)	miR-146a	Decreased in T1D PBMCs	(154)
Seyhan (2016)	miR-148a, -21, -24, -375	Increased in T1D circulation	(153)
Samandari (2017)	miR-24-3p, -146a-5p, -194-5p, -197-3p, -301a-3p, -375	Correlated with β-cell function	(151)

The use of streptozotocin (STZ)-induced diabetic mice and non-obese diabetic (NOD) mice has enabled the identification of circulating miR-375 in these animals (156). One of the major advantages of these models is the high level of certainty that the majority of these animals will become diabetic and so the study was able to measure the circulating miR-375 level prior to the onset of the disease. It found that there was a marked increase in the levels of miR-375 in the plasma of mice treated with STZ, prior to the onset of hyperglycaemia. To strengthen the use of miR-375 as a biomarker within these diabetic models, this miRNA was also found to be increased in the plasma of NOD mice roughly two weeks prior to the onset of diabetes (156). The increase of this miRNA in these models was associated with islet cell death, as isolated islets cultured with cell death inhibitors demonstrated a reduction in extracellular miR-375 levels (156). The finding that acute β-cell death resulted in a detectable rise of miR-375 was supported by another recently published animal study; however, the authors noted that only a very small proportion of circulating miR-375 directly originated from β-cells (157). As they were using a model with β-cell specific miR-375 expression, they could not conclude where the rest of the circulating miR-375 originated. This finding supports the use of this miRNA for the detection of β-cell death but not β-cell function.

1.7. Circulating Cell-free DNA (cfDNA)

As seen with miRNAs, circulating cell free DNA (cfDNA) has been intensively investigated as a diagnostic and prognostic marker for various cancers (158-160). Again, this utilises a less invasive method of assessing an individual's health status using liquid biopsy (e.g. blood, plasma, urine) samples (160). Unlike miRNAs, however, cfDNA has a shorter half-life (minutes to hours) within the peripheral circulation and highly pone to degradation by just two or more freeze-thaw cycles. Previous studies have identified rapid clearance of non-host DNA, mainly by the liver (161; 162). Indeed, a study evaluating the presence of foetal DNA within the circulation of expectant mothers has concluded that this cfDNA has an average half-life of 16.3 mins after the delivery of the neonate (161). More recent investigations in both cancer and islet transplantation have identified a longer half-life of 114-117 mins (163; 164), however, the presence of continual DNA release inherent to these conditions would obfuscate the findings. In the progression to T1D it has been postulated that the β-cell mass of an individual undergoes periods of cell death and recuperation, yet the overall trend of β-cell death (Figure 1-1) means that cfDNA has great potential as a biomarker of T1D progression.

1.7.1. Methylated Insulin DNA

Insulin cfDNA is the current frontrunner as a DNA-based biomarker of β-cell death. As all cell types contain genomic insulin DNA, how does one identify DNA that originates from the pancreatic β-cells? Despite having an identical genome, each cell type within the body contains DNA with a unique methylation pattern that correlates with its specific gene expression profile. The insulin gene, including the promoter region, is typically unmethylated within the pancreatic β-cells and methylated in almost all other cell types, and so researchers have developed assays to attempt to quantify methylated and unmethylated insulin DNA.

DNA methylation is an epigenetic mechanism whereby DNA methyltransferases (DMNTs) place a methyl group onto a cytosine base, converting it to 5-methylcytosine. The cytosine is usually placed next to a guanine, causing two 5-methylcytosines to be created diagonally from each other. These areas within the genome are commonly referred to as CpG sites. DNA methylation is generally regarded as negatively regulating gene expression, although the role of this epigenetic mechanism has not been fully elucidated. There are currently two main methods by which DNA methylation results in transcriptional suppression. Firstly, the addition of the methyl groups is thought to physically block the binding of transcription factors to the promoter regions of the gene of interest. Additionally, studies have found associations between certain DNA methylation sites and histone modifications, however it is uncertain whether the histone modification is required for DNA methylation or vice versa.

The insulin gene, including the upstream promoter region, contains numerous methylation sites. Indeed, DNA methylation is a major factor in the regulation of insulin expression. Using a luciferase construct, Kuroda and colleagues found that methylation of the CpG sites within the insulin promotor resulted in a 90% reduction in expression (165). Intriguingly, subsequent studies have revealed that not all CpG sites show the expected methylation pattern within different tissues (unmethylated in β-cells, methylated in all other tissues). A recent study by Husseiny and colleagues concluded that intron 1, exon 2 and intron 2 do not show any tissue-specific methylation pattern (166). Furthermore, only five of the nine known methylation sites in the promoter region demonstrated consistent methylation within the other non-pancreatic tissues analysed (166). To identify the death of the pancreatic β- cells in the presence of normal cellular turnover, the CpG sites of interest must display a highly unique methylation pattern. Some CpG sites, including those both upstream (-234, -206, -69 and -19 bases) and downstream (+63) of the transcription start site (TSS), not only have significantly different

levels of methylation between different tissues, but also between pancreatic α- and β-cells (167). This gives weight to the preposition that differentially methylated insulin DNA has the potential as a highly specific marker of islet β-cell death.

Another consideration during such selection of the sites is the stability of the DNA methylation, especially during periods of cellular stress. Methylation analyses of islets from individuals with T2D, which are often undergoing extensive inflammatory stress, demonstrate that not all CpG sites are consistently methylated (167). CpG sites, including +63, -102 and -180 (relative to the TSS), are more likely to be methylated within T2D islets, while -19, -69, -135, and -206 show no difference in methylation (166). All of this previous data should be taken into account when selecting methylation sites for biomarker studies.

1.7.2. Methylated and Unmethylated Insulin cfDNA in T1D

Currently, there are three main groups, headed by Professors Mirmira (USA), Herold (USA), and Dor (Israel), investigating the use of methylated/unmethylated insulin cfDNA as a marker of β-cell death, each with their own approach.

Professor Mirmira's team have focused upon one particular CpG site located upstream of the TSS (-69), using both nested qPCR and digital droplet PCR approaches (168; 169). This particular site demonstrates consistent demethylation within the pancreatic β-cells, even while under cellular stress, and high levels of methylation in other tissues (166; 167). The most recent paper from this group evaluated serum samples from paediatric patients within 2-days from clinical diagnosis of T1D, and then 8-weeks and 1-year later (168). They identified that the levels of both methylated and unmethylated insulin DNA were increased in these individuals compared to non-diabetic control subjects, but that they decreased over time and returned to control levels by 1-year post-diagnosis (168). These findings support the notion

that the progression of T1D causes systemic stress on an individual, causing a release of methylated as well as unmethylated insulin DNA into peripheral circulation. Xeno-rejection of transplanted human islets resulted in a significant increase of unmethylated, but not methylated, insulin cfDNA, again suggesting that islets are not the source of the methylated copies (168). Furthermore, as the disease progresses post-diagnosis there is reduced β-cell mass to contribute to the circulating unmethylated insulin DNA levels.

Professor Herold's team has chosen to analyse two CpG sites located close to one another within the coding region (+396 and +399) of the insulin gene (170). They have also utilised a digital PCR approach to quantify the absolute copy numbers, however they have chosen to present their data as a ratio of unmethylated/methylated (UM/M) *Ins* DNA (163; 170). As the majority of investigations have focused upon the INS promoter region, there are little data on the specificity or stability of the two chosen methylation sites. A previous manuscript from this group identified that one of the CpG sites, +399, was unmethylated in β-cells and methylated in the majority of kidney cells (171), however the other site, +396, was not mentioned. A recent study from this group attempted to use their digital PCR assay to assess β-cell death within two longitudinal cohorts of at risk individuals from the TrialNet Pathway to Prevention study (163). A modest increase in the average UM/M *Ins* DNA ratio (P=0.048) was found in individuals that progressed to T1D, compared to healthy controls, however when all measurements were assessed independently this difference was abolished (163). Furthermore, this assay was not able to discriminate between high-risk individuals that progressed to T1D and those that did not. Individuals at high-risk of T1D (familial history and presence of islet autoantibodies) would benefit the most from an assay of β-cell death, as it would monitor progression toward T1D and allow early intervention if necessary. Therefore, a β-cell death assay must be sensitive enough to distinguish and stratify these individuals.

Professor Yuval Dor's group has taken a much different platform; they have used a combination of Illumina 450K methylation arrays and next generation sequencing to identify a cluster of six CpG sites within the INS gene promoter region (172). These sites are in close proximity to one another. These sites are not able to distinguish patients with T1D from healthy controls when analysed individually, but when assessed in combination they demonstrate a signal within the circulation of T1D patients that is absent in healthy controls (172). It is important to note, however, that bisulfite sequencing has previously identified differential methylation of CpG sites between β-cells and kidney that was later debunked by more extensive analysis (166). Additionally, bisulfite sequencing protocols are sample- and costs-prohibitive for many other research groups in utilising this approach on large biobank cohorts. The three main areas of DNA methylation can be seen in Figure 1.5. Table 1-B compares the two main technical approaches for quantitation of methylated and unmethylated insulin cfDNA.

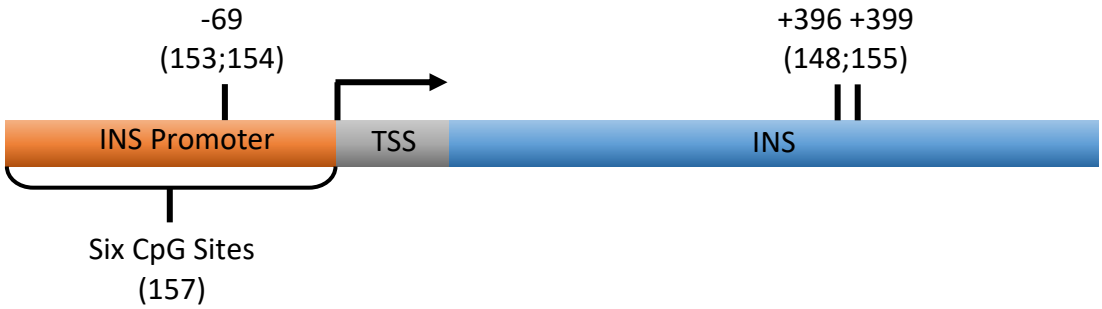

Figure 1-5. Methylation sites investigated as markers of β-cell death

Nine CpG sites have been identified within the insulin gene, including the upstream promoter region. They are potential markers of β-cell death due to their differential methylation pattern. Diagrammatical representation of the insulin coding region, not drawn to scale. INS = insulin, TSS = transcriptional start site.

Table 1-B. Approaches to Insulin cfDNA Quantitation

Group	*1*	*2*	*3*
Head of group	Mirmira (168)	Herold (163; 170)	Dor (172)
CpG site(s)	-69	+396, +399	Six undisclosed sites
Quantitation method	Digital droplet PCR (Bio-Rad)	Nested PCR/Digital droplet PCR (Bio-Rad)	Bisulfite sequencing (Illumina)
Volume of plasma required (mL)	0.03 – 0.05	0.2	0.2 – 1.0
DNA extraction method	QIAmp DNA Blood kit (Qiagen) with Poly(A) carrier (Sigma)	QIAmp DNA Blood kit (Qiagen)	QIAquick kit (Qiagen)
Number of rxns/run[†]	8 – 96	8 – 96	Up to 96, depending on use of barcodes
Time required for quantitation and analysis	+++	+++	+
Costs[‡]	+++	+++	++

[†]Based on the possible reactions that can be assessed on each platform in a single run on a single instrument. [‡]Based on inferred costs based on prices for studies in Sydney, Australia. Rating scale = + poor, ++ good, +++ excellent.

1.8. Preliminary Data

Prior to the commencement of this PhD project, the Hardikar laboratory invested significant effort in investigating the role of ncRNAs in the developing human pancreas and their potential application as T1D biomarkers. A summary of the findings of these experiments carried out by Dr. Mugdha Joglekar and A/Prof Anand Hardikar and their teams are detailed in the following sections, and form the basis on which this thesis is built.

1.8.1. Non-coding RNAs in the Developing Human Pancreas

In order to understand the microRNAs that are expressed during human pancreas development, the Hardikar lab obtained ethics and collected human fetal pancreatic samples from aborted human fetuses and assessed samples between 14-36 weeks of gestational age as well as adult pancreatic islets obtained from pancreatectomized samples using the SOLiD NGS platform. Following analysis and identification of miRNAs that increased in abundance during human pancreas development, the 300 most abundant microRNAs were then validated using TaqMan-based qPCR technology. Interestingly, a subset of these were found to increase in abundance during pancreatic development and remain highly expressed in adult islets (Figure 1-6a). To confirm that these ncRNAs are expressed within human islets *in situ*, these investigtors performed a combination of immunocytochemistry and fluorescent *in situ* hybridisation (FISH), or immune-FISH technique. This technique was used to confirm if the precursor microRNA molecule and/or the mature miRNA molecule were expressed within insulin-producing islet cells (Figure 1-6b). Interestingly, it was observed that some microRNAs, such as the pri-miR-375 was expressed in almost all of the human islet cells but the mature miR-375 appeared to be present only in a subset of these cells (Figure 1-6b) thereby demonstrating that yet unidentified microRNA processing mechanisms regulate the

expression of mature microRNA within islet cells. Some of these findings were assessed using a technique of single cell PCR wherein these investigators confirmed that mature miR-375 appears to be expressed in the non-β-islet cells than the β-cells within the pancreatic islets (96). These studies led to identification of candidate microRNAs that are i) found to increase in abundance in developing human pancreas; ii) found to be present in adult human pancreatic islet cells; and iii) had mature microRNA gene transcripts expressed in relevant pancreatic cells. Such candidate were selected for further evaluation/validation using *in vitro* and cross-sectional analyses discussed below.

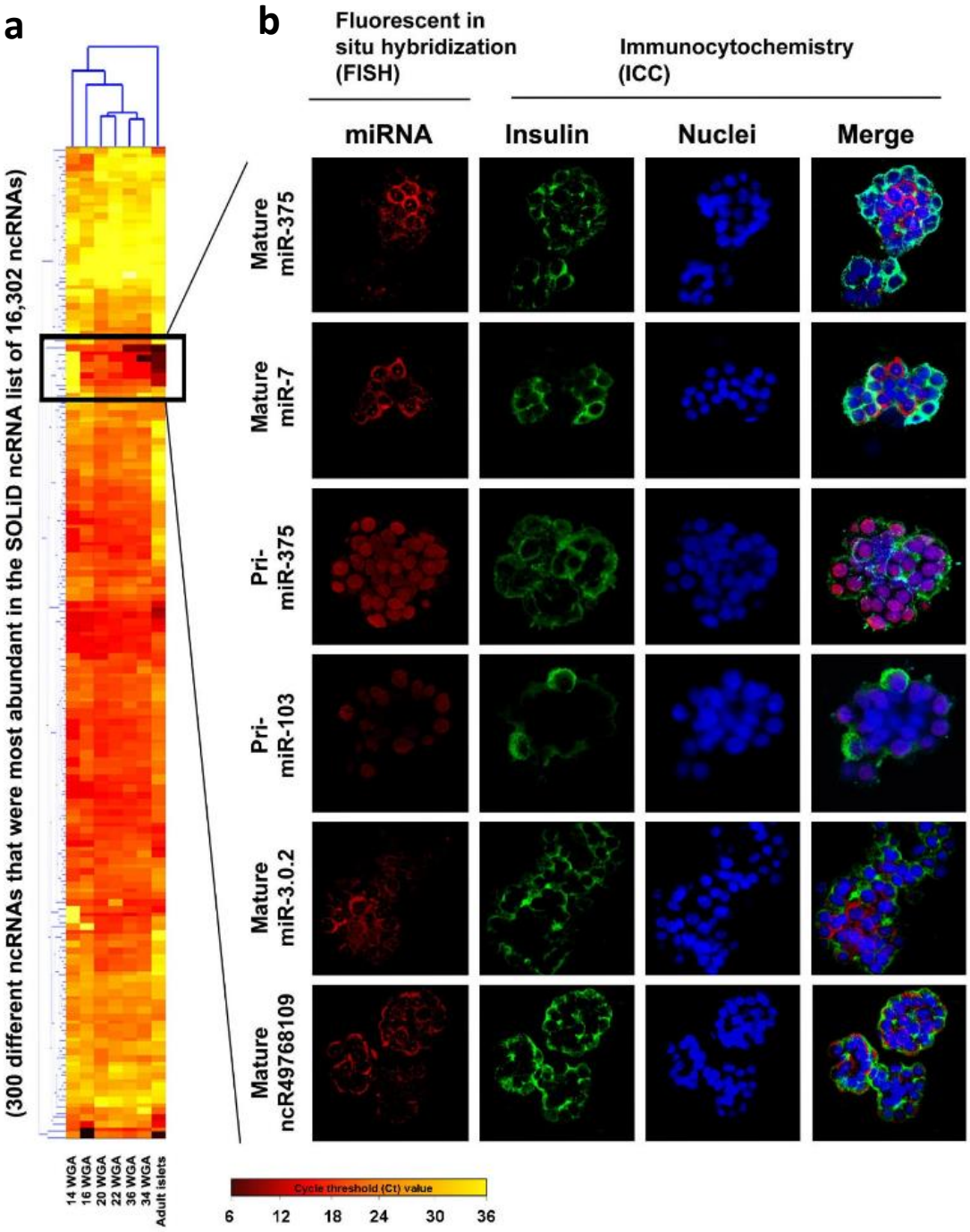

Figure 1-6. Non-coding RNA expression in the developing human pancreas

(a) Heat map of the 300 most abundant ncRNAs in the developing pancreas, identified by SOLiD NGS and validated by qPCR. (b) Confirmation of precursor and mature miRNA expression within adult islets using immuno-FISH. WGA = weeks of gestational age. Unpublished data from Hardikar Lab (credit: Joglekar MV *et al.*).

1.8.2. Circulating MicroRNA Signature in T1D

To assess whether the RAPID signature had potential as circulating biomarkers of T1D, our laboratory quantified their abundance within Non-Obese Diabetic (NOD) mice, as well as clinical samples from human subjects with and without T1D. The NOD mouse model has been extensively utilised as a model of T1D due to their genetic predisposition for autoimmune diabetes (173) (discussed in more detail in Chapter 3). The RAPID miRNAs were found to be elevated in the circulation of female NOD mice, both before and after the confirmation of diabetes, compared to mice that are not genetically pre-disposed (female non-diabetic C57BL/6 mice) to diabetes (Figure 1-7).

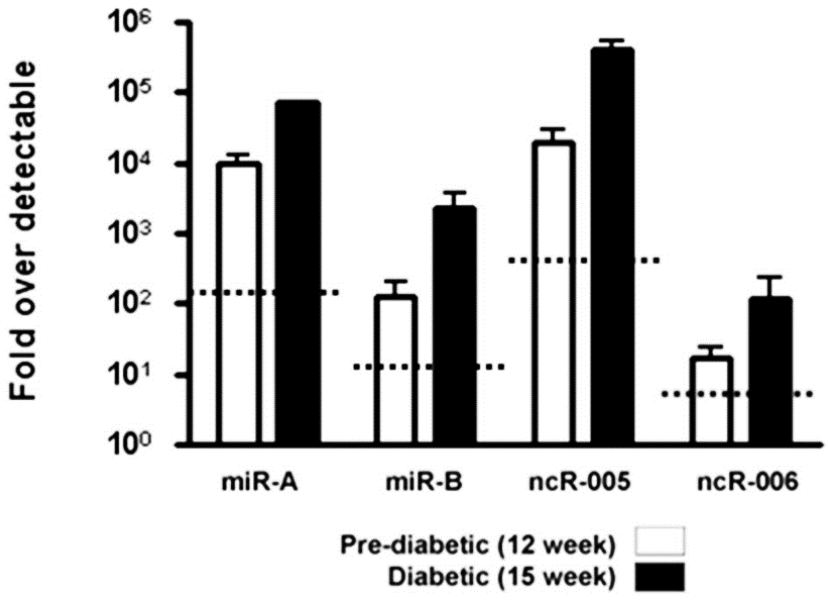

Figure 1-7. RAPID signature miRNAs in NOD mice

Four representative RAPID signature miRNAs were elevated in the circulation of female pre-diabetic and diabetic NOD mice, compared to female non-diabetic C57BL/6 mice (dotted line). Mean ± SEM. Unpublished data from Hardikar Lab (credit: Joglekar MV *et al*.).

The RAPID miRNAs were also found to be elevated in the circulating of human subjects with T1D (N=7), compared to age and gender matched controls (N=7) (Figure 1-8). Interestingly, these miRNAs were observed at high levels even up to 50 years post T1D diagnosis.

These data highlight the potential of miRNAs as circulating biomarkers of T1D. This thesis aims to extend existing findings to add to the RAPID signature miRNAs and validate a signature of candidate microRNAs as well as insulin cfDNA as biomarkers of β-cell death and the progression to T1D.

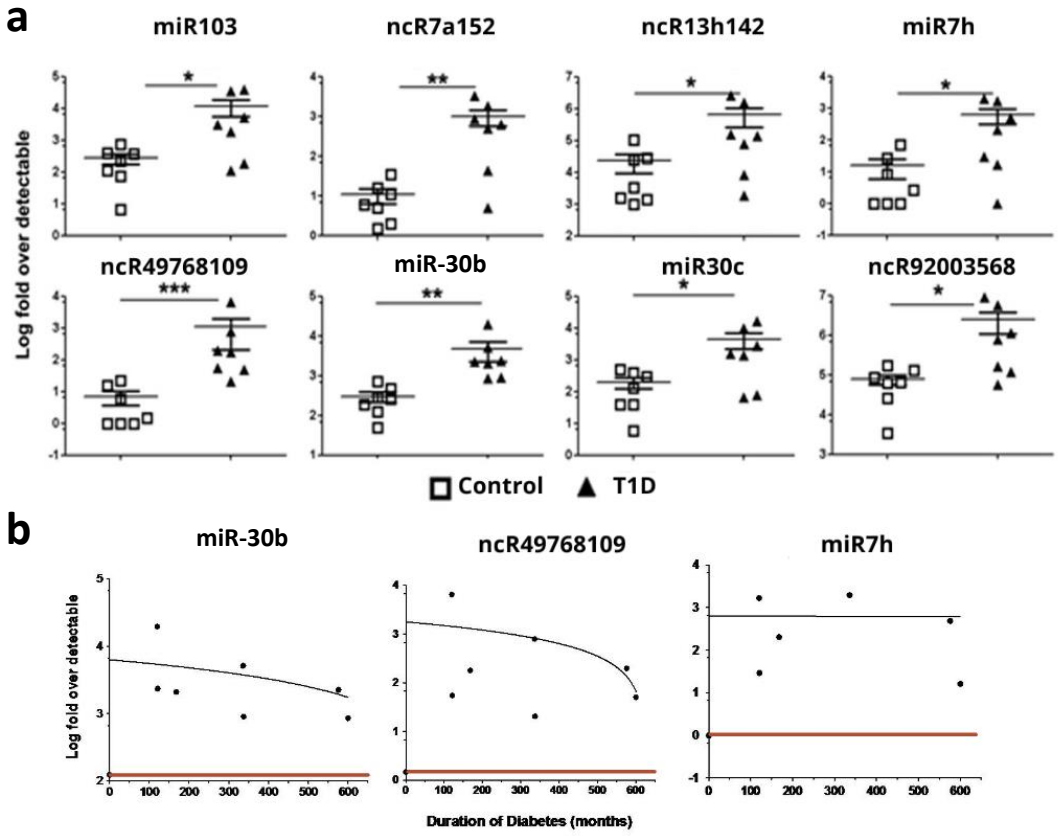

Figure 1-8. RAPID miRNAs in subjects with T1D

(a) RAPID miRNAs were elevated in the circulation of 7 subjects with T1D (filled triangles), compared to 7 age and gender matched controls (open squares). (b) RAPID miRNAs remain highly expressed within T1D circulation up to 50 years post-diagnosis, N=7. Black line = non-linear regression. Red line = abundance within control subjects. Mean ± SEM. * P<0.05, ** P<0.01, *** P<0.001. Unpublished data from Hardikar Lab (credit: Joglekar MV *et al*.).

1.9. Identification of a Candidate MicroRNA Signature

The miRNA signature investigated throughout this thesis was predominantly based upon the RAPID signature discussed in the previous section as well as Islet-specific microRNAs assessed through discovery analyses on over 500 different human tissues; including over 150 cadaveric human islets, (as part of the PhD thesis of Wilson Wong - Hardikar lab; supervisors: A/Prof. Anand Hardikar and Dr. Mugdha Joglekar). To ensure the inclusion of other microRNAs that are possibly reseased from non-pancreatic tissues, circulating miRNAs were also profiled in individuals with T1D and their age and gender matched controls (outlined in Chapter 4). Additionally, miRNAs previously identified within the literature as differentially abundant in T1D and its complications were also included. This forms the PREDICT T1D study signature, which is validated through this thesis and continues to be confirmed in other individuals progressing to T1D in the Hardikar lab.

This resulted in the generation of a signature of 50 candidate miRNAs, collectively known as the PREDICT T1D (Plasma RNA Evaluation and Diagnosis In Children progressing To Type 1 Diabetes) Signature (Figure 1-9). Intriguingly, less than half of these 50 miRNAs have been previously identified in the development and function of the pancreas (Table 1-C), although further research may change this figure. This correlates with the hypothesis that cellular stress outside of the pancreas can contribute to the circulating miRNA signature.

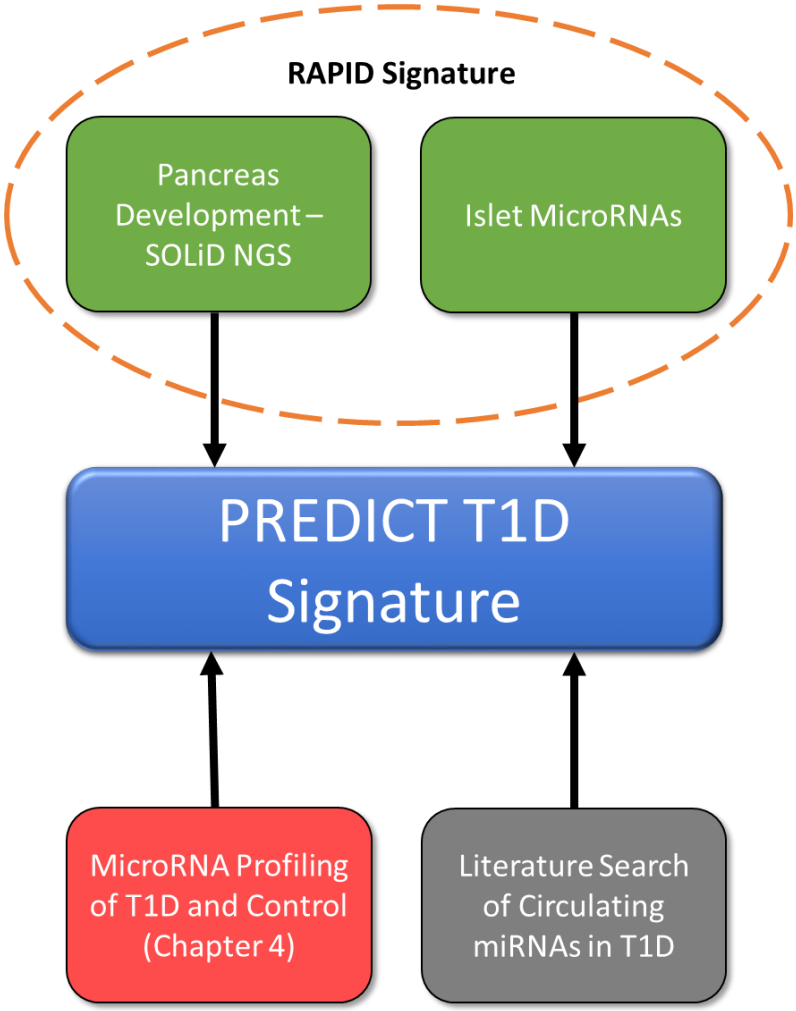

Figure 1-9. Identification of the MicroRNA Signature Assessed Within this Thesis

The miRNA signature investigated within this thesis was built upon the RAPID Signature, however additional miRNA candidates were identified through miRNA profiling of clinical samples and extensive literature searches of circulating miRNAs in T1D. The resulting signature of 50 miRNAs is known as the PREDICT T1D Signature. The RAPID Study from the Hardikar lab represents "**R**NA-based **A**nalysis and **P**rediction of **I**slet **D**eath", while the PREDICT T1D study is the JDRF Australia-funded T1D CRN fellowship to A/Prof Hardikar and represents "**P**lasma **R**NA **E**valuation for **D**iagnosis of β-cell death and vascular health **I**n **C**hildren and adults progressing **T**o **T**ype **1** **D**iabetes".

Additionally, only 20 of these miRNAs have been previously reported in T1D circulation, indicating that the preliminary signature discussed here may provide up to 30 novel biomarkers.

Table 1-C Candidate miRNAs

MicroRNA	Islet Development, Function, or T1D Dysfunction	T1D Circulation
let-7e	(174)	-
miR-103	-	-
miR-125a-5p	-	-
miR-125b	(175)	
miR-126	(176)[a]	(153)
miR-127	(177)	-
miR-145	(178)	-
miR-146a	(116)[b]	(154)[c]
miR-148a	(179)	(148; 153)
miR-152	-	(148)
miR-155	-	-
miR-15b	(180)	-
miR-16	(180)	-
miR-181a	-	(148)
miR-186	(181)[b]	-
miR-188	-	-
miR-199a-3p	-	-
miR-200a	(182)[b]	(148)
miR-20a	-	-
miR-21	-	(153)
miR-210	-	(148)
miR-22-5p	-	-
miR-220c	-	-
miR-222	-	(183)[d]
miR-223	-	-
miR-24	(179)	(148; 153)
miR-25	-	(148)

MicroRNA	Islet Development, Function, or T1D Dysfunction	T1D Circulation
miR-26a	(179)	(148)
miR-26b	-	-
miR-27a	-	(148)
miR-27b	(176)[a] (184)	(148)
miR-29a	(185)[d]	(148)
miR-301b	-	-
miR-30a-5p	(186)	(148)
miR-30b	(186)	-
miR-30c	(186)	-
miR-30e-3p	(186)	-
miR-326	-	(152)
miR-340-3p	-	-
miR-34a	(116)[b]	(153)
miR-374	-	-
miR-375	(96; 101; 102; 115)	(153; 187)
miR-409-5p	-	-
miR-558	-	-
miR-625	-	-
miR-7	(83; 84; 96; 100)	-
miR-9	(96)	-
miR-92a	-	-
miR-93	-	(150)
miR-99b	-	-

[a] Detected in islet extracellular vesicles.
[b] Detected in insulin producing cells differentiated from hSCs.
[c] Detected in PBMCs.
[d] Rodent model.

1.10. Objectives and Significance

This thesis intends to build upon the existing data on miRNA and cfDNA release during T1D progression. The studies discussed in the previous sections highlight the potential of both circulating miRNAs and insulin DNA as biomarkers of β-cell death. These studies, however, have yet to characterise and validate a clinically relevant molecular signature of β-cell death. A signature comprised of both circulating miRNAs and insulin cfDNA would provide clinicians with a minimally-invasive (blood) test to help identify, monitor and therapeutically manage those individuals undergoing immune-mediated β-cell destruction. The development of a biomarker signature to quantify islet cell loss would help in identifying children or adults at risk of developing T1D and allow preventative treatments, such as incretin drugs, anti-inflammatory drugs, vaccinations and diets, to prevent islet loss and induce regeneration. This project has tremendous implications in diabetes research as early diagnosis can potentially delay the clinical onset of this disease, thereby delaying the onset of diabetic complications and enabling the retention of some endogenous insulin production, which is associated with better glycaemic control and lower risk of chronic complications (6). Severe hypoglycaemia (that requiring assistance from another person for recovery, such as by glucagon or glucose injection) and the end organ complications significantly impact upon an individual's quality and duration of life and result in an increasingly large burden on the health care system.

Furthermore, a molecular signature of β-cell death would allow clinicians to assess the insulin needs of individuals with LADA and with T2D, as well as the rejection of islet transplants. Basic researchers could also utilise such a signature to monitor the efficacy of novel drugs in preventing β-cell toxicityto therapeutic agents.

The hypothesis is that the cellular stress and mortality that occurs during the asymptomatic progression to clinical T1D results in the release of miRNAs (from both β-cells and non-β-cells) and insulin cfDNA (both methylated and unmethylated). Section 1.11 provides a graphical overview of this process and the approaches taken to quantify these circulating molecules.

To test this hypothesis, several objectives must be met:

1. Identify the most appropriate technology for the quantitation of a miRNA biomarker signature (chapter 2)

1) Examine the release of miRNAs and INS cfDNA in *in vitro* and *in vivo* disease models (chapter 3)
2) Profile circulating miRNAs in individuals with established or newly-diagnosed T1D compared to age and gender matched controls (chapter 4)
3) Investigate the PREDICT T1D miRNA signature in the circulation of individuals with established T1D compared to age and gender matched non-diabetic controls (chapter 4)
4) Examine the molecular (miRNA and cfDNA) signature within individuals at high risk of developing T1D, individuals at the point of T1D diagnosis, and individuals post-diagnosis (chapter 5)

1.11. Graphical Overview

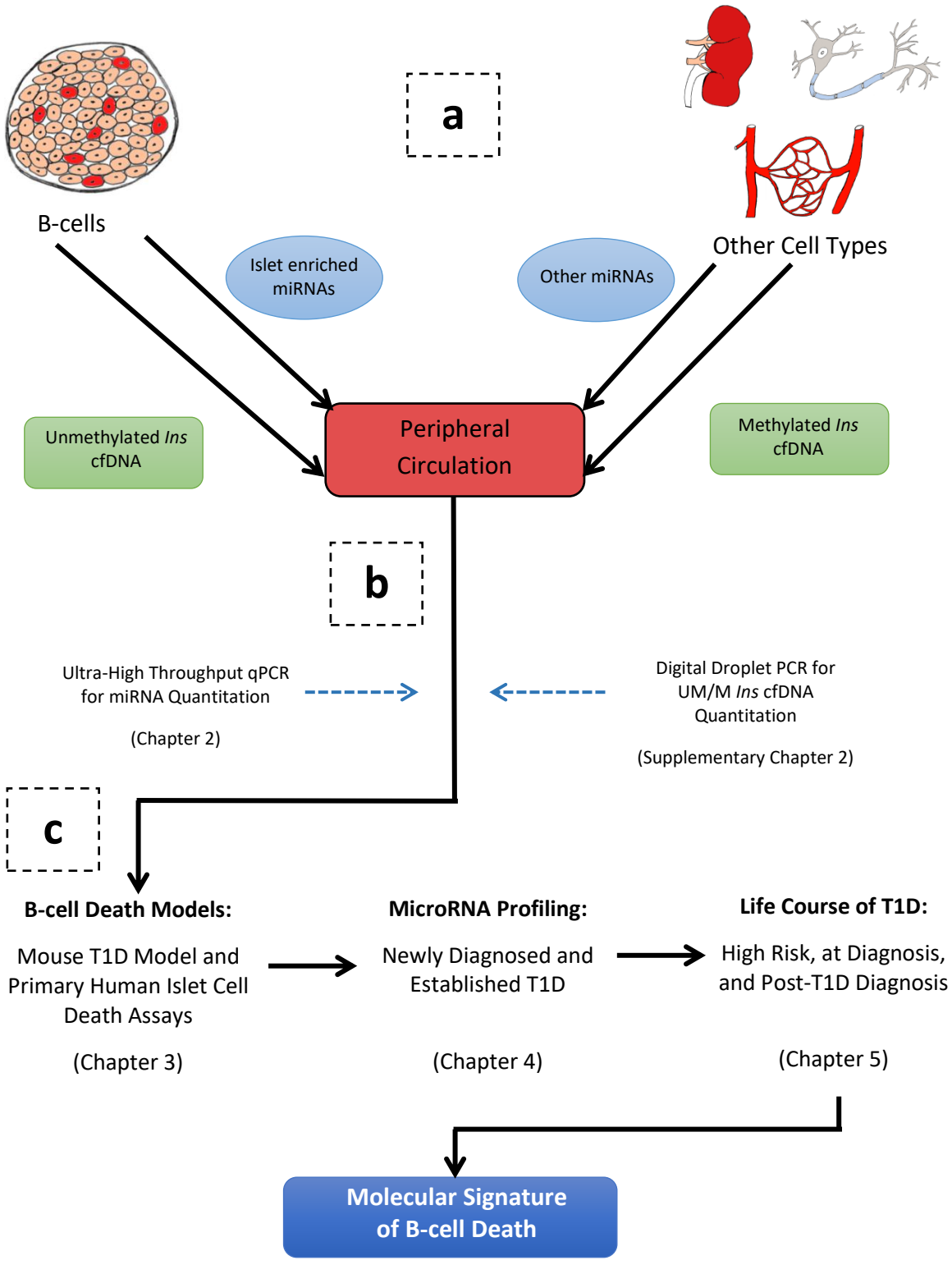

Figure 1-10. Graphical overview

Simplified diagrammatical overview of this thesis. (a) This thesis hypothesises that islet enriched miRNAs and unmethylated insulin (INS) gene cfDNA are released into the circulation during βcell death, while other miRNAs and methylated *Ins* cfDNA could be released from other cell types undergoing cellular stress during the progression to T1D. (b) Two of the molecular techniques utilised in this manuscript are shown with blue dotted arrows. (c) Breakdown of the sample groups used to identify and validate this molecular signature of β-cell death.

2. Assessing High-throughput qPCR Technologies for MicroRNA Signature Detection

2.1. Published Manuscript

Farr R.J., Januszewski A.J., Joglekar, M.V., Liang H., McAulley A.K., Hewitt A.W., Thomas H.E., Loudovaris T., Kay T.W., Jenkins A., and Hardikar, A.A., A comparative analysis of high-throughput platforms for validation of a circulating microRNA signature in diabetic retinopathy. **Scientific Reports**, 2015. 5: p. 10375.

2.2. Chapter Overview

MicroRNAs are now increasingly recognised as biomarkers of disease progression. Several quantitative real-time PCR (qPCR) platforms have been developed to determine the relative levels of microRNAs in biological fluids. We systematically compared the detection of cellular and circulating microRNA using (a) a standard 96-well platform, (b) a high-content microfluidics platform and (c and d) two ultra-high content platforms. We used extensive technical and analytical tools to compute inter- and intra-run variability and concordance measured using fidelity scoring, coefficient of variation and cluster analyses. We also carried out unprejudiced next generation sequencing to identify a microRNA signature for Diabetic Retinopathy (DR), defined as late stage sight threatening DR requiring retinal laser treatment, and systematically assessed the validation of this signature on clinical samples using each of the above four qPCR platforms. The results indicate that sensitivity to measure low copy number microRNAs is inversely related to qPCR reaction volume and that the choice of platform for microRNA biomarker validation should be made based on the abundance of miRNAs of interest.

2.3. Chapter Aims

The studies in this chapter aimed to:

1. assess the reproducibility of micro- and nanofluidic high-throughput qPCR platforms in quantitating cellular and circulating microRNAs;
2. compare the data generated from these platforms with the gold standard 96-well low-throughput qPCR platform, and;
3. validate a representative microRNA signature of diabetic retinopathy (DR), identified through unbiased next generation sequencing analyses, for recognition of the most reliable platform for microRNA profiling.

2.4. Methods

2.4.1. Samples

The study was approved by the University of Sydney Ethics Committee and all samples were collected following written informed consent Total RNA was isolated from human islets (Australian Islet Transplant Consortium) and from serum samples, collected from individuals with or without diabetes. Cellular RNA was isolated as outlined in Appendix A, while serum RNA was isolated as per the protocol in Appendix B. The study was carried out in accordance with the approved guidelines. Samples were tested for a total of 48 miRNAs, selected based upon their expression in small RNA sequencing, their relevance to islet biology or diabetes, or their suitability as housekeeping transcripts. However, six of these 48 miRNAs were identified to be incompatible on the Fluidigm system (see discussion) and therefore all of the analysis for the two platforms is based on comparison of the expression of these 42 miRNAs on all the platforms tested. The 42 miRNAs include the three most commonly used "housekeeping" miRNAs (U6, RNU44 and RNU48). Each PCR reaction was undertaken at least in duplicate. Technical replicates were also included within the same run as well as in different runs, and repeated by upto three users (Ryan J Farr, Mugdha V. Joglekar and Anandwardhan A. Hardikar). No statistically significant variation was seen in data obtained by the three users.

2.4.2. ViiA7

To aid comparison with the pre-amplified samples run on the high-throughput technologies, samples were pre-amplified and run in the 96-well format using 5 µl reaction volumes. Reverse transcription (RT) and pre-amplification (PA) was completed using the Megaplex RT/PA Primer Pools (Life Technologies) using the manufacturer's protocol, with minor changes. Briefly, each sample had an RNA input of 100 ng (measured by Nanodrop), went through 12 cycles of PA

and was diluted 1:40 in nuclease-free water. qPCR was undertaken in 0.1 ml optically clear 96-well plates using TaqMan MicroRNA Primer/Probe mixes and TaqMan Fast Universal PCR Master Mix (2X), No AmpErase UNG (Life Technologies) as described elsewhere (188).

2.4.3. TaqMan Low Density Arrays (TLDA)

RT and pre-amp were undertaken with Megaplex RT/PA Primer Pools using the manufacturer's protocol. Each sample had 80-100 ng RNA input (as measured by Nanodrop), 12 cycles of pre-amplification and was diluted 1:4 with 0.1 x TE pH 8.0. qPCR was completed using TaqMan® Low Density Array human microRNA Panel as previously published (188).

2.4.4. OpenArray (OA)

RT and PA were undertaken with Megaplex RT/PA Primer Pools using the manufacturer's OpenArray microRNA Panel protocol as described elsewhere (188). Briefly, each sample (100 ng input), underwent 12 PA cycles, then was diluted 1:40 in 0.1X TE (pH 8.0), combined with TaqMan OpenArray PCR Master Mix and loaded onto TaqMan OpenArray Human MicroRNA Panel (AccuFill™ system). qPCR was completed using the QuantStudio 12K Flex (Life Technologies).

2.4.5. Dynamic Array (DA)

RT and PA were undertaken with Megaplex RT/PA Primer Pools using the protocol supplied by Fluidigm Corporation. Each sample (input 100 ng), underwent 16 PA cycles (recommended by the manufacturer), then was diluted 1:10 in nuclease-free water, combined with TaqMan MicroRNA Primer/Probe mixes and TaqMan Fast Universal PCR Master Mix (2X), No AmpErase UNG, and loaded onto a 48 × 48 Dynamic Array IFC (Integrated Fluidic Circuit) using the IFC Controller MX. qPCR was performed on the BioMark system (Fluidigm Corporation).

2.4.6. Next Generation Sequencing

RNA was isolated from plasma samples using protocol described earlier (189). SmallRNA libraries generated using the Ion Total RNA-Seq Kit v2 were processed through emulsion PCR using OneTouch 2 (Life Technologies) and the Ion PGM™ Template OT2-200 Kit, then enriched using the OneTouch ES (all Life Technologies). One sample was loaded per Ion-318™ chip and sequenced on Ion PGM using the Ion PGM™ Sequencing 200 Kit v2 (all Life Technologies). The aligned BAM files were analysed using Strand NGS (Strand Life Sciences) and differential miRNA expression was determined by a two-fold change in normalised read number.

2.4.7. Statistical Analysis

The data were analysed using Statistica for Windows analytical software (ver. 12.0, StatSoft, Tulsa, OK). For intra-platform reproducibility analysis, the coefficient of variation (CV%) was calculated between replicate measurements. Data were obtained from the multiple measurements (lowest number of replicates = 2, highest = 8) of 40 transcripts in four samples. miR-140 and miR-320 were excluded due to the lack of results on TLDA and DA platforms respectively.

CT/CRT values could not be compared directly so they were transformed into Z-scores within each platform. Pearson correlation and linear fits were calculated. Level of compression or expansion of data measured on the different platforms were evaluated by comparing the slope of the best fitted line of a least square linear regression of the Z-scores between pairs to the “ideal” slope of 1. Ward’s linkage method and Euclidean distances were used for cluster analysis. Separate dendrograms were generated for each analytical platform. Number of clusters was based on Mojena rule for distances between the dendrogram knots. In each analytical method four clusters were observed. The miRNAs of each cluster were then

calculated using k-means method. MicroRNAs with >15% missing data (across all platforms) were excluded from the calculations; otherwise missing data were replaced by mean. Clusters concordance was estimated by comparing the clusters generated by other platforms with the ViiA7 (“gold standard”). The assignment was declared in concordance if at least two miRNAs were placed in the same cluster by different methods.

2.5. Results

2.5.1. Platform Overview

An overview of the different platforms (Figure 2-1) compared within this chapter can be found in Table 2-A. The ease of workflow and cost analysis was computed considering a study size of > 100 samples and 48 miRNAs to be screened. The ease of the workflow is also a reflection of the time and experience needed to create the cDNA, pre-amplify it and load it onto the respective platform. All software was supplied by the manufacturer and utilised with default recommended parameters.

The raw cycle threshold (CT/CRT) values generated on each platform are plotted in Figure 2-1b. A distinct decrease in CT values is seen in the Dynamic Array, most likely due to the increase in the number of pre-amplification cycles and lower dilution factor (1:10 versus 1:40 for the OpenArray), as recommended for the DA platform. The median CT/CRT value for the entire miRNA dataset analysed is 18.09 for the ViiA7, 15.79 for OA and 12.76 for DA.

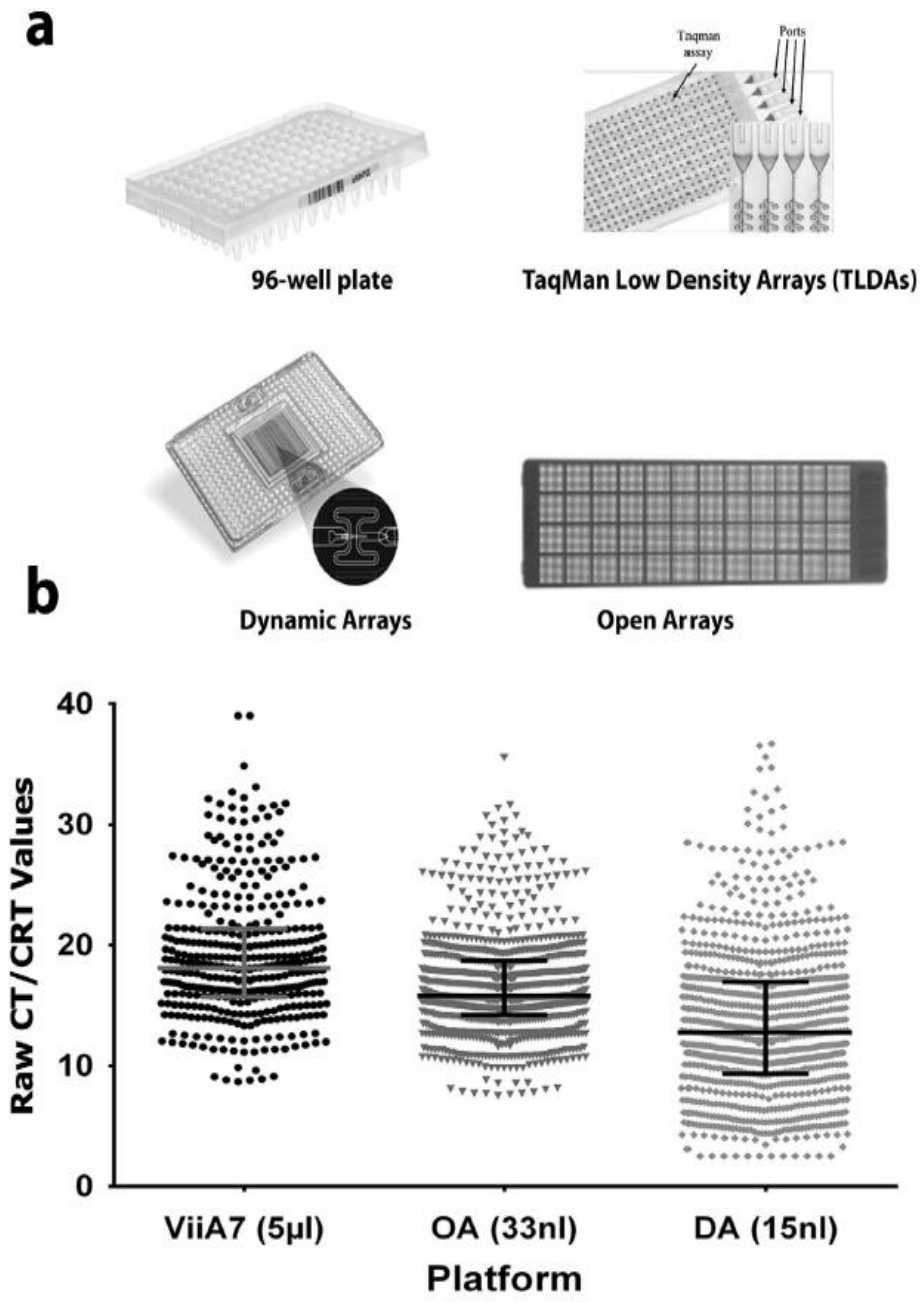

Figure 2-1. qPCR platform overview

(a) Representative pictures of the four platforms. (b) CT/CRT values from all samples.

Table 2-A. Comparison of qPCR platforms

Platform	96-rxns/run (ViiA7)	384 rxns/run (TLDA)	12,228 rxns/run (OpenArray)	2304 rxns/run (Dynamic Array)
RNA Input (ng)	100	100	100	100
RT cycles	40	40	40	40
Pre-amplification (Pre-amp)	Yes	Yes	Yes	Yes
Pre-amp cycles	12	12	12	16
Pre-amp dilution	1:40	1:4	1:40	1:10
PCR volume/rxn	5 µl	1 µl	33 nl	15 nl
Primer/probe°	Individual	Pre-printed	Pre-printed	Pre-printed
Number of rxns/run†	1–96	384	3,072–12,228	2,304–9,216
Ease of workflow	++	+++	+++	++
Costs‡	+	++	+++	++
Ease of analysis§	+++	+++	+++	++

°The use of individually available TaqMan primer/probe assays or pre-printed TaqMan primer/probe assays. Note: we recommend using the individual TaqMan assays for the panel of microRNAs proposed as there may be compatibility issues between off-the-shelf Megaplex primer pools and the individual microRNA TaqMan assay. †Based on the possible reactions that can be assessed on each platform in a single run on a single instrument. ‡Based on actual total costs involved in Sydney, Australia. §Based on our analysis of software capabilities, robustness and ease of use of the software supplied by the manufacturer and ranked by three independent users. Rating scale = + poor, ++ good, +++ excellent.

2.5.2. Platform Variability

To assess the variability of each platform, the co-efficient of variation (CV) was calculated for each microRNA assay (Figure 2-2). The median CV of the replicates was lowest in the 5 µl 96-well platform (0.6%), ranging from 0.1 to 1.9%, then OA at 2.1% (range 0.7–4.6%), TLDA at 8.3% (range 0.3–19.1%) and DA at 9.5% (range 2.2–27.6%).

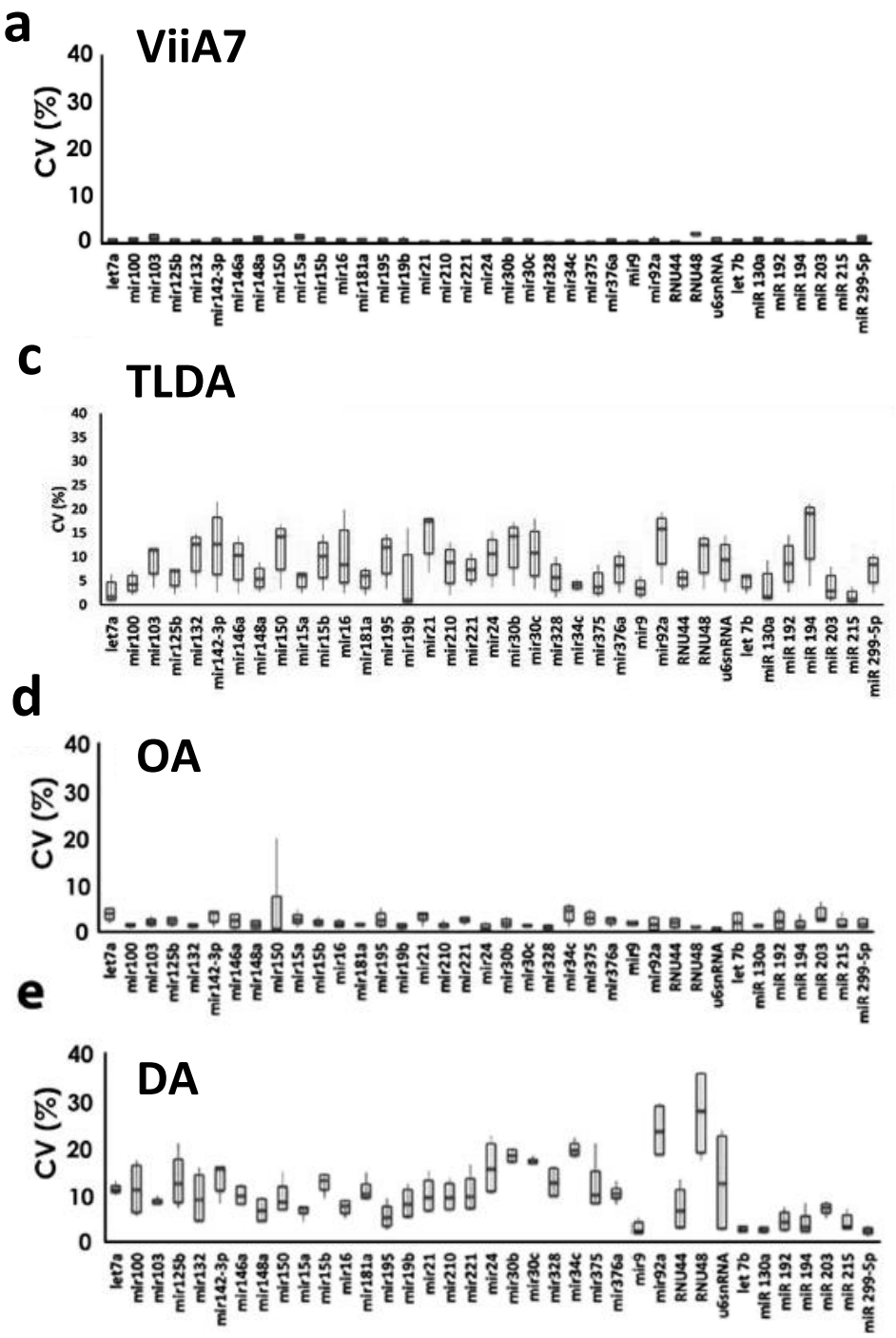

Figure 2-2. Platform co-efficient of variation analysis

Lines indicate median and IQR. Boxplots (median, 10–90th percentile) of the CV distribution for (a) ViiA7, (b) TLDA, (c) OA and (d) DA.

As an indicator of overall reproducibility, the fidelity of each platform was assessed. Fidelity was calculated as the percentage of replicates that differed by less than 1, 2 or 3 CT values and is presented as deviation from fidelity in Figure 2-3a-c and Figure 2-4. The standard 96-well format attained 99.23% fidelity for both 1 and 2 CT values, and 100% fidelity for the 3 CT cut-off. Both OpenArray and Dynamic Array platforms performed capably; 88.1% (OA) and 77.78% (DA) of replicates differed by less than 1 CT, 96.29% (OA) and 91.27% (DA) less than 2 CTs, and 98.41% (OA) and 94.44% (DA) less than 3 CTs. Neither of the high-throughput technologies were able to attain 100% fidelity using these CT cut-off points. This variation of the CT values would effectively translate to ~8-fold difference in transcript abundance. It is worth noting that even if an 8-fold variation between replicates is considered acceptable, 1.59% (OA) and 5.56% (DA) of replicates may still show greater than 8-fold variability. The TLDA platform was able to attain 92.68% fidelity using the 1CT cut-off, and 100% using a 2 or 3 CT cut-off. However, due to a limited number of replicates run on this platform, it is not appropriate to compare this data to the other technologies, and so it is plotted on its own (Figure 2-4). CT values were then segregated into expression levels and the replicate variation plotted (Figure 2-3d-g, 2-4). Ultra-high expression was considered to be CT values less than 10, high expression defined to be a CT value between 10.01 and 20.00, moderate expression between 20.01 and 30.00, and low expression above 30.01. Replicate variability increased across all platforms as the transcript abundance decreased. This was especially apparent in the high-throughput platforms, where replicate variability increased substantially when the transcript was present at moderate or low expression (Figure 2-3d–g). The 96-well plate platform (ViiA7) maintained a CT variation of less than 1 cycle until the target transcript was expressed at low levels (> 30.01 CT; Figure 2-3g).

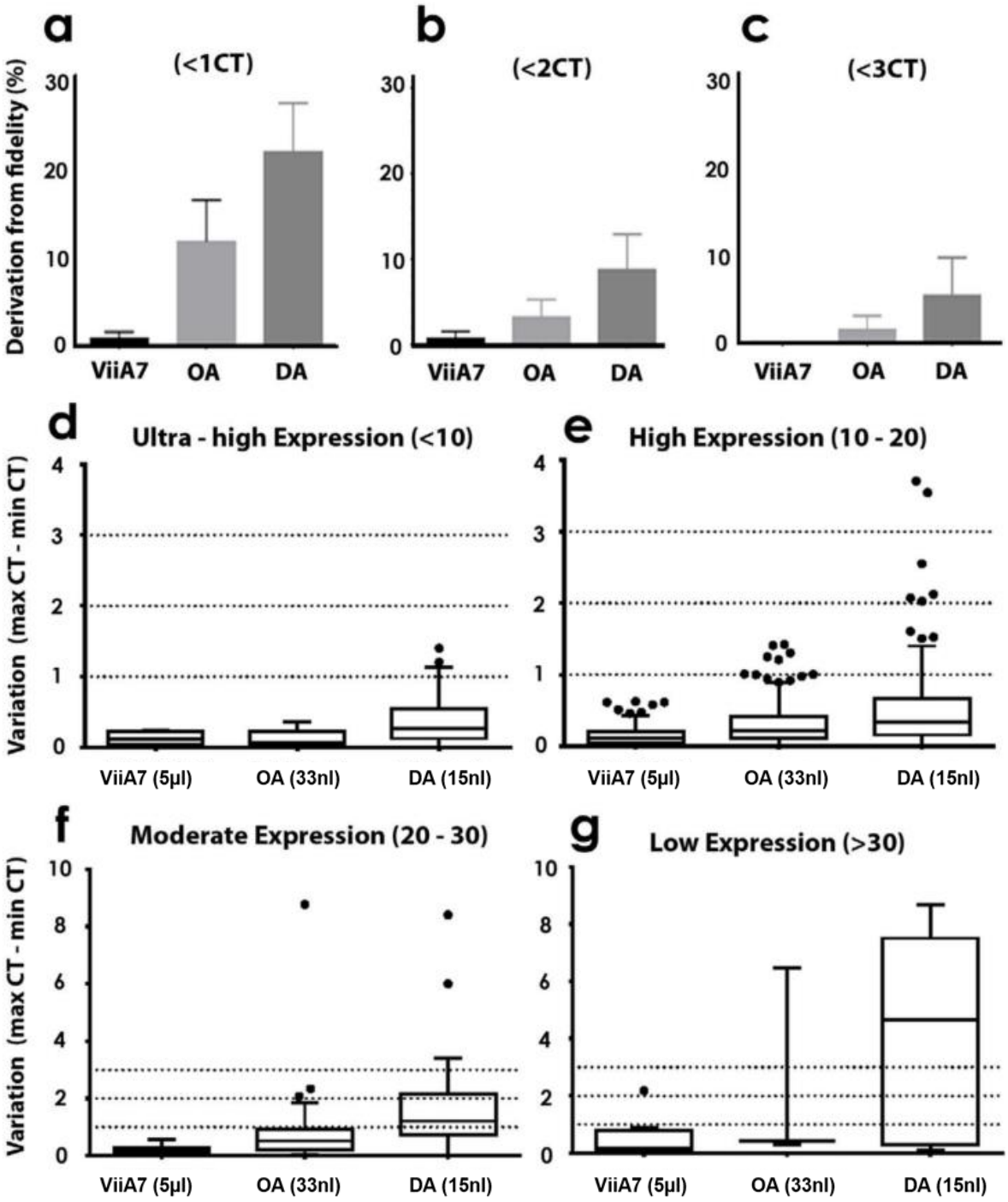

Figure 2-3. Platform variability

(a–c) Fidelity scoring using (a) 1 CT/CRT, (b) 2 CT/CRT or (c) 3 CT/CRT cut-off. Data is presented as deviation from fidelity (100%) and plotted as mean + SEM. (d–g) Tukey boxplots (median + IQR) of variation between replicates (maximum CT/CRT—the minimum CT/CRT) for the f our expression levels, (d) ultra-high (CT/CRT < 10), (e) high (CT/CRT 10-20), (f) moderate (CT/CRT 20-30) and (g) low (CT/CRT > 30). Dotted line is 1, 2 or 3 CT/CRT cut-off used in fidelity scoring.

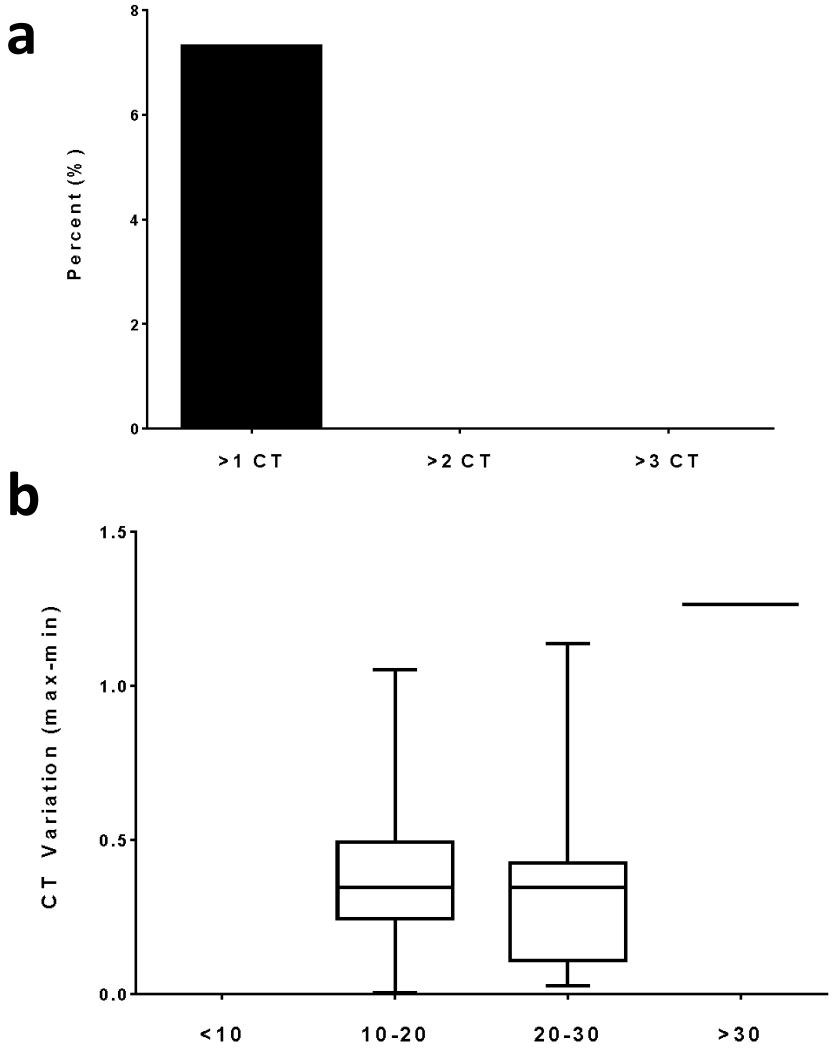

Figure 2-4. TLDA variability

(a) Fidelity scoring using 1 CT/CRT, 2 CT/CRT or 3 CT/CRT cut-off. Data is presented as deviation from fidelity (100%) and plotted as mean + SEM. (b) Spread of variation between replicates (measured as the maximum CT – the minimum CT) for the four expression levels, ultra-high (CT<10), high (CT 10-20), moderate (CT 20-30) and low (CT>30).

The ViiA7 platform thus truly represents the “gold standard” amongst these qPCR platforms as any variation seen for such low level transcripts is potentially due to the Poisson distribution (190). When dealing with low copy transcripts, the Poisson distribution predicts that in a large number of replicates containing an average of one copy of starting template per reaction (rxn), approximately 37% rxns should actually have no copies, only 37% rxns should contain one copy, and 18% rxns should contain two copies (190). Therefore, reliable detection of single copy transcripts in any sample calls for a large number of replicates to assess statistical significance and overcome the limitations of Poisson distribution.

2.5.3. Reproducibility

To determine how reproducible the high-throughput technologies are, RNA extracted from human islet cells and serum was run twice on each of the high-throughput platforms by two different users. The average difference between the two sets of replicates is plotted in Figure 2-5e,f. The OpenArray system produced reproducible results, with the greatest variation being 2.06 cycles, whilst the Dynamic Array system demonstrated larger variation (up to 8.17 cycles). Interestingly, the second repeat on the Dynamic Array system produced consistently lower CT values. This may reflect an increased susceptibility of this platform to user variation. Calibrations performed between the two runs may also have impacted on the results.

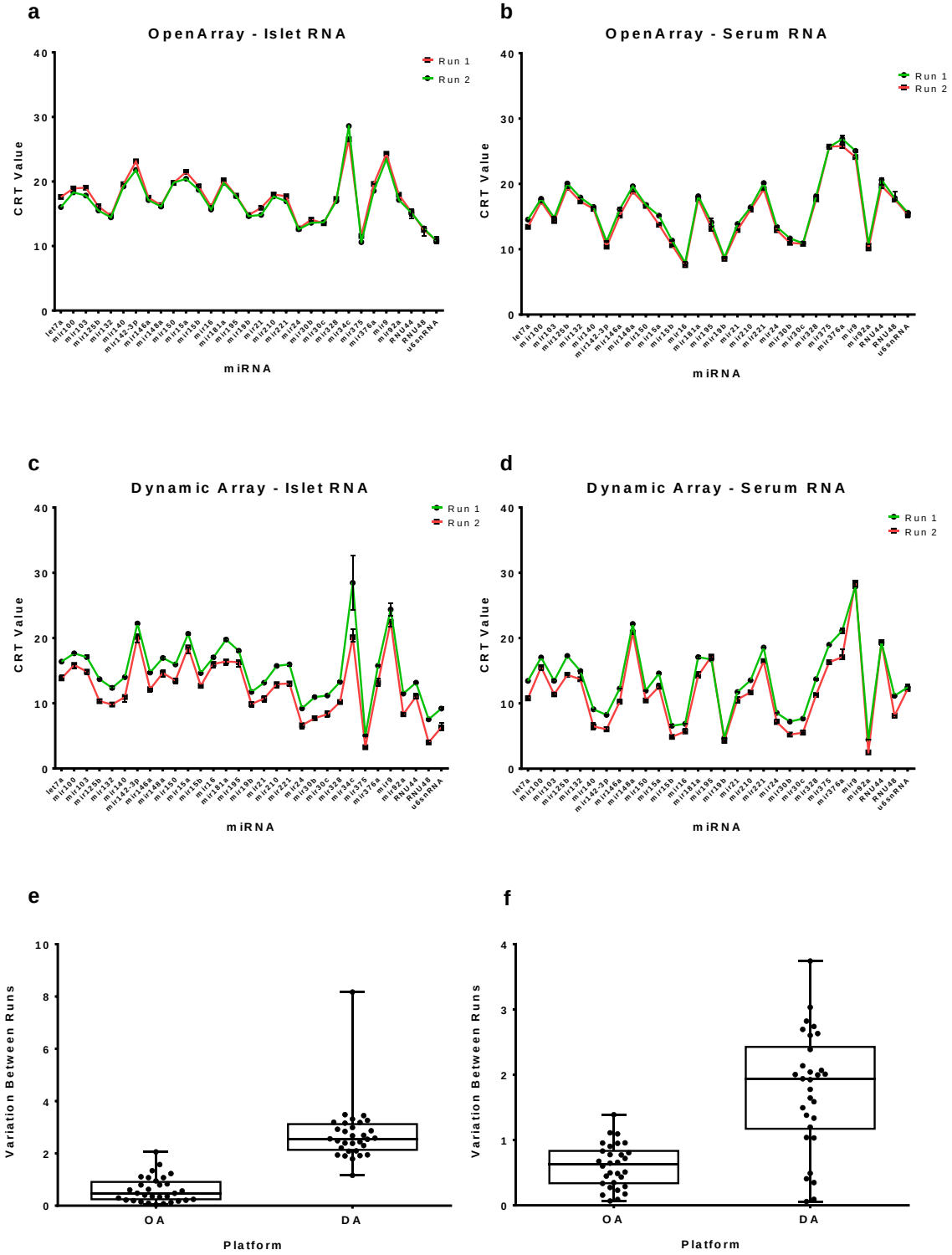

Figure 2-5. High-throughput platform reproducibility

(a-d) RNA from islet cells and human serum was run twice on the (a,c) OA and (b,d) DA (same batch/lot). Data are median ± range. The average difference (boxplots, median and 25th – 75th percentile, whiskers min/max) between runs for each miRNA tested for cellular miRNAs is plotted in (e) and for serum miRNAs in (f).

2.5.4. MicroRNA Signature Detection

One of the ultimate goals of most miRNA expression studies is to determine a biomarker signature related to particular pathology. To assess a biomarker signature for diabetic retinopathy (DR), we used unbiased small RNA sequencing of plasma samples from diabetic individuals with or without retinopathy. While analysing samples from subjects with (DR) and without (No DR; NDR) diabetic retinopathy (Figure 2.6a–d) we selected five miRNAs based on consistent differences between DR and NDR subjects and assessed the detection of such a "fingerprint" (Figure 2.6e) using the four different qPCR platforms. Furthermore, these five miRNAs were detected on all platforms tested. Although other miRNAs displayed a greater differential expression, they were unable to be detected using all of the platforms tested, usually due to the absence of the respective assays. We carried out rigorous analyses (Figure 2.7) to compare differences in expression of this microRNA signature amongst DR and NDR subjects. Interestingly, these analyses demonstrate that the features of miRNA expression (denoted by shaded areas in Figure 2.7) retain their profile across three qPCR platforms - ViiA7 (96-well), TLDA and OA platforms - whilst these same features appear skewed for the DA platform. As expected, the area and feature properties are different for the sequencing platform and vary between the DR and NDR groups amongst the sequencing profile.

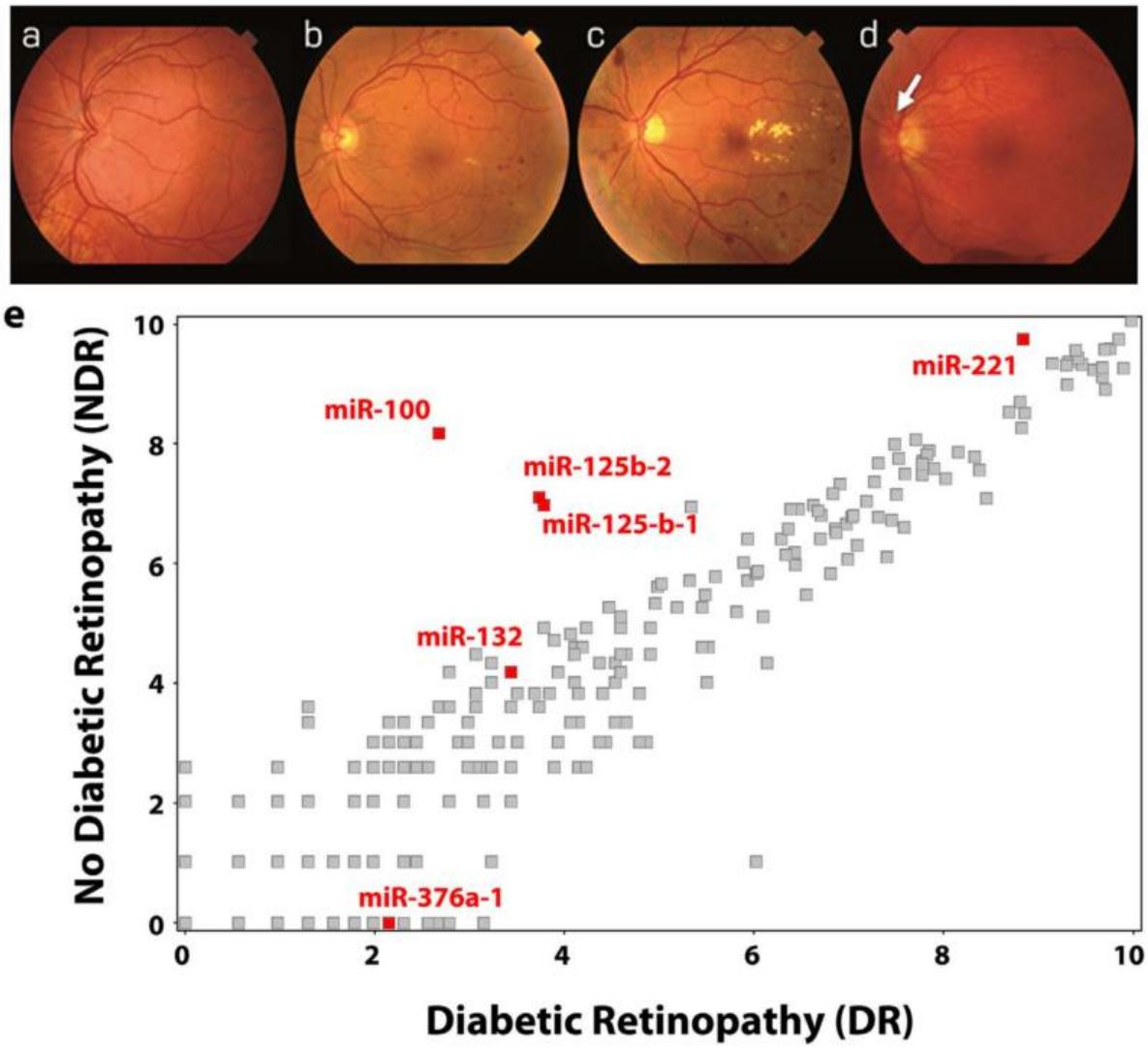

Figure 2-6. A circulating microRNA signature for diabetic retinopathy (DR)

Fundus photographs showing the clinical spectrum of DR: (a) a normal retina—no DR; (b) mild non-proliferative DR, with haemorrhages, microaneurysms and hard exudates; (c) non-proliferative DR; (d) proliferative DR (PDR), at the optic disc (white arrow) and pre-retinal haemorrhage in the inferior retina. (e) MicroRNAs consistently identified in plasma of age and gender matched diabetic individuals with or without severe DR (PDR) following analysis of small RNA sequencing (see text). The miRs that constitute part of the DR biomarker signature are displayed in red.

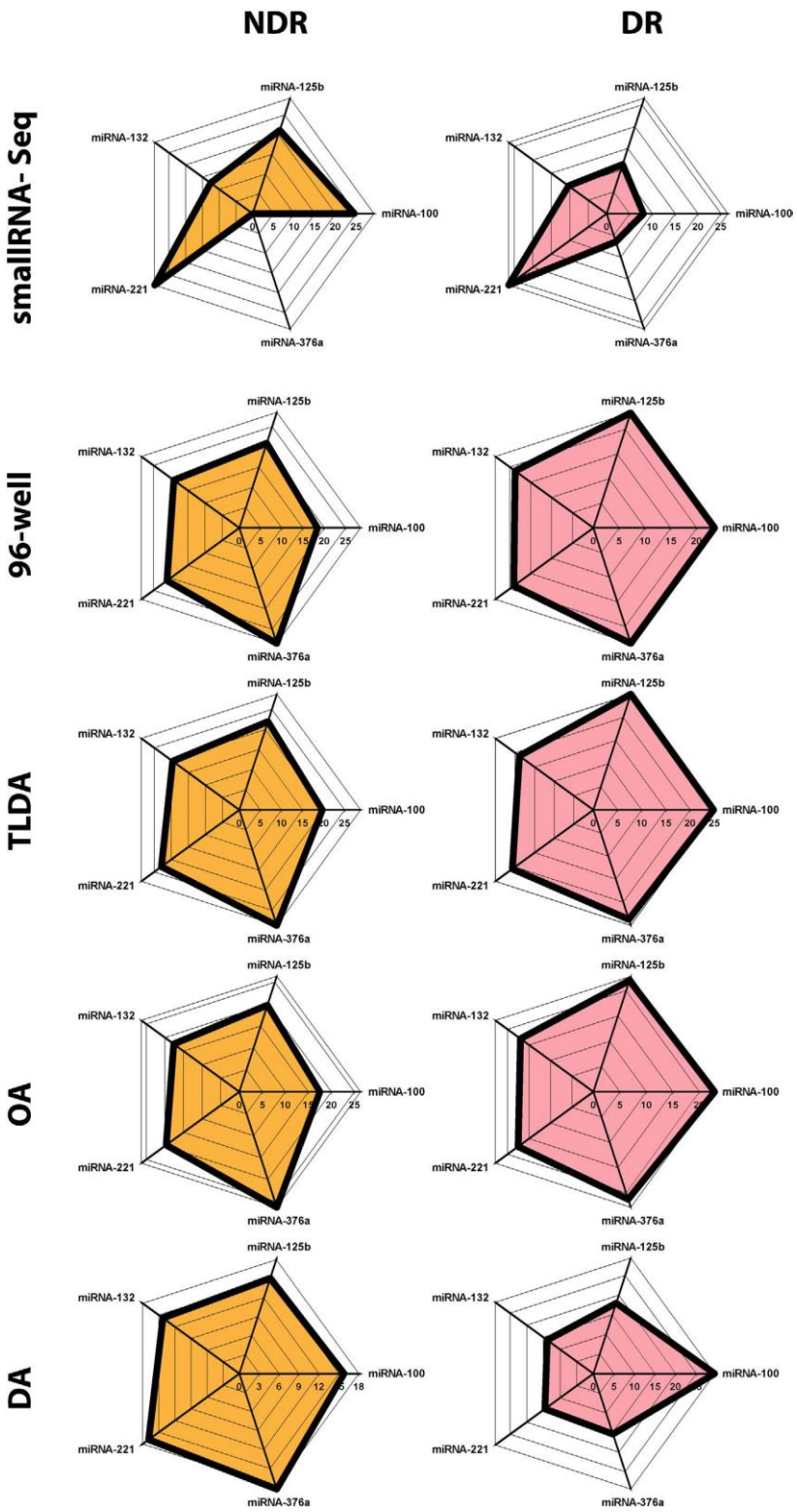

Figure 2-7. NDR and DR microRNA signature profiles

Radar plots of miRNAs signature profiles from small RNA sequencing of two age and gender matched subjects (with (DR) and without (NDR) DR). Based on DR/NDR difference 5 miRNAs were chosen as a "DR biomarker signature". Radar plots were generated using the CT/CRTs for these miRNAs on the four platforms. The results show the profile of the miRNA signature plot differs between NDR and DR in all platforms. The DA delivers a different miRNA signature profiles for DR and NDR. Radar plot axes are normalised reads for small RNA-Seq and CT/CRT for 96-well, TLDA, OA and DA.

2.5.5. Correlation and Cluster Analysis

To determine intra-platform consistency, the correlation between platforms was analysed. We assessed 42 miRNAs (including the DR signature miRs) in four human subject samples (two islet cell samples and two serum samples; a total of 168 matched measurement pairs) and plotted these as pair-wise comparisons against ViiA7 ("gold standard") platform for OA and DA (Figure 2.8). All platforms show good correlations with ViiA7, with the R^2 values 0.88 and 0.66 for OA and DA respectively. The TLDA platform had an R^2 value of 0.91. The lowest compression was observed in OA platform (slope: 0.98) and TLDA (slope: 0.94) whereas DA platform showed the moderate compression with slope 0.81.

Cluster analysis was implemented to determine the ability of these qPCR platforms in allocating miRNAs into distinct clusters. Each platform grouped the microRNAs into four distinct clusters (Figure 2.9). Again, the 96-well ViiA7 platform was used as the benchmark; clusters produced by the other platforms were directly compared to this "gold standard" (Figure 2.10). Comparison of all of the platforms (qPCR and small RNA-Seq) reveal that approximately 8% of miRNAs were assigned to different clusters by OA, 17% by TLDA, 28% by small RNA-Seq, and 39% by DA (Figure 2.10).

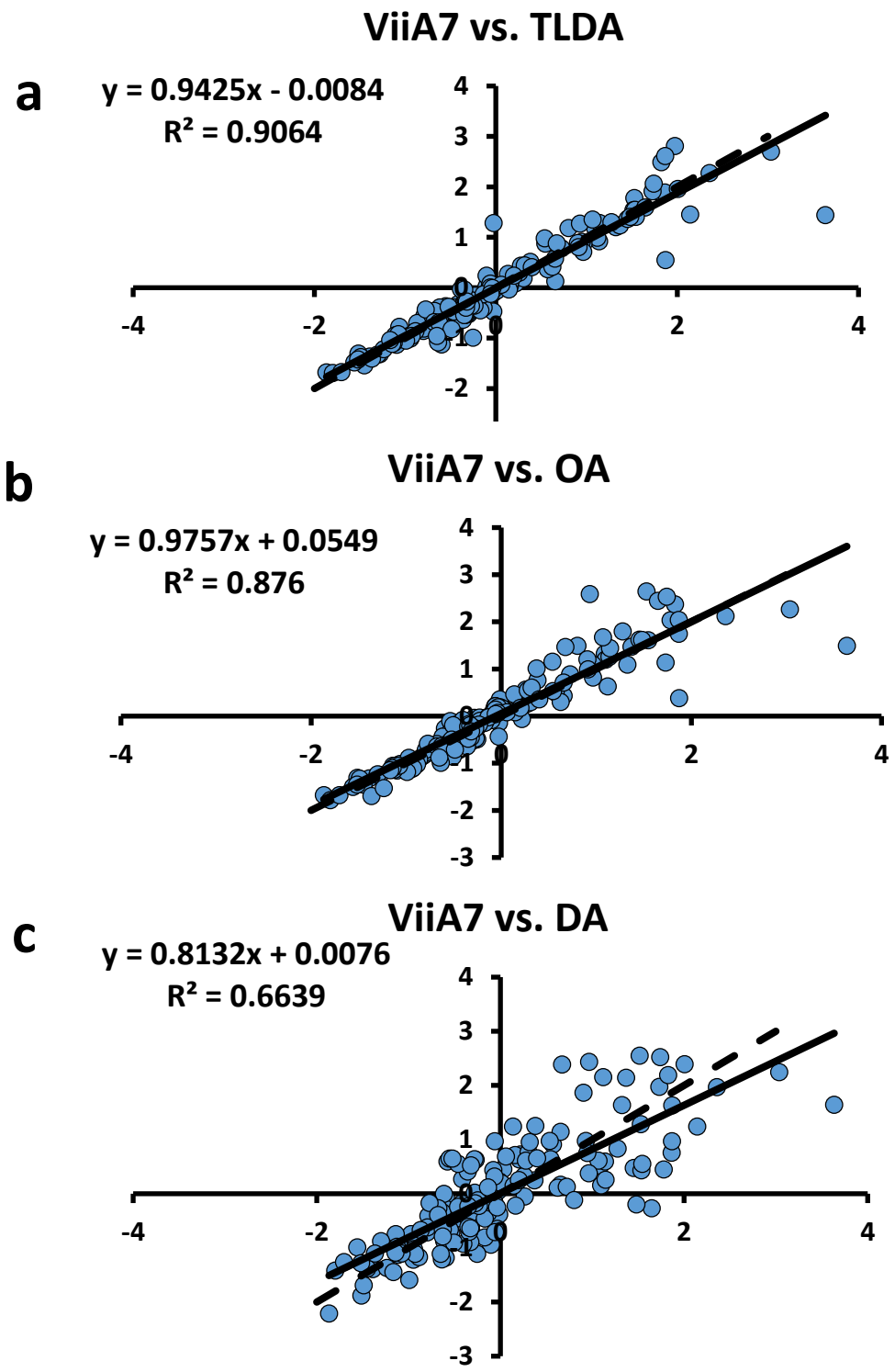

Figure 2-8. Platform correlation

Correlation of Z-scored transformed results between ViiA7 and either (a)TLDA, (b) OA or (c) DA. The hypothetical trend line of slope = 1 (dashed line) represents complete concordance, with the actual trend plotted as a solid line. The slope of the trend line (upper left corner) shows the deviation from 1.

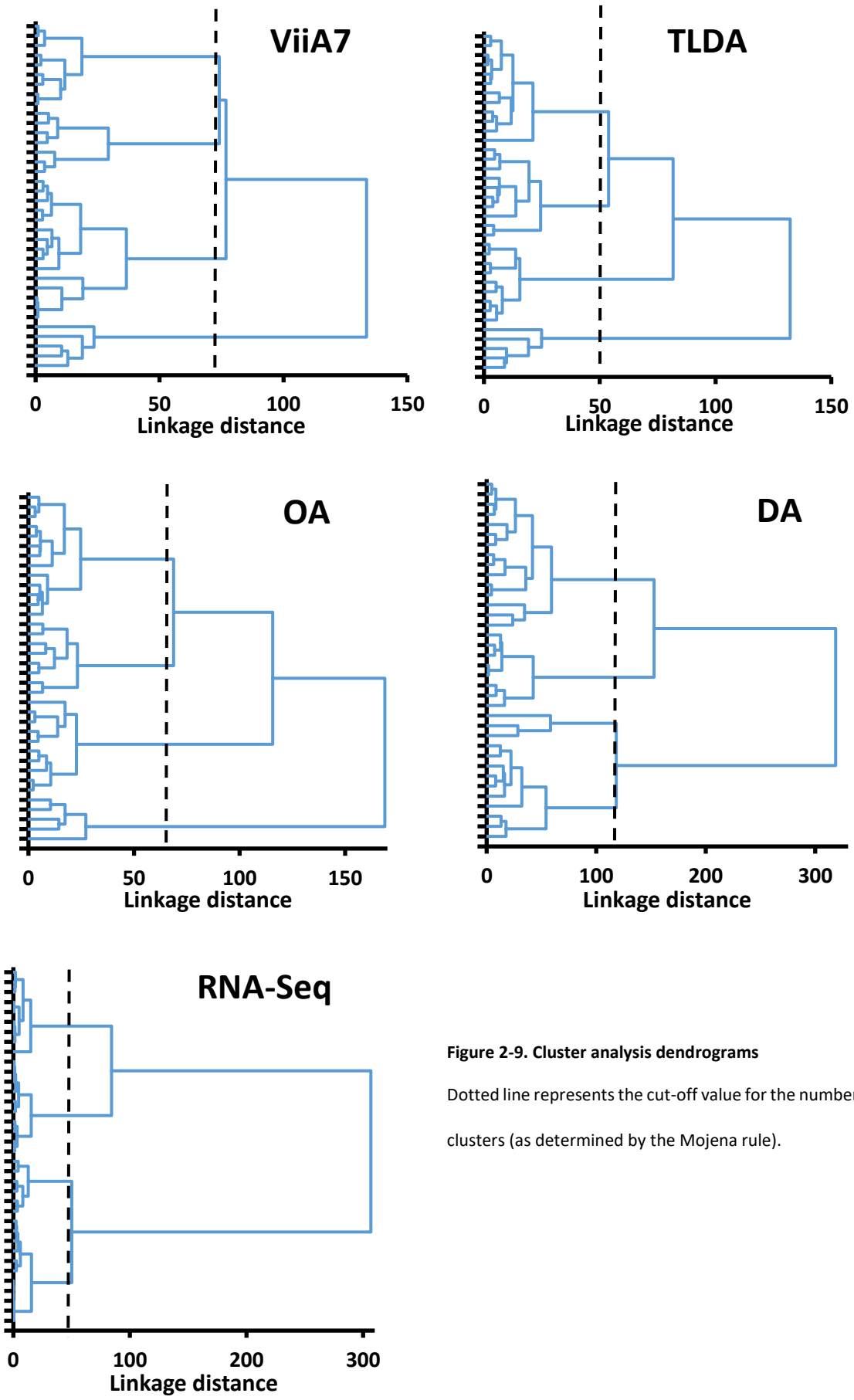

Figure 2-9. Cluster analysis dendrograms

Dotted line represents the cut-off value for the number of clusters (as determined by the Mojena rule).

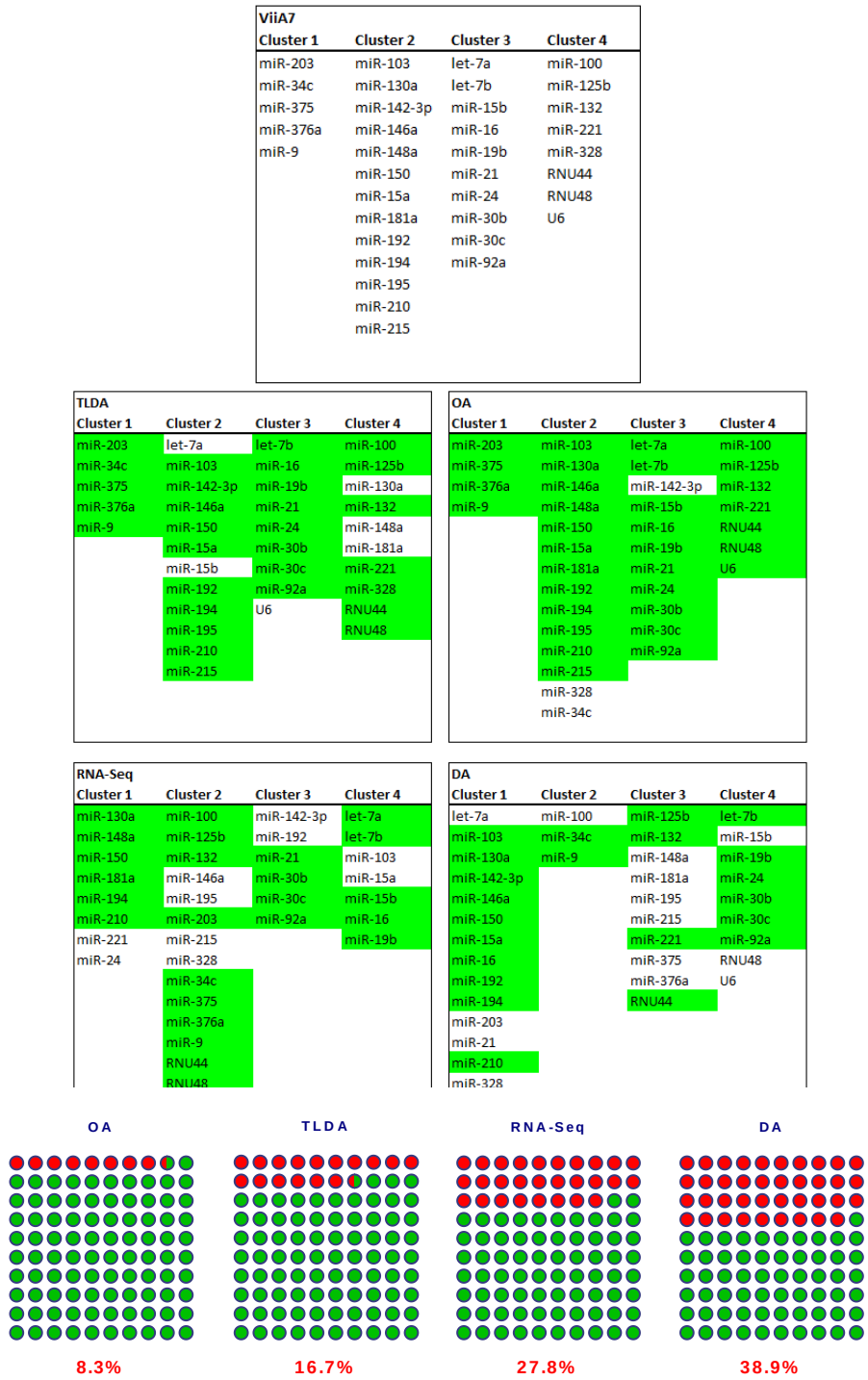

ViiA7			
Cluster 1	Cluster 2	Cluster 3	Cluster 4
miR-203	miR-103	let-7a	miR-100
miR-34c	miR-130a	let-7b	miR-125b
miR-375	miR-142-3p	miR-15b	miR-132
miR-376a	miR-146a	miR-16	miR-221
miR-9	miR-148a	miR-19b	miR-328
	miR-150	miR-21	RNU44
	miR-15a	miR-24	RNU48
	miR-181a	miR-30b	U6
	miR-192	miR-30c	
	miR-194	miR-92a	
	miR-195		
	miR-210		
	miR-215		

TLDA			
Cluster 1	Cluster 2	Cluster 3	Cluster 4
miR-203	let-7a	let-7b	miR-100
miR-34c	miR-103	miR-16	miR-125b
miR-375	miR-142-3p	miR-19b	miR-130a
miR-376a	miR-146a	miR-21	miR-132
miR-9	miR-150	miR-24	miR-148a
	miR-15a	miR-30b	miR-181a
	miR-15b	miR-30c	miR-221
	miR-192	miR-92a	miR-328
	miR-194	U6	RNU44
	miR-195		RNU48
	miR-210		
	miR-215		

OA			
Cluster 1	Cluster 2	Cluster 3	Cluster 4
miR-203	miR-103	let-7a	miR-100
miR-375	miR-130a	let-7b	miR-125b
miR-376a	miR-146a	miR-142-3p	miR-132
miR-9	miR-148a	miR-15b	miR-221
	miR-150	miR-16	RNU44
	miR-15a	miR-19b	RNU48
	miR-181a	miR-21	U6
	miR-192	miR-24	
	miR-194	miR-30b	
	miR-195	miR-30c	
	miR-210	miR-92a	
	miR-215		
	miR-328		
	miR-34c		

RNA-Seq			
Cluster 1	Cluster 2	Cluster 3	Cluster 4
miR-130a	miR-100	miR-142-3p	let-7a
miR-148a	miR-125b	miR-192	let-7b
miR-150	miR-132	miR-21	miR-103
miR-181a	miR-146a	miR-30b	miR-15a
miR-194	miR-195	miR-30c	miR-15b
miR-210	miR-203	miR-92a	miR-16
miR-221	miR-215		miR-19b
miR-24	miR-328		
	miR-34c		
	miR-375		
	miR-376a		
	miR-9		
	RNU44		
	RNU48		

DA			
Cluster 1	Cluster 2	Cluster 3	Cluster 4
let-7a	miR-100	miR-125b	let-7b
miR-103	miR-34c	miR-132	miR-15b
miR-130a	miR-9	miR-148a	miR-19b
miR-142-3p		miR-181a	miR-24
miR-146a		miR-195	miR-30b
miR-150		miR-215	miR-30c
miR-15a		miR-221	miR-92a
miR-16		miR-375	RNU48
miR-192		miR-376a	U6
miR-194		RNU44	
miR-203			
miR-21			
miR-210			
miR-328			

Figure 2-10. MicroRNA cluster classification

(a) MicroRNA clusters as classified by the ViiA7, OA, DA, and RNA-Seq. Highlighted miRNAs represent members belonging to the same cluster as those in the ViiA7 cluster analysis. (b) Percentage dot plot of miRNA cluster classification. ● indicates the percentage of miRNAs that have been correctly classified as compared to the cluster analysis from the ViiA7 platform, while ● indicates those that are misclassified. 8.33% of microRNAs were assigned to different clusters by OA, 16.66% by TLDA, 27.77% by RNA-Seq, and 38.88% by DA.

2.6. Discussion

The appeal of high-throughput technologies is readily apparent; they provide a significant decrease in sample processing time and reagents consumed, with a substantial increase in the volume of data generated in the same time. For researchers within the burgeoning field of miRNA biomarker research, such a tool is immensely desirable, especially when dealing with a multitude of clinical samples from large trials. Such assay performance would also be required should a miRNA profile related to diabetes reach clinical practice. It is imperative that technologies used for quantitative research or in clinical practice be accurate, sensitive and reproducible, and high-throughput platforms must present a similar (if not greater) level of reproducibility offered by current high sensitivity/low-throughput platforms.

The two high-throughput technologies discussed here represent the two most contemporary high-throughput qPCR platforms. The Dynamic Array platform offers a finely crafted plate with a set of individually pressure-tested valves that control the flow of reagents into the microfluidic plate. The OpenArray platform provides a high density PCR plate/slide that allows automated sample loading using a specially designed robotic device (Accufill™). The major difference is that the OpenArray comes with pre-printed miRNA assays while the Dynamic Array provides flexibility to choose the miRNA assays just before setting up the plate. The DA platform thus provides only the "hardware" for users to perform qPCR. Although this flexibility is an advantage, the limitation of the DA is that it heavily depends on the compatibility of the pooled RT primers with the TaqMan real-time PCR assays. Of the 48 miRNAs selected from the TaqMan primer pool A (Life Technologies, CA) six of these assays could not be read on the DA due to incompatibility between the RT and PCR primers. Since the proprietary primer pools are compatible with the primers printed in TaqMan Low Density Arrays (TLDAs) or OpenArray

plates only, the individual assays available from Life Technologies may not be compatible with the multiplex RT pools. Of course, users can avoid this by ordering customised primer pools from Life Technologies to assess a specific set of miRNAs.

In our analysis, the OpenArray system was the most reproducible high-throughput platform tested, with less inter- and intra-run variation than the Dynamic Array. This conclusion correlates with a recent study comparing these platforms for screening genomic mutations in the Ashkenazi Jewish community (191). The OA platform also proffers a simple, cost-effective workflow, with user-friendly software for further analyses.

Our data demonstrate that replicate variability was exacerbated when quantifying low abundance transcripts on any of the platforms. As shown in Figure 2-3, this variability is especially apparent in the high-throughput platforms, highlighting a limitation of these systems. Screening low abundance transcripts on these platforms should be avoided, as even the implementation of a pre-amplification step was insufficient to reduce CT variability. Increasing the number of pre-amplification cycles is not recommended as it would amplify any bias that is introduced in the process. Users of Dynamic Arrays could expect 5.6% of their assays to demonstrate more than 8-fold variability. Any data obtained using DAs with differences less than or around 8-fold need to be re-validated using a high sensitive PCR technology, such as the 96-well platform described herein. For miRNAs detected around a CT value of 30, the standard qPCR format proves more reliable.

For medium-throughput studies, researchers can utilise the TLDA platform. We found a comparable level of reproducibility on this platform when using cards from the same lot, but have observed considerable (13.9%) lot-to-lot variation (188).

Correlation between technologies is required to translate relative gene expression data on different qPCR platforms. Since CT values cannot be directly compared across platforms due to the differences in sample preparation, reaction volume and detection technologies, correlation between z-scored transformed data (Figure 2.8) is a reliable method to compare the data obtained from multiple qPCR technologies. All of the technologies assessed correlated well with the standard 96-well platform, however the OpenArray platform deviated the least from the theoretical ideal value of 1, demonstrating that it correlates extremely well with the staple 96-well format. As such, up or down scaling miRNA qPCR reactions between the ViiA7 and OA platforms will produce parallel data.

Segregation of miRNAs based upon their expression profile is useful for biomarker identification. Our cluster analysis (Figures 2.9 and 2.10) demonstrated that data obtained from all platforms were able to create four distinct miRNA clusters; however, the members of these clusters differed between the platforms. The Dynamic Array generated fundamentally different clusters, making it difficult to identify our test DR miRNA signature (generated through smallRNA sequencing). The OpenArray platform generated the most similar clusters (compared to 96-well), with similar segregation of miRNA DR signature members into clusters giving confidence in validating disease-related microRNA signatures. Although quantitative real time PCR platforms have different sensitivities and efficacies for reproducing the miRNA DR signature we assessed the similarity in data obtained from qPCR versus our sequencing platform. Interestingly, the small RNA-Seq data also generated four distinct clusters, with 27% of the miRNAs misassigned to the four clusters. This may be due to the fact that qPCR and next generation sequencing employ vastly different chemistries to quantitate miRNAs and that the outcome of such comparisons would be largely impacted by the depth of sequencing achieved.

The miRNA signature profile generated by our small RNA sequencing, although representative, demonstrates the importance of rigorously analysing new technologies, especially those that may become routine for biomarker discovery and validation and potentially be used in clinical practice. Figure 2.7 demonstrates the differences in miRNA signature profile detected by multiple platforms.

This report demonstrates the importance of multiple technical factors that can influence the conclusions derived from miRNA qPCR data. Although there are differences in the respective detection systems (QuantStudio for OpenArrays, Biomark HD for Dynamic Arrays), the size of the reaction may also affect the reproducibility of these high-throughput systems. Although both platforms have a reaction volume in nanoliters, the OpenArray reaction volume is 2.2-fold more than the Dynamic Arrays. During the optimisation of our standard (96-well) qPCR analysis for detection of low-copy miRNA/mRNA transcripts, the amplification curves differed by 0.5 cycles when the reaction volume was reduced from 10 µl to 5 µl (not shown here. Considering the Poisson distribution of miRNA templates, this difference can be significant when more than two-fold difference is factored in, even at the nanoliter range.

2.7. Conclusions

The data presented within this chapter demonstrate that the OpenArray system provides the greatest reproducibility of the micro- and nano-fluidic platforms assessed, and this is evident when quantitating both cellular and circulating miRNAs. When compared to the gold-standard 96-well plate system, however, all platforms demonstrated increased variability. This was especially apparent when attempting to quantify low abundance transcripts – a probable consequence of increased throughput and decreased reaction volume. Interestingly, these studies also highlighted the impact of technology on the characterisation of a circulating miRNA signature. The representative DR signature, obtained from NGS studies, displayed a markedly different profile when quantitated on the DA platform.

Although each of the platforms discussed have their own advantages/disadvantages, users need to consider all aspects before choosing an analytical platform, and ideally should test their data across another high-sensitivity platform such as the 96-well platform. These observations provide a useful guide for researchers planning to switch to high-throughput qPCR technologies for quantitative assessment of gene transcripts in large number of research/clinical trial samples. Furthermore, the development of a sensitive, reliable and minimally invasive test with high predictive power for clinical stratification of DR will provide a surrogate marker for clinical trials, improve prognosis information and guide development of future therapies aimed towards preventing the vascular complications of diabetes.

Similar studies as performed herein are likely merited in the future with the refinement of existent systems and likely development of novel systems.

3. *In Vitro* and *In Vivo* Models of β-cell Death

3.1. Chapter Overview

Pancreatic β-cell death and immune cell infiltration are characteristic of the progression to T1D. To understand if these processes result in a significant and detectable release of miRNAs and cfDNA, two models of β-cell death were employed. The first (*in vitro)* model exposed primary human islets cultured in a defined (serum-free) medium to sodium nitroprusside (SNP), a compound known to initiate apoptosis through the generation of nitric oxide (NO) (192) or hydrogen peroxide (193). Exposure to SNP for 24 hours resulted in an increase in islet cell death (measured by DNA fragmentation). The two highest concentrations (1 and 10 mM) caused some miRNAs, but not others, to be significantly released into the surrounding supernatant. This affirms our hypothesis that only select miRNAs are released in response to islet cell stress/death, leading to a circulating miRNA signature. A 1 mM SNP concentration also caused a significant release of both unmethylated and methylated *Ins* cfDNA into the defined culture medium, however 10 mM did not demonstrate a dose-dependent increase, indicating that the cfDNA may have been either rapidly degraded or reached a saturation level for release into the surrounding cellular environment.

To emulate the progression to T1D in an *in vivo* model system, non-obese diabetic (NOD) mice were assessed at 4 to 18 weeks of age. NOD mice demonstrate immune cell infiltration of the pancreatic islets, β-cell destruction and a significant increase in blood glucose levels (BGLs), all of which are confirmed within this chapter. Circulating candidate miRNAs were elevated prior to immune cell infiltration and the dysfunction of glucose homeostasis, and demonstrate significant correlation with fasting BGLs. In contrast, other miRNAs are stable within the NOD

circulation. These data highlight important miRNAs that are released in response to β-cell stress/death using in vitro (human) as well as *in* vivo (mouse) model systems.

3.2. Chapter Aims

Studies in this chapter aimed to:

1. assess the miRNA and cfDNA release in response to SNP-mediated human islet cell death.
2. quantitate circulating miRNA abundance in NOD mice during diabetes progression.
3. identify any associations between circulating miRNAs and measures of β-cell function.

3.3. Methods

3.3.1. Cadaveric Islets

Cadaveric human islets were kindly provided by Associate Professor Wayne Hawthorne and his surgical team at the Westmead Institute, Sydney Australia and Professor Tom Kay and his surgical team at the St Vincent's Institute, Melbourne Australia. Islets were generally obtained from cadaveric pancreas harvested from brain dead donors. The best islet quality/numbers were from pancreas of younger and heavier donors with minimal intensive care stay period and with short cold/warm ischaemic times (61; 194). Islets that were consented for research and were not of the desired quantity/quality to progress into clinical islet transplantation were made available to the Hardikar Lab within 24-48 hours of isolation. Islets from Melbourne and Sydney isolation centers were delivered on wet ice and used for the *in vitro* experiments discussed herein.

3.3.2. Sodium Nitroprusside (SNP) Exposure

Primary cadaveric human islets were exposed to SNP for 24 hours as per the protocol outlined in Appendix G. SNP exposure was conducted at 1 µM, 10 µM, 100 µM, 1 mM and 10 mM.

3.3.3. Flow Cytometry

SNP-induced islet cell death was assessed using flow cytometry as outlined in Appendix L. Briefly, cell death was analysed by separating islets into a single cell suspension and then placing them into a hypotonic buffer containing propidium iodide (PI) to lyse the cells and stain the nuclei. Flow cytometry was then used to assess the size of the nuclei – dying/dead cells have fragmented nuclei, resulting in hypodiploid DNA.

3.3.4. Non-Obese Diabetic (NOD) Mice

Female NOD mice (N=32) were received in two groups of 16; one group was received at 3 weeks of age and studied from 4 weeks of age to 10 weeks of age, while the other group was received at 11 weeks of age and was studied from 12 weeks of age to 18 weeks of age. Four mice were randomly placed into each cage at the beginning of the study; all mice were fed on an *ad libitum* chow diet with unrestricted access to food and water. Each cage was placed in the same room in the middle rack and were exposed to the same day/night schedule. Every two weeks, one cage was fasted overnight for 12-14 hours and all four mice then had plasma, pancreas, liver (and other tissues) collected as per the protocol outlined in Appendix G. Fasting blood glucose concentration (BGL) was recorded as blood was collected via cardiac puncture. Sufficient plasma was unable to be collected from one mouse at week 4 so miRNA results were not obtained. Pancreas and liver samples were stored in 4% paraformaldehyde then given to the Royal Prince Alfred Hospital Pathology Department for paraffin embedding, sectioning, and Haematoxylin and Eosin (H&E) staining. Liver sections were used as negative controls for both H&E staining and immunohistochemistry. All tissues from a mouse were incorporated in a single block to assess the immunostaining and histochemistry for pancreatic as well as non-pancreatic tissues in a single section.

3.3.5. Immunohistochemistry

Pancreas and liver paraffin sections were stained for insulin and glucagon expression using the protocol outline in Appendix K. Insulin was detected using primary polyclonal guinea pig anti-insulin antibodies (Dako) at 1:100 dilution, and secondary anti-guinea pig Alexafluor 488 antibodies (Invitrogen) at 1:100 dilution. Glucagon was detected using mouse polyclonal anti-glucagon antibodies (Sigma) at 1:400 dilution, and secondary anti-mouse Alexafluor 546

antibodies (Invitrogen) at 1:100 dilution. Stained slides were visualised using the Zeiss 510 Meta scanning laser confocal microscope. All thresholds were set below saturation, and all other parameters (including laser power) were identical for all samples. Dye swaps for secondary antibodies were carried out to confirm specificity and staining on a subset of these samples.

3.3.6. RNA Isolation

RNA was isolated from NOD mice EDTA-plasma using the protocol outlined in Appendix B. RNA from cell culture media was isolated using the protocol outline in Appendix B or C. Cellular RNA was isolated using the protocol outlined in Appendix A. RNA was quantitated using a spectrophotometer.

3.3.7. MicroRNA Quantitation

Candidate miRNAs were identified through previous work from the Hardikar lab (discussed in Section 1.7) and through literature searches. MicroRNA abundance was measured using the custom high throughput qPCR protocol outlined in Appendix D. To remove non-specific amplification, results with an AMP score of <1.24 and/or a Cq confidence score of <0.6 were omitted. Results were normalised to the RNA isolation and RT ath-miR spike-in miRNAs (see Supplementary Chapter 1 for optimisation). Transcript abundance was calculated using the fold over detectable method (limit of detection = 39) described earlier (190).

3.3.8. Cell-free DNA Isolation and Bisulfite Conversion

Cell-free DNA was isolated from the cell culture media after islet SNP exposure as per the protocol outlined in Appendix E. All samples underwent one freeze-thaw prior to cfDNA isolation. Bisulfite conversion was completed as per the protocol outlined in Appendix I.

3.3.9. Insulin cfDNA Quantitation

Methylated and unmethylated insulin cfDNA were quantified using the digital droplet PCR protocol outlined in Appendix J. Each plate contained a positive control, which consisted of a mixture of control plasmids (10% unmethylated, 90% methylated plasmid, 1 ng total per reaction), and a no template control (nuclease-free water). Control plasmids, kindly provided by Professor Raghu Mirmira (Indiana University, Indianapolis, Indiana, USA) as part of an existing collaboration with A/Prof. Hardikar, were amplified using the transformation protocol outlined in Appendix H. FAM and VIC thresholds were identified based on the positive control and then applied to the entire plate.

3.4. Results

3.4.1. SNP Exposure Causes Cell Death in Primary Human Islets

Primary human islets were allowed to recuperate in serum-free media for atleast 14 hours prior to culture in the presence of increasing concentrations of SNP for 24 hours. After this time, the islets demonstrated consistent morphological changes indicative of cell death, including blebbing and fragmentation, which is particularly evident in the higher concentrations. The highest concentration of SNP, 10 mM, resulted in striking morphological changes, indicating that this concentration is highly cytotoxic and may also cause necrosis. Figure 3-1 contains representative photographs of human islets prior to exposure and after 24 hours of SNP exposure.

To confirm the apoptotic and/or necrotic effect of SNP, the nuclei of the islet cells were assessed using flow cytometry (Figure 3-2). During such apoptotic cell death, the genomic DNA is fragmented, causing a decrease in PI staining. Normal diploid nuclei in the control islets cultured in media without SNP (Control, Figure 3-2a) have the highest percent of live cells. Hyperdiploid nuclei are seen to the right (increasing PI fluorescence) of the diploid nuclei, indicating cells that were within or had completed the S-phase of the cell cycle prior to mitosis. Hypodiploid (fragmented or degraded) nuclei show reduced PI fluorescence. Reflecting the images seen in Figure 3-1, 10 mM SNP results in extensive cell death and fragmented DNA (Figure 3-2f).

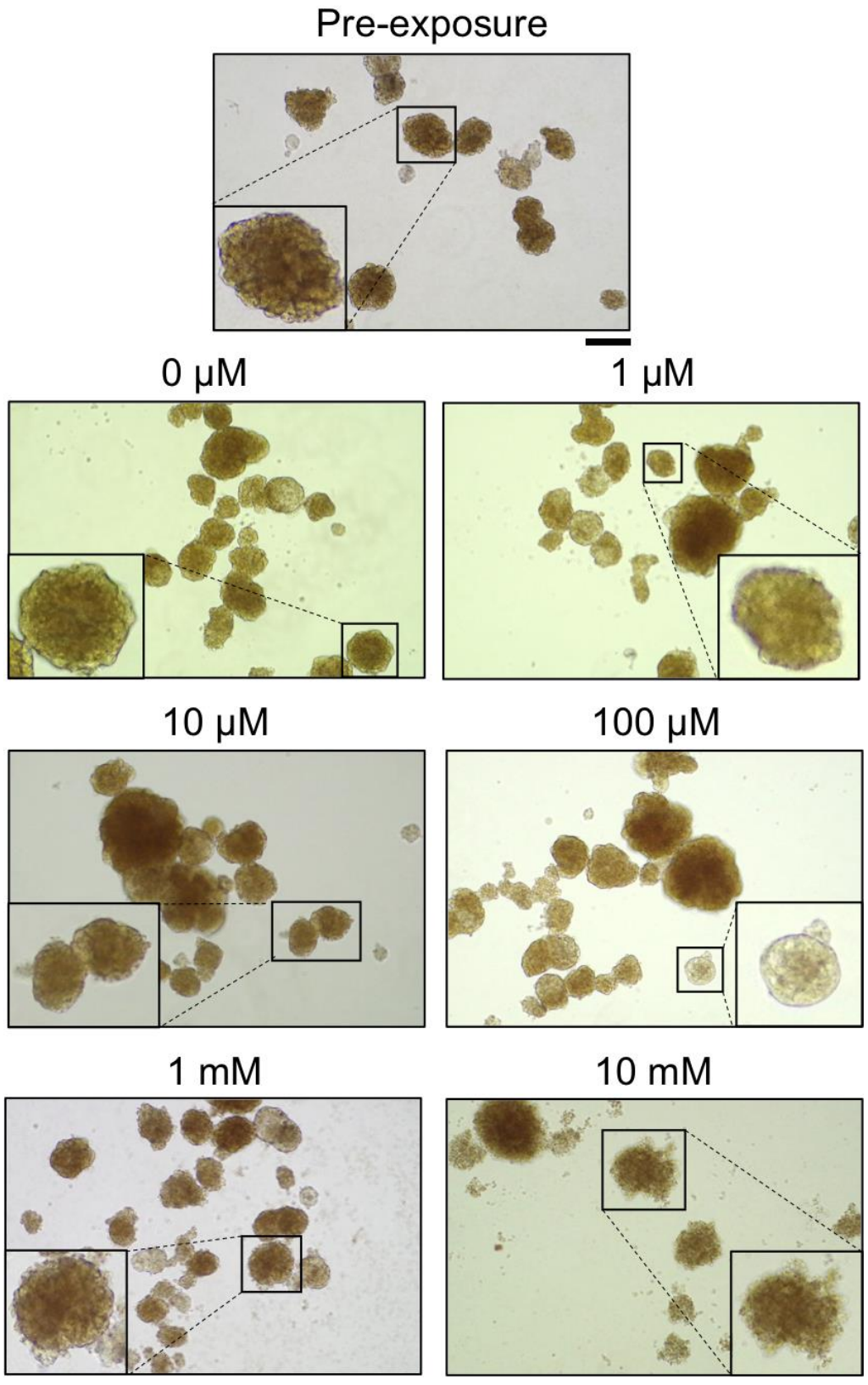

Figure 3-1. Human islets during SNP exposure

Representative images of human primary islets prior to SNP exposure (Pre-exposure) and after 24 hours cultured with serum-free media only (0µM) or serum-free media containing differing concentrations of SNP as indicating above each panel. All images were taken from a single experiment using islets from a single donor. Bar=50µm (all panels except insets).

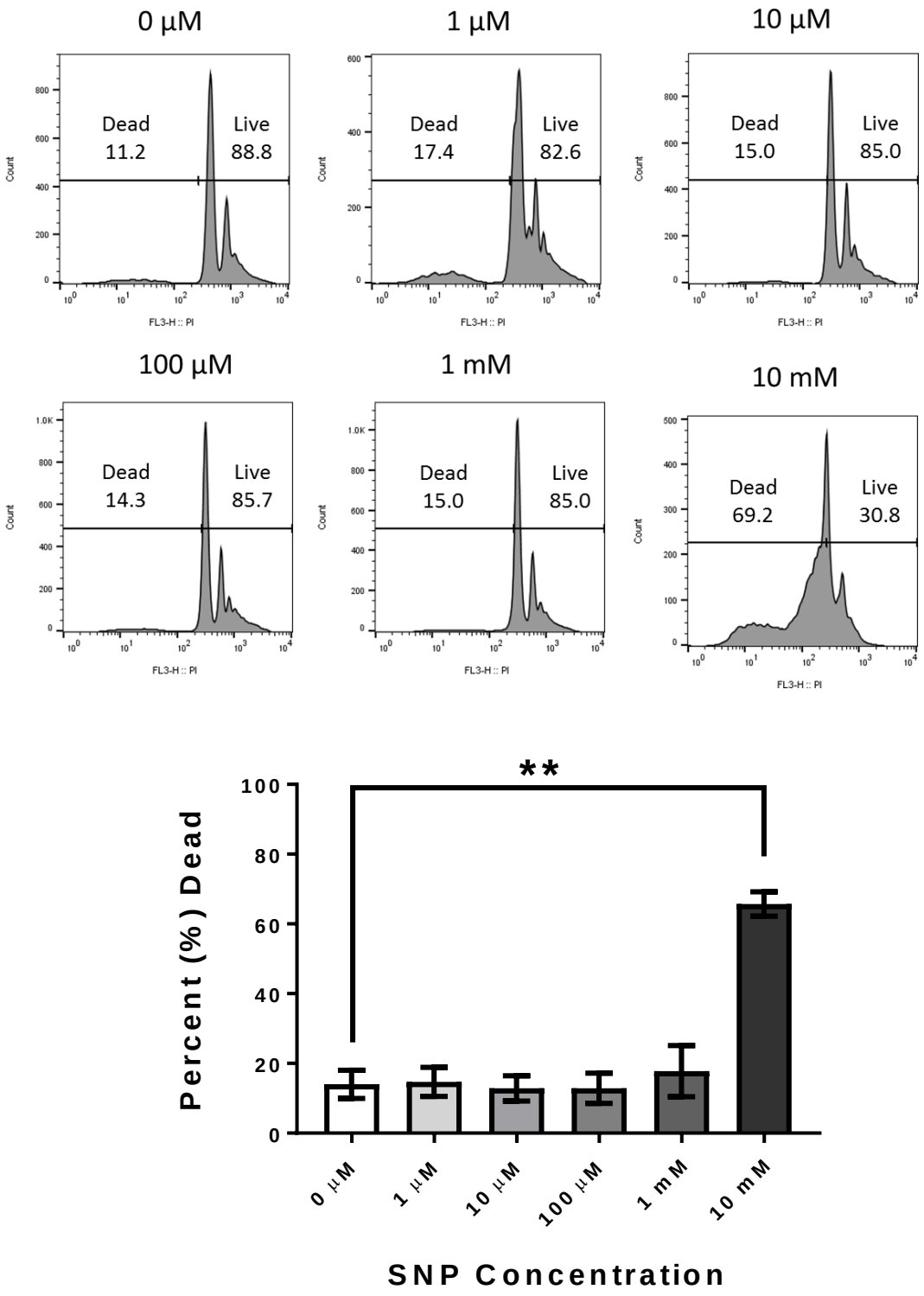

Figure 3-2. SNP causes an increase in DNA fragmentation

(a) Representative flow cytometry results showing an increase cell death with exposure to SNP. (b) Combined results showing a significant increase in cell death at 10 mM SNP. Mean ± SEM. ** P<0.01 (unpaired t-test). All comparisons were made with reference to 0 µM. N = 2-3 independent experiments.

3.4.2. Islet Cell Death Causes a Release of MicroRNAs and Cell-Free DNA

A significant increase in the abundance of 27 miRNAs was found within the supernatant of human islets cultured in the presence of 1 and 10 mM SNP (Figure 3-3). As shown in the previous section, these concentrations result in increased cell death, leading to the release of these miRNAs. When the abundance of these 27 miRNAs was quantified within the cellular fraction, a significant decrease was found in the islets exposed to 10 mM only (Figure 3-4). This suggests that 1 mM SNP results in an active release of these candidate miRNAs in response to the cellular stress. Meanwhile, 10 mM indicates a significant release of the cellular miRNAs due to membrane rupture, a hallmark of necrosis.

Not all miRNAs that were measured demonstrated an increased or dose-dependent release during SNP exposure (Figure 3-5). Intriguingly, two of these miRNAs are commonly utilised "housekeeping" small nucleolar RNAs, U6 and RNU44.

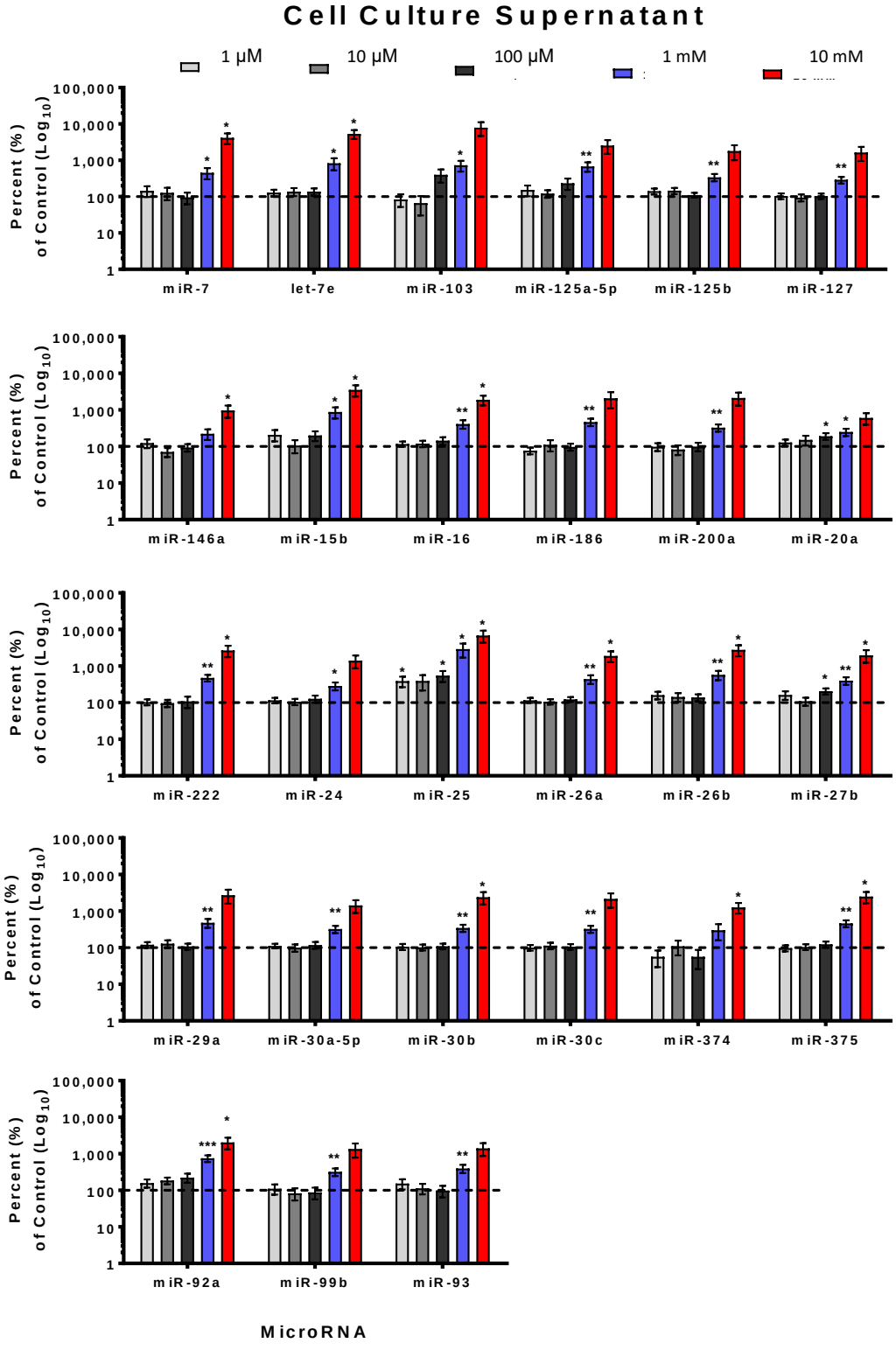

Figure 3-3. Islet SNP exposure causes a release of miRNAs

27 miRNAs were increased in the cell supernatant following a 24-hour exposure to SNP. Mean ± SEM. * P<0.05 ** P<0.01 *** P<0.001 (t-test, deviation from 100%). N = 6-7 islet preps for all concentrations apart from 10 mM (N = 3 islet preps). Each islet preparation was conducted in multiple technical replicates.

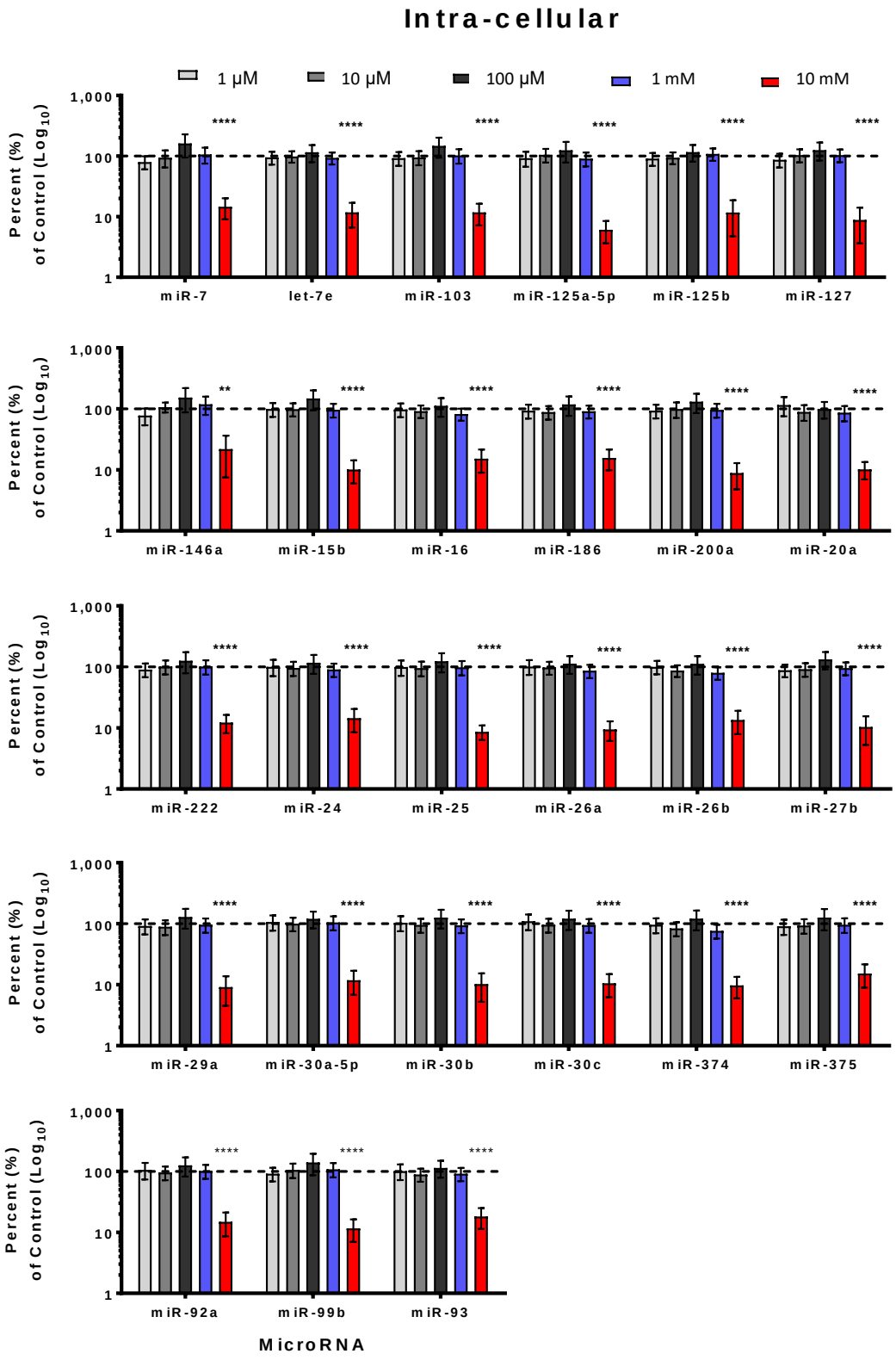

Figure 3-4. Islet SNP exposure causes a decrease in cellular miRNAs

The same 27 miRNAs (as shown in Figure 3-3) were found to be reduced in the cells exposed to 10 mM SNP. Mean ± SEM. ** P<0.01 **** P<0.0001 (t-test, deviation from 100%). N = 6-7 islet preps for all concentrations apart from 10 mM (N = 3 islet preps). Each islet preparation was conducted in multiple technical replicates.

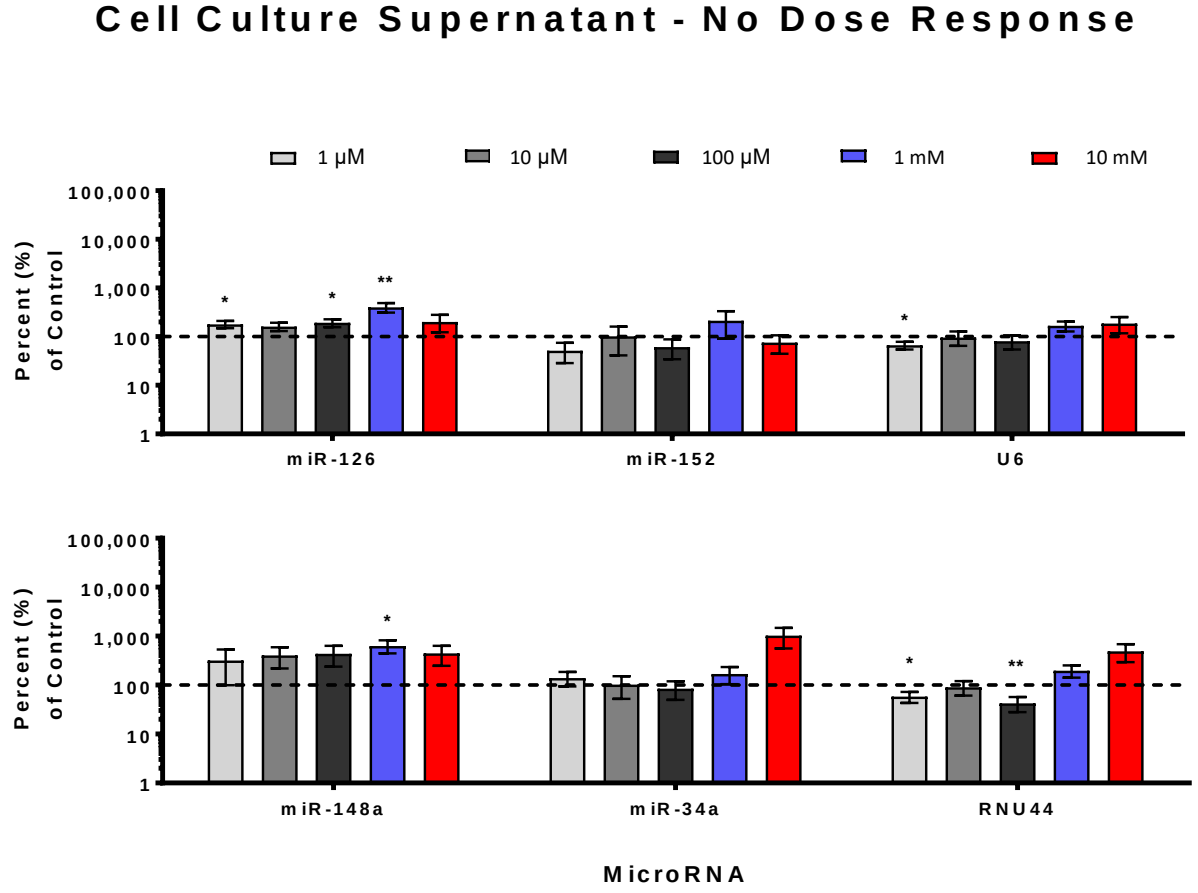

Figure 3-5. Other miRNAs are not released in response to SNP exposure

SNP mediated islet cell death does not cause a significant, or dose-dependent, release of some miRNAs into the cell culture supernatant. Mean ± SEM. * P<0 .05 ** P<0.01 (t-test, deviation from 100%). N = 6-7 islet preps for all concentrations apart from 10 mM (N = 3 islet preps). Each islet preparation was conducted in multiple technical replicates.

Both unmethylated and methylated *Ins* cfDNA was significantly released by islets cultured in the presence of 1 mM SNP (Figure 3-6), mirroring the miRNA release seen in Figure 3-3. When exposed to 10 mM, however, the unmethylated cfDNA did not demonstrate a dose dependent increase. Methylated *Ins* DNA copies were not significantly increased in response to 10 mM SNP. The increase cytotoxic effect of 10 mM SNP, and the associated DNA fragmentation (Figure 3-2), is likely to result in the reduction in detectable cfDNA copies.

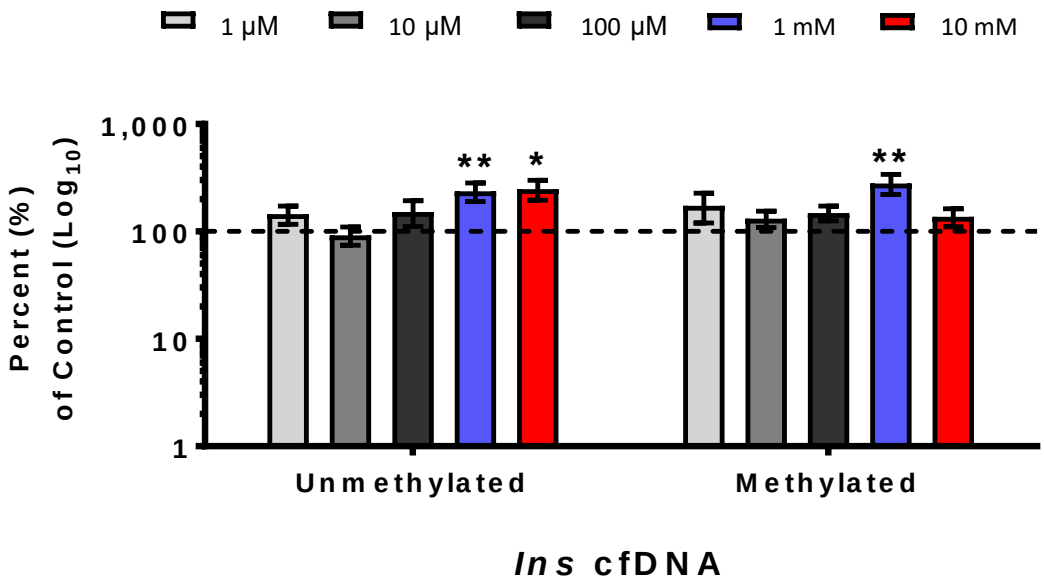

Figure 3-6. Cell-free DNA release due to SNP exposure

N = 6-7 islet preps for all concentrations apart from 10 mM (N = 3 islet preps). Each islet preparation was conducted in multiple technical replicates. Mean ± SEM. * P<0.05 ** P<0.01 (t-test, deviation from 100%).

3.4.3. NOD Mice Demonstrate Immune Infiltration and Loss of Glucose Homeostasis

To model the progression of T1D, NOD mice were housed between 4 to 18 weeks of age, with four mice euthanised every two weeks and samples taken as per Figure 3-7. Due to the volume of plasma needed for RNA isolation and miRNA quantitation, the blood had to be collected via terminal cardiac puncture and so the study was cross-sectional in nature. The mice developed normally, with consistent total and pancreas weight gain over time (Figure 3-8). Fasting BGLs started to rise around 10 weeks of age and became significantly higher at 12 weeks of age (Figure 3-9), consistent with previous reports. The fasting BGLs of the mice at 16 and 18 weeks of age were lower, albeit not significantly so, than those at 12 and 14 weeks of age. All mice were housed and treated identically, however, as the study was cross-sectional and consisted of two groups of animals, inter-animal differences may be observed. Furthermore, changes in stress levels, possibly due to unavoidable construction noise at the Medical Foundation Building during the later time points in the study, unintentional changes in diet manufacturer and the use of non-sterile water provided by the facility to these mice, as well as batch variations in the glucose testing strips may also impact upon the BGL readings during the later time points for this study.

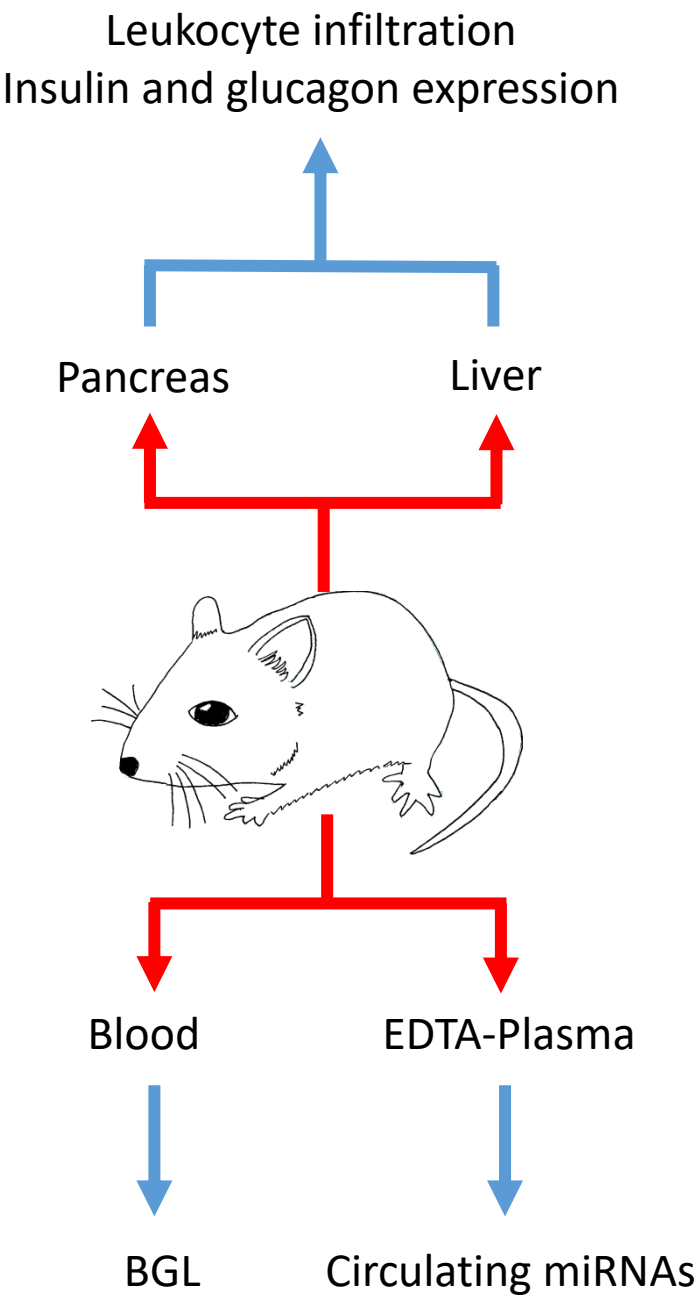

Figure 3-7. Overview of NOD mouse procedure

Every two weeks (from 4-18 weeks of age) four NOD mice were euthanased, and whole blood, ETDA-plasma, pancreas and liver samples were taken. Red arrows indicate the samples, while blue arrows indicate the downstream analysis.

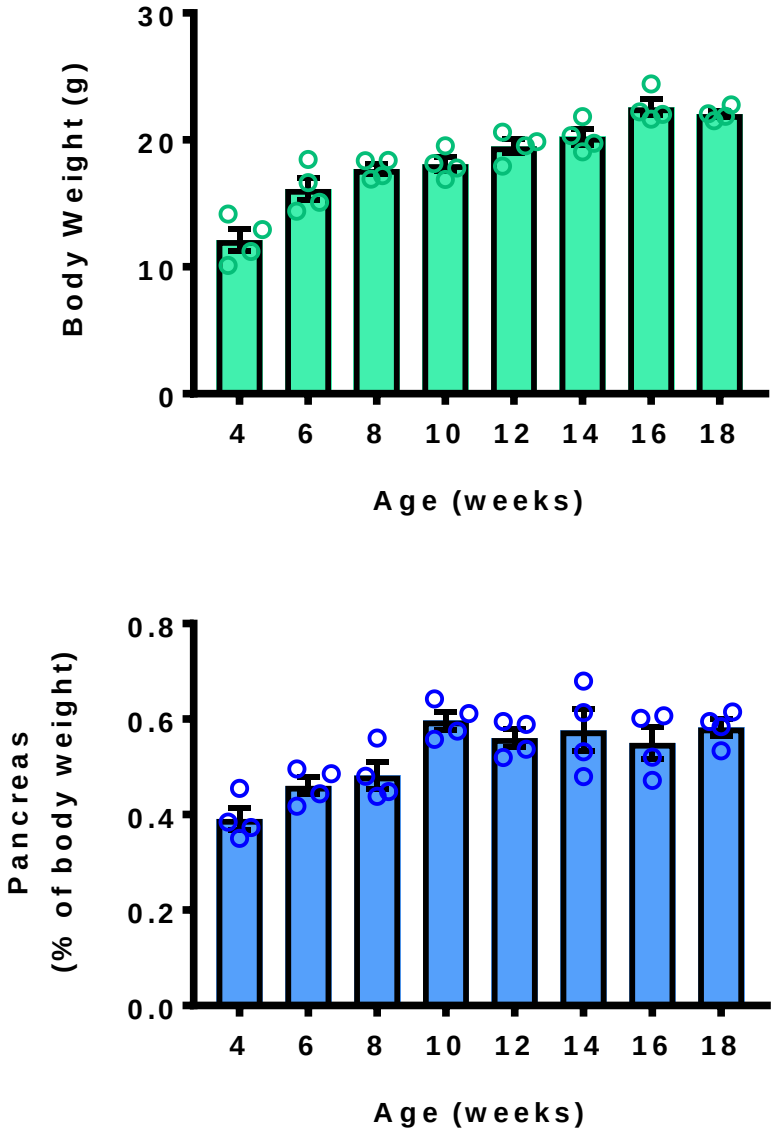

Figure 3-8. NOD mice total body and pancreas weight

(a) Total body weight and (b) pancreas weight of the NOD mice at each age group. Mean ± SEM N = 4 mice/group.

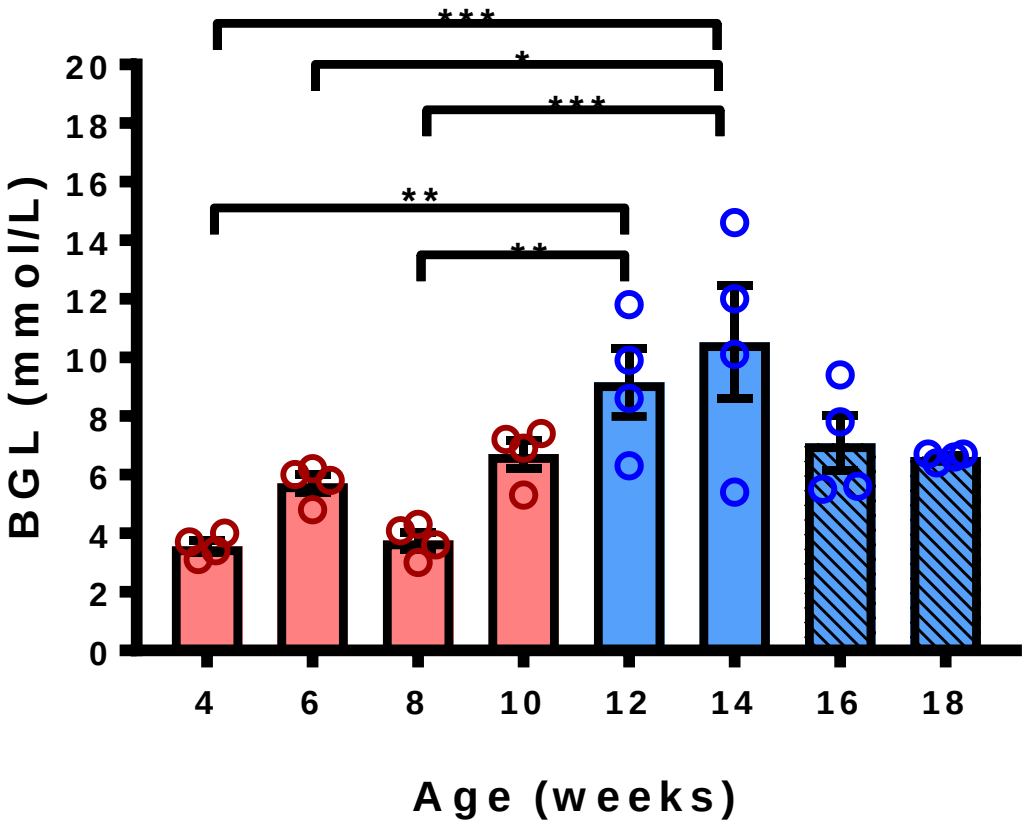

Figure 3-9. NOD mice fasting blood glucose levels

NOD mice were fasted for 12-14 hours overnight prior to BGL measurement. N = 4 mice at each timepoint. Mean ± SEM. Red and blue indicate the two groups of mice used (see section 3.3.4). Hatched bars indicate time points that were omitted for further analysis, possibly due to reasons discussed in section 3.4.3. * = P<0.05 ** = P<0.01 ***= P<0.001. ANOVA with post-hoc Tukey's multiple comparisons test.

The accumulation of immune cells within the periductal areas of the pancreas (peri-insulitis) and within the islets themselves (intra-insulitis) became evident at 6-weeks of age (Figure 3-10). The degree of insulitis was quantified by one investigator using an insulitis score, with 0 = no insulitis, 1 = peri-insulitis with up to 25% of the islet area showing immune infiltration, 2 = 25-50% infiltration, 3 = 50-75% infiltration, and 4 = greater than 75% infiltration. Examples of islets fitting each of these categories can be found in Figure 3-10b.

A noticeably large drop in islets with no insulitis (from 85.3% to 44.8%) can be seen between 6 to 8 weeks of age, prior to the increase in fasting BGL seen in Figure 3-9. Another drop (41.4% to 12.4%) can be seen between 10 and 12 weeks of age as the BGLs significantly increase. By 18 weeks of age, only 1.9% of islets are free from insulitis. No immune infiltration was observed within liver sections from the same mice.

The extensive immune infiltration seen in these animals causes a reduction in insulin expression. Figure 3-11 contains representative images from animals at all time points; immune cells are clearly visible, with insulin staining reduced within the area of infiltration. This is especially evident within the 12-week image (Figure 3-11e), where insulin, but not glucagon, staining is reduced in the periphery of the islet where numerous immune cells have infiltrated. Figure 3-11h demonstrates a quintessential T1D islet; there is no insulin present, indicating a loss of β-cells, but glucagon staining remains substantial, indicating the presence of significant numbers of α-cells. No insulin or glucagon staining was seen within liver sections from the same mice, which were used as a negative control.

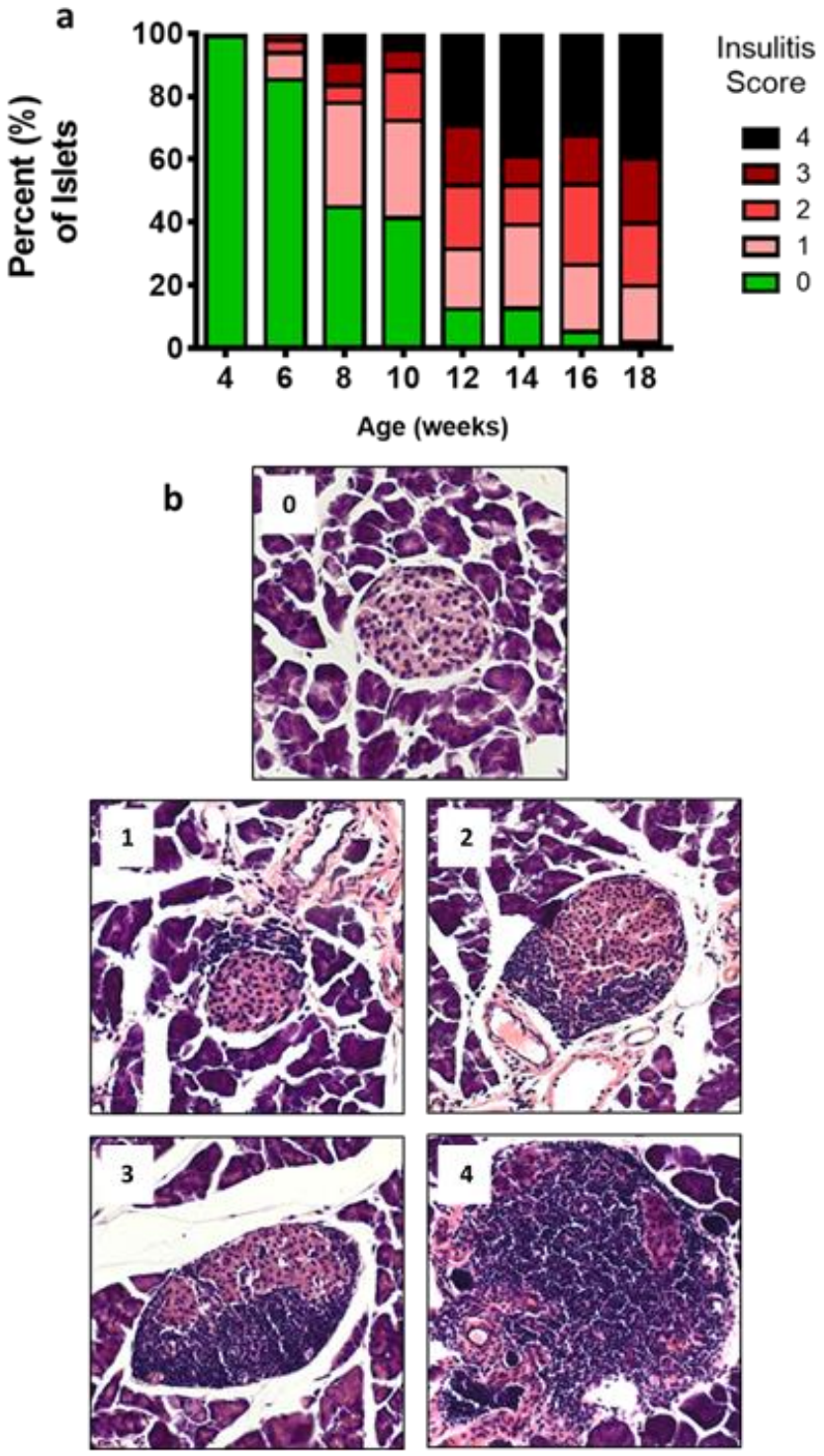

Figure 3-10. NOD insulitis scores

(a) Percentage of islets scored as 0 (no insulitis), 1 (peri-insulitis with up to 25% infiltration), 2 (25-50% infiltration), 3 (50-75% infiltration), or 4 (>75% infiltration). Percentages were based on H&E stained islets from four mice at each time point, with multiple layers being analysed. (b) Representative photos of islets with insulitis scores of 0, 1, 2, 3 or 4. N = 4 mice per time point. Total islet numbers used for calculations = 106 (4wk), 95 (6wk), 145 (8wk), 133 (10wk), 89 (12wk), 64 (14wk), 133 (16wk), 106 (18wk).

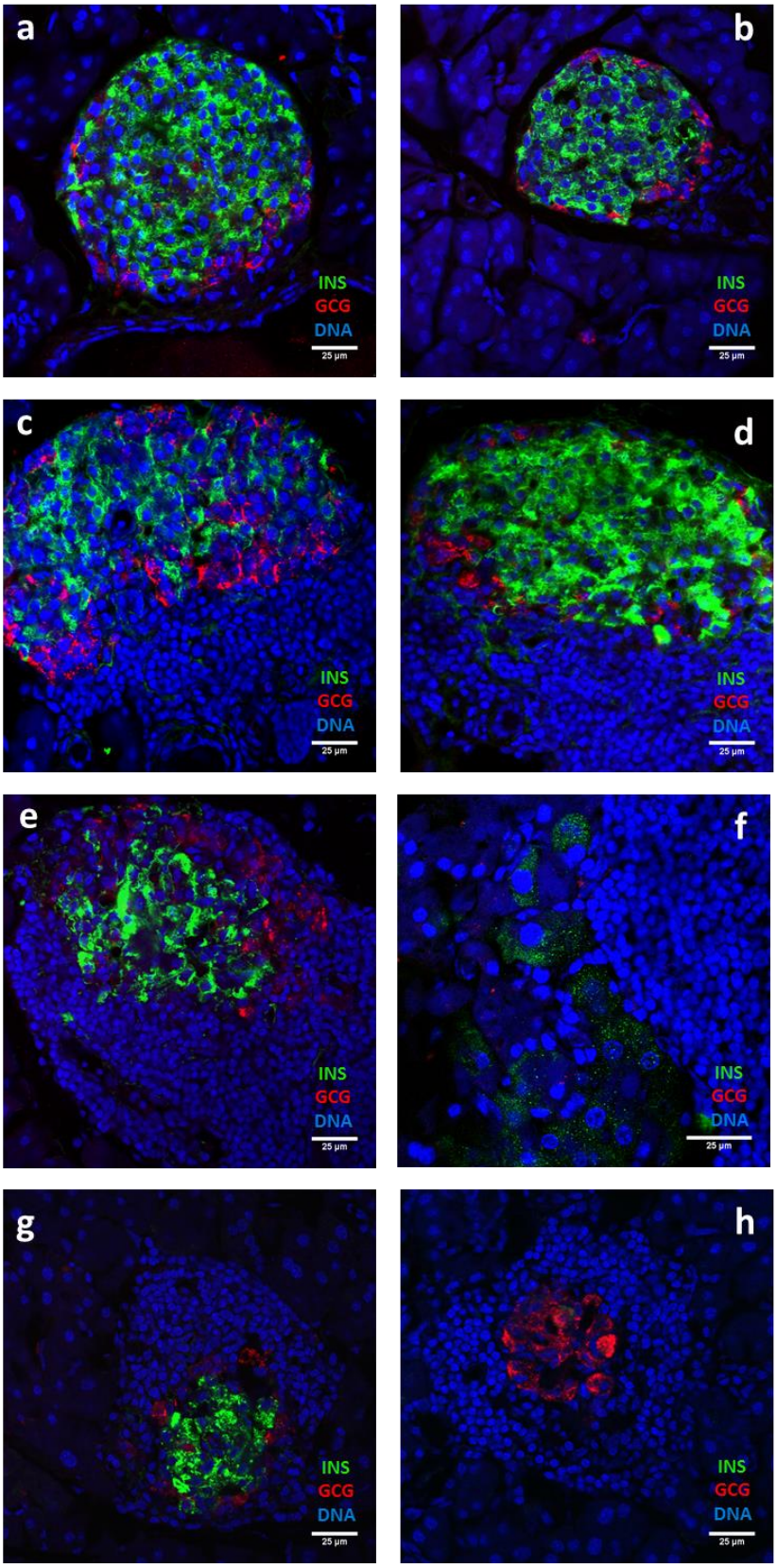

Figure 3-11. Immunostaining of NOD mice islets.

Representative images of insulin (green), glucagon (red) and DNA (blue) stained NOD mice islets at (a) 4, (b) 6, (c) 8, (d) 10, (e) 12, (f) 14, (g) 16, and (h) 18 weeks of age.

3.4.4. Circulating MicroRNAs in NOD Mice

MicroRNA quantitation revealed that a subset of circulating miRNAs was elevated in young NOD mice, prior to significant insulitis and the development of elevated fasting BGLs (Figure 3-12). Due to the abnormally low fasting BGLs of the 16 and 18 week old mice, miRNA abundance trend analysis was conducted both with and without the results from these mice. The overall abundance of these miRNAs decreases over time, with a significant linear trend. The abundance of miR-375, a miRNA that has been identified within the circulation of this mouse model previously (156), can be seen in Figure 3-13. Its abundance spiked in the circulation of mice at 8-weeks of age, although the increase was not a statistically significant one.

Not all circulating miRNAs that were measured demonstrate this pattern of abundance. Figure 3-14 details seven miRNAs that were stable within the circulation of NOD mice throughout all time points. This suggests that the miRNAs identified in Figure 3-12 have an association with the progression to diabetes within this murine model.

Furthermore, to assess whether there was an association between circulating miRNAs and β-cell function, their abundance was compared to the fasting BGL of the same mouse. As above, the abnormal fasting BGL results of the 16 and 18 week old mice necessitated analysis with and without these mice. The correlations were strengthened by omitting data from 16 and 18 week old mice. Interestingly, 17-18 miRNAs were found to have a significant correlation with fasting BGL (Figures 3-15 and 3-16). As with age, the correlation was negative, and so a higher miRNA abundance is indicative of a lower fasting BGL. This strengthens the potential of these miRNAs as indicators or predictors of β-cell function.

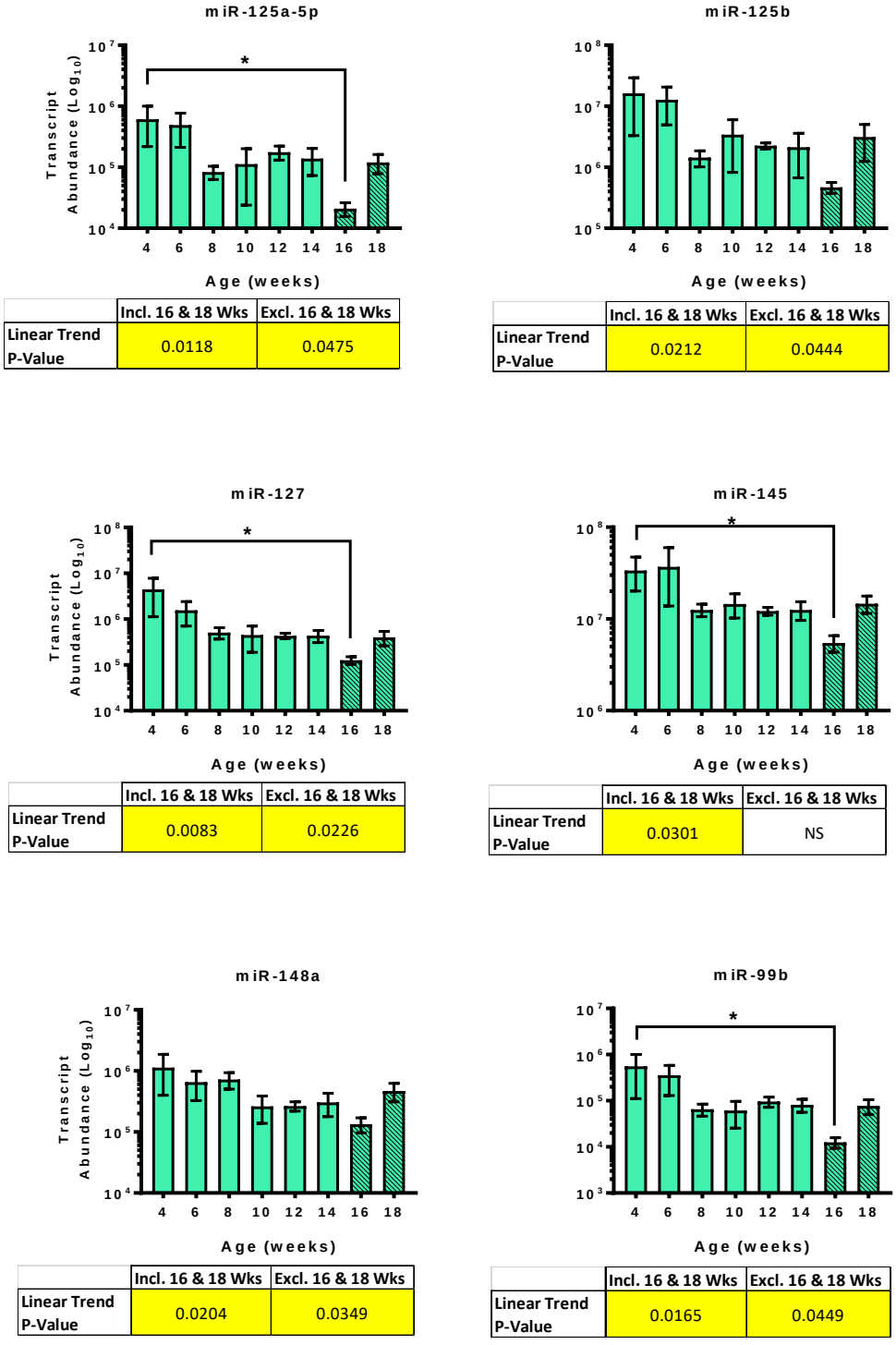

	Incl. 16 & 18 Wks	Excl. 16 & 18 Wks
Linear Trend P-Value	0.0118	0.0475

	Incl. 16 & 18 Wks	Excl. 16 & 18 Wks
Linear Trend P-Value	0.0212	0.0444

	Incl. 16 & 18 Wks	Excl. 16 & 18 Wks
Linear Trend P-Value	0.0083	0.0226

	Incl. 16 & 18 Wks	Excl. 16 & 18 Wks
Linear Trend P-Value	0.0301	NS

	Incl. 16 & 18 Wks	Excl. 16 & 18 Wks
Linear Trend P-Value	0.0204	0.0349

	Incl. 16 & 18 Wks	Excl. 16 & 18 Wks
Linear Trend P-Value	0.0165	0.0449

Figure 3-12.1. Circulating miRNAs change in abundance with age of NOD mice

Circulating miRNAs decrease over time and significantly correlate with age. Mean ± SEM. Linear trend, $P<0.05$ significant. Linear trend P-values are presented below of the respective graph, with the results from 16 and 18 weeks of age included (Incl. 16 & 18 Wks) and excluded (Excl. 16 & 18 Wks). Hatched bars are indicative of omitted groups. N = 4 mice at each time point, except 4 weeks (N=3, see section 3.3.4). * $P<0.05$ (Kruskal-Wallis non-parametric ANOVA with corrected Dunn's multiple comparison test).

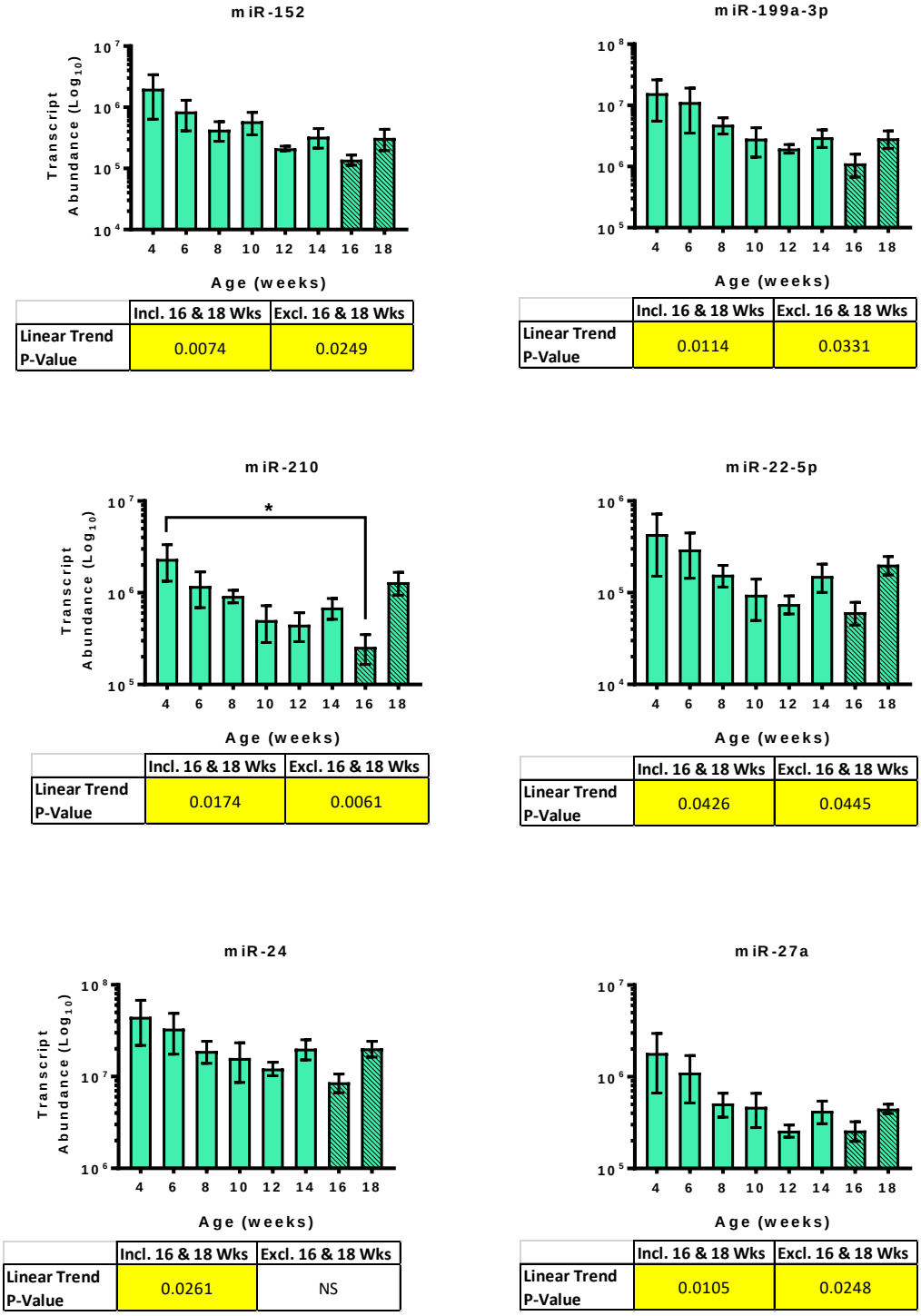

miR-152	Incl. 16 & 18 Wks	Excl. 16 & 18 Wks
Linear Trend P-Value	0.0074	0.0249

miR-199a-3p	Incl. 16 & 18 Wks	Excl. 16 & 18 Wks
Linear Trend P-Value	0.0114	0.0331

miR-210	Incl. 16 & 18 Wks	Excl. 16 & 18 Wks
Linear Trend P-Value	0.0174	0.0061

miR-22-5p	Incl. 16 & 18 Wks	Excl. 16 & 18 Wks
Linear Trend P-Value	0.0426	0.0445

miR-24	Incl. 16 & 18 Wks	Excl. 16 & 18 Wks
Linear Trend P-Value	0.0261	NS

miR-27a	Incl. 16 & 18 Wks	Excl. 16 & 18 Wks
Linear Trend P-Value	0.0105	0.0248

Figure 3-12.2. Circulating miRNAs change in abundance with age of NOD mice

Circulating miRNAs decrease over time and significantly correlate with age. Mean ± SEM. Linear trend, P<0.05 significant. Linear trend P-values are presented below of the respective graph, with the results from 16 and 18 weeks of age included (Incl. 16 & 18 Wks) and excluded (Excl. 16 & 18 Wks). Hatched bars are indicative of omitted groups. N = 4 mice at each time point, except 4 weeks (N=3, see section 3.3.4). * P<0.05 (Kruskal-Wallis non-parametric ANOVA with corrected Dunn's multiple comparison test).

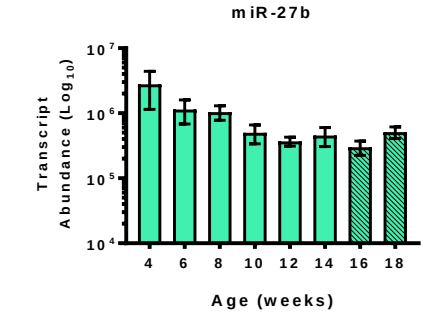

	Incl. 16 & 18 Wks	Excl. 16 & 18 Wks
Linear Trend P-Value	0.0022	0.0077

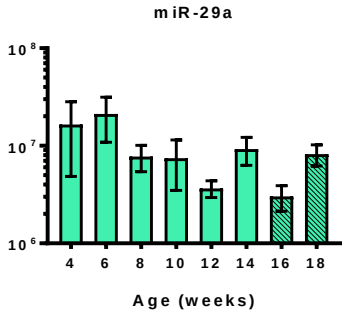

	Incl. 16 & 18 Wks	Excl. 16 & 18 Wks
Linear Trend P-Value	0.0478	NS

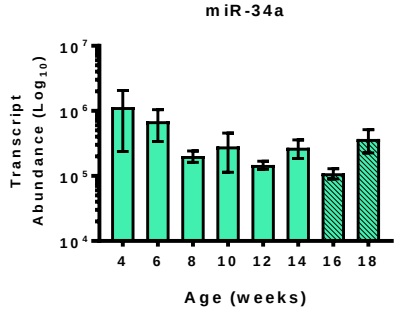

	Incl. 16 & 18 Wks	Excl. 16 & 18 Wks
Linear Trend P-Value	0.0395	NS

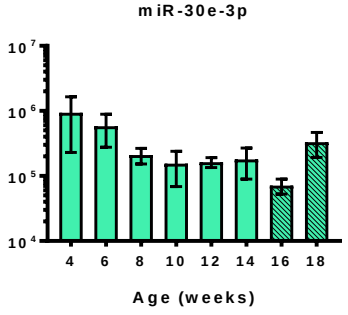

	Incl. 16 & 18 Wks	Excl. 16 & 18 Wks
Linear Trend P-Value	0.0328	0.0360

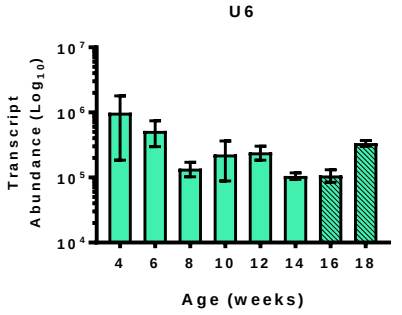

	Incl. 16 & 18 Wks	Excl. 16 & 18 Wks
Linear Trend P-Value	0.0410	0.0417

Figure 3-12.3. Circulating miRNAs change in abundance with age of NOD mice

Circulating miRNAs decrease over time and significantly correlate with age. Mean ± SEM. Linear trend, P<0.05 significant. Linear trend P-values are presented below of the respective graph, with the results from 16 and 18 weeks of age included (Incl. 16 & 18 Wks) and excluded (Excl. 16 & 18 Wks). Hatched bars are indicative of omitted groups. N = 4 mice at each time point, except 4 weeks (N=3, see section 3.3.4).

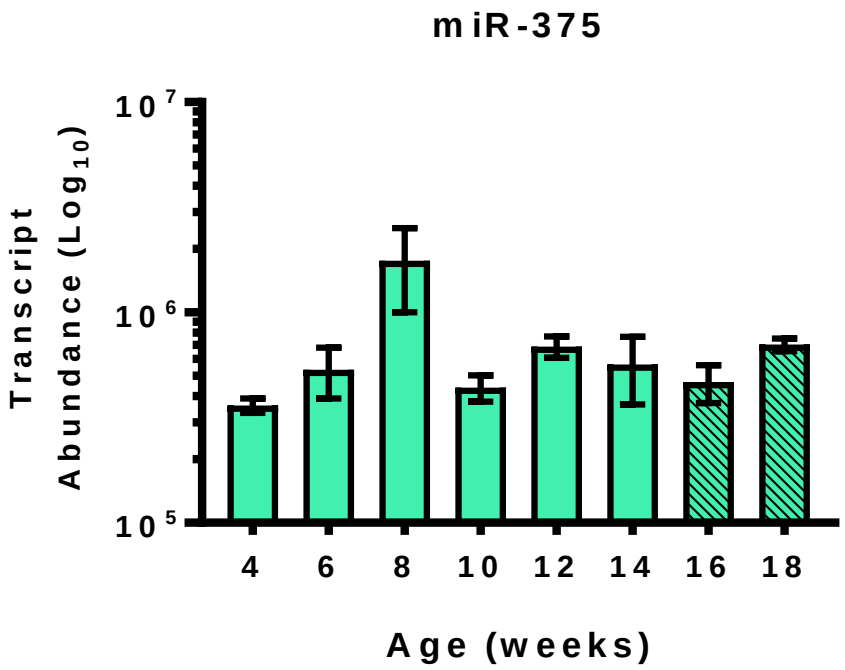

Figure 3-13. MicroRNA-375 abundance peaks at eight weeks of age.

Mean ± SEM. N = 4 mice at each time point, except 4 weeks (N=3, see section 3.3.4). Hatched bars are indicative of groups omitted from other analyses.

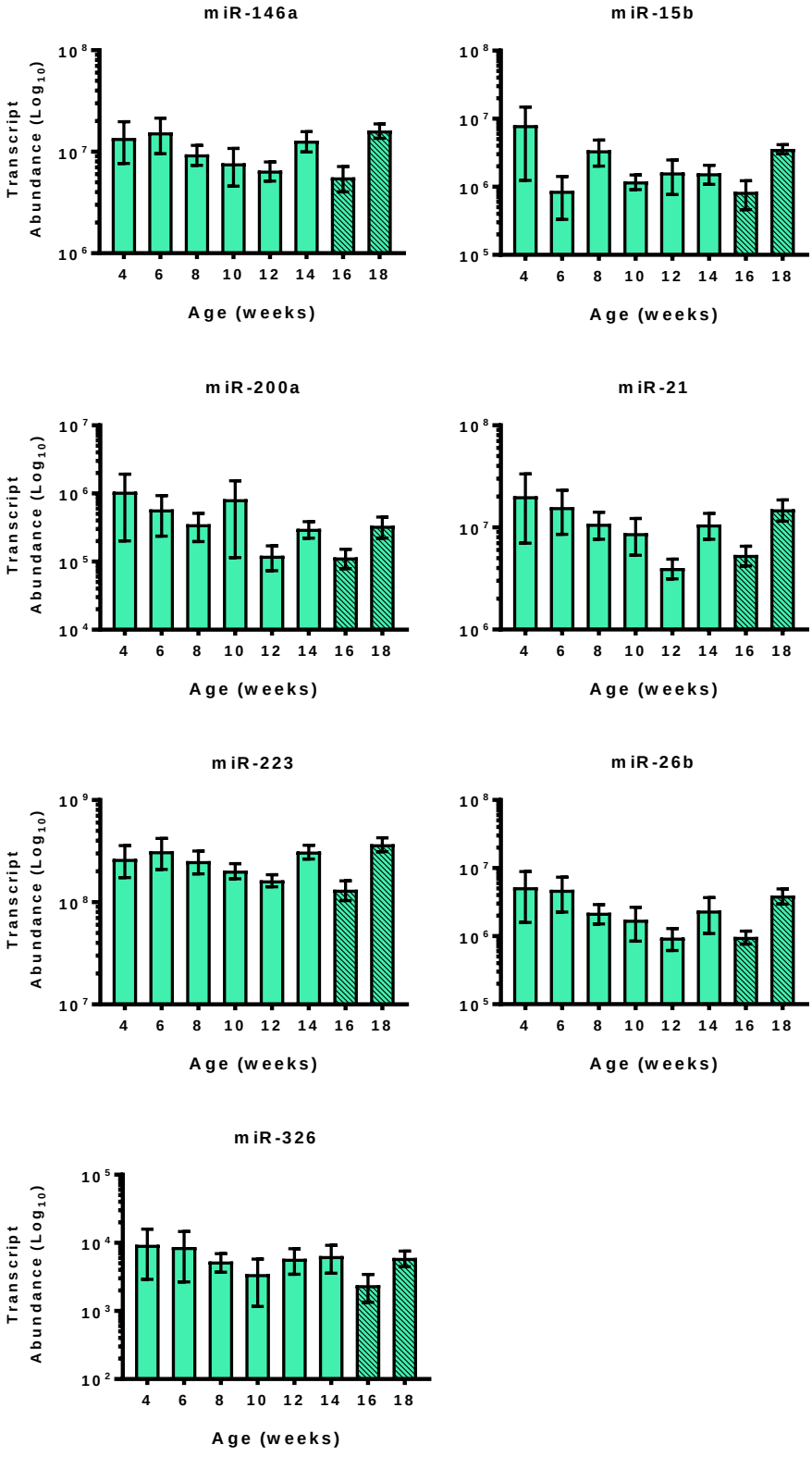

Figure 3-14. Other circulating miRNAs are stable in NOD mice

Seven of the miRNA tested show no significant differences or trends between age groups of NOD mice (with or without omitted groups). Mean ± SEM. N = 4 mice at each time point, except 4 weeks (N=3, see section 3.3.4). Hatched bars are indicative of groups omitted from other analyses.

Including 16 & 18 Weeks

miRNA	Spearman R	P-Value
miR-210	-0.55	0.0013
miR-27b	-0.55	0.0014
miR-199a-3p	-0.51	0.0034
miR-148a	-0.48	0.0058
miR-93	-0.46	0.0100
miR-20a	-0.44	0.0144
miR-22-5p	-0.44	0.0138
miR-186	-0.42	0.0185
miR-30e-3p	-0.41	0.0236
miR-103	-0.40	0.0269
miR-16	-0.39	0.0323
miR-27a	-0.39	0.0324
miR-127	-0.37	0.0434
miR-26b	-0.37	0.0430
miR-30b	-0.37	0.0418
miR-25	-0.36	0.0469
miR-409-5p	-0.36	0.0446

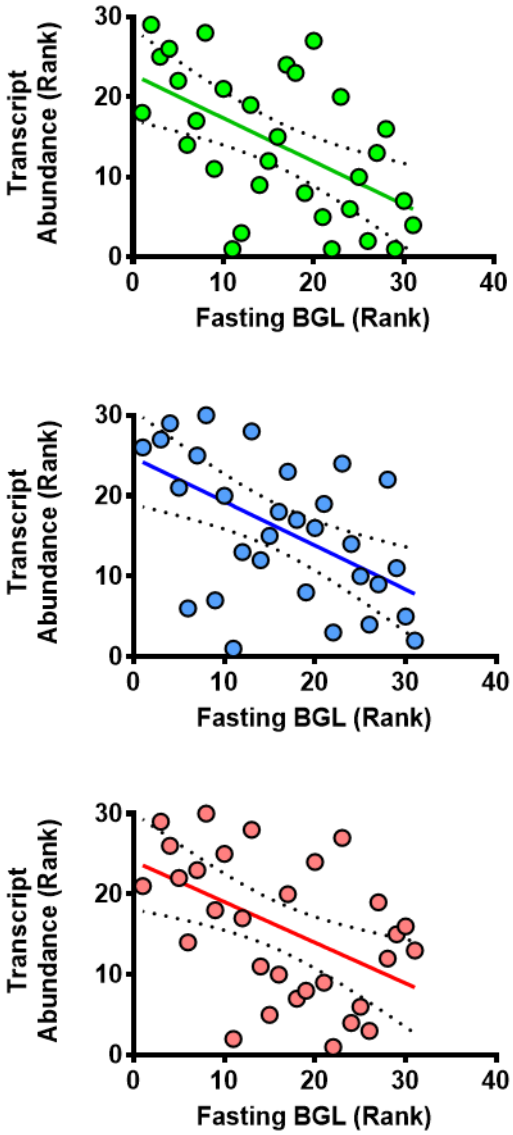

Figure 3-15. Circulating microRNAs correlate with fasting blood glucose in NOD mice

(a) 17 miRNAs were found to significantly correlate with the fasting BGLs in NOD mice. (b) Three representative miRNAs were plotted against the respective fasting BGL using Spearman ranks. Colours correspond to highlighted miRNAs in (a). The line of best fit (solid) with 95% confidence interval (dotted) is shown. N = 27 mice. Spearman correlation, significance P<0.05.

Excluding 16 & 18 Weeks

miRNA	Spearman R	P-Value
miR-210	-0.72	0.0001
miR-27b	-0.64	0.0010
miR-148a	-0.56	0.0054
miR-93	-0.56	0.0059
miR-199a-3p	-0.55	0.0064
miR-186	-0.53	0.0090
miR-22-5p	-0.53	0.0087
miR-20a	-0.52	0.0110
miR-103	-0.49	0.0189
miR-16	-0.49	0.0184
miR-30b	-0.48	0.0216
miR-25	-0.45	0.0305
miR-30e-3p	-0.45	0.0305
miR-27a	-0.44	0.0353
miR-126	-0.43	0.0401
miR-26b	-0.43	0.0427
miR-127	-0.42	0.0433
miR-152	-0.42	0.0460

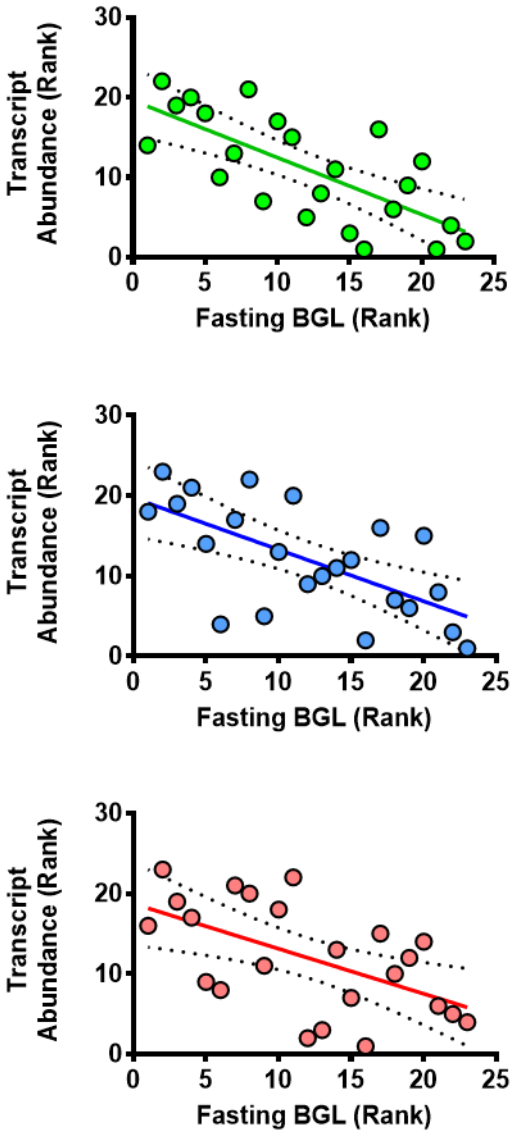

Figure 3-16. Circulating microRNAs demonstrate stronger correlation with fasting blood glucose in NOD mice with 16 and 18 week old groups omitted

(a) 18 miRNAs were found to significantly correlate with the fasting BGLs in NOD mice. (b) Three representative miRNAs were plotted against the respective fasting BGL using Spearman ranks. Data from 16 and 18 week old mice were omitted. Colours correspond to highlighted miRNAs in (a). The line of best fit (solid) with 95% confidence interval (dotted) is shown. N = 27 mice. Spearman correlation, significance P<0.05.

3.5. Discussion

In vitro and *in vivo* models are often utilised to understand and investigate the intricate molecular mechanisms underlying human diseases, such as T1D. They allow researchers to view aspects of disease progression, and its potential molecular mechanisms, in a controlled environment. Within this chapter, two models were used to investigate the central pathophysiology of T1D: β-cell death and immune infiltration. While it must be noted that models such as these may not always translate well to the human condition, they are a cogent starting point that inform subsequent clinically-focused investigations (Chapters 4 and 5).

3.5.1. Replicating Islet Cell Death *In Vitro*

To replicate islet cell death, primary human islets were cultured in the presence of SNP. As this compound is metabolised, it first releases nitric oxide and then subsequently hydrogen peroxide, both of which have been identified as the cause of SNP's apoptotic properties (192; 193). SNP has been utilised for over 20 years to cause cell death in pancreatic islets, with NO highlighted as the causative agent in these cells (192). Indeed, streptozotocin (STZ), a compound with selective β-cell toxicity used to initiate diabetes in animal models, may also function through the generation of NO (195).

SNP was selected to induce islet cell death over more selective β-cell toxins, such as STZ and alloxan, as the investigation was focused on the response of cellular stress and death of the entire islet. While β-cells are the clear victim of immune-mediated T1D, the surrounding cells must also undergo cellular stress as they are caught in the metaphorical cross-fire. Indeed, a reduction of α-cells in patients with T1D (especially fulminant T1D) has been demonstrated previously (196). In support of this, the majority of T1D-associated antigens, such as ICA and GAD, have been found on all endocrine cells, rather than just β-cells (197). Furthermore, STZ

and alloxan both gain entry to β-cells through the GLUT2 transporter; rodent β-cells have an abundance of GLUT2, while human β-cells predominantly utilise GLUT1 (198). This may explain the documented resistance of human islets to STZ-mediated β-cell death (199).

As shown within this chapter, SNP exposure results in significant cell death, with the islets exhibiting morphological signs of apoptosis, such as blebbing (Figure 3-1). An increase in DNA fragmentation and hypodiploid nuclei (Figure 3-2) – a marker of cell death – was also demonstrated, mirroring previous studies (192). The highest concentration, 10 mM, caused rapid cellular disintegration and DNA fragmentation (Figure 3-2f), highlighting the cytotoxicity of SNP at this concentration.

3.5.2. *In Vitro* MicroRNA and Cell-free DNA Release

The cellular stress and death that resulted from SNP exposure caused the release of both miRNAs and cfDNA into the surrounding supernatant (Figures 3-3 and 3-6). Twenty-seven miRNAs displayed a significant, dose-dependent release at 1 and 10 mM, however, the cellular abundance of these miRNAs was only reduced in those islets exposed to 10 mM SNP (Figure 3-4). This suggests that 1 mM SNP initiated an active cellular release of these miRNAs, while 10 mM caused leakage of miRNAs due to a significant rupturing of the plasma membrane. Some of these miRNAs have been identified as important for islet development and function, such as miR-375 (101) and miR-7 (83), while others, such as miR-92a, have not. Whether these miRNAs have a previously unknown islet function, or are only released in response to stress, requires additional investigations. As these 27 miRNAs are stable after active and passive release into the extracellular environment, they display immense potential as biomarkers of islet stress and islet death.

Interestingly, it was only a subset of miRNAs that exhibited a significant, dose-dependent release. Other ncRNAs, such as those outlined in Figure 3-5, are either not released due to islet stress/death, or are rapidly degraded upon exiting a cell. The former explanation is more likely, as miRNAs display impressive stability once outside the cell (discussed in Section 1.5.1.). Two of these are the commonly used "housekeeping" small nucleolar (sno)RNAs, U6 and RNU44. Both of these snoRNAs are highly expressed within animal cells, and so it is intriguing that their extra-cellular abundance did not increase in response to cell death. This gives weight to the notion that the release of specific miRNAs can be used as a signature of islet cell stress/death.

Methylated and unmethylated cell-free *Ins* DNA displayed a slightly different pattern of release. Both cfDNA species increased their copy numbers within the supernatant after human islets were exposed to 1 mM SNP, however 10 mM caused them to plateau (unmethylated) or decrease (methylated), suggesting subsequent degradation (Figure 3-6). The immense cell death evident after 24 hours in 10 mM SNP is likely to have released the entirety of the cellular contents of a large number of islet cells into the extracellular milieu. Unlike miRNAs, cfDNA is not complexed with microvesicles, apoptotic bodies or lipoproteins; this leaves it vulnerable to degradation by endogenous nucleases. This conclusion correlates with previous studies that have found cfDNA's half-life to be exceptionally short (minutes to hours) within the peripheral circulation (163; 164). Alternatively, the release of cfDNA may reach a saturation threshold, causing a plateu of cfDNA abundance in cells treated with ≥1mM SNP.

3.5.3. Modelling Immune Infiltration and T1D Progression

Since its generation in 1980 (173), the NOD mouse model has been extensively used to investigate the progression of autoimmune diabetes. These mice develop extensive immune

infiltration and spontaneously exhibit polyuria, hyperglycaemia and lowered plasma insulin concentrations around 12 weeks of age (173). Interestingly, the incidence of diabetes is highly variable within this model. Unlike humans, there is a clear link between the incidence of diabetes of the sex of the NOD mouse; 80-90% of female mice develop diabetes, while only 30-40% of males develop the disease (173). Due to this, most studies, including the one outlined within this chapter, utilise female NOD mice to ensure high disease incidence. Numerous other factors influence the disease penetrance in this model, including the intestinal microflora (200), temperature (201), diet (202), and even sleep (203).

To ensure that all NOD mice used in this study had the same risk of developing diabetes, all variables were kept constant; four mice were housed in each cage, the cages were placed next to one another in the middle of the rack to minimise temperature variation, and the mice all had unrestricted access to normal chow and non-sterile water. Despite this, a reduction in fasting BGL was seen at 16 and 18 weeks of age, although it was not significantly different to 12- and 14-weeks of age (Figure 3-9). Indeed, the removal of these results strengthened the correlation between circulating miRNAs and fasting BGLs (Figures 3-15 and 3-16). The NOD mice detailed in this chapter demonstrated extensive insulitis (Figure 3-10), commencing around 6-weeks of age, and a significant increase in fasting BGL at 12-weeks of age (Figure 3-9), mirroring previous reports (173). A limitation of this study, however, was the use of a single investigator to grade to insulitis, with no data on reproducibility. Despite the variability of disease incidence seen in this animal model, the results outlined here support its use as a model of T1D.

3.5.4. Circulating MicroRNAs and B-cell Function

NOD mice represent an exciting model to investigate the change in circulating miRNAs during the progression to T1D. Despite the many differences between mice and man, miRNAs display an impressive conservation between animal species (204). Due to this, the majority (86%) of the miRNAs that were investigated in NOD mice have homologs in humans.

Technical limitations meant that the study described here was conducted in a cross-sectional manner, however, these results give an insight into circulating miRNA abundance as these mice progress to autoimmune diabetes. Seventeen miRNAs were found to be elevated in the circulation of 4-week old NOD mice and subsequently declined over time (Figure 3-12). Indeed, these miRNAs demonstrated a significant linear trend. As these mice get older, their risk of developing diabetes increases (173), and so these miRNA present as possible markers of progression to T1D. Interestingly, these miRNAs were elevated prior to any evidence of insulitis, which began around 6-weeks of age, and elevated fasting BGL, which was significantly higher by 12-weeks of age. While circulating miRNA abundance may be influenced by age (205), the short duration of the study (14-weeks) and the genetic predisposition of this mouse model, point to minimal confounding age-linked effects. Furthermore, miRNA-375 demonstrated a spike in abundance at 8-weeks, prior to the elevation of fasting BGL. Although it was not a significant increase, it reflects an earlier study that identified elevations of this miRNA in the circulation of NOD mice prior to the onset of diabetes (156).

Not all miRNAs demonstrated changes in abundance over time. Seven miRNAs presented here (Figure 3-14) remained stable within NOD circulation at all time points. As with the islet SNP experiments discussed above, these unchanged miRNAs give weight to the notion that specific

miRNAs within circulation can be used as a signature of islet cell stress/death and the progression to autoimmune diabetes.

To assess the β-cell function of NOD mice, the fasting BGL was recorded. Eighteen miRNAs demonstrated a significantly negative correlation with fasting BGL (Figure 3-16). This indicates an association with these miRNAs and β-cell function within this model. Whether these miRNAs directly affect β-cell function or are simply a reflection of it remains to be confirmed. Either way, these miRNAs have potential as markers of β-cell function.

3.6. Conclusions

The use of *in vitro* and *in vivo* models has assisted in the identification of interesting miRNAs in the progression of T1D. Here, we confirm that SNP-mediated β-cell stress/death causes the release of 27 candidate miRNAs (Aim 1). Insulin cfDNA is also released in response to SNP exposure, however it seems to be rapidly degraded at the highest SNP concentration (Aim 1). Circulating miRNAs are also found to be elevated in plasma of NOD mice prior to the presence of insulitis and glycaemic dysfunction. These miRNAs (N=17) continued to decrease through the increasing age groups, with a significant negative correlation between miRNA abundance and age (Aim 2). Additionally, there is an association evident between circulating miRNAs in NOD mice and fasting blood glucose. Nineteen miRNA demonstrate a negative correlation with fasting BGLs, indicating an association between these markers and β-cell function (Aim 3). Taken together, these data give functional insights into miRNA and cfDNA release and highlights miRNAs that merit further analysis in human clinical cohorts.

4. Characterising a Circulating MicroRNA Signature in Patients with Type 1 Diabetes

4.1. Chapter Overview

Type 1 diabetes is a complex, multi-faceted disease. Despite originating through the destruction of pancreatic β-cells, T1D has an enormous systemic impact upon the individual. Hyperglycaemia, hypoglycaemia and glycaemic variability has been shown to have adverse effects on cultured cells, animal models and in humans and to be associated with increased risk of chronic complications (206-208). T1D chronic complications attest to this; chronic stress within the circulatory and nervous systems result in significant damage to numerous organs and tissues. This widespread stress may cause additional miRNAs to be released into the circulation, even before β-cell death or diabetes complications may become clinically evident, thus altering the overall miRNA signature measured in circulation. The level of glycaemic control and drugs such as those used to prevent or treat complications may also impact miRNA signatures, but as yet there are few clinical studies to understand such changes.

Within this chapter, the circulating miRNAs from individuals with newly-diagnosed and established T1D, and their age and gender matched controls have been profiled, using a qPCR panel of 754 miRNA assays. Thirty-one miRNAs were found to have differential abundance (fold change >2, P-value <0.05) within the T1D circulation (27 increased, four decreased). These data, along with the previous data outlined in Section 1.7 and the *in vivo* and *in vitro* modelling data discussed in Chapter 3, allowed the identification of 50 candidate miRNAs as circulating markers of β-cell death. Interestingly, less than half of these have been previously identified in the literature in relation to β-cell development or function, supporting the idea that cellular stress outside of the pancreas contributes to the circulating miRNA profile. These

miRNAs then underwent preliminary assessment in a larger clinical cohort of patients with established T1D and their age and gender matched non-diabetic controls. Two of the miRNAs were confirmed to be increased in the circulation of these T1D individuals, while additional subsets were found to associate with residual C-peptide, disease duration and microvascular complications in T1D. This exploratory approach highlights the potential of these miRNAs post-diagnosis.

4.2. Chapter Aims

Studies in this chapter aimed to:

1. identify miRNAs that have differential abundance within the circulating plasma or serum of patients with newly diagnosed and established T1D, compared to their age and gender matched controls;
2. compile a signature of miRNAs with potential to reflect β-cell death, and
3. assess these miRNAs in a larger group of individuals with established T1D, including any association with clinical characteristics such as residual C-peptide, disease duration and the presence of microvascular complications.

4.3. Methods

4.3.1. Sample Cohorts

Six serum samples from patients with newly diagnosed T1D, as well as further six age and gender matched control subjects, were kindly provided by Professor Maria Craig. Samples were taken ≤5 days after T1D diagnosis. Plasma samples from patients with established T1D (N=183, mean disease duration 20 years) and age and gender matched controls (N=141) were kindly provided by Professor Alicia Jenkins. A subset of these were used for the initial miRNA profiling (N=3 from each group). Differentially abundant miRNAs in newly-diagnosed and/or long-standing T1D circulation were selected for further analysis.

4.3.2. RNA Isolation

RNA was isolated using the manual method outlined in Appendix B. RNA concentration and purity was assessed using a spectrophotometer.

4.3.3. C-peptide

C-peptide levels were carried out by Dr. Andrzej Januszewki (NHMRC CTC, Sydney Australia) using the ultra-sensitive ELISA (Mercodia), with a detection limit of 1.25 pmol/L.

4.3.4. MicroRNA Profiling

MicroRNA profiling was undertaken using OpenArray Human miRNA qPCR Panels (Applied Biosystems) utilising the protocol published previously. To remove non-specific amplification, assays with an AMP score <1.24 were omitted. Data were normalised using the global normalisation method (209). Differential abundance was classified as a >2-fold change with a P-value <0.05. The newly diagnosed and established T1D groups were analysed separately to avoid confounding the results.

4.3.5. Candidate MicroRNA Assessment

The 50 candidate miRNAs were assessed using Custom OpenArray miRNA qPCR panels (Applied Biosystems) using the protocol outlined in Appendix D. To remove non-specific amplification, assays with an AMP score <1.24 were omitted. Data was normalised to the RNA isolation and RT ath-miR spike-ins. For details of these, please refer to Supplementary Chapter 1. All changes between groups were required to differ by at least one cycle, regardless of the statistical significance, as this is the smallest difference detectable by qPCR.

4.3.6. Data Presentation and Statistical Analysis

MicroRNA profiling results are presented using a volcano plot (Figure 4-2), with >2-fold change (or 1 cycle difference) and $P<0.05$ regarded as a significant change.

To compare miRNA abundance between groups, the normalised CRT values of both groups were investigated. The average difference between groups had to exceed one cycle (or a doubling of the amplicon), as this is the minimum difference that qPCR can detect. Significant differences were identified using a t-test on any group comparisons with a >1 CRT difference. MicroRNAs displaying a significant difference between groups ($P<0.05$) were presented as transcript abundance using the fold over detectable method (limit of detection is 39 cycles) described earlier (190). Due to the exponential nature of this method, differences were confirmed using the non-parametric Mann-Whitney U-test with significance deemed $P<0.05$. An overview of this procedure can be found in Figure 4-1. Correlations were assessed using non-parametric Spearman method, with significance $P<0.05$. No corrections were made for multiple comparisons, as this chapter has an exploratory focus and so strives to minimise type II (false negative) errors.

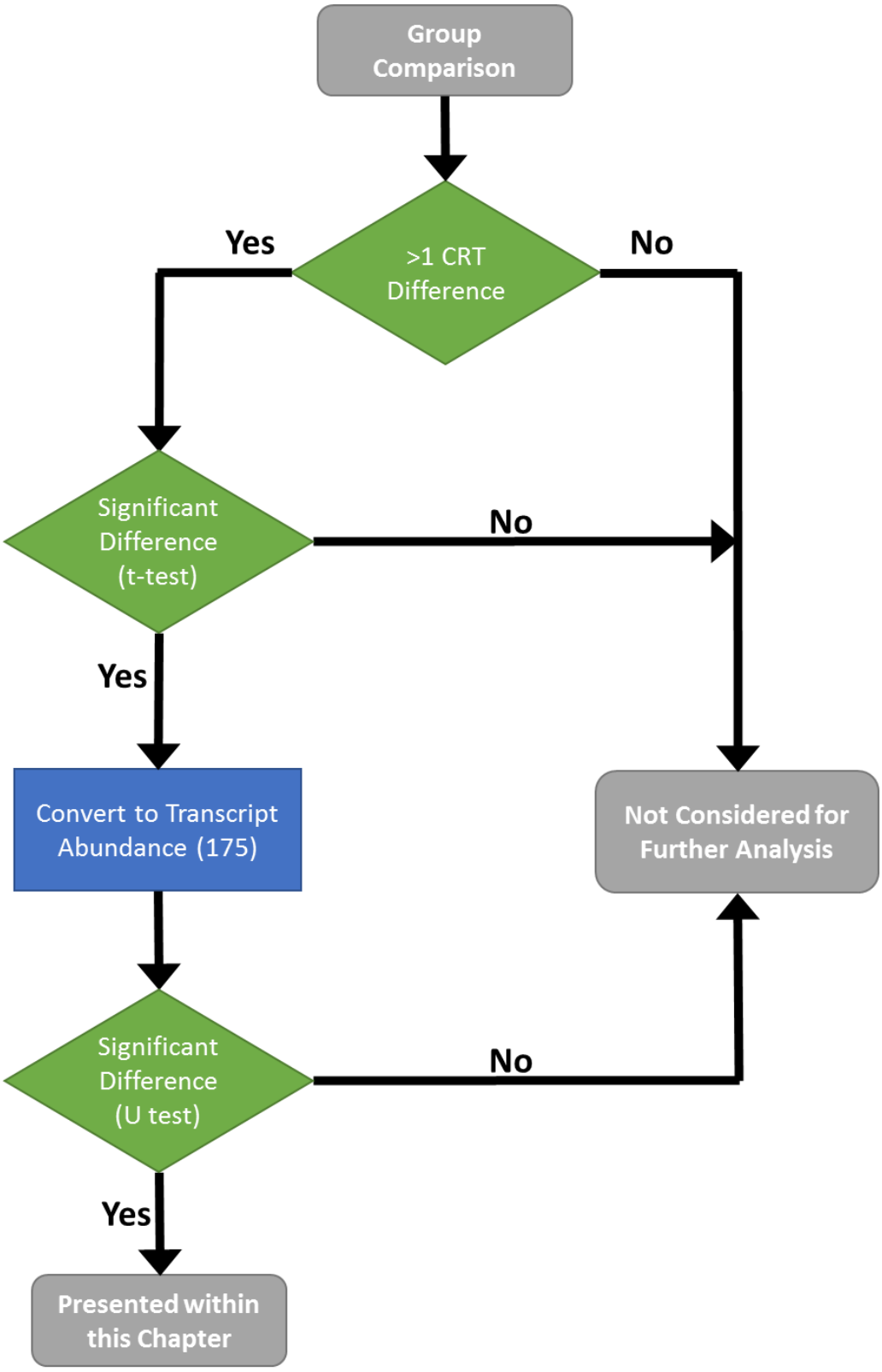

Figure 4-1. Flowchart for data analysis

Diagrammatical overview of the analytic process of identifying significant differences in miRNA abundance within different groups. U test refers to Mann-Whitney U test as described in Section 4.3.6.

4.4. Results

4.4.1. Differential MicroRNA Abundance in T1D Circulation

MicroRNA profiling of serum and plasma samples from individuals with newly diagnosed or established T1D (ND-T1D and E-T1D respectively) revealed 31 miRNAs that were either increased or decreased within T1D circulation (ND-T1D and/or E-T1D circulation) compared to age and gender matched controls. The majority of these (27 miRNAs) were increased, suggesting that they were released as a result of the cell stress/death that is associated with T1D. Figure 4-2 provides an overview of all detectable miRNAs, including those with significantly different abundance. In Figure 4-2b, three miRNAs with the largest or most significant changes are plotted.

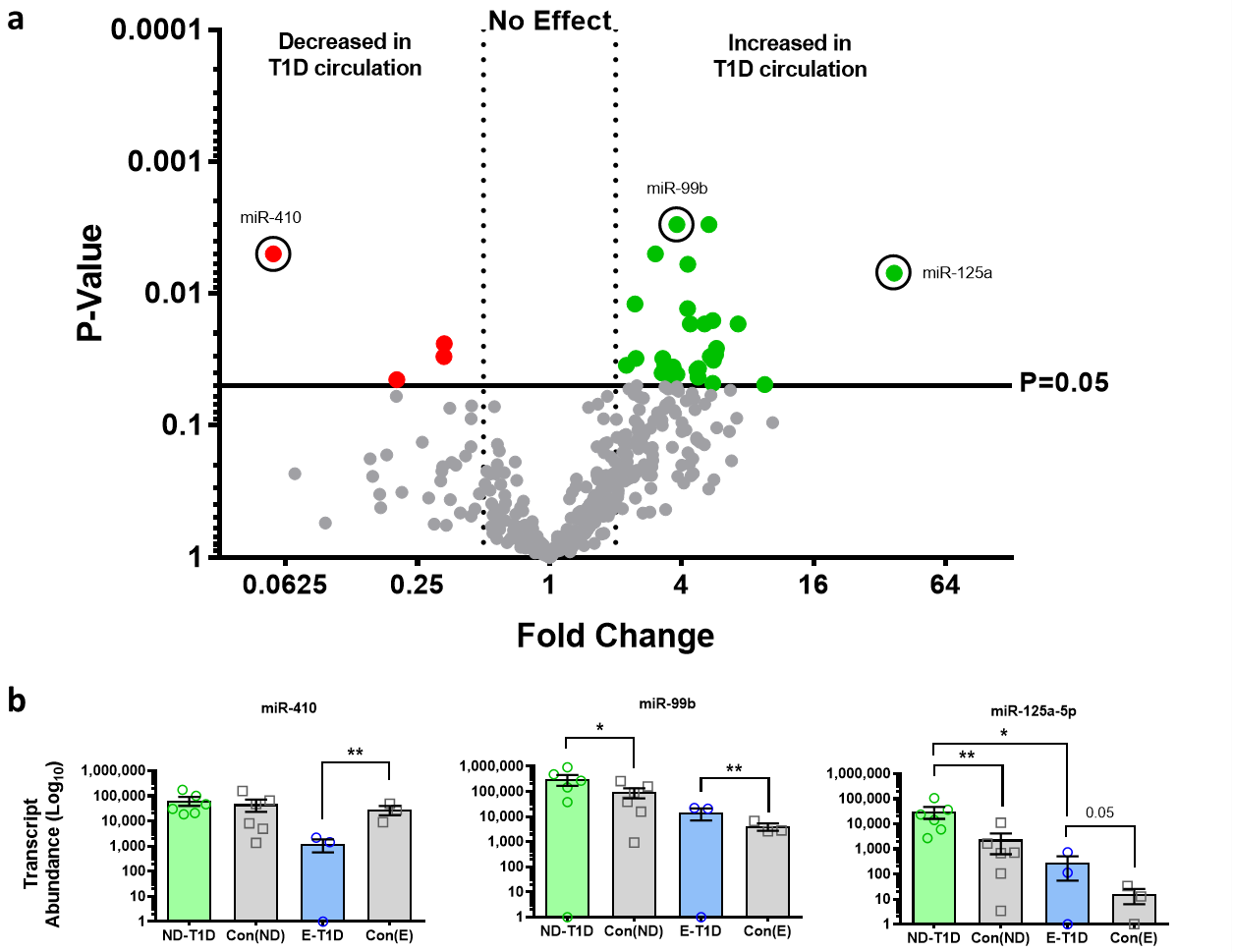

Figure 4-2. Circulating microRNA profiling of patients with T1D

(a) Volcano plot of differentially abundant miRNAs measured within the circulation of patients with newly-diagnosed (ND-T1D) and established (E-T1D) T1D, compared to age and gender matched controls (Con(ND) and Con(E) respectively). Dotted line = 2-fold change. (b) Subset of significant miRNAs highlighted in (a) with newly diagnosed T1D and controls in green and established T1D and controls in blue. Mean ± SEM. N = 9 T1D (6 ND-T1D, 3 E-T1D), 9 Control (6 ND-Con, 3 E-Con). * P<0.05, ** P<0.01.

MicroRNA-410 was significantly decreased in the individuals with established T1D, but not the newly diagnosed T1D group. The other miRNAs, miR-99b and miR-125a, show an increase in the circulation of both ND-T1D and E-T1D compared to the age and gender matched controls.

Based on the results outlined above, in combination with the previously generated data (discussed in section 1.8), a list of 50 candidate miRNAs was generated (Table 1-A).

4.4.2. Assessment of Candidate MicroRNAs in Patients with Established T1D

As a preliminary assessment of this miRNA signature, the levels of these miRNAs were quantified within the plasma of 180 individuals with established T1D and 138 age and gender controls. The group characteristics are outlined in Table 4-B.

Table 4-B. Cohort summary of patients with established T1D and their age and gender matched non-diabetic controls

	T1D	Controls	P-value
N	180	138	-
Females, %	61	51	ns[a]
Age, yrs (mean ± SD)	38.9 ± 1.05	39.0 ± 1.26	ns[b]
T1D Duration, yrs (mean ± SD)	20 ± 13	-	-
HbA1c (mean ± SD)	8.0 ± 1.3% 64.4 ± 14.7 mmol/mol	5.1 ± 0.4% 32.7 ± 3.9 mmol/mol	<0.0001[b]
Microvascular Cx, N	58	-	-

[a] Chi-square test
[b] T-test

Within the T1D group, 58 individuals (32.2%) presented with microvascular complications (Cx), defined as proliferative retinopathy and/or increased albuminuria.

Two miRNAs, miR-146a and miR-22-5p, were confirmed to be elevated in the circulation of subjects with established T1D (Figure 4-3). Interestingly, only miR-146a has been previously reported as differentially abundant in T1D circulation (154).

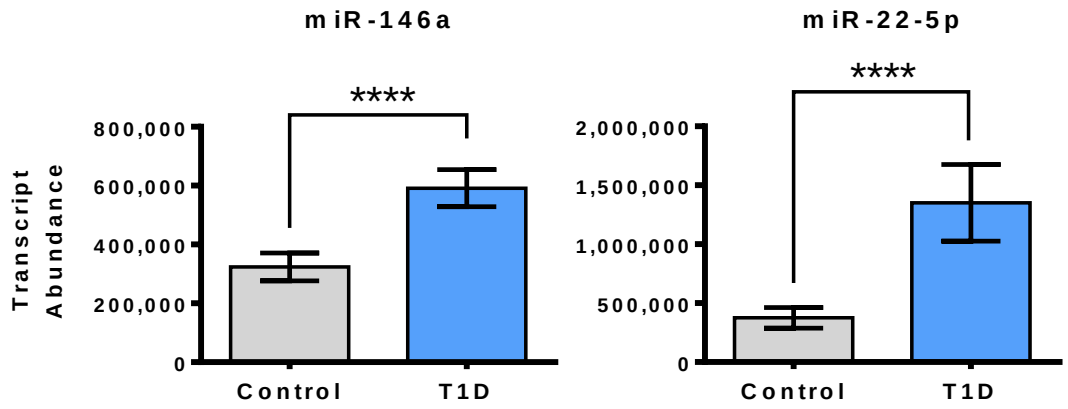

Figure 4-3. MicroRNAs are elevated in T1D circulation

Two miRNAs were found to be significantly elevated in the circulation of individuals with established T1D compared to age and gender matched controls. N = 138 controls, 180 T1D. **** P<0.0001. Mean ± SEM.

4.4.3. Circulating MicroRNAs Differ with C-peptide and HbA1c Status

C-peptide levels were measured as an indicator of residual β-cell function. Controls subjects had an average C-peptide concentration of 559.5 ± 245.4 pM, while T1D subject had 29.3 ± 87.6 pM (P<0.0001, unpaired t-test with Welch's correction). Due to the use of an ultra-sensitive ELISA, C-peptide was detectable in 123 of the T1D subjects. Five miRNAs were found to be significantly elevated in the circulation of T1D subjects with detectable C-peptide as compared against those with no detectable C-peptide (Figure 4-4). Furthermore, eight miRNAs

had a significantly positive correlation with detectable C-peptide concentrations in T1D subjects (Table 4-C). MicroRNA-222 and -99b were found be to both significantly elevated in those with detectable C-peptide and positively correlate with the levels, indicating an association between these miRNAs and β-cell function. No correlation between miRNA abundance and C-peptide level was found in control subjects.

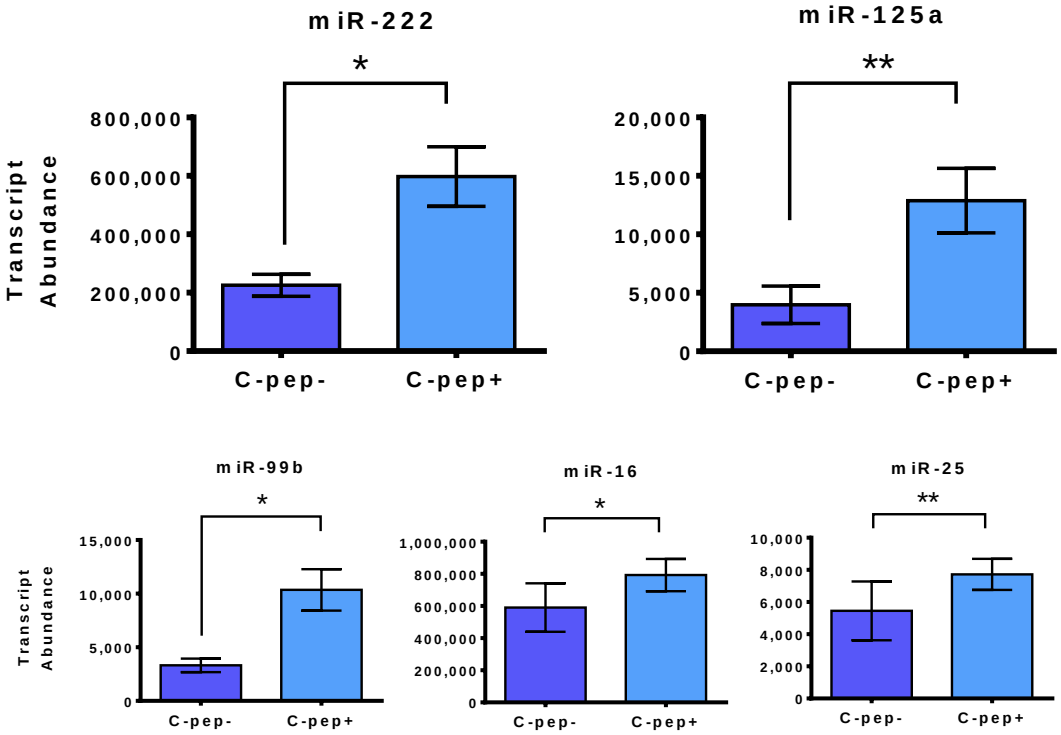

Figure 4-4. MicroRNAs differ by C-peptide status

Five miRNAs were significantly elevated in the circulation of T1D patients with detectable C-peptide (C-pep+), compared to those without detectable C-peptide (C-pep-). N = 53 C-pep-, 123 C-pep+. Mean ± SEM.

Table 4-C. MicroRNAs positively correlate with detectable T1D C-peptide levels

miRNA	Spearman R	P
miR-375	0.32	0.00027
miR-24	0.21	0.021
miR-93	0.21	0.016
miR-21	0.19	0.035
miR-22-5p	0.19	0.035
miR-99b	0.18	0.045
miR-222	0.18	0.044
miR-92a	0.18	0.048

Spearman correlation, P<0.05 significant. N = 123.

HbA1c levels were measured as an indicator of glycaemic variability. As expected, there was a significant difference in the HbA1c levels of the Control and T1D subjects (Table 4-B). Three miRNAs displayed a significant negative correlation with the HbA1c levels of the control subjects (Table 4-D). Interestingly, one of these, miR-25, displayed a similar correlation in T1D subjects. MicroRNA-375 displayed a significant positive correlation with the HbA1c levels of T1D subjects.

Table 4-D MicroRNAs correlate with HbA1c levels in control and T1D subjects

Group	miRNA	Spearman R	P
Control	miR-25	-0.34	0.0001
Control	miR-16	-0.23	0.0094
Control	miR-20a	-0.18	0.046
T1D	miR-25	-0.18	0.022
T1D	miR-375	0.16	0.041

Spearman correlation, P<0.05 significant. Control N =122, T1D N = 168.

4.4.4. Disease Duration and Microvascular Complications

Of the candidate miRNAs outlined in this chapter, eight demonstrate a decreased abundance in T1D subjects that had lived with the disease for greater than 20 years (Figure 4-5). This cut-off point of 20 years was chosen as this was the average disease duration for this group. Additionally, nine miRNAs significantly correlated with disease duration, with all but one decreasing with time post-diagnosis (Table 4-E). MicroRNA-24, -27a, -27b, -93, and -199a-3p were found to both decrease significantly in those T1D subjects with a disease duration >20 years and negatively correlate with disease duration, indicating an association between these miRNAs and the progression of T1D post-diagnosis.

Similarly, seven of the miRNA candidates were decreased in T1D subjects that had microvascular complications (Figure 4-6). The longer that an individual has T1D, the higher their risk of developing associated complications, including those of the microvasculature such as retinopathy. Three of these, miR-27b, -103, and-199a-3p, were previous identified to be significantly reduced in T1D subjects with longer disease duration.

Figure 4-5. Lower circulating miRNAs levels associated with with longer T1D duration

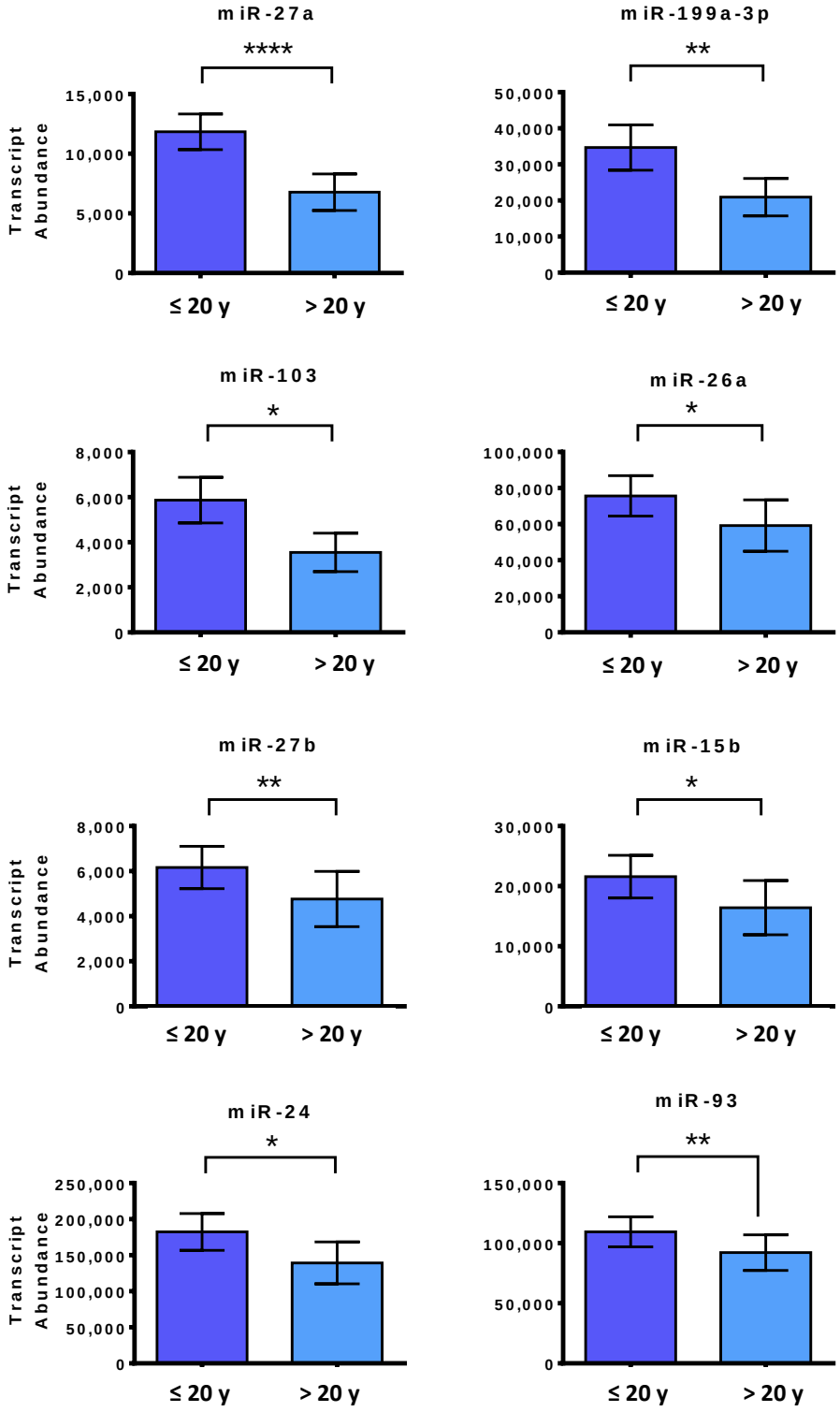

Eight miRNAs have significantly lower abundance in T1D patients with longer disease duration (greater than 20 years post-diagnosis, >20y) compared to those with shorter duration (less than or equal to 20 years post-diagnosis, ≤20y). N = 98 (≤20y), 82 (>20y). * P<0.05 ** P<0.01 **** P<0.0001. Mean ± SEM.

Table 4-E. MicroRNAs correlate with T1D duration

miRNA	Spearman R	P
miR-27a	-0.24	0.0016
miR-199a-3p	-0.19	0.012
miR-146a	-0.18	0.02
miR-93	-0.18	0.015
miR-20a	-0.17	0.023
miR-24	-0.16	0.037
miR-222	-0.16	0.036
miR-27b	-0.15	0.045
miR-126	-0.15	0.046
miR-186	0.17	0.028

Spearman correlation, $P<0.05$ significant. N = 173.

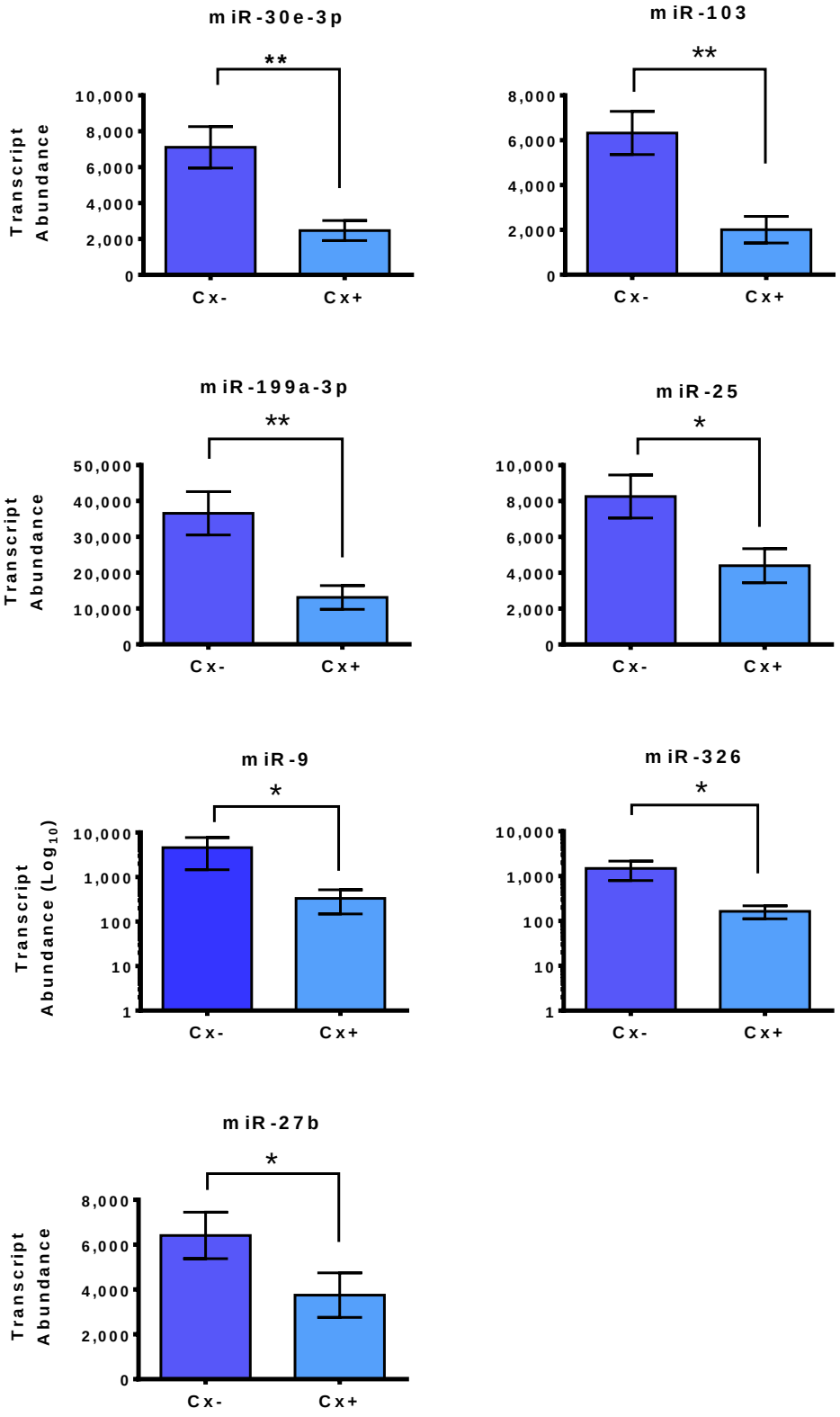

Figure 4-6. Circulating microRNAs are reduced in T1D patients with vs without microvascular complications

Seven miRNAs were significantly reduced in the circulation of T1D patients with microvascular complications (Cx+), compared to those without complications (Cx-). Microvascular complications were defined as proliferative diabetic retinopathy and/or increased albuminuria. N = 117 Cx-, 58 Cx+. Mean ± SEM.

4.5. Discussion

4.5.1. MicroRNA Profiling

Currently, there are over 2,500 mature miRNAs identified within the human genome (miRBase release 21). Due to the enormity of this class of non-coding RNAs, candidate-based approaches, whereby the miRNA/s of interest are decided prior to quantitation, present severe limitations when trying to identify circulating biomarkers. The rise of next generation sequencing has allowed researchers to identify all small non-coding RNAs within a sample, including novel sequences, and so present an unbiased method of ncRNA quantitation. The downside of this technique, however, is its inherent requirement for copious amounts of starting RNA (usually in the order of micrograms). Serum and plasma samples from clinical cohorts are a precious resource; investigators often do not have access to large sample volume to isolate the RNA needed for NGS. Here, 754 miRNAs have been profiled within the serum and plasma of subjects with T1D and their age and gender matched controls using an ultra-high throughput qPCR platform. This allowed the capture of the most abundant and well characterised miRNAs using only 200 ng of RNA isolated from 200 µl of starting sample. Interestingly, these miRNAs do not always show the same difference when examining the ND-T1D and E-T1D groups separately. MicroRNA-410 for example, does not show any difference at the time of diagnosis but is significantly reduced in patients with long-term T1D. This indicates that miR-410 may not be indicative of β-cell death prior to, or at the point of, diagnosis. The resulting data, combined with the data generated from previous experiments, facilitated the identification of 50 miRNAs of interest. These miRNAs have the potential to reflect β-cell death in the progression into T1D as they are important in the development of the human pancreas, and have been seen to be released in *in vitro* islet cell death experiments

and genetically predisposed mouse models. Of course, these miRNAs must be quantitated in other, larger cohorts to fully assess their potential as markers of β-cell death.

Subsequent exploratory assessment of these miRNAs in a larger group of subjects with established T1D and their age and gender matched non-diabetic controls was conducted. This analysis revealed that subsets of these molecules have the potential to not just differentiate between subjects with and without T1D, but also residual β-cell function, disease duration and the presence of microvascular complications. Initial results confirm two miRNAs, miR-22-5p and 146a, were significantly elevated in the circulation of subjects with T1D. MicroRNA-146a has been previously identified with regard to subjects with newly diagnosed T1D (154), although the study was focused upon PBMCs rather than serum or plasma. The authors of this study concluded that miR-146a was decreased in subjects with newly diagnosed T1D, and that its abundance correlated with GADA antibody titres (154). Whether the PBMCs or another cell type are releasing this miRNA into the circulation of individuals with T1D remains to be investigated. Isolating PBMCs from individuals with T1D and culturing them in the presnce of islet antigens would mimic the in situ scenario enabling identification of released miRNAs. The other elevated miRNA, miR-22-5p, has not been the subject of extensive evaluation, presumably due to the fact that until recently it has been known as miR-22*, the antisense or passenger miRNA. This miRNA may present a novel circulating biomarker, however, additional evaluations of this miRNA's abundance in other groups of individuals with T1D must be made.

While these two miRNAs only represent 4% of the original list of candidate miRNAs (Table 1-C), this does not discount the other miRNAs as biomarkers of T1D. As the average disease duration within this cohort was 20 years, the majority of the candidate miRNAs may not be actively released anymore, especially if they were originally released by β-cells. Indeed, the

elevated abundance of these miRNAs two decades after an individual's diagnosis indicates that they are either released from the remaining β-cell fraction still undergoing cell stress/death, or from another cellular source, such as PBMCs, endothelial cells or cardiac muscle (154; 210). In either case, this group provided a preliminary assessment of these candidate miRNAs in subjects with T1D; further analysis of this signature in the progression into T1D will be discussed in the following chapter.

4.5.2. Residual β-cell Function and Glycaemic Variability

C-peptide levels were quantified as a measure of residual β-cell function as it is released in equimolar amounts with insulin. T1D requires the use of exogenous insulin to maintain glucose homeostasis so C-peptide allows an indirect quantitation of endogenous insulin secretion. Due to the increased sensitivity of modern assays, the majority of individuals with T1D were found to be C-peptide positive. Higher miRNA abundance was associated with increased C-peptide expression, and those individuals with detectable C-peptide had significantly higher levels of candidate miRNAs that those without detectable C-peptide. This mirrors what was found in the previous chapter; in NOD mice higher miRNA abundance associated with a lower fasting BGL (Figure 3-14). Indeed, miR-22-5p and miR-93 were both found to significantly correlate with C-peptide concentrations in humans with established T1D, and fasting BGL in NOD mice (positive and negative correlations respectively). Despite the clear association of these candidate miRNAs with β-cell function, no correlation was found with C-peptide levels in non-diabetic control individuals, indicating that these miRNAs may be indirect markers of function rather than directly involved in the manufacturing, processing or secretion of insulin.

Circulating microRNA abundance was also compared to the HbA1c levels, a measure of glycaemic variability. Here, three miRNAs significantly correlated with HbA1c levels in control subjects, and two miRNAs correlated with levels in T1D subjects. Interestingly, one miRNA, miR-25, was found to negatively correlate with HbA1c levels in both control and T1D subjects; therefore, an increase in the miR-25 abundance relects a decrease in HbA1c levels. This miRNA was shown to be significantly increased in T1D subjects with detectable C-peptide (Figure 4-4), and so the decrease in HbA1c levels may be a result of increased insulin secretion. Furthermore, miR-375 was found to have a positive correlation with HbA1c levels, indicating that its increased abundance in circulation may reflect greater β-cell injury or death, a relationship that has been previously reported (156; 157).

4.5.3. Microvascular Complications

Another area of significant interest within diabetes research is the identification of circulation biomarkers of diabetic complications. Complications, such as retinopathy, nephropathy and neuropathy, have dramatic impacts on the quality of life of individuals with T1D, and so early detection and stratification is vital. Understanding of the mechanisms of vascular tissue damage and protection are also of interest, as they may help identify and validate therapeutic targets and/or agents. Within this cohort, seven miRNAs were found to be significantly decreased within T1D subjects with microvascular complications. Of these, three have been previously reported in retinopathy or nephropathy. A recent examination of two T1D retinopathy clinical trials identified a higher abundance of miR-27b within an individual's serum resulted in a decreased risk of developing the condition (OR = 0.67) (211). This finding correlates with the decrease found in the plasma of T1D individuals with microvascular complications outlined in this chapter. MicroRNA-199a-3p has also been implicated in DR, with a decrease of this miRNA found within the retina of STZ-treated rats (212). Again, this is

in line with the findings presented here, and this change within the retina could potentially contribute to the reduction in circulating miR-199a-3p.

A recently published paper has delved into the role of miR-25 in the early stages of diabetic nephropathy (213). Intriguingly, the authors found that the precursor and mature miR-25 was decreased within the glomeruli of STZ-treated C57BL/6 mice, but the primary miRNA was increased. This was found to result from the inhibition of DGCR8 (also known as Pasha), an important RNA binding protein involved in the initial processing of primary miRNA transcripts (see section 1.4.1). The subsequent decrease of this miRNA resulted in an increase in one miR-25's validated targets, NOX4 (213), which has a well-known role in the development of diabetic nephropathy (214). This decrease in the production of mature miR-25 may result in the reduction of circulating miR-25 seen in T1D individuals with microvascular complications.

The other miRNAs identified within this chapter (mir-9, -30e-3p, -103, and -326) have remarkable potential as biomarkers of diabetic complications. Further investigation needs to be completed to confirm the role of these molecules in diabetic complications, including the source tissue. Caution must be applied to miR-103, however, as this miRNA was also identified as reduced in patients who have been living with T1D for longer than 20 years. Longer disease duration can be a risk factor for complications and so any change seen could be from longer duration rather than complications.

4.6. Conclusions

The miRNA profiling and preliminary assessment outlined within this chapter gives credence to the notion that miRNAs have potential as circulating biomarkers in T1D. MicroRNA profiling of circulating plasma/serum samples from patients with newly diagnosed and established T1D, and their age and gender matched controls, highlighted 31 differentially abundant miRNAs. This data, combined with the preliminary data and literature searches (see Figure 1-9), resulted in a list of 50 miRNA candidates being generated. Subsets of these 50 miRNAs had differential abundance when examining T1D and controls, as well as C-peptide levels, disease duration and microvascular complications within the T1D group. These results suggest that these miRNAs have potential as biomarkers of additional aspects of T1D, however, as β-cell death and T1D progression is the focus of this project they will undergo further examination with this focus in the next chapter.

5. Molecular Signature in Type 1 Diabetes Progression

5.1. Chapter Overview

The previous chapters have been focussed upon the different stages in identifying and characterising a circulating signature of various aspects of diabetes, specifically Type 1 diabetes (T1D): identifying the appropriate technology, modelling the disease, and profiling the samples from patients. This chapter is focussed on assessing this molecular signature during the life course of T1D. Samples and related data kindly provided by collaborators, Professors Maria Craig (UNSW, Sydney, Australia), Tim Jones (UWA, Perth, Australia), Alicia Jenkins (University of Sydney, Sydney, Australia) and Kristina Rother (NIH, Bethesda, USA), have allowed the quantitation of the molecular signature in the circulation of 19 individuals at high risk of T1D (prior to diagnosis), 199 subjects at or within 48 hours from clinical diagnosis of T1D, 57 after diagnosis (within 6 weeks and 12 months), and 220 with long-standing T1D (20 years post-diagnosis).

Both unmethylated and methylated *Ins* cfDNA decrease within the circulation of individuals at the point of diagnosis, but then return to levels similar to pre-diagnosis within 6 weeks. Individuals at 20 years after diagnosis, however, show decreased unmethylated and methylated insulin cfDNA abundance. The miRNA signature displays a different profile within high risk individuals and those at the time of T1D diagnosis, when compared to individuals soon after diagnosis. When analysed individually, the miRNAs tended to conform to four general patterns of expression, with the majority displaying increased abundance in the high risk group. Interestingly, the miRNAs tended to reflect the immune and glycaemic status of individuals when T1D diagnosis occurs. Twenty-three of the fifty miRNAs demonstrated a

linear tend with GAD autoantibody titres, while eight miRNAs, as well as insulin cfDNA, had a quadratic trend with HbA1c levels at diagnosis.

Additional analysis conducted on individuals with newly diagnosed T1D treated with ingested interferon-α found that immune modulation caused a change in the abundance of seven candidate circulating miRNAs.

5.2. Chapter Aims

Studies presented within this chapter aimed to:

1. assess the microRNA and insulin cfDNA signature in peripheral circulation of individuals before, during, and after T1D diagnosis;
2. investigate whether insulin cfDNA or candidate miRNAs are indicative of the immune status or glucose control over three months (as measured by HbA1c) in individuals at diagnosis; and
3. identify any effects that immune modulation may play on the molecular signature.

5.3. Methods

5.3.1. Sample Cohorts

5.3.1.1. Children at High Risk of T1D

Plasma and serum samples and related data from 19 children at high risk of developing T1D were kindly provided by Professor Maria Craig and her team at the Prince of Wales Hospital Virology Research Laboratory in Sydney. These samples are comprised of children whoe's parent(s) or sibling had T1D, with 79% also presenting with islet autoantibodies. These children are currently being followed by Prof. Craig and her team as part of an on-going prospective study to assess whether they develop T1D, and so the individuals analysed in this chapter have an average of 3.5 samples taken at different time points (3.2 ± 2.4 (mean ± SD) years of follow-up) (Table 5-A).

5.3.1.2. Children at T1D Diagnosis

Plasma samples and related clinical data from 199 children at T1D diagnosis were kindly provided by Professor Timothy Jones and his team from the Princess Margaret Hospital in Perth. These samples were taken, mostly within two days from clinical diagnosis of T1D (Table 5-A).

5.3.1.3. Individuals Within the First Year of T1D Diagnosis

Paediatric (N=115) and adult (N=40) plasma samples from N=57/40 individuals respectively with T1D were kindly provided by Professor Kristina Rother and her team at the National Institute of Health in Bethesda, USA. Paediatric samples were taken from subjects within 6-weeks of T1D diagnosis. Subjects were then randomly assigned to receive daily ingested human recombinant interferon-α (hrIFNα), at either 5,000 or 30,000 units, or a placebo for

one year, as published previously (51). The baseline samples from this cohort form the <6 Weeks Post Dx group, while the placebo samples taken until 12 months form the <12 Months Post Dx group, outlined in Table 5-A.

5.3.1.4. Individuals with Long-standing T1D

Samples and related clinical data from patients with long-standing T1D were kindly provided by Professor Alicia Jenkins and her team from the NHMRC Clinical Trials Centre, Sydney and the University of Melbourne Dept. of Medicine (St. Vincent's) Health, Melbourne (N=180, see Table 4-B), and Professor Kristina Rother and her team at the National Institute of Health in Bethesda, USA. Professor Rother's samples came from a previously published cohort on the effects of exenatide on patients with long-standing T1D (215), however all samples tested here were taken from individuals at screening (N=40), prior to any intervention. Together, these samples were taken from individuals with an average of 20 years disease duration (Table 5-A). The use of individuals with long standing T1D provides a more thorough investigation of the changes in circulating miRNAs and insulin cfDNA during the life course of T1D.

5.3.2. RNA Isolation

RNA was isolated using either the manual RNA isolation protocol outlined in Appendix B, or the automated protocol outlined in Appendix C. Isolated RNA concentration was quantitated using a spectrophotometer.

5.3.3. MicroRNA Quantitation

The signature of 50 miRNAs, discussed in the previous chapter, was quantitated using custom OpenArray gene expression slides. RT, PA, and qPCR was undertaken as per the protocol outlined in Appendix D. Each of the slides also contained assays for RNA isolation and RT spike-in miRNAs (ath-miRs, see Supplementary Chapter 1), as well as a negative control

(ath-miR-394) and two endogenous controls (U6 and RNU44). To remove non-specific amplification, results with an AMP score of <1.24 and/or a Cq confidence score of <0.6 were omitted. Results were normalised to the RNA isolation and RT ath-miR spike-in miRNAs (see Supplementary Chapter 1 for optimisation). Any samples with detectable amplification within the negative control assay were removed from the analysis. Repeats and slide controls were also employed to ensure the integrity of the clinical data; the results of these can be found in the Supplementary Data.

5.3.4. Cell-free DNA Isolation and Bisulfite Conversion

Cell-free DNA was isolated from 50 µl of serum or plasma using the protocol outlined in Appendix E, and bisulfite conversion was undertaken using the protocol outlined in Appendix I.

5.3.5. Insulin cfDNA Quantitation

Methylated and unmethylated insulin cfDNA were quantified using the digital droplet PCR protocol outlined in Appendix J. Each plate contained a positive control, which consisted of a mixture of control plasmids (10% unmethylated, 90% methylated plasmid, 1 ng total per reaction), and a no template control (nuclease-free water). Control plasmids, kindly provided by Professor Raghu Mirmira at Indiana University USA as part of an existing collaboration with A/ Prof. Hardikar, were amplified using the transformation protocol outlined in Appendix H. FAM and VIC thresholds were identified based on the positive control and then applied to the entire plate. In addition to the controls, repeats were employed to ensure the integrity of the data; the results of these can be found in the Supplementary Data.

5.3.6. Data Presentation and Statistical Analysis

In the previous chapter, differences between groups were confirmed to be >1 cycle and then tested for significance. As there are five groups to analyse in this chapter for each miRNA, differences were confirmed to be >1 cycle after testing for significance to streamline analysis. Firstly, microRNA data is converted from CRT to transcript abundance using the fold over detectable method (limit of detection is 39 cycles) described earlier (190). Linear trend analysis was performed, with the P-value reported if <0.05. Kruskal-Wallis non-parametric ANOVA was used to assess changes within groups. Any miRNA that demonstrated a significant difference ($P<0.05$) was further investigated using Dunn's test (corrected for multiple comparisons) to identify which pairs of groups demonstrated a significant difference. An adjusted P value of <0.05 indicated significance. Any miRNA displaying a significant difference was then confirmed to show a >1 cycle difference between the compared groups. To be deemed a significant difference the miRNA must display atleast >1 cycle difference and an adjusted P-value of <0.05. Figure 5-1 gives an overview of this analysis.

Insulin cfDNA is presented as either copies/µl, or log transformed copies/µl as described earlier (168) and differences were assessed using Kruskal-Wallis non-parametric ANOVA with corrected Dunn's multiple comparison test.

Linear or quadratic regression was used to determine trend significance ($P<0.05$) between miRNA abundance and clinical parameters at T1D diagnosis.

To assess changes due to interferon treatment, data are kept as CRT and repeated measures ANOVA was used to identify any differences between treatment groups, time points or the interaction between treatment and time. Sum of squares test was used to identify and significant differences in treatment groups at individual time points.

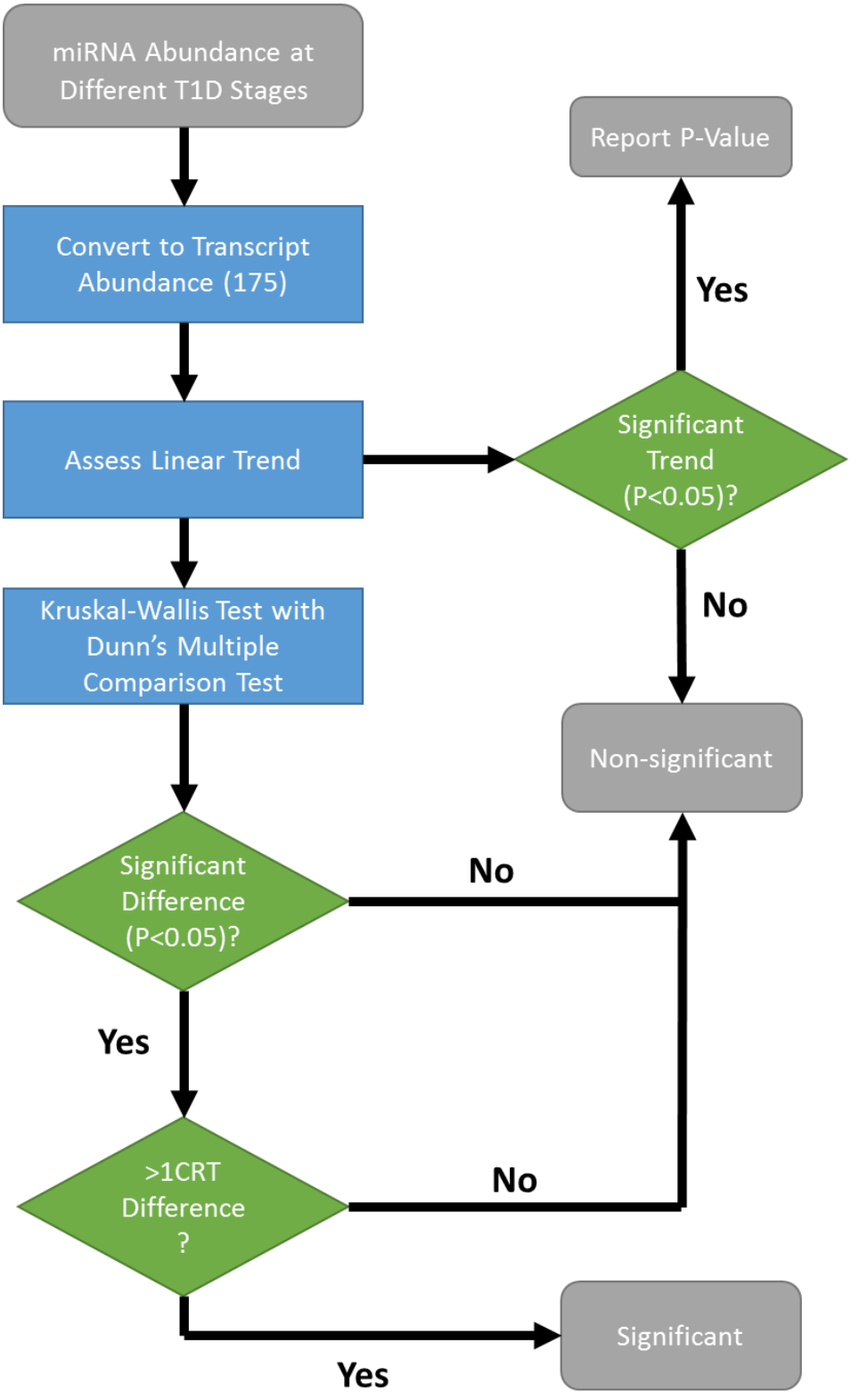

Figure 5-1. Flowchart for data analysis

Diagrammatical overview of the analytic process of identifying significant differences in miRNA abundance within different stages of T1D progression.

5.4. Results

5.4.1. T1D Progression – Sample Details

The details of the samples used in the assessment of the molecular signature in the progression of T1D can be found in Table 5-A. A significant difference was found in the age, HbA1c levels, and gender proportions between the groups.

To assess whether age impacted upon the abundance of the candidate miRNAs and insulin cfDNA, Spearman correlations were conducted independently for each cohort. No significant correlation (R^2>0.1, P<0.05) was observed between age and any miRNA or cfDNA within any group or cohort.

Multiple t-tests (with a false discovery rate of 1%) were employed to identify gender differences. No candidate miRNA or cfDNA significantly differed (P<0.05) between genders for any of the cohorts. Therefore, no adjustments were made for age or gender. Furthermore, as HbA1c levels are indicative of the stage of T1D, and may influence the molecular signature, no adjustments were made.

Table 5-A. Details of samples used in the analysis of T1D progression

	High Risk	At Diagnosis (Dx)	<6 Weeks Post-Dx	6 Weeks - 12 Months Post-Dx	20 Years Post-Dx	P-Value
Cohort (Section)[a]	1 (5.3.1.1)	2 (5.3.1.2)	3A (5.3.1.3)	3B (5.3.1.3)	4 (5.3.1.4)	-
Subjects, N	19	199	57	19	220	-
Time point samples per subject, N (mean ± SD)	3.5 ± 1.6	1	1	3 ± 1.2	1	-
Females, %	58	47	32	37	57	0.0047[b]
Age, yrs (mean ± SD)	7.0 ± 4.0	8.6 ± 4.1	10.1 ± 4.6	9.4 ± 4.0[c]	39.5 ± 13.5	<0.0001[d]
Time since diagnosis	-	2 ± 1.4 days (mean ± SD)	Up to 6 weeks	Between 6 weeks and 12 months	20.2 ± 12.7 years	-
HbA1c, % (mean ± SD)	NA	11.6 ± 2.06	7.5 ± 1.2	6.97 ± 1.03	7.9 ± 1.3	<0.0001[d]
HbA1c, mmol/mol (mean ± SD)		103.2 ± 22.5	58.3 ± 13.0	53.2 ± 11.2	63.3 ± 14.5	<0.0001[d]

NA = Not available
[a] See section text for further details.
[b] Chi-square test
[c] Calculated using the age at the beginning of the study
[d] ANOVA

5.4.2. MicroRNA Abundance Changes During T1D Progression

Cluster analysis reveals that the High Risk and At Diagnosis groups have a similar miRNA profile (Figure 5-2). Interestingly, the individuals within 6 weeks and 12 months post-diagnosis cluster differently, and demonstrate a lower abundance of multiple miRNA (lighter colour, higher cycle threshold). Those patients with a disease duration of 20 years cluster slightly closer to those at high risk and at diagnosis, however, their expression profile seems distinct.

The individual candidate miRNAs presented with four overarching patterns of expression throughout the life course of T1D. The majority of the miRNAs demonstrated higher abundance in the High Risk and/or At Dx groups (Figure 5-3.1, 3.2, 3.3, and 3.4). Some of these miRNAs, such as miR-99b, increase in abundance in the 20 Years Post-Dx group. Interestingly, the snoRNA U6 was highly elevated in those at high risk of T1D and demonstrated a significantly linear trend.

Three other miRNAs, miR-125a-5p, -146a, and -375, tended to be elevated at diagnosis (Figure 5-4). MicroRNA-375 was significantly elevated at diagnosis, compared to those at high risk, and then decreased in the subsequent groups.

Furthermore, eight miRNAs demonstrated the highest, albeit variable, abundance within the <12 Months Post-Dx group and then decreased in the 20 Years Post-Dx group (Figure 5-5.1 and 5.2). Finally, miR-152 and -186 are increased in the 20 Years Post-Dx group, both with significant linear trends indicating successive increases in abundance throughout the life course of T1D (Figure 5-6).

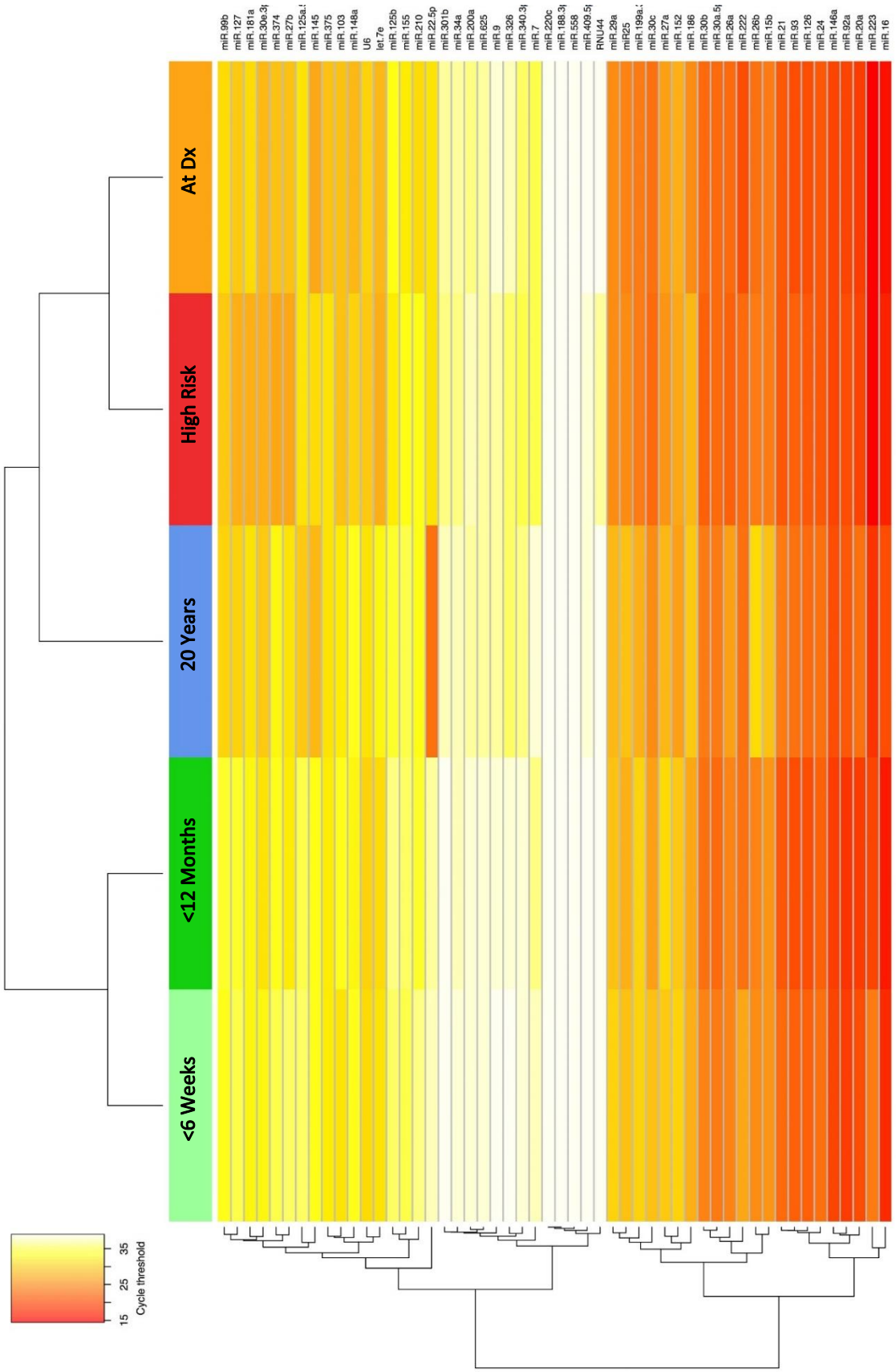

Figure 5-2. Heatmap of miRNA signature expression during T1D progression

Each square represents the mean value of the particular miRNA in each cohort. Complete linkage, Euclidean distance. N = 75 (High Risk), 187 (At Dx), 54 (<6 Wks and <12 Mths Post-Dx), 218 (20 Yrs Post-Dx).

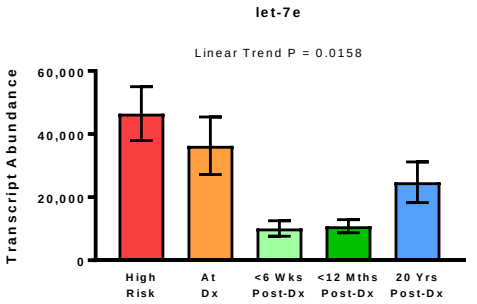

Comparison	Adjusted P	Comparison	Adjusted P
High Risk vs At Dx	NS	At Dx vs <12 Mths	0.0498
High Risk vs <6Wks	0.0001	At Dx vs 20 Yrs	<0.0001
High Risk vs <12 Mths	0.0006	<6 Wks vs <12 Mths	NS
High Risk Vs 20 Yrs	<0.0001	<6 Wks vs 20 Yrs	NS
At Dx vs <6 Wks	0.0139	<12 Mths vs 20 Yrs	NS

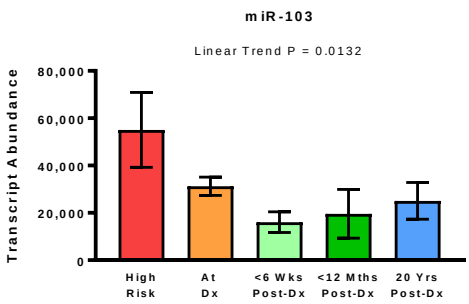

Comparison	Adjusted P	Comparison	Adjusted P
High Risk vs At Dx	NS	At Dx vs <12 Mths	<0.0001
High Risk vs <6Wks	NS	At Dx vs 20 Yrs	<0.0001
High Risk vs <12 Mths	<0.0001	<6 Wks vs <12 Mths	NS
High Risk Vs 20 Yrs	0.0001	<6 Wks vs 20 Yrs	NS
At Dx vs <6 Wks	0.023	<12 Mths vs 20 Yrs	NS

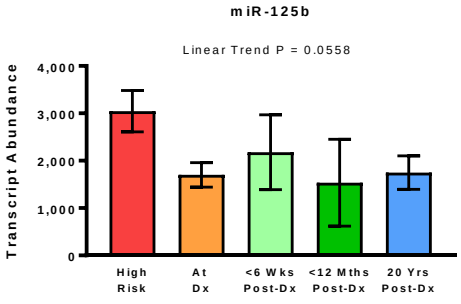

Comparison	Adjusted P	Comparison	Adjusted P
High Risk vs At Dx	NS	At Dx vs <12 Mths	0.0077
High Risk vs <6Wks	0.0005	At Dx vs 20 Yrs	NS
High Risk vs <12 Mths	<0.0001	<6 Wks vs <12 Mths	NS
High Risk Vs 20 Yrs	0.0005	<6 Wks vs 20 Yrs	NS
At Dx vs <6 Wks	NS	<12 Mths vs 20 Yrs	NS

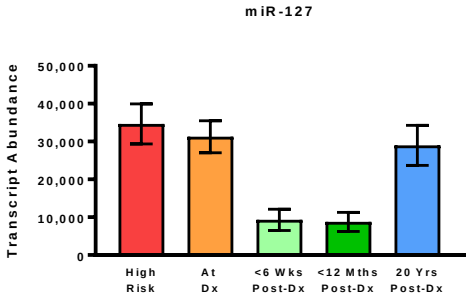

Comparison	Adjusted P	Comparison	Adjusted P
High Risk vs At Dx	NS	At Dx vs <12 Mths	<0.0001
High Risk vs <6Wks	<0.0001	At Dx vs 20 Yrs	NS
High Risk vs <12 Mths	<0.0001	<6 Wks vs <12 Mths	NS
High Risk Vs 20 Yrs	0.0141	<6 Wks vs 20 Yrs	0.0016
At Dx vs <6 Wks	<0.0001	<12 Mths vs 20 Yrs	0.0037

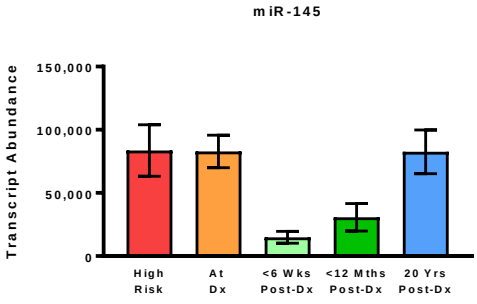

Comparison	Adjusted P	Comparison	Adjusted P
High Risk vs At Dx	0.0461	At Dx vs <12 Mths	0.0002
High Risk vs <6Wks	NS	At Dx vs 20 Yrs	NS
High Risk vs <12 Mths	NS	<6 Wks vs <12 Mths	NS
High Risk Vs 20 Yrs	NS	<6 Wks vs 20 Yrs	<0.0001
At Dx vs <6 Wks	<0.0001	<12 Mths vs 20 Yrs	0.0029

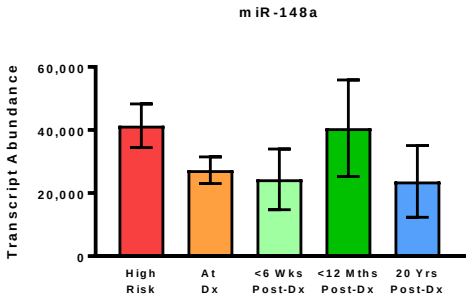

Comparison	Adjusted P	Comparison	Adjusted P
High Risk vs At Dx	NS	At Dx vs <12 Mths	NS
High Risk vs <6Wks	0.004	At Dx vs 20 Yrs	<0.0001
High Risk vs <12 Mths	NS	<6 Wks vs <12 Mths	NS
High Risk Vs 20 Yrs	<0.0001	<6 Wks vs 20 Yrs	NS
At Dx vs <6 Wks	0.0005	<12 Mths vs 20 Yrs	NS

Figure 5-3.1. MicroRNAs are elevated in high risk individuals and at T1D diagnosis

N = 75 (High Risk), 187 (At Dx), 54 (<6 Wks and <12 Mths Post-Dx), 218 (20 Yrs Post-Dx). Mean ± SEM. Multiple comparisons and adjusted P-values are listed in the table below each graph. Significant differences are highlighted. Linear trend significance $P < 0.05$.

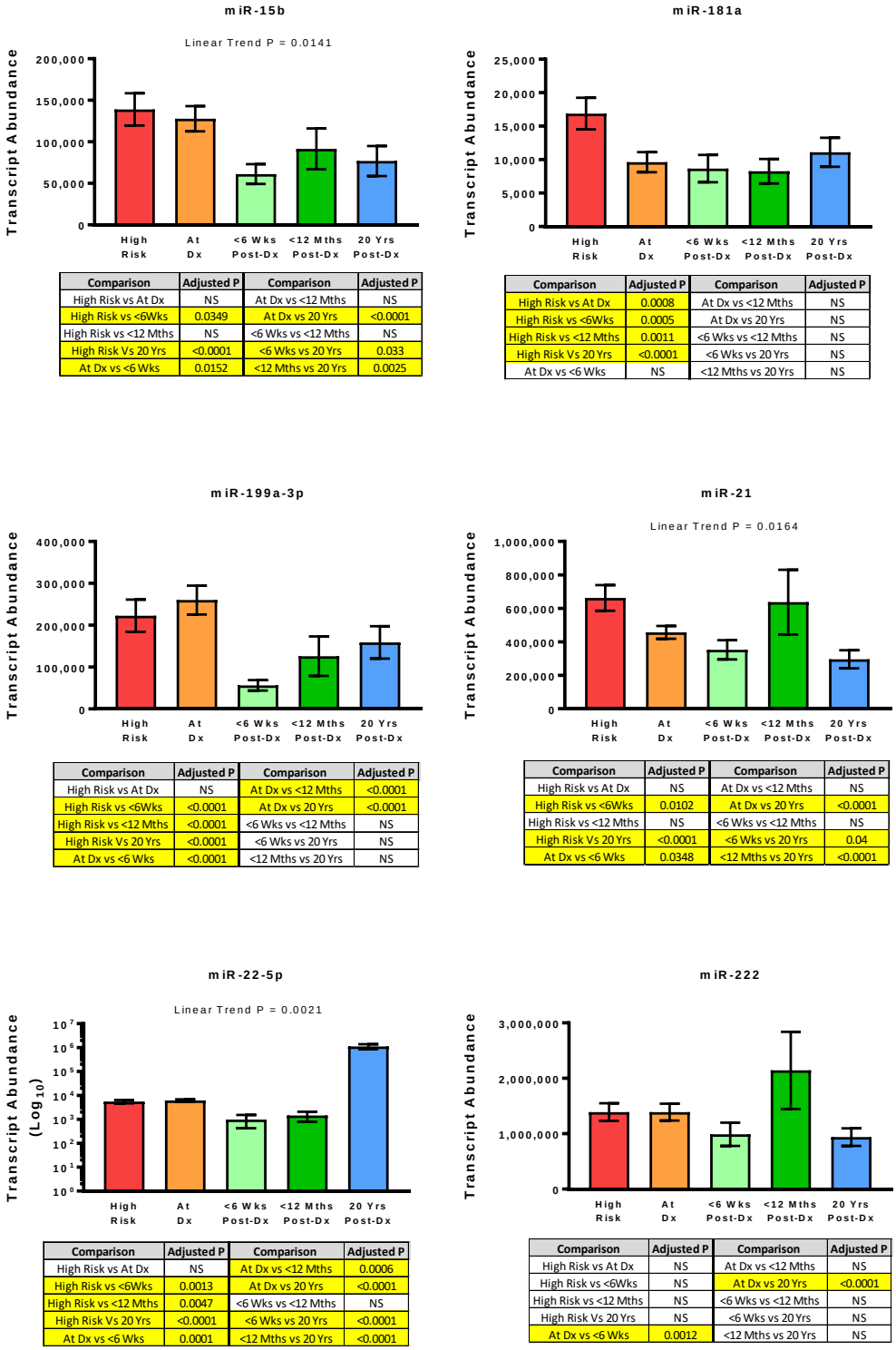

Comparison	Adjusted P	Comparison	Adjusted P
High Risk vs At Dx	NS	At Dx vs <12 Mths	NS
High Risk vs <6Wks	0.0349	At Dx vs 20 Yrs	<0.0001
High Risk vs <12 Mths	NS	<6 Wks vs <12 Mths	NS
High Risk Vs 20 Yrs	<0.0001	<6 Wks vs 20 Yrs	0.033
At Dx vs <6 Wks	0.0152	<12 Mths vs 20 Yrs	0.0025

Comparison	Adjusted P	Comparison	Adjusted P
High Risk vs At Dx	0.0008	At Dx vs <12 Mths	NS
High Risk vs <6Wks	0.0005	At Dx vs 20 Yrs	NS
High Risk vs <12 Mths	0.0011	<6 Wks vs <12 Mths	NS
High Risk Vs 20 Yrs	<0.0001	<6 Wks vs 20 Yrs	NS
At Dx vs <6 Wks	NS	<12 Mths vs 20 Yrs	NS

Comparison	Adjusted P	Comparison	Adjusted P
High Risk vs At Dx	NS	At Dx vs <12 Mths	<0.0001
High Risk vs <6Wks	<0.0001	At Dx vs 20 Yrs	<0.0001
High Risk vs <12 Mths	<0.0001	<6 Wks vs <12 Mths	NS
High Risk Vs 20 Yrs	<0.0001	<6 Wks vs 20 Yrs	NS
At Dx vs <6 Wks	<0.0001	<12 Mths vs 20 Yrs	NS

Comparison	Adjusted P	Comparison	Adjusted P
High Risk vs At Dx	NS	At Dx vs <12 Mths	NS
High Risk vs <6Wks	0.0102	At Dx vs 20 Yrs	<0.0001
High Risk vs <12 Mths	NS	<6 Wks vs <12 Mths	NS
High Risk Vs 20 Yrs	<0.0001	<6 Wks vs 20 Yrs	0.04
At Dx vs <6 Wks	0.0348	<12 Mths vs 20 Yrs	<0.0001

Comparison	Adjusted P	Comparison	Adjusted P
High Risk vs At Dx	NS	At Dx vs <12 Mths	0.0006
High Risk vs <6Wks	0.0013	At Dx vs 20 Yrs	<0.0001
High Risk vs <12 Mths	0.0047	<6 Wks vs <12 Mths	NS
High Risk Vs 20 Yrs	<0.0001	<6 Wks vs 20 Yrs	<0.0001
At Dx vs <6 Wks	0.0001	<12 Mths vs 20 Yrs	<0.0001

Comparison	Adjusted P	Comparison	Adjusted P
High Risk vs At Dx	NS	At Dx vs <12 Mths	NS
High Risk vs <6Wks	NS	At Dx vs 20 Yrs	<0.0001
High Risk vs <12 Mths	NS	<6 Wks vs <12 Mths	NS
High Risk Vs 20 Yrs	NS	<6 Wks vs 20 Yrs	NS
At Dx vs <6 Wks	0.0012	<12 Mths vs 20 Yrs	NS

Figure 5-3.2. MicroRNAs are elevated in high risk individuals and at T1D diagnosis

N = 75 (High Risk), 187 (At Dx), 54 (<6 Wks and <12 Mths Post-Dx), 218 (20 Yrs Post-Dx). Mean ± SEM. Multiple comparisons and adjusted P-values are listed in the table below each graph. Significant differences are highlighted. Linear trend significance $P < 0.05$.

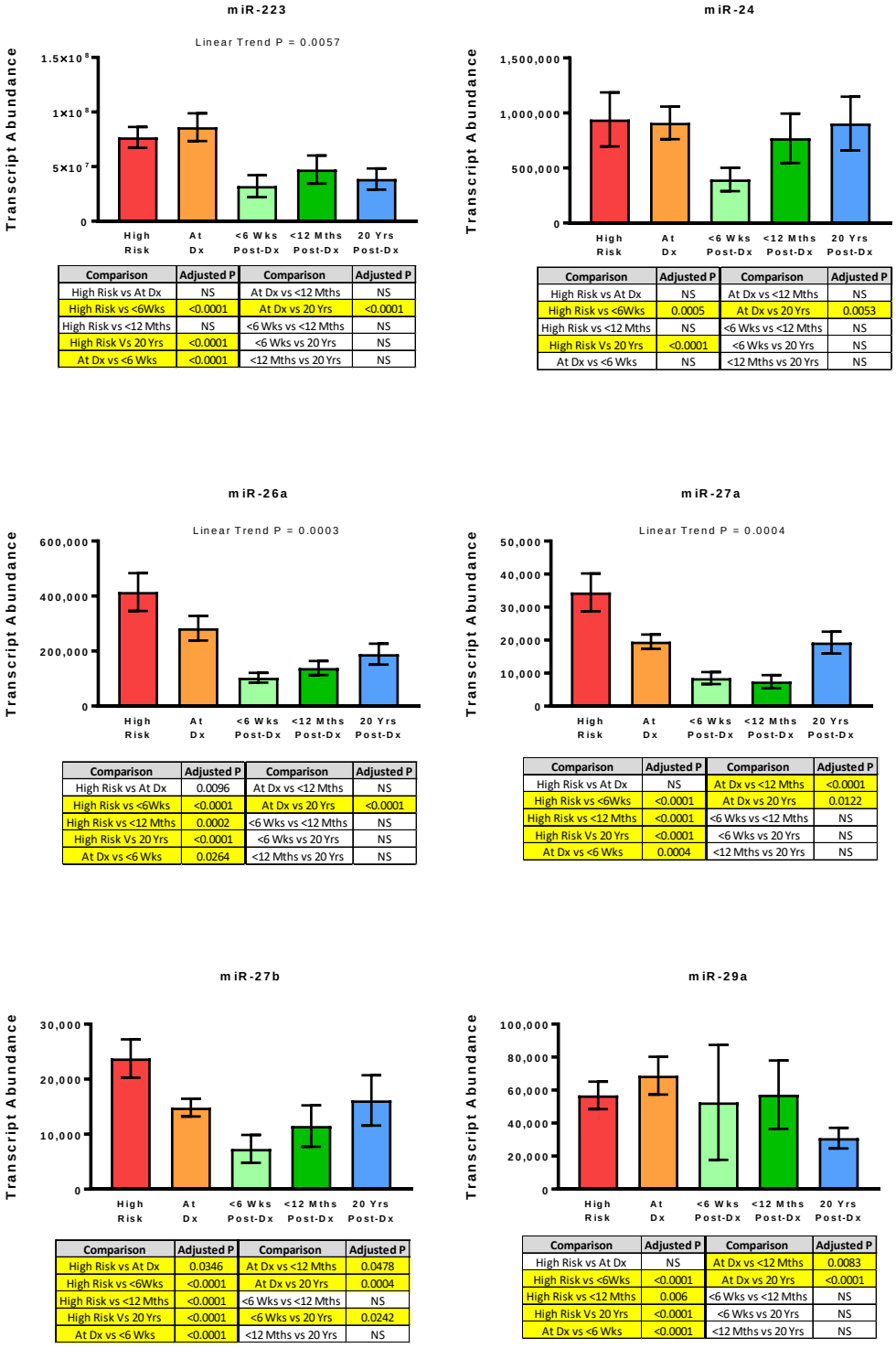

Comparison	Adjusted P	Comparison	Adjusted P
High Risk vs At Dx	NS	At Dx vs <12 Mths	NS
High Risk vs <6Wks	<0.0001	At Dx vs 20 Yrs	<0.0001
High Risk vs <12 Mths	NS	<6 Wks vs <12 Mths	NS
High Risk Vs 20 Yrs	<0.0001	<6 Wks vs 20 Yrs	NS
At Dx vs <6 Wks	<0.0001	<12 Mths vs 20 Yrs	NS

Comparison	Adjusted P	Comparison	Adjusted P
High Risk vs At Dx	NS	At Dx vs <12 Mths	NS
High Risk vs <6Wks	0.0005	At Dx vs 20 Yrs	0.0053
High Risk vs <12 Mths	NS	<6 Wks vs <12 Mths	NS
High Risk Vs 20 Yrs	<0.0001	<6 Wks vs 20 Yrs	NS
At Dx vs <6 Wks	NS	<12 Mths vs 20 Yrs	NS

Comparison	Adjusted P	Comparison	Adjusted P
High Risk vs At Dx	0.0096	At Dx vs <12 Mths	NS
High Risk vs <6Wks	<0.0001	At Dx vs 20 Yrs	<0.0001
High Risk vs <12 Mths	0.0002	<6 Wks vs <12 Mths	NS
High Risk Vs 20 Yrs	<0.0001	<6 Wks vs 20 Yrs	NS
At Dx vs <6 Wks	0.0264	<12 Mths vs 20 Yrs	NS

Comparison	Adjusted P	Comparison	Adjusted P
High Risk vs At Dx	NS	At Dx vs <12 Mths	<0.0001
High Risk vs <6Wks	<0.0001	At Dx vs 20 Yrs	0.0122
High Risk vs <12 Mths	<0.0001	<6 Wks vs <12 Mths	NS
High Risk Vs 20 Yrs	<0.0001	<6 Wks vs 20 Yrs	NS
At Dx vs <6 Wks	0.0004	<12 Mths vs 20 Yrs	NS

Comparison	Adjusted P	Comparison	Adjusted P
High Risk vs At Dx	0.0346	At Dx vs <12 Mths	0.0478
High Risk vs <6Wks	<0.0001	At Dx vs 20 Yrs	0.0004
High Risk vs <12 Mths	<0.0001	<6 Wks vs <12 Mths	NS
High Risk Vs 20 Yrs	<0.0001	<6 Wks vs 20 Yrs	0.0242
At Dx vs <6 Wks	<0.0001	<12 Mths vs 20 Yrs	NS

Comparison	Adjusted P	Comparison	Adjusted P
High Risk vs At Dx	NS	At Dx vs <12 Mths	0.0083
High Risk vs <6Wks	<0.0001	At Dx vs 20 Yrs	<0.0001
High Risk vs <12 Mths	0.006	<6 Wks vs <12 Mths	NS
High Risk Vs 20 Yrs	<0.0001	<6 Wks vs 20 Yrs	NS
At Dx vs <6 Wks	<0.0001	<12 Mths vs 20 Yrs	NS

Figure 5-3.3. MicroRNAs are elevated in high risk individuals and at T1D diagnosis

N = 75 (High Risk), 187 (At Dx), 54 (<6 Wks and <12 Mths Post-Dx), 218 (20 Yrs Post-Dx). Mean ± SEM. Multiple comparisons and adjusted P-values are listed in the table below each graph. Significant differences are highlighted. Linear trend significance $P < 0.05$.

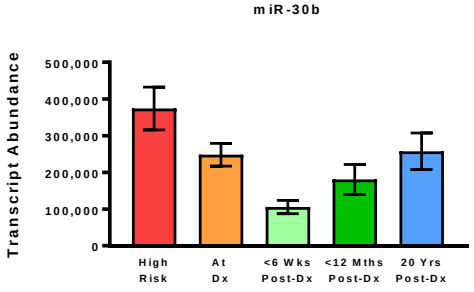

Comparison	Adjusted P	Comparison	Adjusted P
High Risk vs At Dx	NS	At Dx vs <12 Mths	NS
High Risk vs <6Wks	<0.0001	At Dx vs 20 Yrs	0.0016
High Risk vs <12 Mths	0.0038	<6 Wks vs <12 Mths	NS
High Risk Vs 20 Yrs	<0.0001	<6 Wks vs 20 Yrs	NS
At Dx vs <6 Wks	0.0013	<12 Mths vs 20 Yrs	NS

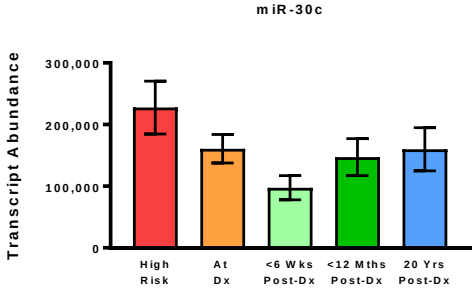

Comparison	Adjusted P	Comparison	Adjusted P
High Risk vs At Dx	NS	At Dx vs <12 Mths	NS
High Risk vs <6Wks	<0.0001	At Dx vs 20 Yrs	0.0004
High Risk vs <12 Mths	0.0254	<6 Wks vs <12 Mths	NS
High Risk Vs 20 Yrs	<0.0001	<6 Wks vs 20 Yrs	NS
At Dx vs <6 Wks	0.0248	<12 Mths vs 20 Yrs	NS

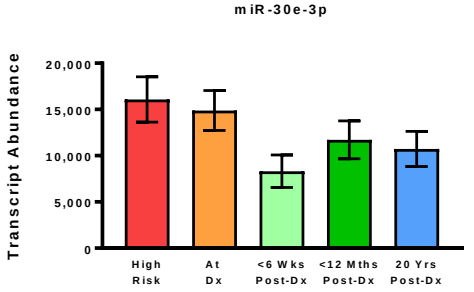

Comparison	Adjusted P	Comparison	Adjusted P
High Risk vs At Dx	NS	At Dx vs <12 Mths	NS
High Risk vs <6Wks	<0.0001	At Dx vs 20 Yrs	0.0126
High Risk vs <12 Mths	0.0244	<6 Wks vs <12 Mths	NS
High Risk Vs 20 Yrs	<0.0001	<6 Wks vs 20 Yrs	NS
At Dx vs <6 Wks	0.0226	<12 Mths vs 20 Yrs	NS

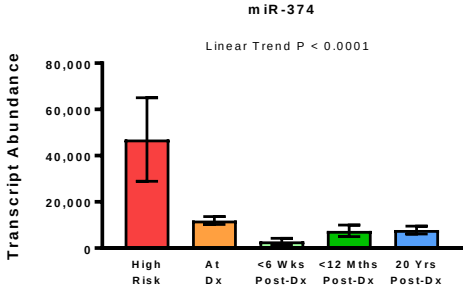

Comparison	Adjusted P	Comparison	Adjusted P
High Risk vs At Dx	NS	At Dx vs <12 Mths	<0.0001
High Risk vs <6Wks	<0.0001	At Dx vs 20 Yrs	<0.0001
High Risk vs <12 Mths	<0.0001	<6 Wks vs <12 Mths	NS
High Risk Vs 20 Yrs	<0.0001	<6 Wks vs 20 Yrs	NS
At Dx vs <6 Wks	<0.0001	<12 Mths vs 20 Yrs	NS

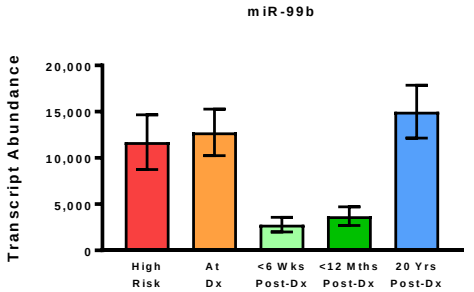

Comparison	Adjusted P	Comparison	Adjusted P
High Risk vs At Dx	NS	At Dx vs <12 Mths	0.0024
High Risk vs <6Wks	0.0002	At Dx vs 20 Yrs	NS
High Risk vs <12 Mths	0.0005	<6 Wks vs <12 Mths	NS
High Risk Vs 20 Yrs	NS	<6 Wks vs 20 Yrs	0.0001
At Dx vs <6 Wks	0.0011	<12 Mths vs 20 Yrs	0.0002

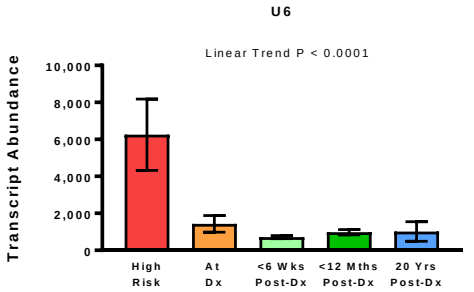

Comparison	Adjusted P	Comparison	Adjusted P
High Risk vs At Dx	NS	At Dx vs <12 Mths	NS
High Risk vs <6Wks	NS	At Dx vs 20 Yrs	<0.0001
High Risk vs <12 Mths	NS	<6 Wks vs <12 Mths	NS
High Risk Vs 20 Yrs	<0.0001	<6 Wks vs 20 Yrs	<0.0001
At Dx vs <6 Wks	NS	<12 Mths vs 20 Yrs	<0.0001

Figure 5-3.4. MicroRNAs are elevated in high risk individuals and at T1D diagnosis

N = 75 (High Risk), 187 (At Dx), 54 (<6 Wks and <12 Mths Post-Dx), 218 (20 Yrs Post-Dx). Mean ± SEM. Multiple comparisons and adjusted P-values are listed in the table below each graph. Significant differences are highlighted. Linear trend significance $P < 0.05$.

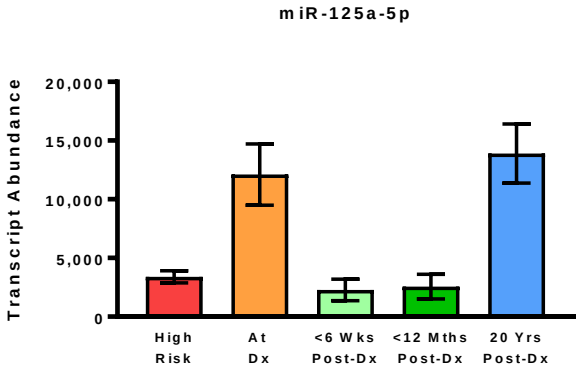

Comparison	Adjusted P	Comparison	Adjusted P
High Risk vs At Dx	NS	At Dx vs <12 Mths	0.0005
High Risk vs <6Wks	0.0038	At Dx vs 20 Yrs	NS
High Risk vs <12 Mths	0.0241	<6 Wks vs <12 Mths	NS
High Risk Vs 20 Yrs	NS	<6 Wks vs 20 Yrs	<0.0001
At Dx vs <6 Wks	<0.0001	<12 Mths vs 20 Yrs	<0.0001

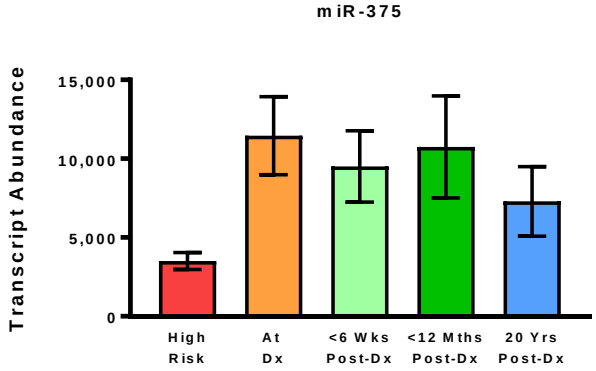

Comparison	Adjusted P	Comparison	Adjusted P
High Risk vs At Dx	0.0047	At Dx vs <12 Mths	0.0368
High Risk vs <6Wks	NS	At Dx vs 20 Yrs	<0.0001
High Risk vs <12 Mths	NS	<6 Wks vs <12 Mths	NS
High Risk Vs 20 Yrs	NS	<6 Wks vs 20 Yrs	NS
At Dx vs <6 Wks	0.0373	<12 Mths vs 20 Yrs	NS

Figure 5-4. Two miRNAs are elevated at T1D diagnosis

N = 75 (High Risk), 187 (At Dx), 54 (<6 Wks and <12 Mths Post-Dx), 218 (20 Yrs Post-Dx). Mean ± SEM. Multiple comparisons and adjusted P-values are listed in the table below each graph.

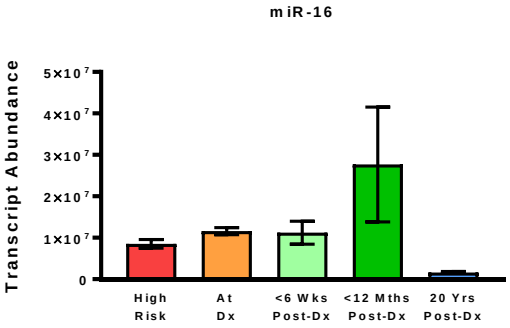

Comparison	Adjusted P	Comparison	Adjusted P
High Risk vs At Dx	0.0113	At Dx vs <12 Mths	NS
High Risk vs <6Wks	NS	At Dx vs 20 Yrs	<0.0001
High Risk vs <12 Mths	NS	<6 Wks vs <12 Mths	NS
High Risk Vs 20 Yrs	<0.0001	<6 Wks vs 20 Yrs	<0.0001
At Dx vs <6 Wks	0.0003	<12 Mths vs 20 Yrs	<0.0001

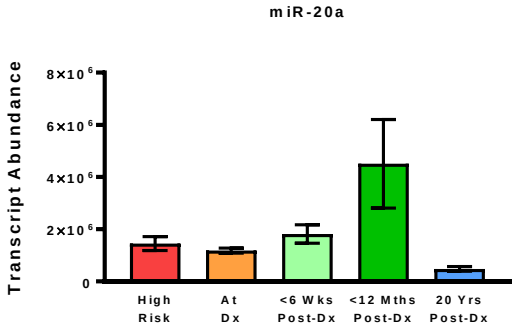

Comparison	Adjusted P	Comparison	Adjusted P
High Risk vs At Dx	NS	At Dx vs <12 Mths	NS
High Risk vs <6Wks	NS	At Dx vs 20 Yrs	<0.0001
High Risk vs <12 Mths	NS	<6 Wks vs <12 Mths	NS
High Risk Vs 20 Yrs	<0.0001	<6 Wks vs 20 Yrs	<0.0001
At Dx vs <6 Wks	NS	<12 Mths vs 20 Yrs	<0.0001

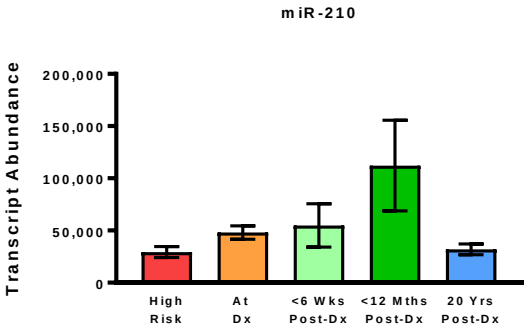

Comparison	Adjusted P	Comparison	Adjusted P
High Risk vs At Dx	NS	At Dx vs <12 Mths	NS
High Risk vs <6Wks	NS	At Dx vs 20 Yrs	0.0225
High Risk vs <12 Mths	NS	<6 Wks vs <12 Mths	NS
High Risk Vs 20 Yrs	NS	<6 Wks vs 20 Yrs	NS
At Dx vs <6 Wks	0.0009	<12 Mths vs 20 Yrs	NS

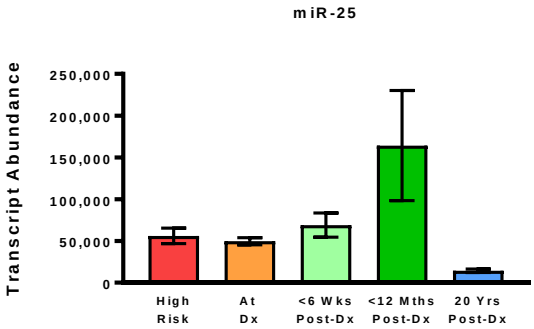

Comparison	Adjusted P	Comparison	Adjusted P
High Risk vs At Dx	NS	At Dx vs <12 Mths	NS
High Risk vs <6Wks	NS	At Dx vs 20 Yrs	<0.0001
High Risk vs <12 Mths	NS	<6 Wks vs <12 Mths	NS
High Risk Vs 20 Yrs	<0.0001	<6 Wks vs 20 Yrs	NS
At Dx vs <6 Wks	0.0121	<12 Mths vs 20 Yrs	<0.0001

Figure 5-5.1 Candidate miRNAs increase in the 12 months following T1D diagnosis

N = 75 (High Risk), 187 (At Dx), 54 (<6 Wks and <12 Mths Post-Dx), 218 (20 Yrs Post-Dx). Mean ± SEM. Multiple comparisons and adjusted P-values are listed in the table below each graph. Significant differences are highlighted.

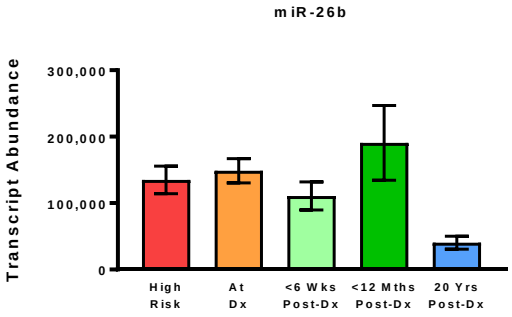

Comparison	Adjusted P	Comparison	Adjusted P
High Risk vs At Dx	NS	At Dx vs <12 Mths	NS
High Risk vs <6Wks	NS	At Dx vs 20 Yrs	<0.0001
High Risk vs <12 Mths	NS	<6 Wks vs <12 Mths	NS
High Risk Vs 20 Yrs	<0.0001	<6 Wks vs 20 Yrs	<0.0001
At Dx vs <6 Wks	NS	<12 Mths vs 20 Yrs	<0.0001

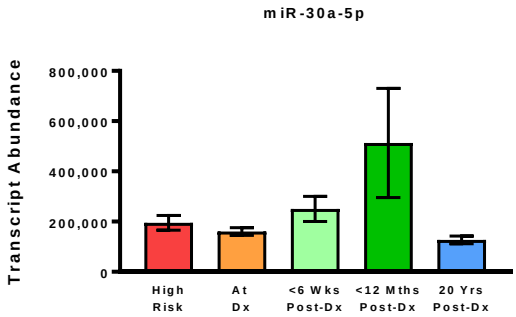

Comparison	Adjusted P	Comparison	Adjusted P
High Risk vs At Dx	NS	At Dx vs <12 Mths	NS
High Risk vs <6Wks	NS	At Dx vs 20 Yrs	NS
High Risk vs <12 Mths	NS	<6 Wks vs <12 Mths	NS
High Risk Vs 20 Yrs	0.0005	<6 Wks vs 20 Yrs	NS
At Dx vs <6 Wks	NS	<12 Mths vs 20 Yrs	0.0012

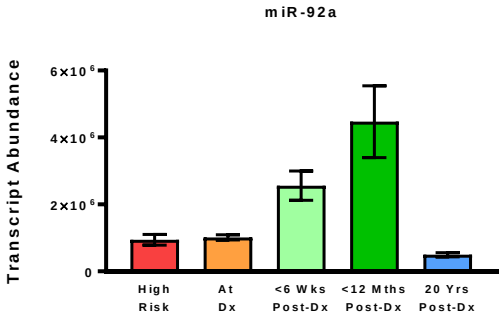

Comparison	Adjusted P	Comparison	Adjusted P
High Risk vs At Dx	NS	At Dx vs <12 Mths	0.0037
High Risk vs <6Wks	0.0094	At Dx vs 20 Yrs	<0.0001
High Risk vs <12 Mths	<0.0001	<6 Wks vs <12 Mths	NS
High Risk Vs 20 Yrs	NS	<6 Wks vs 20 Yrs	<0.0001
At Dx vs <6 Wks	NS	<12 Mths vs 20 Yrs	<0.0001

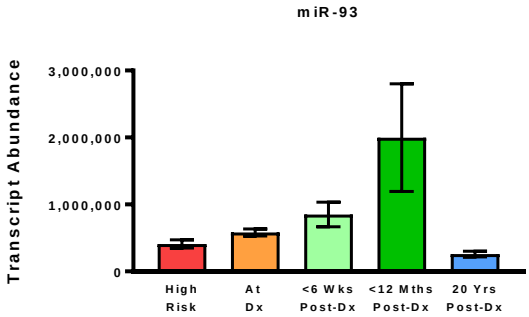

Comparison	Adjusted P	Comparison	Adjusted P
High Risk vs At Dx	NS	At Dx vs <12 Mths	NS
High Risk vs <6Wks	NS	At Dx vs 20 Yrs	<0.0001
High Risk vs <12 Mths	NS	<6 Wks vs <12 Mths	NS
High Risk Vs 20 Yrs	<0.0001	<6 Wks vs 20 Yrs	<0.0001
At Dx vs <6 Wks	NS	<12 Mths vs 20 Yrs	<0.0001

Figure 5-5.2 Candidate miRNAs increase in the 12 months following T1D diagnosis

N = 75 (High Risk), 187 (At Dx), 54 (<6 Wks and <12 Mths Post-Dx), 218 (20 Yrs Post-Dx). Mean ± SEM. Multiple comparisons and adjusted P-values are listed in the table below each graph. Significant differences are highlighted.

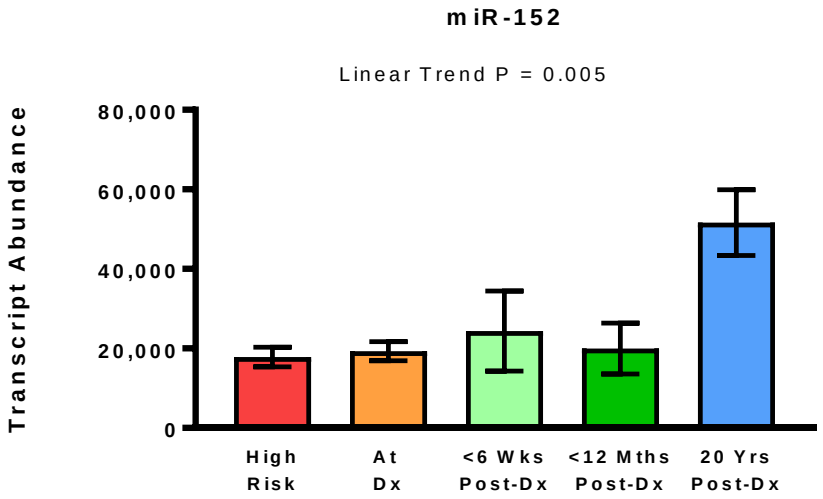

Comparison	Adjusted P	Comparison	Adjusted P
High Risk vs At Dx	NS	At Dx vs <12 Mths	NS
High Risk vs <6Wks	NS	At Dx vs 20 Yrs	0.0045
High Risk vs <12 Mths	NS	<6 Wks vs <12 Mths	NS
High Risk Vs 20 Yrs	NS	<6 Wks vs 20 Yrs	0.0025
At Dx vs <6 Wks	NS	<12 Mths vs 20 Yrs	0.0021

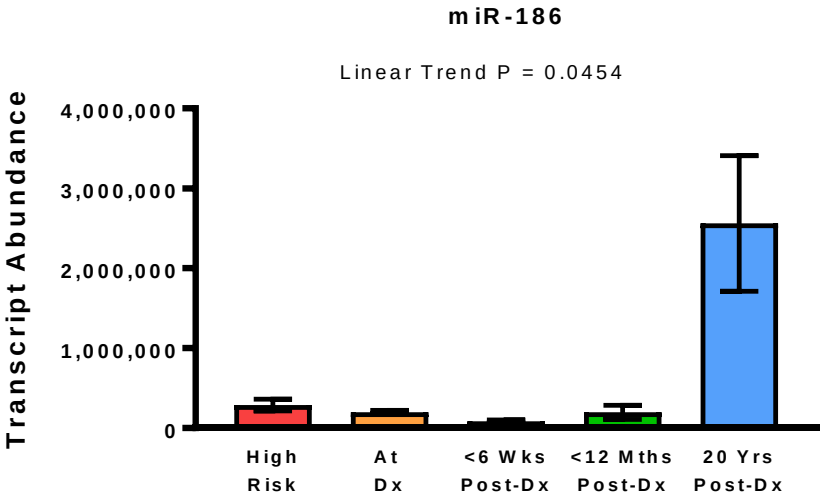

Comparison	Adjusted P	Comparison	Adjusted P
High Risk vs At Dx	NS	At Dx vs <12 Mths	NS
High Risk vs <6Wks	NS	At Dx vs 20 Yrs	<0.0001
High Risk vs <12 Mths	NS	<6 Wks vs <12 Mths	NS
High Risk Vs 20 Yrs	NS	<6 Wks vs 20 Yrs	NS
At Dx vs <6 Wks	0.0273	<12 Mths vs 20 Yrs	NS

Figure 5-6. MicroRNA-152 and -186 are elevated in patients with long-standing T1D

N = 75 (High Risk), 187 (At Dx), 54 (<6 Wks and <12 Mths Post-Dx), 218 (20 Yrs Post-Dx). Mean ± SEM. Multiple comparisons and adjusted P-values are listed in the table below each graph. Significant differences are highlighted. Linear trend significance $P < 0.05$.

5.4.3. Cell-free DNA Decreases at Diagnosis

In contrast with the miRNA signature, methylated insulin cfDNA decreases significantly at the point of T1D diagnosis (Figure 5-7). In the following 6 week and 12 month period, the abundance of these cfDNA species returns to levels similar to that found in the high risk group, and then decrease again in the 20 Years Post-Dx group. The methylated insulin cfDNA demonstrates a similar pattern, however not all of the changes are statistically significant.

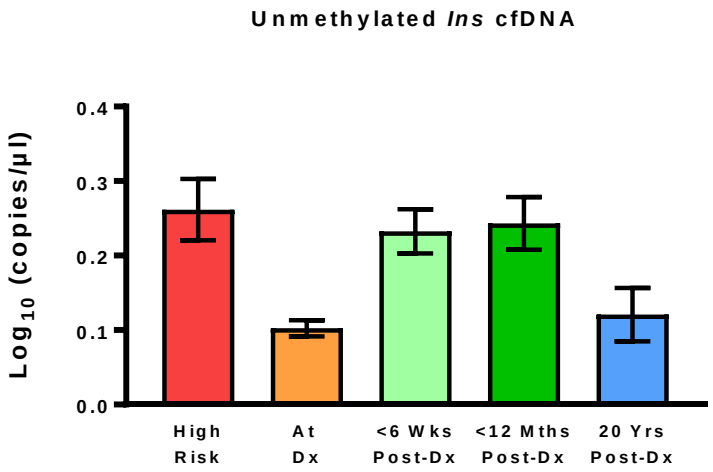

Comparison	Adjusted P	Comparison	Adjusted P
High Risk vs At Dx	<0.0001	At Dx vs <12 Mths	<0.0001
High Risk vs <6Wks	NS	At Dx vs 20 Yrs	NS
High Risk vs <12 Mths	NS	<6 Wks vs <12 Mths	NS
High Risk Vs 20 Yrs	0.0048	<6 Wks vs 20 Yrs	0.0039
At Dx vs <6 Wks	<0.0001	<12 Mths vs 20 Yrs	0.0009

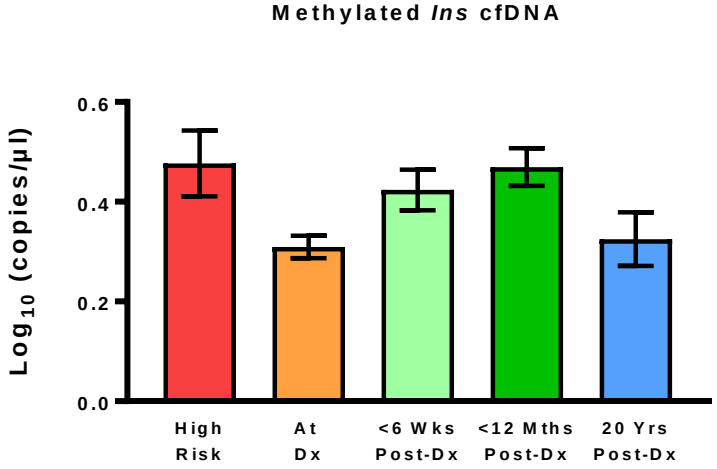

Comparison	Adjusted P	Comparison	Adjusted P
High Risk vs At Dx	NS	At Dx vs <12 Mths	<0.0001
High Risk vs <6Wks	NS	At Dx vs 20 Yrs	NS
High Risk vs <12 Mths	NS	<6 Wks vs <12 Mths	NS
High Risk Vs 20 Yrs	NS	<6 Wks vs 20 Yrs	NS
At Dx vs <6 Wks	0.0185	<12 Mths vs 20 Yrs	0.0286

Figure 5-7. Insulin cfDNA is reduced at T1D diagnosis

N = 61 (High Risk), 198 (At Dx), 57 (<6 Weeks Post-Dx), 59 (<12 Months Post-Dx), 40 (20 Years Post-Dx). Mean ± SEM. Multiple comparisons and adjusted P-values are listed in the table below each graph. Significant differences are highlighted.

5.4.4. MicroRNAs Correspond to GAD Autoantibody Titres at Diagnosis

To assess whether the candidate miRNAs could reflect the immune status of individuals at the point of diagnosis, associations between miRNA abundance and islet autoantibody titres were examined. Within the cohort of 199 individuals at T1D diagnosis, the majority had data for GADA (89.9%) and IA-2 (85.4%) titres, with 77.7% and 92.3% of these being seropositive for GADA and IA-2 respectively. IA-2 did not show any significant associations with the candidate miRNAs or cfDNA. When analysed in tertiles (Table 5-B), a clear linear trend formed between GADA titres and twenty-three candidate miRNAs (Figure 5-8). The abundance of these miRNAs increased with GADA titres, with a significant increase found in tertile 3, providing evidence that these miRNAs are reflective of the immune status of individuals at diagnosis.

Table 5-B. Tertiles of GADA titres in individuals at T1D diagnosis

GADA Tertile	Individuals (N)	Range (U/ml)	Median (U/ml)
Negative	35	-	-
1	43	1.3 – 5.3	3.55
2	41	5.7 – 27	17.00
3	48	30 – 2000	295.00

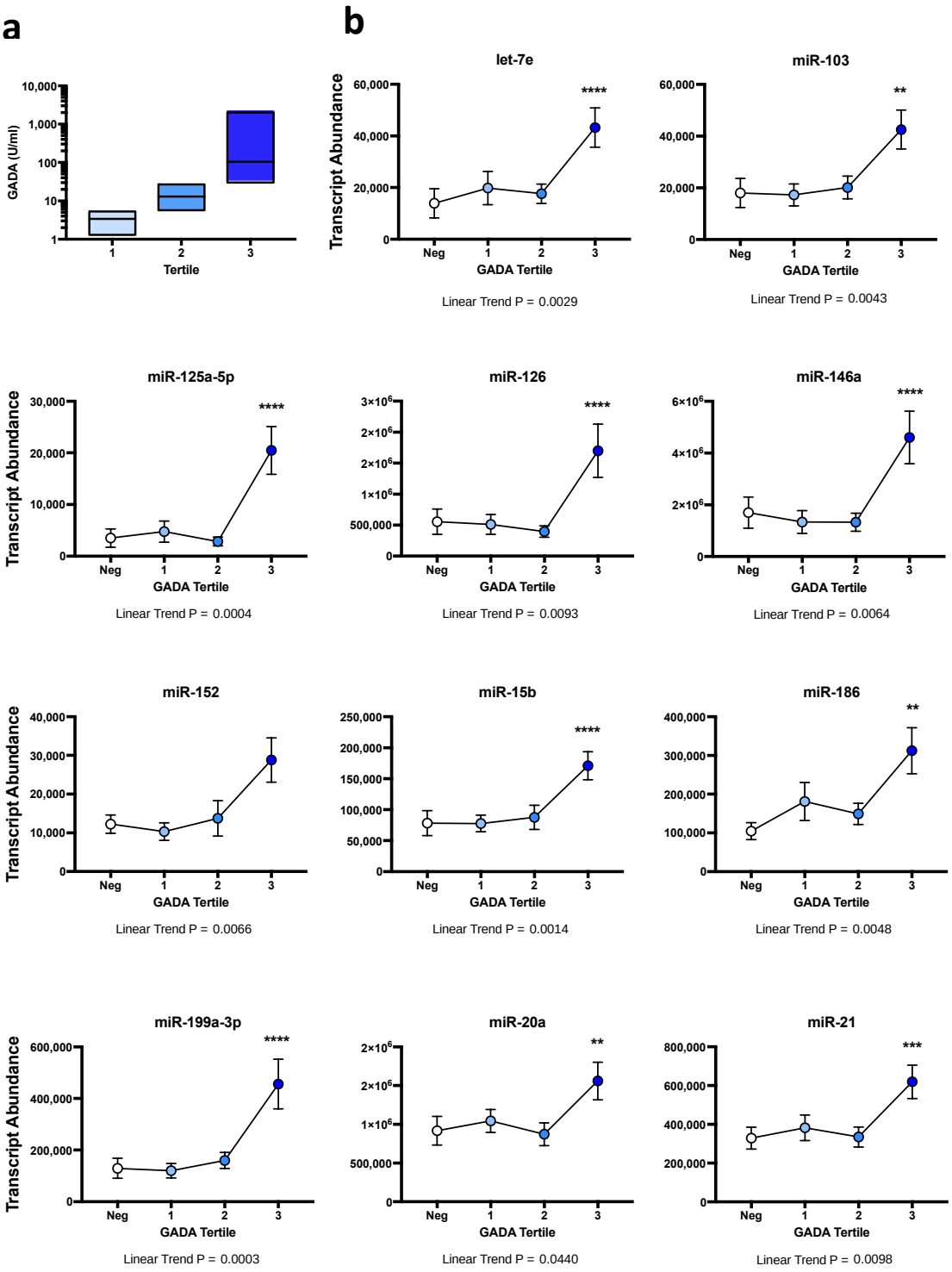

Figure 5-8.1. Candidate miRNAs correspond to GADA titres at T1D diagnosis

(a) Box plot (median, min-max) of GADA tertile spread. (b) MicroRNA abundance in seronegative individuals, and those in each GADA tertile. Mean ± SEM. Linear trend significance $P < 0.05$. ** Adjusted $P < 0.01$, *** Adjusted $P < 0.001$, **** Adjusted $P < 0.0001$ compared to Neg (Kruskal-Wallis non-parametric one-way ANOVA with corrected Dunn's multiple comparison test).

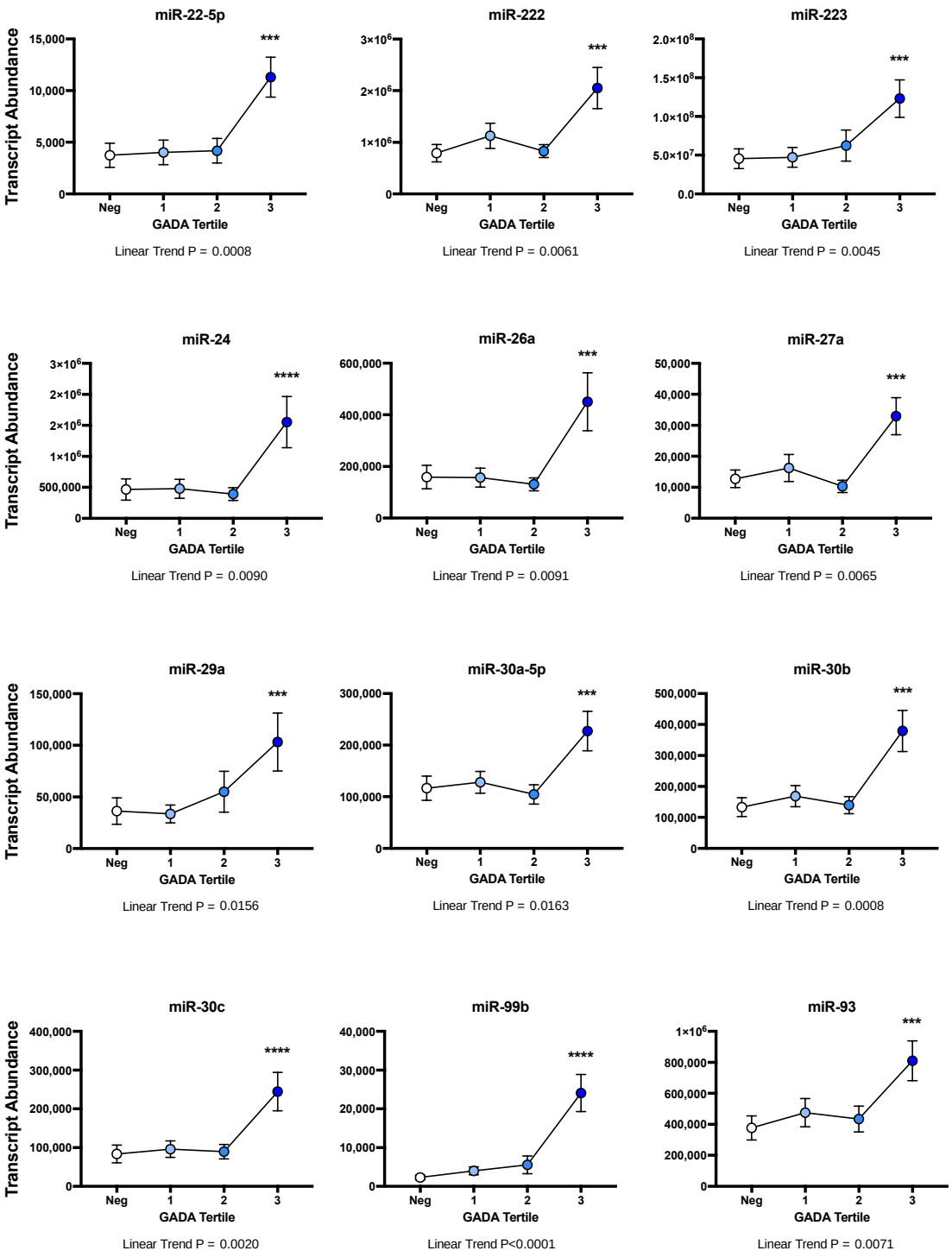

Figure 5-8.2. Candidate miRNAs correspond to GADA titres at T1D diagnosis

MicroRNA abundance in seronegative individuals (Neg), and those in each GADA tertile. Mean ± SEM. Linear trend significance $P < 0.05$. ** Adjusted $P < 0.01$, *** Adjusted $P < 0.001$, **** Adjusted $P < 0.0001$ compared to Neg (Kruskal-Wallis non-parametric one-way ANOVA with corrected Dunn's multiple comparison test).

5.4.5. MicroRNAs and Cell-free DNA Associate with HbA1c Levels at Diagnosis

To investigate whether the molecular signature was indicative of β-cell function, it was compared to HbA1c levels measured at diagnosis. As with GADA titres, the HbA1c levels of individuals at diagnosis were split into tertiles and the trend analysed. The details of the tertiles can be found in Table 5-C. Methylated and unmethylated insulin cfDNA, as well as eight candidate miRNAs demonstrated a significant association with HbA1c levels. Unlike GADA titres, all of these molecules demonstrated a quadratic trend, with abundance increasing in tertiles 2 and then dropping again in tertile 3 (Figure 5-9). It must be noted that 14% was the upper limit of detection (any results higher than this were reported as 14.1%) of the HbA1c assay used at the Princess Margaret Hospital, and so tertile 3 could contain individuals with a higher HbA1c at diagnosis.

Table 5-C. HbA1c tertiles of individuals at T1D diagnosis

HbA1c Tertile	Individuals (N)	Range (%)	Median (%)
1	62	6.1 – 10.7	9.3
2	62	10.8 – 12.8	12.0
3	63	12.9 – 14.1*	14.1

* The highest reported value for glycated haemoglobin was 14.1% by the pathology lab. In Tertile 3, 58.7% of individuals had a HbA1c reported at 14.1%.

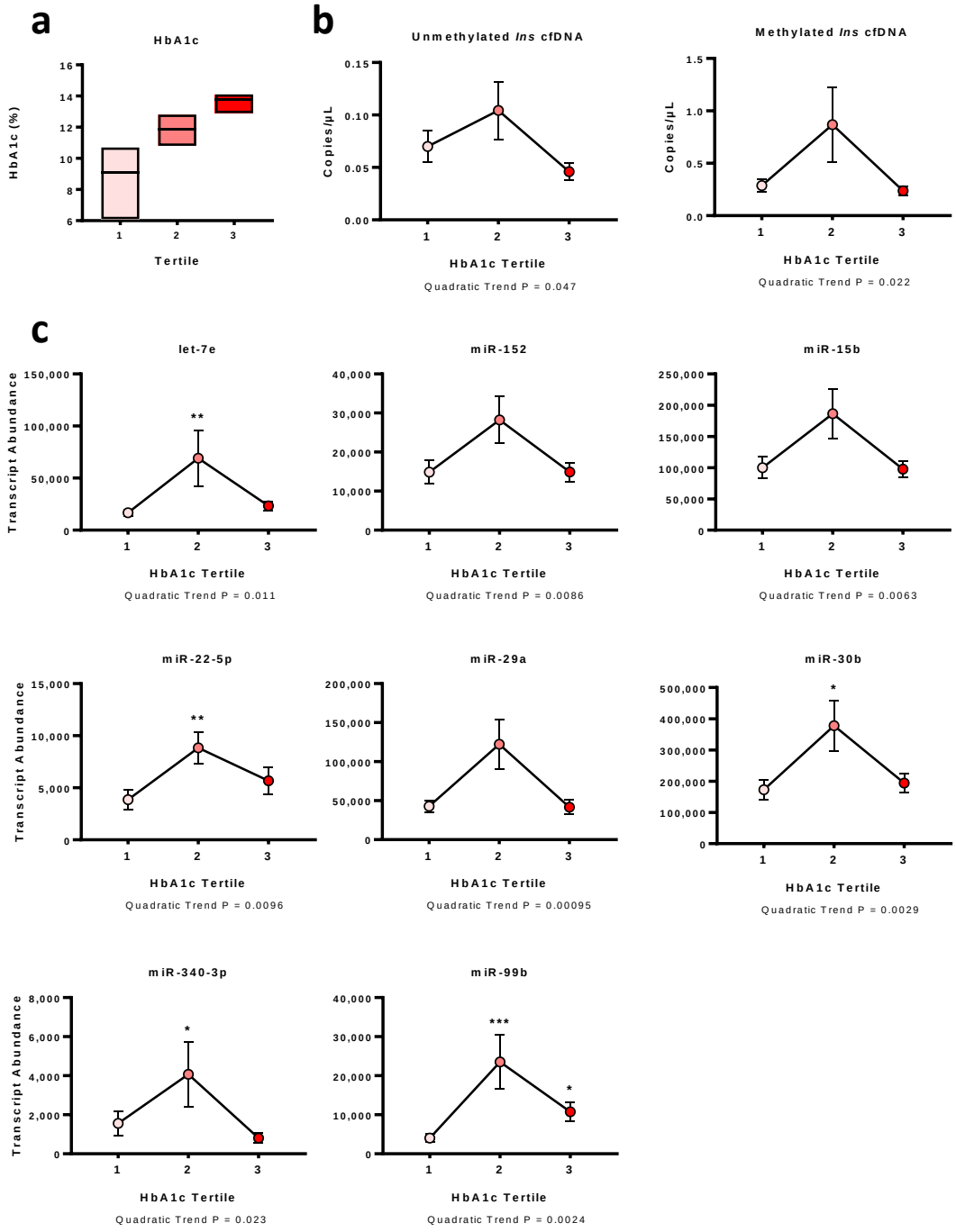

Figure 5-9. Insulin cfDNA and candidate miRNAs have a quadratic relationship with HbA1c at T1D diagnosis

(a) Boxplot (median, min-max) of HbA1c tertiles. Cell-free DNA (b) and eight candidate miRNAs (c) demonstrate a quadratic relationship with tertiles of HbA1c at diagnosis. Mean ± SEM. Quadratic trend significance $P < 0.05$.

* Adjusted $P < 0.05$, ** Adjusted $P < 0.01$, *** Adjusted $P < 0.001$, compared to tertile 1 (Kruskal-Wallis non-parametric one-way ANOVA with corrected Dunn's multiple comparison test).

5.4.6. Immune Modulation Affects the Circulating Molecular Signature

Immune modulation has been proposed as a clinical tool to reduce the loss of residual β-cell loss after T1D diagnosis. To assess whether the immune modulatory effect of ingested interferon-α causes a change in the molecular signature of β-cell death investigated throughout this thesis, the cfDNA and miRNA abundance was measured within the circulation of individuals randomised to placebo, 5,000 units, or 30,000 units of hrIFNα, as published previously (51). Plasma samples were taken from these individuals at baseline (within 6 weeks after diagnosis) and then four subsequent time points. Table 5-D details the average duration of each time point. Both methylated and unmethylated insulin cfDNA show no significant change over time or between treatment groups. Three miRNAs, miR-27b, -145, and -223, demonstrate a significant ($P<0.05$) elevation in abundance in the placebo group at one time point (Figure 5-10). A further four miRNAs, miR-21, -24, -92a, and -152, show a trend toward elevated abundance in the placebo group (indicated by a P-value between 0.5 and 0.1). Interestingly, miR-27b also demonstrated a significant difference between time points ($P=0.0329$) and a significant interaction between time and treatment ($P = 0.0398$ measured by repeated measures ANOVA). This indicates that the IFNα treatment had a significant impact upon this miRNA over the course of the study.

Table 5-D. Time points for IFNα or placebo treatment samples

Time Point	Individuals, N (Placebo/5,000/30,000)	Days After Baseline (mean ± SD)
T0	13/8/10	0
T1	13/8/10	102.2 ± 17.3
T2	13/8/10	203.2 ± 16.3
T3	13/8/10	307.2 ± 22.4
T4	13/8/10	420.5 ±43.8

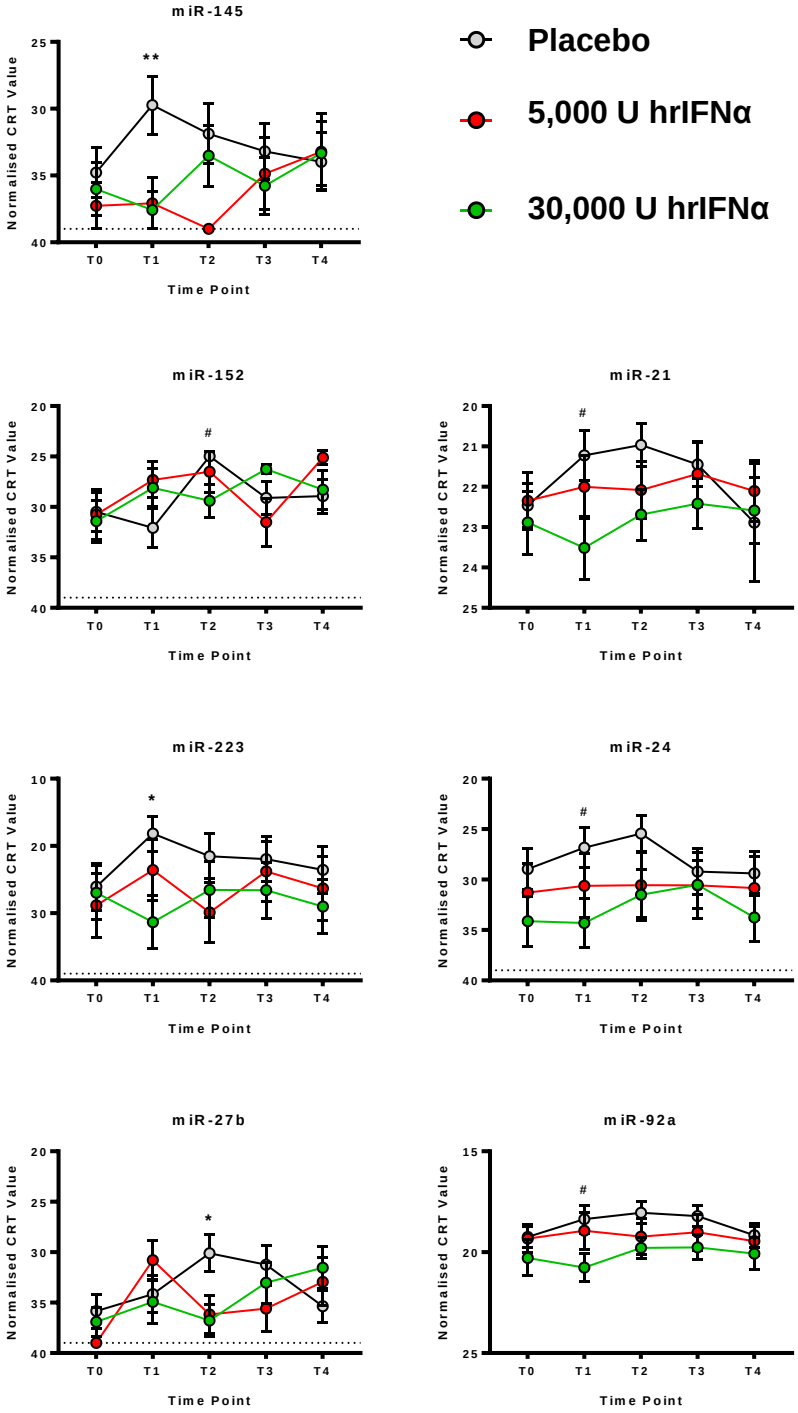

Figure 5-10. Changes in miRNA abundance during treatment with hrIFNα or placebo

Placebo (grey), 5,000 units (red) or 30,000 units (green) of hrIFNα at baseline and four subsequent time points. * P < 0.05 # P < 0.1 between treatments at the respective time point (test of sum of squares). Mean ± SEM. Dotted line is the limit of detection (CRT = 39).

5.5. Discussion

5.5.1. Circulating MicroRNA Signature During T1D Progression

Previous studies have demonstrated that miRNAs display differential abundance within the circulation of individuals with T1D (148-150; 152; 154; 216). What they have yet to demonstrate, however, is the change in abundance that these small ncRNAs may show during the progression T1D – before, during and after diagnosis. Data from this chapter demonstrate that individuals at high risk of T1D (prior to diagnosis) and those at the point of diagnosis present with an elevated abundance of numerous candidate miRNA identified throughout the remainder of this thesis. Indeed, some of these miRNAs, such as let-7e and miR-103, show a significant linear trend, indicating a progressive decline after diagnosis. Furthermore, three of these miRNAs, miR-26a, -27a and -374, exhibit similar patterns of abundance within the circulation of NOD mice as they progressed to T1D (Figure 3-12). They were elevated in the mice prior to the onset of T1D and reduced as they progressed.

This elevated abundance may be indicative of the chronic underlying β-cell death in the progression to clinical disease. Indeed, this may be one of the reasons as to why many of the miRNAs display the lowest abundance in the 6 week period following diagnosis; many patients enter a “honeymoon phase”, or partial remission, soon after diagnosis, where the combination of increased immune tolerance and decreased glucotoxicity and lipotoxicity reduce β-cell stress (217). Unfortunately, this phase does not last; the majority of patients who enter the honeymoon phase exit it within 12 months (218). The subsequent return of β-cell stress may drive the increased abundance of select miRNAs, such as miR-21, -27b, and -222, seen in the <12 months post-Dx group (Figure 5-3) . Interestingly, some of these miRNAs, including miR-127, -145, -22-5p, 27b, -99b, 125a-5p, -152, and -186, significantly rise in the

circulation of patients with long-standing T1D, compared with those who were newly-diagnosed. This may be indicative of β-cell regeneration and the return of a stressed state in these individuals.

Not all of the miRNAs were elevated prior to diagnosis. MicroRNA-375 was significantly increased at diagnosis compared to those at high risk. Previous findings (mouse models) reported that only a minute proportion (~1%) of miR-375 is actively released into the circulation by β-cells, and so this miRNA may be an indicator of acute cell death at diagnosis (157). While this miRNAs displays an association with T1D, their use as markers to stratify those at high risk may be limited.

5.5.2. Insulin Cell-free DNA Abundance During T1D Progression

Unlike the candidate miRNAs, both methylated and unmethylated insulin cfDNA decreased at diagnosis and then returning to levels similar to those prior to diagnosis with 12 months (Figure 5-5). Patients with long-standing T1D (20 years post Dx) display decreased levels of insulin cfDNA, similar to that at diagnosis. This finding is at odds with previous work completed by Professor Mirmira's group, who found them to be elevated at diagnosis and then decrease over the following 8 week and 12 month period (168). This study did not evaluate the levels in patients with a long disease duration.

The finding that the insulin cfDNA is reduced in our hands at the point of diagnosis, in contrast to opposing findings on similar (at diagnosis) samples by Prof. Mirmira's group, demands further analysis of such at –diagnosis samples with shared analytical as well as sample collection protocols to confirm the potential use of these molecules as biomarkers of T1D progression. Furthermore, the propensity of these molecules to degrade once released from dying cells (seen in the short reported half-life (161; 163; 164) and the islet cell death data

discussed in Chapter 3), may explain why previous studies have not been able to easily identify individuals that progress to T1D using insulin cfDNA assessment (163). Additionally, freeze-thaw cycles negatively impact upon the detectable abundance of cfDNA (data not shown). This, as well as other parameters, including sample collection, storage conditions and assay sensitivity, may account for the discord between multiple research groups.Collaborative studies planned between the Hardikar (Sydney) and Mirmira (Indianapolis) groups will potentially address these issues in the coming months through exchange of protocols and deidentified sample sets for validation across the two labs.

5.5.3. Clinical Parameters at T1D Diagnosis

Another important potential use for a molecular signature of T1D progression is to predict or assess the immune function and glycaemic control of patients. In this chapter, the relationship between the molecular signature and antibody tertiles, as well as HbA1c, at the point of diagnosis was also investigated.

Few studies have examined associations between circulating miRNAs and autoantibody titres in subjects with T1D (152; 154). Here, this study has identified 23 miRNAs that have a significantly positive linear relationship with GADA titres, including miR-146a, which has previously been identified as reduced in PBMCs with increasing GADA titres (154). This reduction in PBMCs may reflect a release of this miRNA into circulation. Increased titres of GADA may reflect an increase in immune-mediated islet cell death, causing an increase in circulating miRNAs. Furthermore, when the tertiles were examined individually, the majority of the identified miRNAs were significantly elevated in tertile 3 when compared to the negative group or tertiles 1 and 2 (Figure 5-6). These individuals may be undergoing immense islet cell stress or death.

Glycated haemoglobin is a common measure for average BGLs over the previous three-month period and is used to monitor glucose control in people with diabetes. This measure has also been investigated as both a diagnostic criterion (219) and a predictive marker (220) of diabetes progression. Both cfDNA and eight miRNAs demonstrated a significant trend with HbA1c levels, however it presented as a quadratic relationship (Figure 5-7). This means that those individuals with the lowest and highest tertiles of HbA1c demonstrated lower abundance of these markers, when compared to the middle tertile. Increased glycaemic variability within the second tertile may explain this increase, with tertile 1 and 3 predicted to have consistently lower or higher BGLs respectively. Another explanation is that those with a lower HbA1c (tertile 1) present with less aggressive β-cell loss at diagnosis, while those at the upper tertile have lost a significant portion of functional β-cell mass. Both situations would result in decreased release of these microRNA biomarkers. Further investigation is required to disseminate the relationship between these markers and measures of glycaemic control. For example, the measurement of fructosamine or 1,5-anhydroglucitol in these patients would allow the estimation of glycaemic control within a much shorter time span (1 to 2 weeks instead of 3 months) (221) to investigate the relationship between these markers short-term changes in blood glucose. Such measurements (i.e Fructosamine assays for glycated albumin or the GlycoMark test for 1’5 anhydroglucitol) may be of specific importance in other cohorts of islet graft recepients, which are planned for future analysis at the Hardikar lab. Since islet cell death is known to stabilize within 2 to 14 days post-islet transplantation, these measurements will provide valuable information to understand the abundance of these molecular biomarkers (microRNAs and insulin cfDNA) in such individuals.

5.5.4. Effects of Immune Modulation on the Molecular Signature of B-cell Death

Immune modulation has been presented as a potential therapy for subjects with newly diagnosed T1D to preserve the residual β-cell function. Residual β-cell function was previously shown to correlate with decreased complication rates (6) and so preservation of this would have a significant clinical impact. Ingested IFNα has previously been shown to reduce the incidence of diabetes in NOD mice (222) and has been investigated as a treatment for multiple sclerosis (223), however its exact biological function remains unclear. The study conducted by Rother and colleagues investigating the use of ingested hrIFNα found that the lower dose (5,000 units/day) resulted in a significant increase in β-cell function assessed via stimulated C-peptide AUC when compared to placebo or 30,000 units (51). These samples were analysed within this chapter, with seven candidate miRNAs showing changes (Figure 5-8). Overall, treatment with ingested hrIFNα seemed to reduce miRNA abundance. This suggests that modulating the immune system causes a decrease in the markers of β-cell death, which was clinically diagnosed as increase in β-cell function (C-peptide AUC). Additional investigations must be conducted to determine differences between the 5,000 units/day and the 30,000 units/day hrIFNα doses. As mentioned previously, increased residual C-peptide is associated with a lower risk of chronic complications (6), and so these therapeutic agents and the markers of β-cell death and C-peptide secretion could be immensely useful in assessing the prognosis of T1D individuals.

5.5.5. Strengths and Limitations

This study is the first to offer an insight into circulating miRNAs and cfDNA in individuals before, during and after T1D diagnosis, both in those newly diagnosed as well as those with long-standing disease and in response to immunomodulation with IFNα. The inclusion of

children at high risk of developing T1D is a significant strength. Although not all of the children will develop T1D, their high risk status provides a crucial starting point. Samples are still being collected from this group, and so further analysis may be completed in the future when it is clear as to which individuals have progressed to clinical disease.

Furthermore, the inclusion of almost 200 individuals at the point of diagnosis allows the assessment of these circulating markers with minimal medical intervention (application of exogenous insulin). A number of samples from this cohort were taken on the day of diagnosis. Other studies have utilised samples from newly-diagnosed patients, some only one month post-diagnosis (151; 224), however one cannot discount the effects of medical intervention or the honeymoon phase during this time.

As with all studies, there are limitations. The high risk and <12 months post-Dx groups both contained a small number of individuals (N=19) but analysed multiple samples taken on different time points. This could assert individual bias into the results and should be repeated with larger numbers of individuals. Furthermore, not a significant number of age and gender matched control samples were assessed to ensure that the signature allowed clear identification and stratification between these groups. Unfortunately, gaining blood samples from healthy children tends to be difficult, however, this analysis will be completed in the near future as part of the PREDICT T1D study ld by A/Prof. Anand Hardikar at the NHMRC CTC, University of Sydney. This study will also include ~400 and ~700 at diagnosis of T1D individuals from HongKong and India, with another subset of samples from Denmark and the Middle East. These future studies planned by A/Prof Hardikar as part of the PREDICT T1D study will also provide insights in understanding the potential of these molecular biomarkers in T1D

individuals from different ethenic backgrounds. Control samples from age and gender matched healthy (non-diabetic) children and adults are available for future analyses.

5.6. Conclusions

The miRNA signature identified throughout this thesis exhibits incredible potential to monitor individuals progressing to T1D as well as understand the effects of potential therapeutics. The abundance of these circulating molecules show significantly different profiles in individuals before, during and after T1D diagnosis. The majority (N=27) of the miRNAs are elevated in people at high risk of T1D, those at the point of diagnosis, or both. Other miRNAs reach peak abundance within 12 months (N=8) or 20 years after diagnosis (N=2). They also demonstrate relationships with clinical parameters at diagnosis, including GADA titres and HbA1c. The linear relationship seen between miRNA abundance and GADA titres indicates an association between these miRNAs and immune function. Insulin cfDNA needs further validation for its potential use as a direct biomarker of islet β-cell death and T1D progression, as it decreases at the point of diagnosis and after 20 years, making it difficult to stratify individuals solely based on cfDNA analysis. It does, however, show a significant relationship with glycaemic control at diagnosis. Future studies described above will help to ascertain and cross-validate these findings through more rigorous and detailed shairing of protocols, deidentified samples and testing in larger numbers of ethnically diverse study samples.

The application of immune modulatory therapy to subjects with newly diagnosed T1D causes a shift in the miRNA signature of β-cell death. The use of hrIFNα often resulted in a decrease in miRNA abundance. This underscores the use of these microRNAs as an indicator of the residual functional β-cell mass preservation during immune-mediated β-cell death in individuals with Type 1 Diabetes.

6. Conclusions

This thesis, and the four years of work dedicated to its composition, details the journey of identification and characterisation of a molecular signature of β-cell death and T1D progression. There are numerous conclusions to be made from this body of work, each discussed in detail in the relevant chapters. Together, these chapters highlight the impact that the choice of a technology/platform can make on a miRNA signature, the central use of models of disease, and the importance of unbiased profiling. Due to the completion of these initial stages, the resulting molecular signature displays great potential in identifying individuals before, during and after T1D diagnosis.

This thesis investigated the use of a preliminary miRNA signature as a biomarker of β-cell death and T1D progression. As discussed within the introduction, there were 50 miRNAs that made up this preliminary signature. Figure 6-1 gives an overview of some of the important miRNAs highlighted through the studies outlined in this thesis. Seven of these miRNAs were found to be released due to islet cell stress/death, elevated in NOD mice, and elevated in human clinical samples from individuals at high risk of T1D or at the point of diagnosis. These miRNAs should be the focus of subsequent investigations in order to further refine this signature. While this thesis describes a substantial body of evidence for the use of these miRNAs as biomarkers of β-cell death, it is important to note that 10 miRNAs that were initially identified did not show significant changes during islet SNP exposure, NOD mice progression, or in high risk individuals or patients at the point of diagnosis (Figure 6-1).

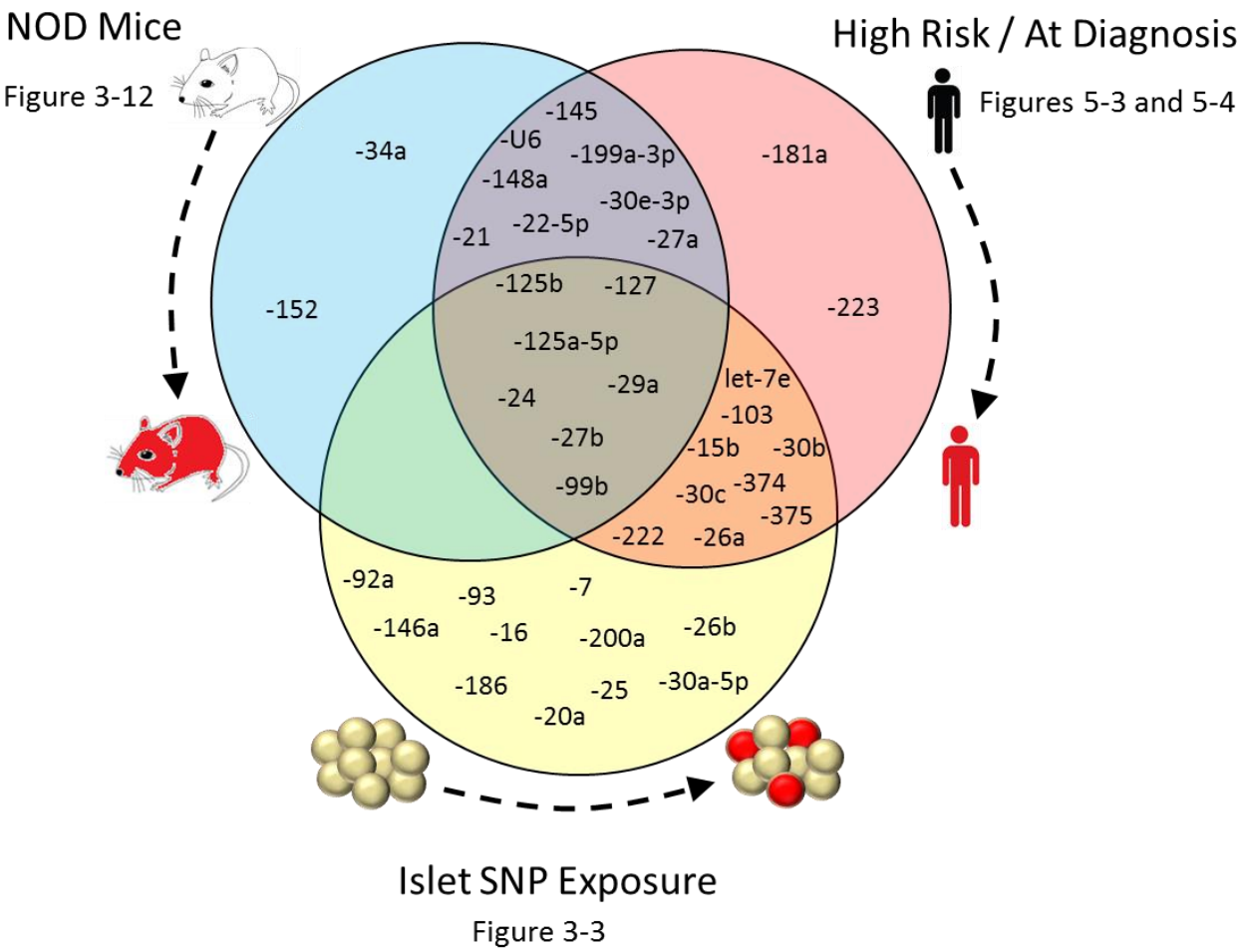

Figure 6-1. Overview of major miRNA findings

Venn diagram of PREDICT T1D miRNAs found to be elevated in NOD mice (blue circle), released after human islet SNP exposure (yellow circle), elevated in individuals at high risk of T1D or at the point of diagnosis (red circle), or a combination of all three. MicroRNA-9, -126, -155, -188, -210, -220c, -301b, -326, -340-3p, -409-5p, -558, and -625 were not found to significantly change in any of these studies.

6.1. Implications of Thesis Findings

The data presented within this thesis has wide ranging implications for researchers and clinicians interested in monitoring the progression of individuals to T1D or response to potential therapeutics, or indeed anyone investigating the use of miRNAs as biomarkers of islet β-cell death and diabetes progression. First and foremost, the technology used to identify and characterise circulating miRNAs can have a tremendous impact upon the final signature. This is a factor that seldom receives the attention it deserves. For the signature to have proven efficacy, and to make this transition to diagnostics, the detection method must be highly reliable and reproducible. Furthermore, the studies presented in Chapter 2 demonstrate that moving to higher throughput platforms resulted in a reduction of sensitivity, especially for the low abundance transcripts. A balance must be struck between sensitivity and throughput; this is especially difficult due to the immense number of human miRNAs that one needs to assess.

Using the OpenArray technology, a signature of miRNAs that are released during islet cell stress/death, which are elevated in NOD mice prior to immune infiltration and glycaemic dysfunction, and those that are differentially abundant in subjects with T1D compared with controls, and whose levels change during T1D progression, were identified. Although the signature requires further refinement to increase its power to stratify individuals undergoing β-cell death, it presents a solid platform from which to do so. This is underscored by the evident associations of these miRNAs with measures of autoimmunity, glycaemic control and β-cell function.

Methylated and unmethylated insulin cfDNA, the focus of much recent interest, did not appear to function as efficiently as a marker of β-cell death. While it was released during islet cell death assays, it can be promptly degraded; a finding in line with previous studies that

identified a short half-life of cfDNA *in vivo* (161; 163; 164). Furthermore, insulin cfDNA was decreased at the point of diagnosis and after 20 years, which is in contrast to a report (168) on similar at-diagnosis of T1D samples, necessitating further testing/validation of these biomarkers. This observation is also significantly different to previous studies employing methylated and unmethylated insulin cfDNA as a biomarker of T1D progression (163; 168; 172). These molecules do, however, demonstrate an association with glycaemic control at diagnosis, and so their use as clinical markers should not be dismissed without future testing.

In conclusion, these thesis findings support the use of circulating miRNAs and cfDNA as markers of pancreatic islet β-cell death, T1D progression, immune function and glucose homeostasis .

6.2. Future Directions

The present study was planned by A/Prof. Anandwardhan A. Hardikar (NHMRC CTC, University of Sydney), as part of his JDRF Australia T1D Clinical Research Network fellowship. Future investigations can build upon and refine the findings outlined in this thesis. In particular future studies will focus on refining the signature to achieve the desired power to stratify individuals who progress to T1D. To enable this, the following studies will be performed:

1. Assessment of this signature in low risk children without T1Dto assess who do and do not progress to T1D over time. This would confirm its elevation and determine the power with which one can utilise it to discriminate between these populations. These studies are currently being carried out on pediatric plasma samples obtained through Professors Kim Donaghue and Alicia Jenkins.
2. Refinement of this signature coupled with further analysis in high risk individuals that do and do not progress to T1D would highlight the power of this signature to identify and stratify progressors.
3. Longitudinal studies are needed to investigate whether this molecular signature could predict the time to diagnosis. As demonstrated earlier, the microRNA abundance-based prediction of residual C-peptide mass will help in understanding the potential benefit conferred by a treatment strategy (eg. Interferon therapy).

In addition to the important studies outlined above, it would be of great interest to researchers to:

4. Identify the tissue of origin of the miRNAs. As discussed earlier, not all of the candidate miRNAs are release by islets, and so studies could aim to identify which other cell types are responsible for their release into circulation. Such studies are already being

carried out as part of another PhD project in the Hardikar lab wherein microRNA discovery analyses in several hundreds of human tissues (including islets), will generate expression maps of tissue-nriched microRNAs.

5. Assess whether the release is active or passive. Active release would suggest that the miRNAs are not merely markers of disease but signalling molecules released in response to stress.
6. As each microRNA can target several mRNAs, it would be important to investigate the mRNA target(s) for a signature of microRNAs so as to identify whether these miRNAs have a role in bringing about β-cell death rather than just being circulating biomarkers of the process.

Future studies that are underway in the Hardikar lab as well as in several other leading laboratories worldwide will help to address these and several other important questions in understanding the potential of these molecular biomarkers of β-cell death. The data presented through this thesis offer further advance to the existing data from the Hardikar lab in terms of protocol optimization, T1D biomarker discovery and clinical validation studies that will help to guide further research. Hopefully, future studies will answer these and many other questions in predicting the progression to Type 1 Diabetes and offer simpler and more powerful tools to assessing the potential of such therapies in preserving functional β-cell mass in individuals at high risk of Type 1 Diabetes.

Supplementary Chapter 1: MicroRNA Spike-in Optimisation

S1.1. Chapter Overview

The use of endogenous controls is a crucial aspect of many techniques utilised in molecular biology. Many ncRNAs have been identified and utilised as endogenous controls in plasma and serum samples, however there has not been a consensus regarding which ncRNA/s are the most effective controls for this sample type. Due to the cell-free nature of serum and plasma, all ncRNAs present within these samples originally came from the surrounding cells, either through organised secretion, or as a result of cellular stress and/or death.

The expression of 11 commonly used endogenous controls was analysed within these circulating samples. These studies identified that the oftn-cited “housekeeping” microRNAs have marked variability within biofluids. The use of synthetic spike-in miRNAs was therefore optimised taking into consideration the microRNAs from two genetically diverse organisms; *Caenorhabditis elegans* and *Arabidopsis thaliana*, as potential spike-in controls for both RNA isolation and reverse transcription. The optimal spike-in amount was optimized to be 250 femtomoles (fmol) for RNA isolation and 150 attomoles (amol) for reverse transcription. Interestingly, while none of the synthetic miRNAs demonstrated homology to human ncRNAs, *C. elegans* miRNAs were detectable in sample that did not contain the spike-in, indicating some cross-talk in the miRNA assays designed for these analysis. Furthermore, the use of an automated RNA isolation technology greatly improved the stability of spike in controls, possibly as a result of less human error. The use of synthetic non-human miRNAs to control for introduced variability allows researchers to avoid inherent issues with circulating endogenous controls.

S1.2. Chapter Aims

Studies in this chapter aimed to:

1. assess the suitability of commonly used endogenous control ncRNAs for normalisation of qPCR data;
2. investigate the use of synthetic miRNA spike-in molecules as controls for variation introduced during different stages along the RNA isolation and reverse transcription workflow for microRNA estimation;
3. (a) identify the optimal amount of spike-in to be added, and (b) at which protocol step to do so; and
4. compare the impact of manual versus automated RNA isolation on the recovery of spike-in controls.

S1.3. Methods

S1.3.1. Synthetic MicroRNAs

Synthetic miRNAs were selected from the nematode *Caenorhabditis elegans* and the plant *Arabidopsis thaliana*. The names and sequences can be found below:

Organism	miRNA	Sequence (5'-3')
Caenorhabditis elegans	cel-miR-39	UCACCGGGUGUAAAUCAGCUUG
	cel-miR-54	UACCCGUAAUCUUCAUAAUCCGAG
	cel-miR-238	UUUGUACUCCGAUGCCAUUCAGA
Arabidopsis thaliana	ath-miR-159a	UUUGGAUUGAAGGGAGCUCUA
	ath-miR-172a	AGAAUCUUGAUGAUGCUGCAU

Table S1-A. Synthetic microRNA sequences.

All synthetic miRNAs were manufactured by Sigma. The miRNAs were reconstituted in nuclease-free water and spiked-in at the appropriate amount to the relevant samples. Each of these synthetic miRNAs were compared with human miRNA database using the BLASTN function of miRBase. None of these sequences exhibited homology to known human miRNAs.

S1.3.2. RNA Isolation

RNA was isolated from plasma samples using the manual SOP outlined in Appendix B or the automated SOP outlined in Appendix C, apart from the spike-in step. Synthetic miRNAs were added at differing amounts and at different steps within the manual SOP as outlined within the results. For each comparison, plasma samples were mixed thoroughly and then aliquots

were created for each experimental condition, thereby eliminating any differences from improper mixing and sampling. The samples that underwent automated RNA isolation did so as per the SOP outlined in Appendix C.

S1.3.3. Reverse Transcription and Quantitative PCR

Reverse transcription and quantitative PCR for all spike-in comparisons was conducted using the 96-well plate protocol published previously (188). The samples included in the manual versus automated RNA isolation comparison underwent RT, pre-amplification and qPCR as per the OpenArray LSI protocol outlined in Appendix D.

S1.4. Results

S1.4.1. Endogenous Controls

The abundance of eleven small nucleolar (sno)RNAs were measured in four plasma samples. These snoRNAs are commonly utilised as endogenous controls, however Figure S1-1 shows that these ncRNAs demonstrate marked variability. Indeed, six of the eleven ncRNAs were undetectable in one or more of the samples tested. U6, the most commonly used ncRNA endogenous control, had a higher abundance than the other ncRNAs tested, although it demonstrated considerable variability between samples, with a CT range of 21.7 to 28.9.

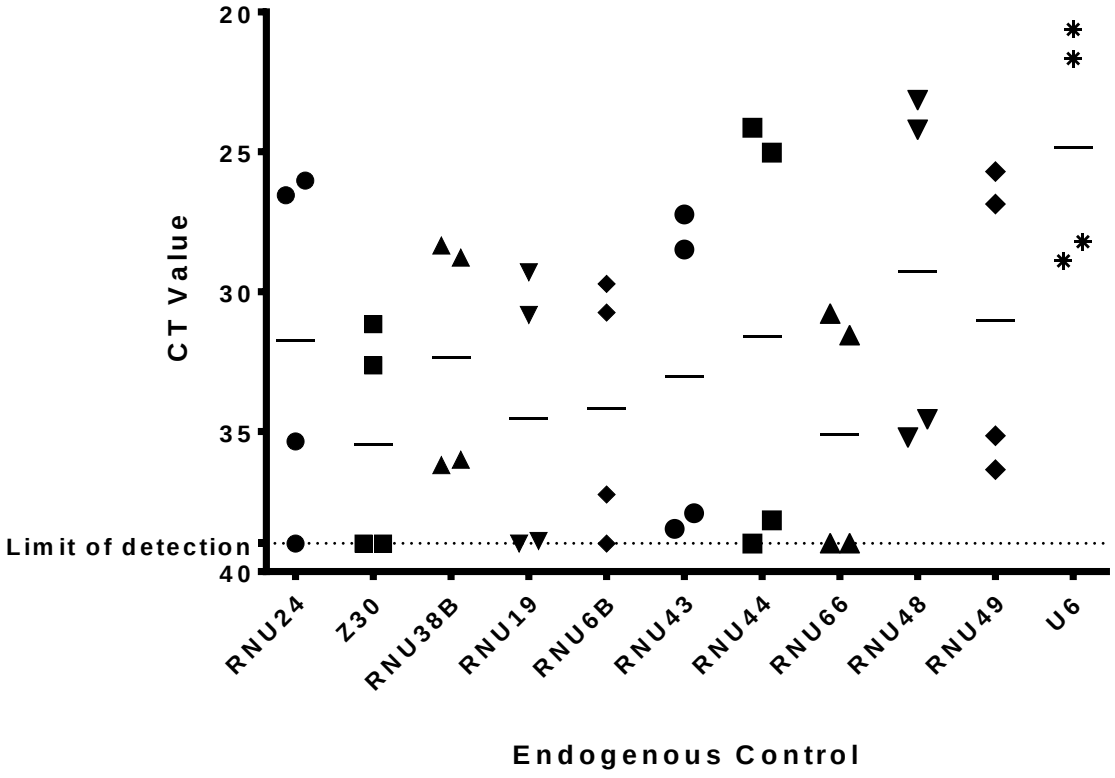

Figure S1-1. Circulating endogenous ncRNA controls demonstrate marked variability

Eleven ncRNAs commonly used as endogenous controls were measured using RNA isolated from four plasma samples. Each sample was run in duplicate. Limit of detection (dotted line) is 39 cycles. Solid line = mean.

S1.4.2. Synthetic *Caenorhabditis elegans* MicroRNAs

To determine the optimal RNA isolation spike-in amount, four differing amounts of *C. elegans* miRNAs, cel-mir-39, -54 and -238, were added to three plasma samples during RNA isolation. The abundance of these spike-in miRNAs can be found in Figure S1-2. The optimal amount was deemed to be 250 fmol as it displays a final abundance that will work effectively on both low, medium and high-throughput qPCR systems. Medium and high-throughput qPCR systems, such as the TLDA and OpenArray platforms respectively, require pre-amplification before quantitation, which may reduce the CT value. Therefore, using 2.5 pmol of spike-in that displays an average CT value of 10.1 on a low-throughput platform may not be assessed accurately on higher throughput technologies. Interestingly, the endogenous U6 also seems to decrease in abundance with the *C. elegans* spike-in, despite being isolated from the same plasma sample.

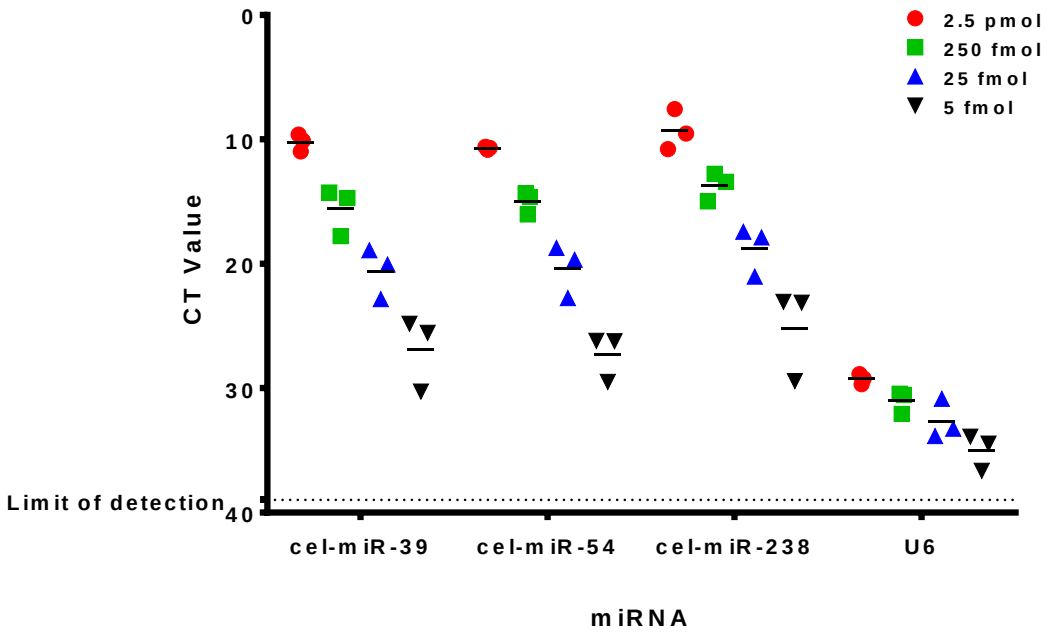

Figure S1-2. Optimisation of synthetic miRNA input for RNA isolation.

Three synthetic *C. elegans* miRNAs (cel-miR-39, cel-miR-54 and cel-miR-238) were spiked into plasma samples during RNA isolation at 2.5 picomoles (pmol), 250 fmol, 25 fmol or 5 fmol. These miRNAs were then quantitated via qPCR. U6 is included as an indicator of endogenous miRNA. Limit of detection (dotted line) is 39 cycles. Solid line = mean.

When samples were assessed with and without *C. elegans* RNA isolation spike-in, those without the spike in still demonstrated amplification, albeit at a much lower CT (Figure S1-3). This suggests the possibility of assay crosstalk or sequence homology with an as-yet uncharacterised human miRNA. This severely undermines the use of *C. elegans* miRNAs as synthetic RNA isolation controls.

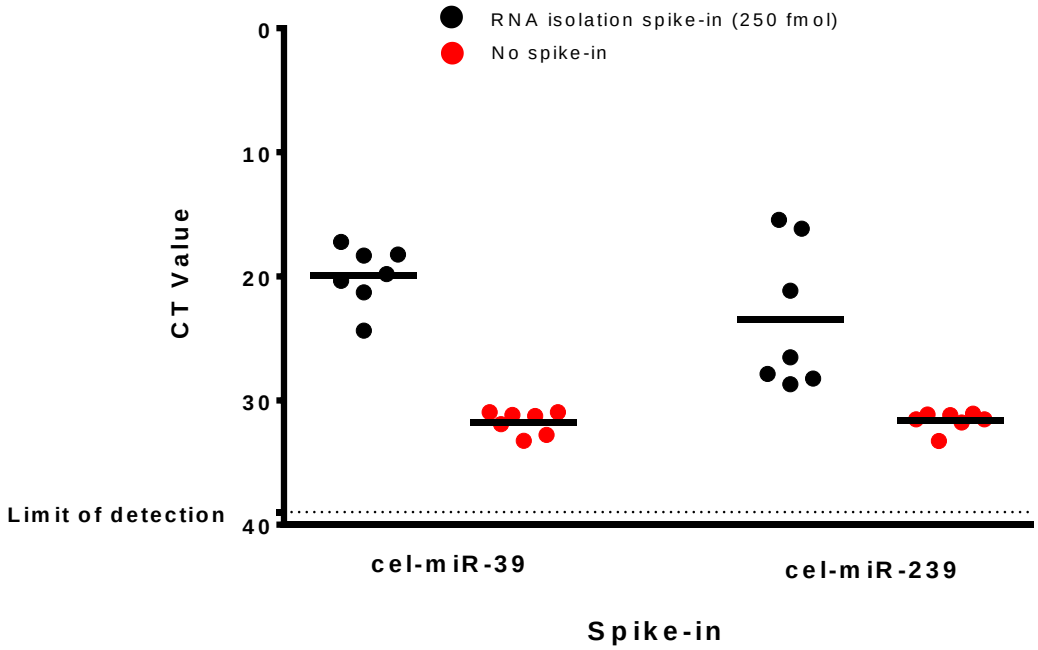

Figure S1-3. Evaluation of synthetic *C. elegans* microRNAs as controls for RNA isolation.

Two synthetic miRNAs (cel-miR-39 and -238) were spiked into plasma samples during RNA isolation (black circles). They were then quantitated via qPCR and compared to the same plasma samples with no spike in miRNAs (No spike-in, red circles). N = 7 per group. Limit of detection (dotted line) is 39 cycles. Solid line = mean.

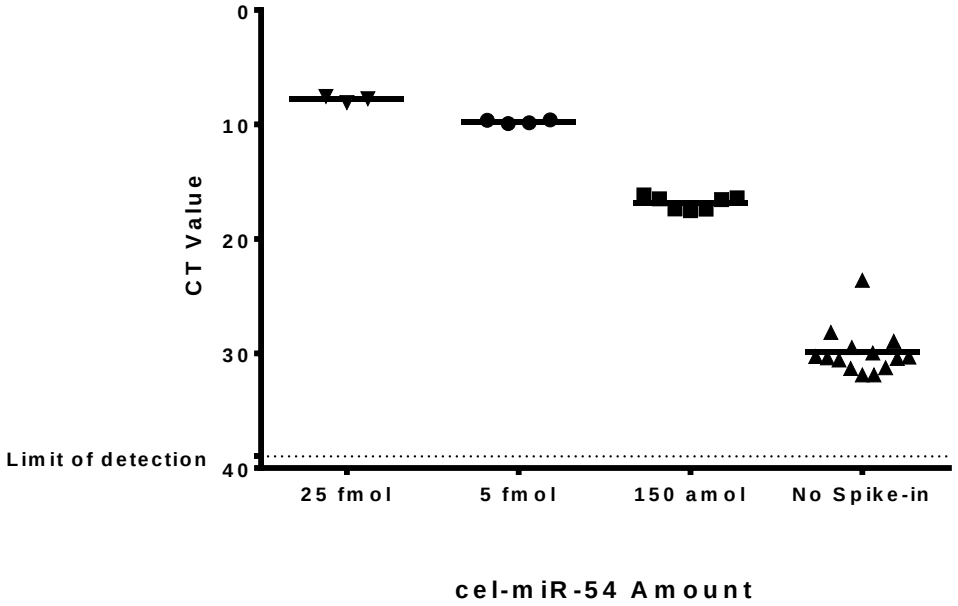

Figure S1-4. Optimisation of synthetic miRNA input for reverse transcription.

Cel-miR-54 was added to the reverse transcription reaction at 25 fmol, 5 fmol or 150 amol and then quantitated by qPCR. Limit of detection (dotted line) is 39 cycles. N = 3 for 25 fmol (upside down triangles), 4 for 5 fmol (circles), 7 for 150 amol (squares), and 14 for No spike-in (triangles). Solid line = mean.

One *C. elegans* miRNA, cel-miR-54, was selected to optimise the amount needed for a reverse transcription spike-in. As there should be ~100% conversion of miRNAs during this process, the amount of spike in was reduced to either 25 fmol, 5 fmol or 150 attomoles (amol) per reaction. The abundance of these spike-in miRNAs can be found in Figure S1-4. As with the RNA isolation spike-in, 150 amol was deemed to be the optimal RT spike-in amount as it displays a final abundance (average CT = 16.8) that will work effectively on both low, medium and high-throughput qPCR systems. Again, samples without the *C. elegans* spike-in still displayed amplification (average CT = 29.9), undermining the use of this miRNA as an RT control.

S1.4.3. Synthetic *Arabidopsis thaliana* MicroRNAs

Although the use of *C. elegans* miRNAs allowed for the optimisation of RNA isolation and RT spike-in amounts, the detection of these miRNAs in samples with no spike-in added undermines the efficacy of these molecules as controls. As such, miRNAs from another model organism, *Arabidopsis thaliana*, were assessed as RNA isolation and RT spike-in controls (Figure S1-5).

Two *A. thaliana* miRNAs, ath-miR-159a and -179a, were used for RNA isolation and RT respectively. One sample displayed significantly lower RNA isolation spike-in, possibly due to the variability of manual RNA isolation. The other samples displayed minimal variability (CT range 17-17.4). Ath-miR-159a was not detectable in samples with no spike-in. The majority of samples without the RT spike-in had no detectable ath-miR-172a. One sample demonstrated very low abundance of ath-miR-172a (CT = 36.3). One sample demonstrated very low abundance of ath-miR-172a (CT = 36.3). Endogenous U6 abundance was not affected by the presence of ath-miR spike-ins.

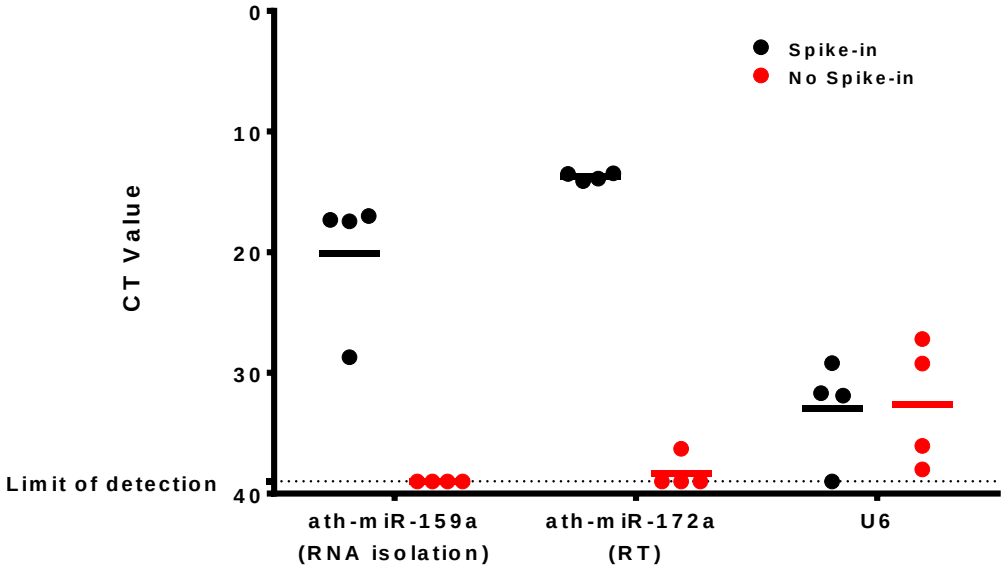

Figure S1-5. Evaluation of synthetic *A. thaliana* microRNAs as controls for RNA isolation and reverse transcription.

250 fmol of ath-miR-159a was added to four plasma samples during RNA isolation, and 150 amol ath-miR-172a was added during reverse transcription. They were then quantitated via qPCR. U6 is included as an indicator of endogenous miRNA. Limit of detection (dotted line) is 39 cycles. Solid line = mean.

To determine the optimal stage of RNA isolation to introduce the synthetic ath-miR spike-in, 250 fmol was added directly to the plasma sample, after the addition of the TRIzol reagent (step 4 of the SOP in Appendix B) or after incubation with TRIzol (step 5 of the SOP). Despite adding the ath-miR spike-in to the plasma sample ~5 mins prior to the addition of the TRIzol reagent, significant degradation of this miRNA was seen when measured via qPCR (Figure S1-6). No significant difference was observed when the spike-in was added after TRIzol addition or incubation.

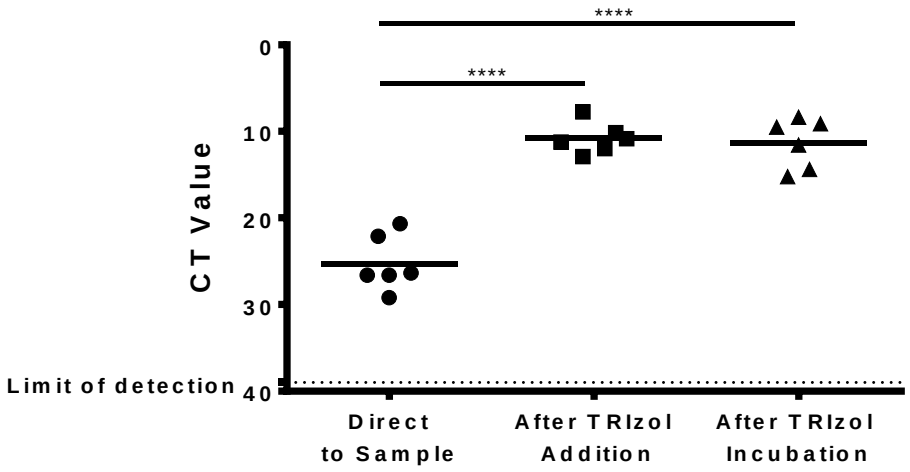

Figure S1-6. Addition of spike-in control during different steps of RNA isolation.

250 fmol of ath-miR-172a was added to six plasma samples at different steps in the RNA isolation protocol. Isolated RNA was quantitated for ath-miR-172a expression via qPCR. Limit of detection (dotted line) is 39 cycles. Solid line = mean. **** P<0.0001 (T-test).

S1.4.4. Manual Versus Automated RNA Isolation

To determine the efficacy of automated RNA isolation (QIAcube HT), plasma samples underwent manual and automated RNA isolation using 250 fmol ath-miR spike-in. These were then quantitated using the OpenArray qPCR platform; the CRT values are shown in Figure S1-7. The manual RNA isolation protocol resulted in a lower average abundance of the ath-miR spike-in. The manual method also demonstrated a large spread of CRT values, while the automated method only had two samples with a CRT value >10.

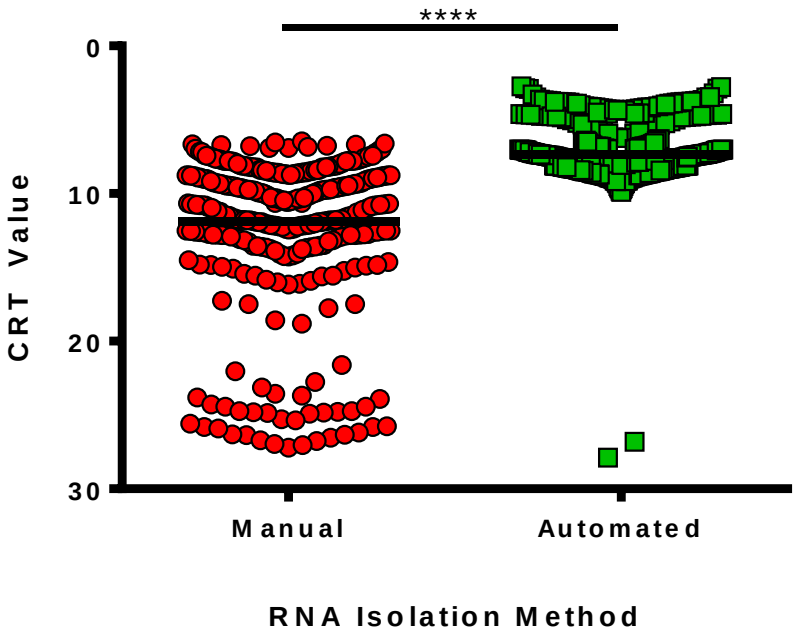

Figure S1-7. Manual versus automated RNA isolation.

Quantitation of the ath-miR spike-in added to plasma samples that underwent manual (red circles) and automated (green squares) RNA isolation. N = 367 manual, 633 automated. Solid line = mean. **** P<0.0001 (T-test).

S1.5. Discussion

Controls are essential in many facets of molecular biology, including qPCR. They allow researchers to account for variability introduced during the experimental procedure or subsequent analysis. The use of these controls relies on the basis that their expression, inspit of being low or high in abundance, is within the measurable (linear) range and is unchanged in different conditions or across different groups of individuals. As shown in this chapter, the commonly used endogenous snoRNAs, such as U6 and RNU6B (225; 226), demonstrated marked variability within circulating plasma samples. Indeed, some of these ncRNAs were undetectable in some samples, making them ineffectual controls for this sample type.

A growing number of studies are employing synthetic miRNA spike-ins to their samples as an alternative to endogenous controls. The majority of these use *C. elegans* derived miRNAs, particularly the three described here, cel-miR-39, -54, and -238 (227; 228). This may be due largely to the fact that they utilise Qiagen miRNA isolation kits, which routinely include or recommend synthetic cel-miR-39 as a spike-in control. All three of these cel-miRs were detectable within human plasma samples (Figures S1-3 and S1-4), despite no spike-in being added, and no homology to known human miRNAs. This suggests a possible crosstalk between miRNA assays, or homology to unknown human ncRNAs. Either possibility undermines the use of this family of miRNAs as spike-in controls. Furthermore, endogenous U6 appeared to decrease with the cel-miR spike-in. As these experiments were conducted using identical plasma samples, this indicates that cel-miR spike-ins could impact the quantitation of endogenous miRNAs. These data demonstrate that synthetic cel-miR spike-in controls may have troubling effects upon generated data and should not be utilised as controls.

Synthetic miRNAs derived from *Arabidopsis thaliana* do not seem to share these unintended effects. Plasma samples absent of the ath-miR RNA isolation spike-ins demonstrated no detectable amplification when using the associated assays. One spike-in negative sample had detectable ath-miR RT spike-in, however the transcript abundance was very low (CT = 36.3) and so may have been unintentional contamination when setting up the RT reactions. The abundance of endogenous U6 was unchanged with the addition of ath-miR spike-in. Previously, naked cel-miRs were found to degrade quickly when added into plasma sample due to the inherent nuclease activity. This correlates with the data presented here (Figure S1-6), and confirms that the spike-in must be introduced after the addition of TRIzol, which denatures these enzymes. Due to these results, ath-miR spike-in controls were introduced to the RNA isolation and RT protocols that are used throughout this thesis.

The RNA isolation protocol has also been adapted to take place upon an automated platform (QIAcube-HT), which not only increases the sample throughput, but also increases the retrieval of the spike-in and reduces sample-to-sample variability (Figure S1-7).

S1.6. Conclusions

Synthetic *Arabidopsis thaliana* miRNAs were found to be the most effective spike-in controls, when utilised at 250 fmol (RNA isolation) or 150 amol (RT). Furthermore, the RNA isolation protocol was optimised by identifying the optimal step to introduce the spike-in, as well moving the procedure to an automated platform. By comparing and optimising these processes, any introduced variability in the generated data will be minimised.

Supplementary Chapter 2: Digital PCR Platform Comparison

S2.1. Chapter Overview

Digital PCR (dPCR) is becoming an increasingly popular method of quantifying nucleic acids as it is able to provide absolute quantitation of target gene/transcript copies, thereby offering a more sensitive and absolutely quantifiable technology than conventional real-time qPCR technologies that allow relative quantification of target genes/transcripts. It is a technological refinement of qPCR that is achieved by splitting the clonal amplification into thousands of distinct reactions. By reading the fluorescence of each of these reactions as positive (the sequence of interest is present) or negative (no sequence of interest), digital PCR can apply the Poisson distribution to calculate the absolute copy number of the sequence of interest. Like any other technique, multiple platforms have been developed to utilise it and these must be compared to ensure robust reproducibility and ease of use.

This chapter compares two of the three currently available digital PCR platforms; the QuantStudio 3D (QS3D, Applied Biosystems) and the QX200 (Bio-Rad). The third currently available platform (RainDrop Plus™ Digital PCR system from RainDance®) was not assessed due to unavailability of a distributor in Australia at the time of this testing. The QS3D uses a finely-crafted chip with 20 thousand individual wells to partition the amplification reaction, while the QX200 system relies on a droplet generator that splits the PCR reaction into up to 20 thousand aqueous droplets within an emulsion oil. The reproducibility of each platform was assessed using mixtures of methylated and unmethylated insulin DNA plasmids, obtained from Professor RG Mirmira, as part of an existing collaboration with A/Prof. Hardikar. The QX200 was more reproducible than the QS3D, and allows a significantly higher number of

samples to be analysed in each run. The QS3D produced higher copy numbers but also detected copies in the no template controls more frequently. Overall, the QX200 provided the reproducibility and throughput needed for large scale clinical analysis. These analyses were carried out prior to finalization of procurement of the digital PCR platform in the Hardikar lab. All samples and data described in the thesis were assessed on the BioRad® QX200 system using droplets generated on the automated droplet generator from BioRad®.

S2.2. Chapter Aims

Studies in this chapter aimed to:

- assess the reproducibility of the QS3D and QX200 digital PCR platforms, and
- compare their ease of use, as well as the capability of their softwares for downstream analysis.

S2.3. Methods

S2.3.1. Plasmids

Unmethylated (UM) and methylated (M) *Ins* plasmids were kindly provided by Professor Raghu Mirmira from Indiana University, USA as part of the existing collaboration with A/Prof. Hardikar, NHMRC CTC, University of Sydney. Plasmids were amplified using the plasmid transformation protocol outlined in Appendix H. Purified plasmids were combined to create solutions with varying percentages of each unmethylated (UM) and methylated (M) plasmids. The percentages used were 100, 99.9, 99, 90, 75, 50, 25, 10, 1, 0.1 and 0%. Each mixture had the remaining percentage made of the other plasmid (i.e. the 90% UM plasmid solution had 10% M plasmid). Each solution had a final concentration of 0.5 pg/µl.

S2.3.2. Digital PCR

Digital PCR was completed using manual droplet generation/chip loading as per the respective manufacturer's protocol. Each plasmid mixture (described in S2.4.1) and a no template control (NTC) was run in triplicate. To effectively compare the two platforms, the digital PCR reaction was identical: 1X QuantStudio 3D Digital PCR Mastermix v2 (Applied Biosystems) or 1X ddPCR Supermix for Probes (No dUTP) (Bio-Rad), 1X Custom TaqMan SNP assay AH21BH1, 10U EcoR1, nuclease-free water and 0.5 pg (1 µl) of the plasmid mix. Once the reactions were partitioned, they were thermocycled using the following cycling conditions: 95°C for 10 mins, 40 cycles (94°C for 3 mins, 57.5°C for 1 min), 98°C for 10 mins, 12°C hold. The ramp rate for thermocyling was set to 2˚C/sec for all steps.

S2.4. Results

S2.4.1. Overview of Digital PCR Platforms

Figure S2-1 gives an overview of the dPCR technologies that have been compared; the QuantSudio 3D system uses a chip containing 20,000 wells (Figure S2-1b), while the QX200 generates up to the same number of oil droplets (Figure S2-1d). During normal operation, however, neither of these platforms utilise the maximum 20,000 partitions. Rather, the QS3D employed 17,300 ± 624.3 (mean ± SD) wells and the QX200 generated 16,524 ± 1863 (mean ± SD) usable droplets (Figure S2-2). While both platforms had enough partitions to estimate absolute copy numbers, the QS3D demonstrated more consistent partitioning.

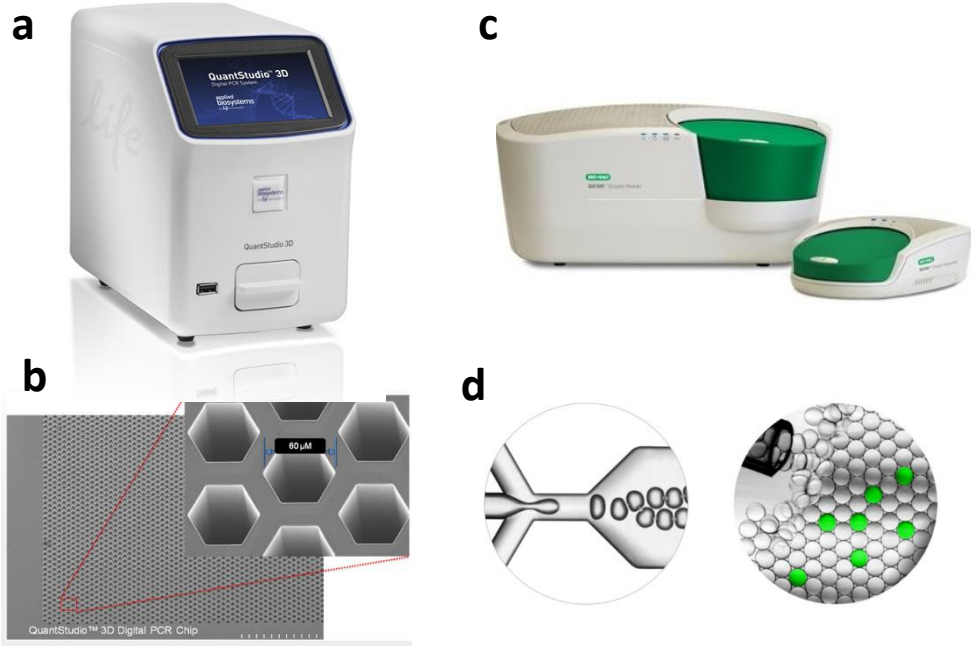

Figure S2-1. Digital PCR platforms

(a-b) QS3D platform with (a) chip reader and (b) close-up of QS3D chip wells. (c-d) QX200 platform with (c) manual droplet generator (right) and reader (left), and (d) generated dPCR droplets. Images taken from each of the manufacturer's websites.

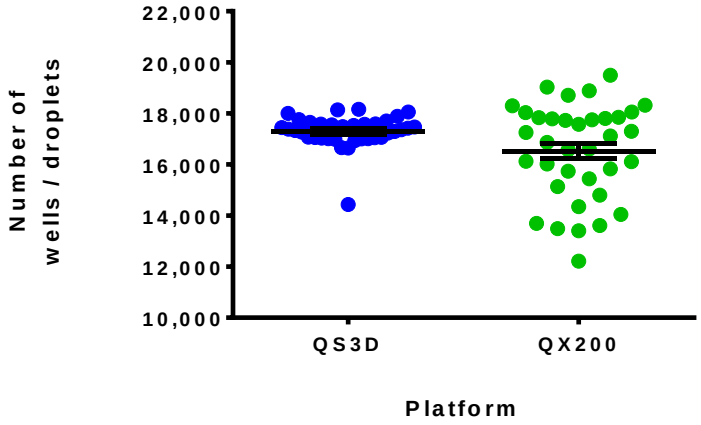

Figure S2-2. Number of partitions created for digital PCR.

Scatterplot showing the number of wells (QS3D, blue) or droplets (QX200, green) utilised for the calculation of absolute DNA copy numbers. N = 36 per group. Mean ± SEM.

Once the dPCR reactions have been completed, a threshold must be placed on both the FAM and VIC fluorescence to determine which partitions are negative for both probe, which are positive for a single probe, and which are positive for both probes. As seen in Figure S2-3, the QX200 consistently separates droplets into these four distinct populations. The identification of these populations varies on the QS3D platform, resulting in an overlay with no discernible populations. This makes setting a threshold for multiple samples difficult using this platform.

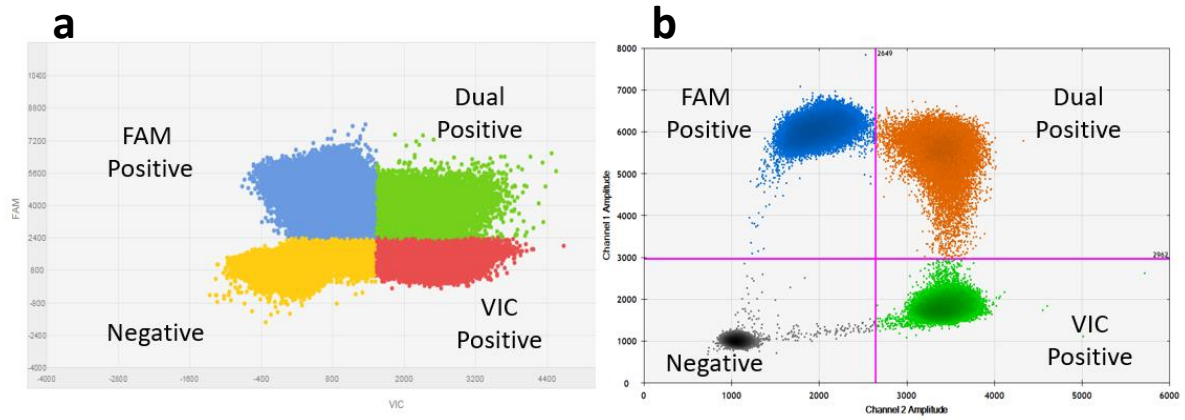

Figure S2-3. Overlay of dPCR results

Overlay of negative, single probe positive (FAM or VIC) and dual positive wells/droplets from 36 dPCR reactions run on the (a) QS3D and (b) QX200.

Additional comparative parameters are listed in Table S2-A. The QS3D is more suited to lower throughput experiments as the minimum number of samples required to complete a run is lower than the QX200. However, the time needed to load and partition a sample is significantly longer using the QS3D, meaning that the maximum number of sample that can be run in a single day is dramatically less. This increase in throughput using the QX200 can be further expanded utilising an automated droplet generator. Unfortunately, the QS3D had no automated platform at the time of this comparison, or even until the submission of this thesis.

Table S2-A. Digital PCR platform comparison

	QS3D	QX200
Minimum samples per run	4*	8
Maximum samples per run	24	96
Maximum samples per day	48	192
Time to load one sample (mins)	5	1
Ease of loading	++	+++
Ease of analysis	+++	+++
Possibility of automation?	No	Yes

* Whilst one sample can be run at a time, the included reagents necessitate multiples of four to be run to avoid wastage.

S2.1.1. Digital PCR Platform Accuracy and Reproducibility

The plasmid mixtures outlined in S2.4.1 were analysed on both dPCR platforms, with their expected and observed percentages plotted in Figure S2-4. Data obtained from both platforms show that the methylated *Ins* plasmid was estimated to have a greater percentage than expected in all combinations (Figure S2-4). This may be due to the fact that the probes only differ by one base and so some crosstalk may occur. Indeed, FAM positive wells/droplets show a small degree of VIC fluorescence, while those positive for VIC show a small amount of FAM fluorescence (Figure S2-3).

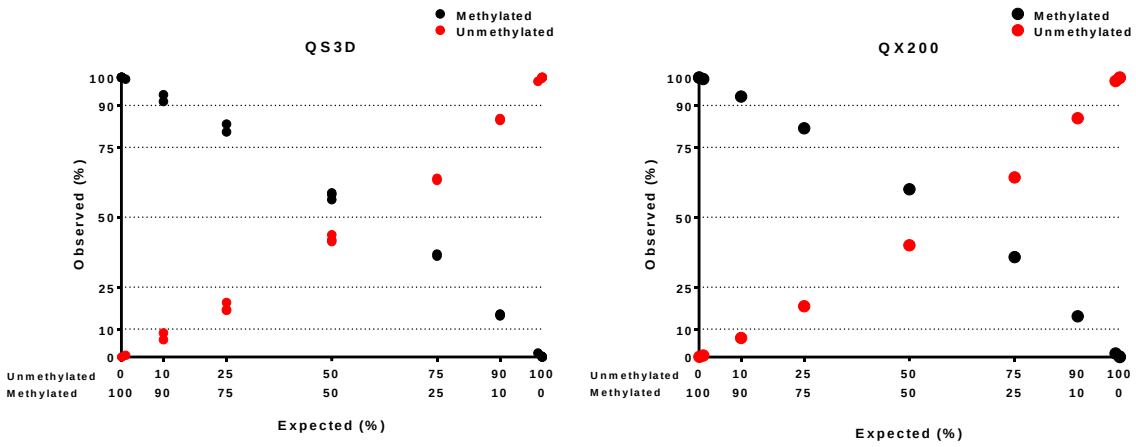

Figure S2-4. Expected versus observed plasmid mixtures.

Dotted lines are expected percentages. Each plasmid mixture was run in triplicate.

Interestingly, when the absolute copy numbers were examined, the QS3D demonstrated consistently higher measurements than the QX200 (Figure S2-5). However, the measurements obtained from the QS3D also demonstrated a higher level of variability, with significantly higher assay CVs than the QX200 platform (Figure S2-6).

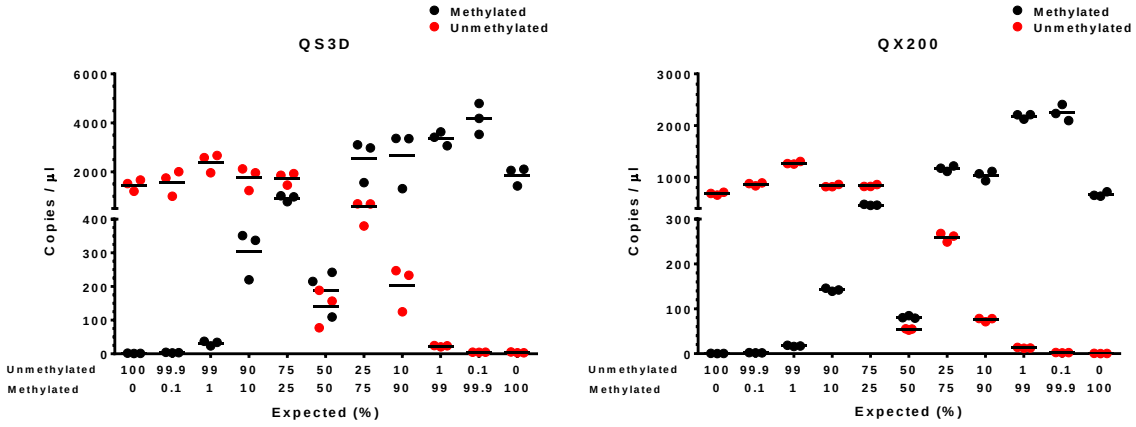

Figure S2-5. Absolute quantification of plasmid mixtures.

Absolute copy numbers generated from QS3D and QX200 platforms. Each plasmid mixture was run in triplicate. Solid line = mean.

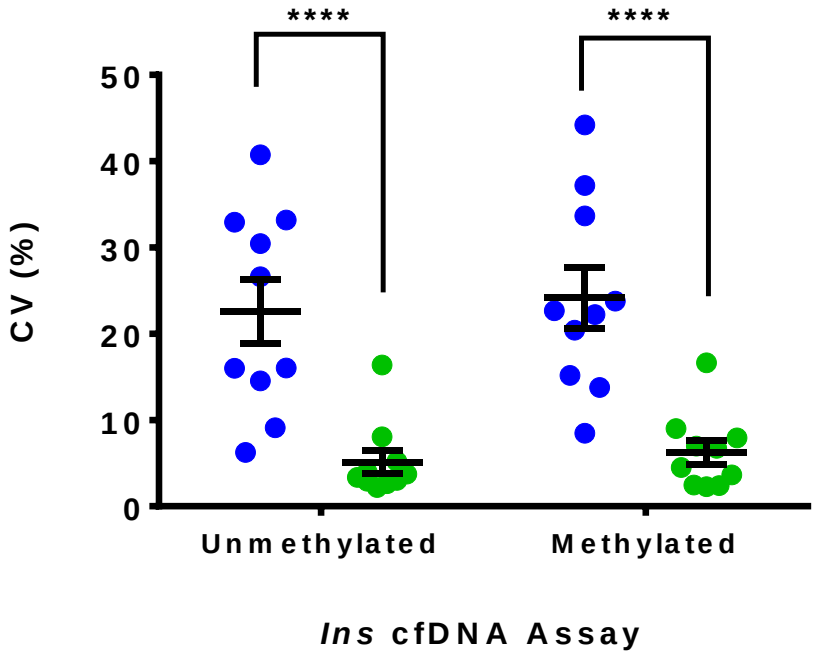

Figure S2-6. Digital PCR coefficient of variation analysis

CV distribution for unmethylated and methylated assays run on QS3D (blue) and QX200 (green). Mean ± SEM. ****P<0.0001.

Finally, when NTCs were analysed on the dPCR platforms, the QS3D detected DNA copies more frequently than the QX200 (Figure S2-7). This may be due to an inherent overestimation of DNA copy numbers, which could then explain why plasmid copy numbers were also elevated compared to the QX200, or an increased risk of contamination as all plasmids and NTCs were run together.

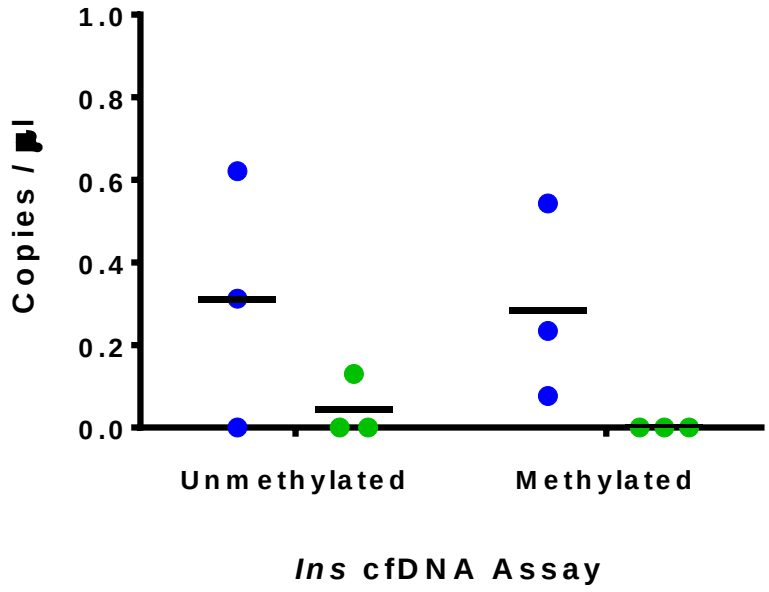

Figure S2-7. Absolute quantitation of no template controls.

NTC was run in triplicate on the QS3D (blue) and QX200 (green) platforms. Solid line = mean.

S2.2. Discussion

Digital PCR offers advantages over other PCR technologies; it allows absolute quantitation of very low nucleic acid copy numbers, and therefore is able to detect much smaller differences between samples. As a result, it is the favoured method of quantitating the low levels of circulating cfDNA. As discussed within Chapter 2, the choice of technology can heavily influence the generation and reproducibility of the data. As such, the two currently available dPCR technologies, the QuantStudio 3D and the QX200 were directly compared in this chapter. Despite generating consistently more reaction partitions, the QS3D demonstrated greater sample variability than the QX200 (Figure S2-6) and was therefore the least preferred system. Studies planned and carried out herein led to the procurement of the BioRad QX200 system with the manual as well as the automated droplet generators in the Hardikar lab.

S2.3. Conclusions

This analysis has demonstrated that the QX200 dPCR system has greater reproducibility, throughput and ease of use, when compared to the QS3D. As such, it is the preferable platform to undertake cfDNA quantitation in larger clinical cohorts.

Supplementary Data: Clinical Data Integrity

Standard operating procedures in the Hardikar Lab emphasize on the need for replicates, repeats and controls. These are introduced in every sample assay procedure carried out in the lab so as to ensure data integrity, especially when assessing large number of clinical samples within the same plate/slide or across multiple plates/slides. As a general rule, specific requests to the manufacturer were made to order OpenArrays from the same batch and also to cross-check assay performance between different batches. For the custom OpenArray slides, the sample that lay at position A1 was repeated at a random position in the same slide. This “repeat” sample would allow identification of any position effects for the same assay on the array. One sample was chosen at the start to the study to be present at the same position (D12) on each slide. This “Control”sample ensured the performance of these OpenArrays across different plates, across different runs as well as between different batches of arrays. Technical “replicates” were carried out to assess for any variation in the automated array loading procedres. A schematic representation of the plate map/desin is presented in Figure SD-1.

The intra-slide repeats demonstrated significantly high correlation with their corresponding sample (Figure SD-2), while the inter-assay control exhibited low coefficient of variation (Figure SD-3). This indicates little variation both within and across OpenArray slides.

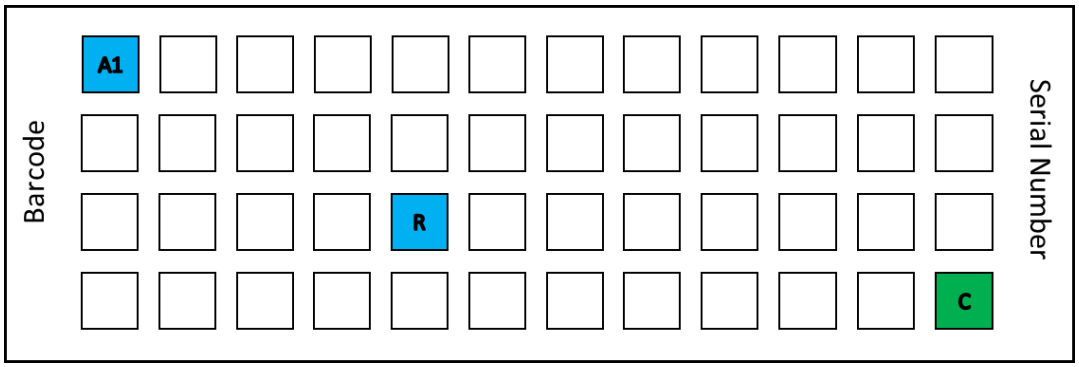

Figure SD-1. Schematic of control samples for custom OpenArray slides

The sample at position A1 (blue) is repeated at a random position (R, blue) throughout the slide (intra-slide repeat). A control sample is placed at position D12 (C, green) on every slide (inter-assay control).

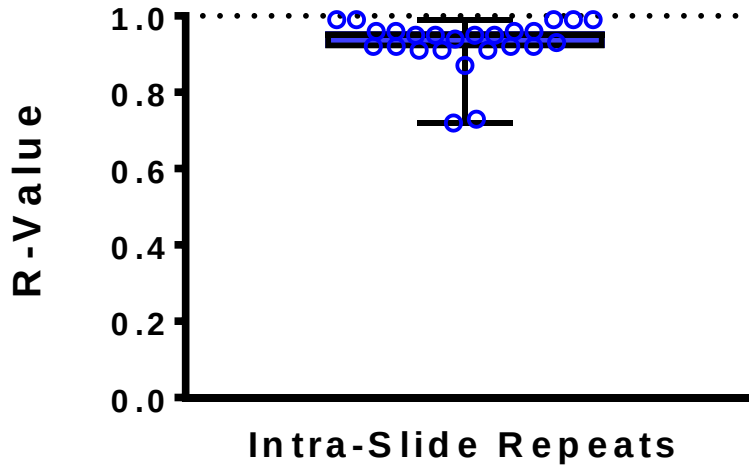

Figure SD-2. Correlation of intra-slide repeats

Box and whiskers plot of Spearman R-values for correlations between samples located at position A1 and their repeats. All correlations P<0.0001. Mean = 0.93. Median = 0.95. Whiskers = min/max. N = 25 samples.

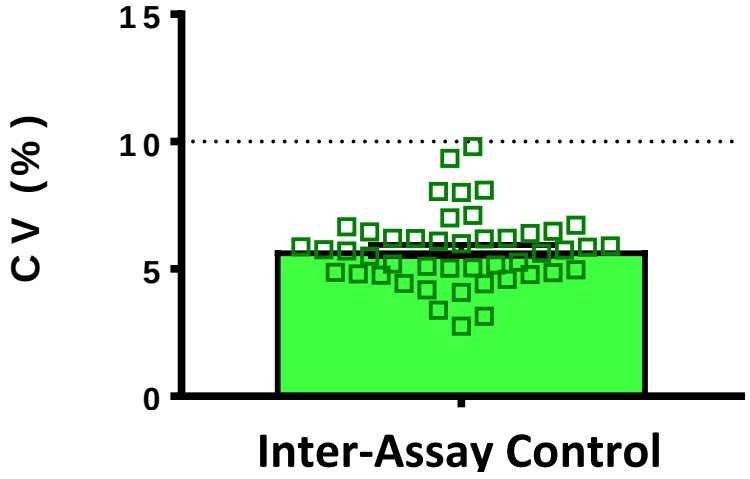

Figure SD-3. Coefficient of variation analysis of inter-assay control

CVs are plotted for all detectable miRNAs within the inter-assay control sample. Mean ± SEM. N = 46 miRNAs.

As the ddPCR plates all contained positive plasmid controls, only repeats were conducted. As seen in Figure SD-4, the repeats demonstrated a highly significant correlation with their original sample, indicating minimal technical variation.

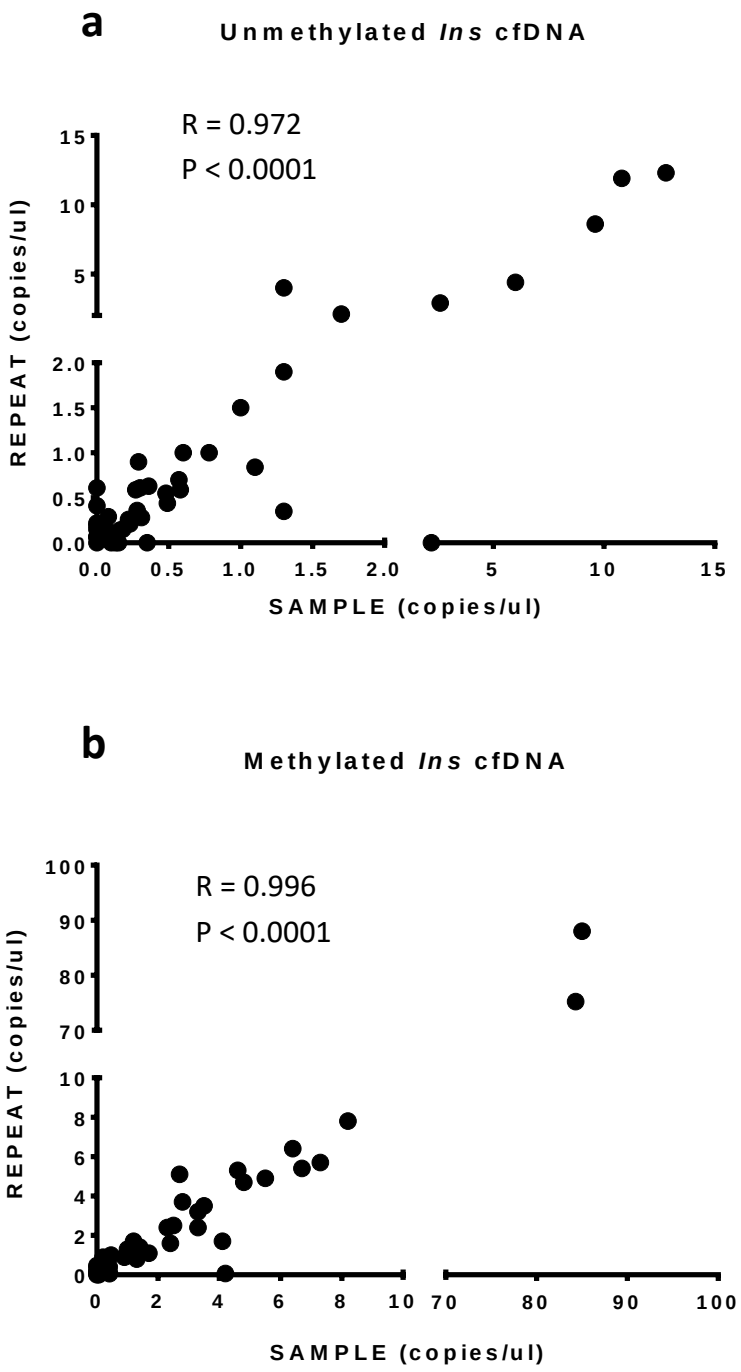

Figure SD-4. Digital droplet PCR sample repeat correlations

(a) Unmethylated and (b) methylated *Ins* cfDNA correlations for samples repeated on the ddPCR platform. Pearson R. N = 54 pairs.

These supplementary datasets demonstrate the optimization procedures that were finalized prior to *in vitro*, animal model and clinical sample assessment, presented in this thesis. These optimization procedures help to achieve the desired clarity for reproducing the findings presented in this thesis as well as to provide a guide for similar studies from other research groups in assessing a large number of biomarkers using the molecular technologicalworkflows described in this thesis.

7. References

1. Zajac J, Shrestha A, Patel P, Poretsky L: The Main Events in the History of Diabetes Mellitus. In *Principles of Diabetes Mellitus* Poretsky L, Ed. New York, USA, Springer, 2010, p. 3-18

2. Medvei VC. *The History of Clinical Endocrinology: Comprehensive Account of Endocrinology from Earliest Times to Present Day*. USA, The Parthenon Publishing Group, 1993

3. Best CH, Scott DA. *The Preparation of Insulin*. The Journal of Biological Chemistry 1923;57:709-723

4. Atkinson MA, Eisenbarth GS, Michels AW. *Type 1 diabetes*. Lancet 2014;383:69-82

5. Skyler JS, Greenbaum CJ, Lachin JM, Leschek E, Rafkin-Mervis L, Savage P, Spain L, Type 1 Diabetes TrialNet Study G. *Type 1 Diabetes TrialNet--an international collaborative clinical trials network*. Annals of the New York Academy of Sciences 2008;1150:14-24

6. Steffes MW, Sibley S, Jackson M, Thomas W. *Beta-cell function and the development of diabetes-related complications in the diabetes control and complications trial*. Diabetes care 2003;26:832-836

7. Orchard TJ, Costacou T, Kretowski A, Nesto RW. *Type 1 diabetes and coronary artery disease*. Diabetes care 2006;29:2528-2538

8. Eckel RH, Eisenbarth GS. *Autoimmune diabetes inflames the heart*. Science translational medicine 2012;4:138fs118

9. AIHW (Ed.). *Incidence of type 1 diabetes in Australia 2000–2013*. Canberra: AIHW, 2013

10. NDSS (Ed.). *Type 1 Diabetes*. Diabetes Australia, 2016

11. Dall TM, Mann SE, Zhang Y, Quick WW, Seifert RF, Martin J, Huang EA, Zhang S. *Distinguishing the economic costs associated with type 1 and type 2 diabetes*. Population health management 2009;12:103-110

12. Tao B, Pietropaolo M, Atkinson M, Schatz D, Taylor D. *Estimating the cost of type 1 diabetes in the U.S.: a propensity score matching method*. PLoS One 2010;5:e11501

13. Colagiuri S, Brnabic A, Gomez M, Fitzgerald B, Buckley A, R C (Eds.). *DiabCo$t Australia Type 1: Assessing the burden of Type 1 Diabetes in Australia*. Canberra, 2009

14. Shaw J, Tanamas S. *Diabetes: the silent pandemic and its impact on Australia* Diabetes Australia and the Juvenile Diabetes Research Institute, 2012

15. Klinke DJ, 2nd. *Extent of beta cell destruction is important but insufficient to predict the onset of type 1 diabetes mellitus*. PLoS One 2008;3:e1374

16. Leete P, Willcox A, Krogvold L, Dahl-Jorgensen K, Foulis AK, Richardson SJ, Morgan NG. *Differential insulitic profiles determine the extent of beta cell destruction and the age at onset of type 1 diabetes*. Diabetes 2016;

17. Pugliese A, Yang M, Kusmarteva I, Heiple T, Vendrame F, Wasserfall C, Rowe P, Moraski JM, Ball S, Jebson L, Schatz DA, Gianani R, Burke GW, Nierras C, Staeva T, Kaddis JS, Campbell-Thompson M, Atkinson MA. *The Juvenile Diabetes Research Foundation Network for Pancreatic Organ Donors with Diabetes (nPOD) Program: goals, operational model and emerging findings*. Pediatric diabetes 2014;15:1-9

18. Eisenbarth GS. *Type I diabetes mellitus. A chronic autoimmune disease*. The New England journal of medicine 1986;314:1360-1368

19. Hardikar AA, Karandikar MS, Bhonde RR. *Effect of partial pancreatectomy on diabetic status in BALB/c mice*. The Journal of endocrinology 1999;162:189-195

20. Kallman F, Grobstein C. *Fine Structure of Differentiating Mouse Pancreatic Exocrine Cells in Transfilter Culture*. J Cell Biol 1964;20:399-413

21. Davis AK, DuBose SN, Haller MJ, Miller KM, DiMeglio LA, Bethin KE, Goland RS, Greenberg EM, Liljenquist DR, Ahmann AJ, Marcovina SM, Peters AL, Beck RW, Greenbaum CJ. *Prevalence of detectable C-Peptide according to age at diagnosis and duration of type 1 diabetes*. Diabetes care 2015;38:476-481

22. Noble JA, Erlich HA. *Genetics of type 1 diabetes*. Cold Spring Harbor perspectives in medicine 2012;2:a007732

23. Noble JA. *Immunogenetics of type 1 diabetes: A comprehensive review*. Journal of autoimmunity 2015;64:101-112

24. Singal DP, Blajchman MA. *Histocompatibility (HL-A) Antigens, Lymphocytotoxic Antibodies and Tissue Antibodies in Patients with Diabetes Mellitus*. Diabetes 1973;22:429-432

25. Ke X. *Presence of multiple independent effects in risk loci of common complex human diseases*. American journal of human genetics 2012;91:185-192

26. Pugliese A, Boulware D, Yu L, Babu S, Steck AK, Becker D, Rodriguez H, DiMeglio L, Evans-Molina C, Harrison LC, Schatz D, Palmer JP, Greenbaum C, Eisenbarth GS, Sosenko JM. *The HLA-DRB1*15:01-DQA1*01:02-DQB1*06:02 haplotype protects autoantibody-positive relatives from type 1 diabetes throughout the stages of disease progression*. Diabetes 2016;

27. Erlich H, Valdes AM, Noble J, Carlson JA, Varney M, Concannon P, Mychaleckyj JC, Todd JA, Bonella P, Fear AL, Lavant E, Louey A, Moonsamy P. *HLA DR-DQ haplotypes and genotypes and type 1 diabetes risk: analysis of the type 1 diabetes genetics consortium families*. Diabetes 2008;57:1084-1092

28. Patente TA, Monteiro MB, Vieira SM, Rossi da Silva ME, Nery M, Queiroz M, Azevedo MJ, Canani LH, Parisi MC, Pavin EJ, Mainardi D, Javor J, Velho G, Coimbra CN, Correa-Giannella ML. *Linkage disequilibrium with HLA-DRB1-DQB1 haplotypes explains the association of TNF-308G>A variant with type 1 diabetes in a Brazilian cohort*. Gene 2015;568:50-54

29. Shin HD, Yang SW, Kim DH, Park Y. *Independent association of tumor necrosis factor polymorphism with type 1 diabetes susceptibility*. Annals of the New York Academy of Sciences 2008;1150:76-85

30. Gambelunghe G, Ghaderi M, Cosentino A, Falorni A, Brunetti P, Sanjeevi CB. *Association of MHC Class I chain-related A (MIC-A) gene polymorphism with Type I diabetes*. Diabetologia 2000;43:507-514

31. Lhotta K, Auinger M, Kronenberg F, Irsigler K, Konig P. *Polymorphism of complement C4 and susceptibility to IDDM and microvascular complications*. Diabetes care 1996;19:53-55

32. Marron MP, Raffel LJ, Garchon HJ, Jacob CO, Serrano-Rios M, Martinez Larrad MT, Teng WP, Park Y, Zhang ZX, Goldstein DR, Tao YW, Beaurain G, Bach JF, Huang HS, Luo DF, Zeidler A, Rotter JI, Yang MC, Modilevsky T, Maclaren NK, She JX. *Insulin-dependent diabetes mellitus (IDDM) is associated with CTLA4 polymorphisms in multiple ethnic groups*. Human molecular genetics 1997;6:1275-1282

33. Wang J, Liu L, Ma J, Sun F, Zhao Z, Gu M. *Common variants on cytotoxic T lymphocyte antigen-4 polymorphisms contributes to type 1 diabetes susceptibility: evidence based on 58 studies*. PLoS One 2014;9:e85982

34. Bell GI, Horita S, Karam JH. *A polymorphic locus near the human insulin gene is associated with insulin-dependent diabetes mellitus*. Diabetes 1984;33:176-183

35. Pugliese A, Zeller M, Fernandez A, Jr., Zalcberg LJ, Bartlett RJ, Ricordi C, Pietropaolo M, Eisenbarth GS, Bennett ST, Patel DD. *The insulin gene is transcribed in the human thymus and transcription levels correlated with allelic variation at the INS VNTR-IDDM2 susceptibility locus for type 1 diabetes*. Nat Genet 1997;15:293-297

36. Vafiadis P, Bennett ST, Todd JA, Nadeau J, Grabs R, Goodyer CG, Wickramasinghe S, Colle E, Polychronakos C. *Insulin expression in human thymus is modulated by INS VNTR alleles at the IDDM2 locus*. Nat Genet 1997;15:289-292

37. Kent SC, Chen Y, Bregoli L, Clemmings SM, Kenyon NS, Ricordi C, Hering BJ, Hafler DA. *Expanded T cells from pancreatic lymph nodes of type 1 diabetic subjects recognize an insulin epitope*. Nature 2005;435:224-228

38. Zhang L, Nakayama M, Eisenbarth GS. *Insulin as an autoantigen in NOD/human diabetes*. Current opinion in immunology 2008;20:111-118

39. Soltesz G, Patterson CC, Dahlquist G, Group ES. *Worldwide childhood type 1 diabetes incidence--what can we learn from epidemiology?* Pediatric diabetes 2007;8 Suppl 6:6-14

40. Gillespie KM, Bain SC, Barnett AH, Bingley PJ, Christie MR, Gill GV, Gale EA. *The rising incidence of childhood type 1 diabetes and reduced contribution of high-risk HLA haplotypes*. Lancet 2004;364:1699-1700

41. Gulden E, Wong FS, Wen L. *The gut microbiota and Type 1 Diabetes*. Clin Immunol 2015;159:143-153

42. Knip M, Simell O. *Environmental triggers of type 1 diabetes*. Cold Spring Harbor perspectives in medicine 2012;2:a007690

43. Korsgren S, Molin Y, Salmela K, Lundgren T, Melhus A, Korsgren O. *On the etiology of type 1 diabetes: a new animal model signifying a decisive role for bacteria eliciting an adverse innate immunity response*. Am J Pathol 2012;181:1735-1748

44. Cardwell CR, Stene LC, Joner G, Cinek O, Svensson J, Goldacre MJ, Parslow RC, Pozzilli P, Brigis G, Stoyanov D, Urbonaite B, Sipetic S, Schober E, Ionescu-Tirgoviste C, Devoti G, de Beaufort CE, Buschard K, Patterson CC. *Caesarean section is associated with an increased risk of childhood-onset type 1 diabetes mellitus: a meta-analysis of observational studies*. Diabetologia 2008;51:726-735

45. Okada H, Kuhn C, Feillet H, Bach JF. *The 'hygiene hypothesis' for autoimmune and allergic diseases: an update*. Clinical and experimental immunology 2010;160:1-9

46. Thomas HE, Trapani JA, Kay TW. *The role of perforin and granzymes in diabetes*. Cell Death Differ 2010;17:577-585

47. Dudek NL, Thomas HE, Mariana L, Sutherland RM, Allison J, Estella E, Angstetra E, Trapani JA, Santamaria P, Lew AM, Kay TW. *Cytotoxic T-cells from T-cell receptor transgenic NOD8.3 mice destroy beta-cells via the perforin and Fas pathways*. Diabetes 2006;55:2412-2418

48. Lehuen A, Diana J, Zaccone P, Cooke A. *Immune cell crosstalk in type 1 diabetes*. Nat Rev Immunol 2010;10:501-513

49. Ziegler A-G, Bonifacio E. *Age-related islet autoantibody incidence in offspring of patients with type 1 diabetes*. Diabetologia 2012;55:1937-1943

50. Davis TM, Zimmet P, Davis WA, Bruce DG, Fida S, Mackay IR. *Autoantibodies to glutamic acid decarboxylase in diabetic patients from a multi-ethnic Australian community: the Fremantle Diabetes Study*. Diabetic medicine : a journal of the British Diabetic Association 2000;17:667-674

51. Rother KI, Brown RJ, Morales MM, Wright E, Duan Z, Campbell C, Hardin DS, Popovic J, McEvoy RC, Harlan DM, Orlander PR, Brod SA. *Effect of Ingested Interferon-α on β-Cell Function in Children With New-Onset Type 1 Diabetes*. Diabetes care 2009;32:1250-1255

52. Rother KI, Spain LM, Wesley RA, Digon BJ, Baron A, Chen K, Nelson P, Dosch H-M, Palmer JP, Brooks-Worrell B, Ring M, Harlan DM. *Effects of Exenatide Alone and in Combination With Daclizumab on β-Cell Function in Long-Standing Type 1 Diabetes*. Diabetes care 2009;32:2251-2257

53. Bonifacio E, Hummel M, Walter M, Schmid S, Ziegler A-G. *IDDM1 and Multiple Family History of Type 1 Diabetes Combine to Identify Neonates at High Risk for Type 1 Diabetes*. Diabetes care 2004;27:2695-2700

54. Hemminki K, Li X, Sundquist J, Sundquist K. *Familial association between type 1 diabetes and other autoimmune and related diseases*. Diabetologia 2009;52:1820-1828

55. Ziegler A-G, Nepom GT. *Prediction and Pathogenesis in Type 1 Diabetes*. Immunity 2010;32:468-478

56. Eisenbarth GS. *Update in Type 1 Diabetes*. The Journal of Clinical Endocrinology & Metabolism 2007;92:2403-2407

57. Achenbach P, Warncke K, Reiter J, Naserke HE, Williams AJK, Bingley PJ, Bonifacio E, Ziegler A-G. *Stratification of Type 1 Diabetes Risk on the Basis of Islet Autoantibody Characteristics*. Diabetes 2004;53:384-392

58. Parikka V, Näntö-Salonen K, Saarinen M, Simell T, Ilonen J, Hyöty H, Veijola R, Knip M, Simell O. *Early seroconversion and rapidly increasing autoantibody concentrations predict prepubertal manifestation of type 1 diabetes in children at genetic risk*. Diabetologia 2012;55:1926-1936

59. Steck AK, Johnson K, Barriga KJ, Miao D, Yu L, Hutton JC, Eisenbarth GS, Rewers MJ. *Age of Islet Autoantibody Appearance and Mean Levels of Insulin, but Not GAD or IA-2 Autoantibodies, Predict Age of Diagnosis of Type 1 Diabetes*. Diabetes Autoimmunity Study in the Young 2011;34:1397-1399

60. Yu J, Yu L, Bugawan TL, Erlich HA, Barriga K, Hoffman M, Rewers M, Eisenbarth GS. *Transient Antiislet Autoantibodies: Infrequent Occurrence and Lack of Association with "Genetic" Risk Factors*. The Journal of Clinical Endocrinology & Metabolism 2000;85:2421-2428

61. Hawthorne WJ. Beta cell therapies for type 1 diabetes - *In* Hardikar AA (Ed) Pancreatic Islet Biology, Stem Cell Biology and Regenerative Medicine Series. In *Pancreatic Islet Biology*, 2016, p. 285-323

62. O'Connell PJ, Holmes-Walker DJ, Goodman D, Hawthorne WJ, Loudovaris T, Gunton JE, Thomas HE, Grey ST, Drogemuller CJ, Ward GM, Torpy DJ, Coates PT, Kay TW, Australian Islet Transplant C. *Multicenter Australian trial of islet transplantation: improving accessibility and outcomes*. American journal of transplantation : official journal of the American Society of Transplantation and the American Society of Transplant Surgeons 2013;13:1850-1858

63. Kauffman SA. *Metabolic stability and epigenesis in randomly constructed genetic nets*. Journal of theoretical biology 1969;22:437-467

64. Taft RJ, Pheasant M, Mattick JS. *The relationship between non-protein-coding DNA and eukaryotic complexity*. BioEssays : news and reviews in molecular, cellular and developmental biology 2007;29:288-299

65. Lee RC, Feinbaum RL, Ambros V. *The C. elegans heterochronic gene lin-4 encodes small RNAs with antisense complementarity to lin-14*. Cell 1993;75:843-854

66. Kozomara A, Griffiths-Jones S. *miRBase: annotating high confidence microRNAs using deep sequencing data*. Nucleic Acids Res 2014;42:D68-73

67. Lewis BP, Burge CB, Bartel DP. *Conserved seed pairing, often flanked by adenosines, indicates that thousands of human genes are microRNA targets*. Cell 2005;120:15-20

68. Wu S, Huang S, Ding J, Zhao Y, Liang L, Liu T, Zhan R, He X. *Multiple microRNAs modulate p21Cip1/Waf1 expression by directly targeting its 3' untranslated region*. Oncogene 2010;29:2302-2308

69. Lee Y, Jeon K, Lee JT, Kim S, Kim VN. *MicroRNA maturation: stepwise processing and subcellular localization*. EMBO J 2002;21:4663-4670

70. Lee Y, Kim M, Han J, Yeom KH, Lee S, Baek SH, Kim VN. *MicroRNA genes are transcribed by RNA polymerase II*. EMBO J 2004;23:4051-4060

71. Denli AM, Tops BB, Plasterk RH, Ketting RF, Hannon GJ. *Processing of primary microRNAs by the Microprocessor complex*. Nature 2004;432:231-235

72. Zeng Y, Cullen BR. *Efficient processing of primary microRNA hairpins by Drosha requires flanking nonstructured RNA sequences*. J Biol Chem 2005;280:27595-27603

73. Fukuda T, Yamagata K, Fujiyama S, Matsumoto T, Koshida I, Yoshimura K, Mihara M, Naitou M, Endoh H, Nakamura T, Akimoto C, Yamamoto Y, Katagiri T, Foulds C, Takezawa S, Kitagawa H, Takeyama K, O'Malley BW, Kato S. *DEAD-box RNA helicase subunits of the Drosha complex are required for processing of rRNA and a subset of microRNAs*. Nat Cell Biol 2007;9:604-611

74. Lund E, Guttinger S, Calado A, Dahlberg JE, Kutay U. *Nuclear export of microRNA precursors*. Science 2004;303:95-98

75. Bernstein E, Caudy AA, Hammond SM, Hannon GJ. *Role for a bidentate ribonuclease in the initiation step of RNA interference*. Nature 2001;409:363-366

76. Ha M, Kim VN. *Regulation of microRNA biogenesis*. Nature reviews Molecular cell biology 2014;15:509-524

77. Meijer HA, Smith EM, Bushell M. *Regulation of miRNA strand selection: follow the leader?* Biochemical Society transactions 2014;42:1135-1140

78. Ha I, Wightman B, Ruvkun G. *A bulged lin-4/lin-14 RNA duplex is sufficient for Caenorhabditis elegans lin-14 temporal gradient formation*. Genes & development 1996;10:3041-3050

79. Hausser J, Zavolan M. *Identification and consequences of miRNA-target interactions--beyond repression of gene expression*. Nat Rev Genet 2014;15:599-612

80. Liu J, Carmell MA, Rivas FV, Marsden CG, Thomson JM, Song JJ, Hammond SM, Joshua-Tor L, Hannon GJ. *Argonaute2 is the catalytic engine of mammalian RNAi*. Science 2004;305:1437-1441

81. Huntzinger E, Izaurralde E. *Gene silencing by microRNAs: contributions of translational repression and mRNA decay*. Nat Rev Genet 2011;12:99-110

82. Farr RJ, Taylor CJ, Satoor SN, Williams MD, Joglekar MV. *From Cradle to the Grave: Tissue-specific microRNA signatures in detecting clinical progression of diabetes*. Non-coding RNAs in Endocrinology 2013:16-27

83. Bravo-Egana V, Rosero S, Molano RD, Pileggi A, Ricordi C, Dominguez-Bendala J, Pastori RL. *Quantitative differential expression analysis reveals miR-7 as major islet microRNA*. Biochem Biophys Res Commun 2008;366:922-926

84. Correa-Medina M, Bravo-Egana V, Rosero S, Ricordi C, Edlund H, Diez J, Pastori RL. *MicroRNA miR-7 is preferentially expressed in endocrine cells of the developing and adult human pancreas*. Gene Expr Patterns 2009;9:193-199

85. Davalos A, Goedeke L, Smibert P, Ramirez CM, Warrier NP, Andreo U, Cirera-Salinas D, Rayner K, Suresh U, Pastor-Pareja JC, Esplugues E, Fisher EA, Penalva LO, Moore KJ, Suarez Y, Lai EC, Fernandez-Hernando C. *miR-33a/b contribute to the regulation of fatty acid metabolism and insulin signaling*. Proc Natl Acad Sci U S A 2011;108:9232-9237

86. Elia L, Contu R, Quintavalle M, Varrone F, Chimenti C, Russo MA, Cimino V, De Marinis L, Frustaci A, Catalucci D, Condorelli G. *Reciprocal regulation of microRNA-1 and insulin-like growth factor-1 signal transduction cascade in cardiac and skeletal muscle in physiological and pathological conditions*. Circulation 2009;120:2377-2385

87. Esau C, Davis S, Murray SF, Yu XX, Pandey SK, Pear M, Watts L, Booten SL, Graham M, McKay R, Subramaniam A, Propp S, Lollo BA, Freier S, Bennett CF, Bhanot S, Monia BP. *miR-122 regulation of lipid metabolism revealed by in vivo antisense targeting*. Cell Metab 2006;3:87-98

88. Esau C, Kang X, Peralta E, Hanson E, Marcusson EG, Ravichandran LV, Sun Y, Koo S, Perera RJ, Jain R, Dean NM, Freier SM, Bennett CF, Lollo B, Griffey R. *MicroRNA-143 regulates adipocyte differentiation*. J Biol Chem 2004;279:52361-52365

89. Granjon A, Gustin MP, Rieusset J, Lefai E, Meugnier E, Guller I, Cerutti C, Paultre C, Disse E, Rabasa-Lhoret R, Laville M, Vidal H, Rome S. *The microRNA signature in response to insulin reveals its implication in the transcriptional action of insulin in human skeletal muscle and the role of a sterol regulatory element-binding protein-1c/myocyte enhancer factor 2C pathway*. Diabetes 2009;58:2555-2564

90. Grueter CE, van Rooij E, Johnson BA, DeLeon SM, Sutherland LB, Qi X, Gautron L, Elmquist JK, Bassel-Duby R, Olson EN. *A cardiac microRNA governs systemic energy homeostasis by regulation of MED13*. Cell 2012;149:671-683

91. He A, Zhu L, Gupta N, Chang Y, Fang F. *Overexpression of micro ribonucleic acid 29, highly up-regulated in diabetic rats, leads to insulin resistance in 3T3-L1 adipocytes*. Mol Endocrinol 2007;21:2785-2794

92. Herrera BM, Lockstone HE, Taylor JM, Ria M, Barrett A, Collins S, Kaisaki P, Argoud K, Fernandez C, Travers ME, Grew JP, Randall JC, Gloyn AL, Gauguier D, McCarthy MI, Lindgren CM. *Global microRNA expression profiles in insulin target tissues in a spontaneous rat model of type 2 diabetes*. Diabetologia 2010;53:1099-1109

93. Horie T, Ono K, Nishi H, Iwanaga Y, Nagao K, Kinoshita M, Kuwabara Y, Takanabe R, Hasegawa K, Kita T, Kimura T. *MicroRNA-133 regulates the expression of GLUT4 by targeting KLF15 and is involved in metabolic control in cardiac myocytes*. Biochem Biophys Res Commun 2009;389:315-320

94. Huang B, Qin W, Zhao B, Shi Y, Yao C, Li J, Xiao H, Jin Y. *MicroRNA expression profiling in diabetic GK rat model*. Acta biochimica et biophysica Sinica 2009;41:472-477

95. Huang M, Xu H, Xie S, Zhou H, Qu L. *Insulin-like growth factor-1 receptor is regulated by microRNA-133 during skeletal myogenesis*. PLoS One 2011;6

96. Joglekar MV, Joglekar VM, Hardikar AA. *Expression of islet-specific microRNAs during human pancreatic development*. Gene Expr Patterns 2009;9:109-113

97. Jordan SD, Kruger M, Willmes DM, Redemann N, Wunderlich FT, Bronneke HS, Merkwirth C, Kashkar H, Olkkonen VM, Bottger T, Braun T, Seibler J, Bruning JC. *Obesity-induced overexpression of miRNA-143 inhibits insulin-stimulated AKT activation and impairs glucose metabolism*. Nature cell biology 2011;13:434-446

98. Liang J, Liu C, Qiao A, Cui Y, Zhang H, Cui A, Zhang S, Yang Y, Xiao X, Chen Y, Fang F, Chang Y. *MicroRNA-29a-c decrease fasting blood glucose levels by negatively regulating hepatic gluconeogenesis*. Journal of hepatology 2013;58:535-542

99. Lu H, Buchan RJ, Cook SA. *MicroRNA-223 regulates Glut4 expression and cardiomyocyte glucose metabolism*. Cardiovasc Res 2010;86:410-420

100. Nieto M, Hevia P, Garcia E, Klein D, Alvarez-Cubela S, Bravo-Egana V, Rosero S, Damaris Molano R, Vargas N, Ricordi C, Pileggi A, Diez J, Dominguez-Bendala J, Pastori RL. *Antisense miR-7 impairs insulin expression in developing pancreas and in cultured pancreatic buds*. Cell Transplant 2012;21:1761-1774

101. Poy MN, Eliasson L, Krutzfeldt J, Kuwajima S, Ma X, Macdonald PE, Pfeffer S, Tuschl T, Rajewsky N, Rorsman P, Stoffel M. *A pancreatic islet-specific microRNA regulates insulin secretion*. Nature 2004;432:226-230

102. Poy MN, Hausser J, Trajkovski M, Braun M, Collins S, Rorsman P, Zavolan M, Stoffel M. *miR-375 maintains normal pancreatic alpha- and beta-cell mass*. Proc Natl Acad Sci U S A 2009;106:5813-5818

103. Roggli E, Britan A, Gattesco S, Lin-Marq N, Abderrahmani A, Meda P, Regazzi R. *Involvement of microRNAs in the cytotoxic effects exerted by proinflammatory cytokines on pancreatic beta-cells*. Diabetes 2010;59:978-986

104. Ryu HS, Park SY, Ma D, Zhang J, Lee W. *The induction of microRNA targeting IRS-1 is involved in the development of insulin resistance under conditions of mitochondrial dysfunction in hepatocytes*. PLoS One 2011;6:e17343

105. Sekine S, Ogawa R, Ito R, Hiraoka N, McManus MT, Kanai Y, Hebrok M. *Disruption of Dicer1 induces dysregulated fetal gene expression and promotes hepatocarcinogenesis*. Gastroenterology 2009;136:2304-2315 e2301-2304

106. Tian R, Abel ED. *Responses of GLUT4-deficient hearts to ischemia underscore the importance of glycolysis*. Circulation 2001;103:2961-2966

107. Xie H, Lim B, Lodish HF. *MicroRNAs induced during adipogenesis that accelerate fat cell development are downregulated in obesity*. Diabetes 2009;58:1050-1057

108. Yu XY, Song YH, Geng YJ, Lin QX, Shan ZX, Lin SG, Li Y. *Glucose induces apoptosis of cardiomyocytes via microRNA-1 and IGF-1*. Biochem Biophys Res Commun 2008;376:548-552

109. Zhang Y, Yang L, Gao YF, Fan ZM, Cai XY, Liu MY, Guo XR, Gao CL, Xia ZK. *MicroRNA-106b induces mitochondrial dysfunction and insulin resistance in C2C12 myotubes by targeting mitofusin-2*. Molecular and cellular endocrinology 2013;381:230-240

110. Bernstein E, Kim SY, Carmell MA, Murchison EP, Alcorn H, Li MZ, Mills AA, Elledge SJ, Anderson KV, Hannon GJ. *Dicer is essential for mouse development*. Nat Genet 2003;35:215-217

111. Lynn FC, Skewes-Cox P, Kosaka Y, McManus MT, Harfe BD, German MS. *MicroRNA expression is required for pancreatic islet cell genesis in the mouse*. Diabetes 2007;56:2938-2945

112. Kanji MS, Martin MG, Bhushan A. *Dicer1 is required to repress neuronal fate during endocrine cell maturation*. Diabetes 2013;62:1602-1611

113. Kalis M, Bolmeson C, Esguerra JL, Gupta S, Edlund A, Tormo-Badia N, Speidel D, Holmberg D, Mayans S, Khoo NK, Wendt A, Eliasson L, Cilio CM. *Beta-cell specific deletion of Dicer1 leads to defective insulin secretion and diabetes mellitus*. PLoS One 2011;6:e29166

114. Farr RJ, Joglekar MV, Hardikar AA. *Circulating microRNAs in Diabetes Progression: Discovery, Validation, and Research Translation*. Exs 2015;106:215-244

115. Kloosterman WP, Lagendijk AK, Ketting RF, Moulton JD, Plasterk RH. *Targeted inhibition of miRNA maturation with morpholinos reveals a role for miR-375 in pancreatic islet development*. PLoS Biol 2007;5:e203

116. Wei R, Yang J, Liu GQ, Gao MJ, Hou WF, Zhang L, Gao HW, Liu Y, Chen GA, Hong TP. *Dynamic expression of microRNAs during the differentiation of human embryonic stem cells into insulin-producing cells*. Gene 2013;518:246-255

117. Zhang ZW, Men T, Feng RC, Li YC, Zhou D, Teng CB. *miR-375 inhibits proliferation of mouse pancreatic progenitor cells by targeting YAP1*. Cellular physiology and biochemistry : international journal of experimental cellular physiology, biochemistry, and pharmacology 2013;32:1808-1817

118. El Ouaamari A, Baroukh N, Martens GA, Lebrun P, Pipeleers D, van Obberghen E. *miR-375 targets 3'-phosphoinositide-dependent protein kinase-1 and regulates glucose-induced biological responses in pancreatic beta-cells*. Diabetes 2008;57:2708-2717

119. Taniguchi CM, Emanuelli B, Kahn CR. *Critical nodes in signalling pathways: insights into insulin action*. Nature reviews Molecular cell biology 2006;7:85-96

120. Rafiq I, da Silva Xavier G, Hooper S, Rutter GA. *Glucose-stimulated preproinsulin gene expression and nuclear trans-location of pancreatic duodenum homeobox-1 require activation of phosphatidylinositol 3-kinase but not p38 MAPK/SAPK2*. J Biol Chem 2000;275:15977-15984

121. Dumortier O, Hinault C, Gautier N, Patouraux S, Casamento V, Van Obberghen E. *Maternal protein restriction leads to pancreatic failure in offspring: role of misexpressed microRNA-375*. Diabetes 2014;63:3416-3427

122. Avnit-Sagi T, Vana T, Walker MD. *Transcriptional mechanisms controlling miR-375 gene expression in the pancreas*. Experimental diabetes research 2012;2012:891216

123. Avnit-Sagi T, Kantorovich L, Kredo-Russo S, Hornstein E, Walker MD. *The promoter of the pri-miR-375 gene directs expression selectively to the endocrine pancreas*. PLoS One 2009;4:e5033

124. Keller DM, McWeeney S, Arsenlis A, Drouin J, Wright CV, Wang H, Wollheim CB, White P, Kaestner KH, Goodman RH. *Characterization of pancreatic transcription factor Pdx-1 binding sites using promoter microarray and serial analysis of chromatin occupancy*. J Biol Chem 2007;282:32084-32092

125. Needhamsen M, White RB, Giles KM, Dunlop SA, Thomas MG. *Regulation of Human PAX6 Expression by miR-7*. Evolutionary bioinformatics online 2014;10:107-113

126. Kredo-Russo S, Mandelbaum AD, Ness A, Alon I, Lennox KA, Behlke MA, Hornstein E. *Pancreas-enriched miRNA refines endocrine cell differentiation*. Development 2012;139:3021-3031

127. Kredo-Russo S, Ness A, Mandelbaum AD, Walker MD, Hornstein E. *Regulation of pancreatic microRNA-7 expression*. Experimental diabetes research 2012;2012:695214

128. Poy MN, Spranger M, Stoffel M. *microRNAs and the regulation of glucose and lipid metabolism*. Diabetes Obes Metab 2007;9 Suppl 2:67-73

129. Tsuura Y, Ishida H, Okamoto Y, Kato S, Sakamoto K, Horie M, Ikeda H, Okada Y, Seino Y. *Glucose sensitivity of ATP-sensitive K+ channels is impaired in beta-cells of the GK rat. A new genetic model of NIDDM*. Diabetes 1993;42:1446-1453

130. Gallagher IJ, Scheele C, Keller P, Nielsen AR, Remenyi J, Fischer CP, Roder K, Babraj J, Wahlestedt C, Hutvagner G, Pedersen BK, Timmons JA. *Integration of microRNA changes in vivo identifies novel molecular features of muscle insulin resistance in type 2 diabetes*. Genome Med 2010;2:9

131. Chang J, Nicolas E, Marks D, Sander C, Lerro A, Buendia MA, Xu C, Mason WS, Moloshok T, Bort R, Zaret KS, Taylor JM. *miR-122, a mammalian liver-specific microRNA, is processed*

from hcr mRNA and may downregulate the high affinity cationic amino acid transporter CAT-1. RNA Biol 2004;1:106-113

132. Herrera BM, Lockstone HE, Taylor JM, Wills QF, Kaisaki PJ, Barrett A, Camps C, Fernandez C, Ragoussis J, Gauguier D, McCarthy MI, Lindgren CM. *MicroRNA-125a is over-expressed in insulin target tissues in a spontaneous rat model of Type 2 Diabetes*. BMC Med Genomics 2009;2:54

133. Li S, Chen X, Zhang H, Liang X, Xiang Y, Yu C, Zen K, Li Y, Zhang CY. *Differential expression of microRNAs in mouse liver under aberrant energy metabolic status*. J Lipid Res 2009;50:1756-1765

134. Zhao E, Keller MP, Rabaglia ME, Oler AT, Stapleton DS, Schueler KL, Neto EC, Moon JY, Wang P, Wang IM, Lum PY, Ivanovska I, Cleary M, Greenawalt D, Tsang J, Choi YJ, Kleinhanz R, Shang J, Zhou YP, Howard AD, Zhang BB, Kendziorski C, Thornberry NA, Yandell BS, Schadt EE, Attie AD. *Obesity and genetics regulate microRNAs in islets, liver, and adipose of diabetic mice*. Mamm Genome 2009;20:476-485

135. Shi B, Sepp-Lorenzino L, Prisco M, Linsley P, deAngelis T, Baserga R. *Micro RNA 145 targets the insulin receptor substrate-1 and inhibits the growth of colon cancer cells*. J Biol Chem 2007;282:32582-32590

136. van Rooij E, Sutherland LB, Qi X, Richardson JA, Hill J, Olson EN. *Control of stress-dependent cardiac growth and gene expression by a microRNA*. Science 2007;316:575-579

137. Mallat Y, Tritsch E, Ladouce R, Winter DL, Friguet B, Li Z, Mericskay M. *Proteome modulation in H9c2 cardiac cells by miR-378 and miR-378**. Molecular & Cellular Proteomics 2013;

138. Farr RJ, Joglekar MV, Taylor CJ, Hardikar AA. *Circulating non-coding RNAs as biomarkers of beta cell death in diabetes*. Pediatric endocrinology reviews : PER 2013;11:14-20

139. Joglekar MV, Parekh VS, Hardikar AA. *Islet-specific microRNAs in pancreas development, regeneration and diabetes*. Indian J Exp Biol 2011;49:401-408

140. Mitchell PS, Parkin RK, Kroh EM, Fritz BR, Wyman SK, Pogosova-Agadjanyan EL, Peterson A, Noteboom J, O'Briant KC, Allen A, Lin DW, Urban N, Drescher CW, Knudsen BS, Stirewalt DL, Gentleman R, Vessella RL, Nelson PS, Martin DB, Tewari M. *Circulating microRNAs as stable blood-based markers for cancer detection*. Proc Natl Acad Sci U S A 2008;105:10513-10518

141. Chen X, Ba Y, Ma L, Cai X, Yin Y, Wang K, Guo J, Zhang Y, Chen J, Guo X, Li Q, Li X, Wang W, Wang J, Jiang X, Xiang Y, Xu C, Zheng P, Zhang J, Li R, Zhang H, Shang X, Gong T, Ning G, Zen

K, Zhang CY. *Characterization of microRNAs in serum: a novel class of biomarkers for diagnosis of cancer and other diseases*. Cell Res 2008;18:997-1006

142. Tsui NB, Ng EK, Lo YM. *Stability of endogenous and added RNA in blood specimens, serum, and plasma*. Clinical chemistry 2002;48:1647-1653

143. Collino F, Deregibus MC, Bruno S, Sterpone L, Aghemo G, Viltono L, Tetta C, Camussi G. *Microvesicles derived from adult human bone marrow and tissue specific mesenchymal stem cells shuttle selected pattern of miRNAs*. PLoS One 2010;5:e11803

144. Zernecke A, Bidzhekov K, Noels H, Shagdarsuren E, Gan L, Denecke B, Hristov M, Koppel T, Jahantigh MN, Lutgens E, Wang S, Olson EN, Schober A, Weber C. *Delivery of microRNA-126 by apoptotic bodies induces CXCL12-dependent vascular protection*. Science signaling 2009;2:ra81

145. Diehl P, Fricke A, Sander L, Stamm J, Bassler N, Htun N, Ziemann M, Helbing T, El-Osta A, Jowett JB, Peter K. *Microparticles: major transport vehicles for distinct microRNAs in circulation*. Cardiovasc Res 2012;93:633-644

146. Wang K, Zhang S, Weber J, Baxter D, Galas DJ. *Export of microRNAs and microRNA-protective protein by mammalian cells*. Nucleic Acids Res 2010;38:7248-7259

147. Vickers KC, Palmisano BT, Shoucri BM, Shamburek RD, Remaley AT. *MicroRNAs are transported in plasma and delivered to recipient cells by high-density lipoproteins*. Nat Cell Biol 2011;13:423-433

148. Nielsen LB, Wang C, Sorensen K, Bang-Berthelsen CH, Hansen L, Andersen ML, Hougaard P, Juul A, Zhang CY, Pociot F, Mortensen HB. *Circulating levels of microRNA from children with newly diagnosed type 1 diabetes and healthy controls: evidence that miR-25 associates to residual beta-cell function and glycaemic control during disease progression*. Experimental diabetes research 2012;2012:896362

149. Osipova J, Fischer DC, Dangwal S, Volkmann I, Widera C, Schwarz K, Lorenzen JM, Schreiver C, Jacoby U, Heimhalt M, Thum T, Haffner D. *Diabetes-associated microRNAs in pediatric patients with type 1 diabetes mellitus: a cross-sectional cohort study*. The Journal of clinical endocrinology and metabolism 2014;99:E1661-1665

150. Salas-Perez F, Codner E, Valencia E, Pizarro C, Carrasco E, Perez-Bravo F. *MicroRNAs miR-21a and miR-93 are down regulated in peripheral blood mononuclear cells (PBMCs) from patients with type 1 diabetes*. Immunobiology 2013;218:733-737

151. Samandari N, Mirza AH, Nielsen LB, Kaur S, Hougaard P, Fredheim S, Mortensen HB, Pociot F. *Circulating microRNA levels predict residual beta cell function and glycaemic control in children with type 1 diabetes mellitus*. Diabetologia 2017;60:354-363

152. Sebastiani G, Grieco FA, Spagnuolo I, Galleri L, Cataldo D, Dotta F. *Increased expression of microRNA miR-326 in type 1 diabetic patients with ongoing islet autoimmunity*. Diabetes/metabolism research and reviews 2011;27:862-866

153. Seyhan AA, Nunez Lopez YO, Xie H, Yi F, Mathews C, Pasarica M, Pratley RE. *Pancreas-enriched miRNAs are altered in the circulation of subjects with diabetes: a pilot cross-sectional study*. Sci Rep 2016;6:31479

154. Yang M, Ye L, Wang B, Gao J, Liu R, Hong J, Wang W, Gu W, Ning G. *Decreased miR-146 expression in peripheral blood mononuclear cells is correlated with ongoing islet autoimmunity in type 1 diabetes patients 1miR-146*. Journal of diabetes 2015;7:158-165

155. Pozzilli P, Di Mario U. *Autoimmune diabetes not requiring insulin at diagnosis (latent autoimmune diabetes of the adult): definition, characterization, and potential prevention*. Diabetes care 2001;24:1460-1467

156. Erener S, Mojibian M, Fox JK, Denroche HC, Kieffer TJ. *Circulating miR-375 as a biomarker of beta-cell death and diabetes in mice*. Endocrinology 2013;154:603-608

157. Latreille M, Herrmanns K, Renwick N, Tuschl T, Malecki MT, McCarthy MI, Owen KR, Rulicke T, Stoffel M. *miR-375 gene dosage in pancreatic beta-cells: implications for regulation of beta-cell mass and biomarker development*. J Mol Med (Berl) 2015;

158. El Messaoudi S, Mouliere F, Du Manoir S, Bascoul-Mollevi C, Gillet B, Nouaille M, Fiess C, Crapez E, Bibeau F, Theillet CG, Mazard T, Pezet D, Mathonnet M, Ychou M, Thierry AR. *Circulating DNA as a strong multi-marker prognostic tool for metastatic colorectal cancer patient management care*. Clin Cancer Res 2016;

159. Primerano S, Burnelli R, Carraro E, Pillon M, Elia C, Farruggia P, Sala A, Vinti L, Buffardi S, Basso G, Mascarin M, Mussolin L. *Kinetics of Circulating Plasma Cell-Free DNA in Paediatric Classical Hodgkin Lymphoma*. Journal of Cancer 2016;7:364-366

160. Connolly ID, Li Y, Gephart MH, Nagpal S. *The "Liquid Biopsy": the Role of Circulating DNA and RNA in Central Nervous System Tumors*. Current neurology and neuroscience reports 2016;16:25

161. Lo YM, Zhang J, Leung TN, Lau TK, Chang AM, Hjelm NM. *Rapid clearance of fetal DNA from maternal plasma*. American journal of human genetics 1999;64:218-224

162. Gauthier VJ, Tyler LN, Mannik M. *Blood clearance kinetics and liver uptake of mononucleosomes in mice*. J Immunol 1996;156:1151-1156

163. Herold KC, Usmani-Brown S, Ghazi T, Lebastchi J, Beam CA, Bellin MD, Ledizet M, Sosenko JM, Krischer JP, Palmer JP. *beta cell death and dysfunction during type 1 diabetes development in at-risk individuals*. The Journal of clinical investigation 2015;125:1163-1173

164. Diehl F, Schmidt K, Choti MA, Romans K, Goodman S, Li M, Thornton K, Agrawal N, Sokoll L, Szabo SA, Kinzler KW, Vogelstein B, Diaz LA, Jr. *Circulating mutant DNA to assess tumor dynamics*. Nature medicine 2008;14:985-990

165. Kuroda A, Rauch TA, Todorov I, Ku HT, Al-Abdullah IH, Kandeel F, Mullen Y, Pfeifer GP, Ferreri K. *Insulin gene expression is regulated by DNA methylation*. PLoS One 2009;4:e6953

166. Husseiny MI, Kaye A, Zebadua E, Kandeel F, Ferreri K. *Tissue-specific methylation of human insulin gene and PCR assay for monitoring beta cell death*. PLoS One 2014;9:e94591

167. Yang BT, Dayeh TA, Kirkpatrick CL, Taneera J, Kumar R, Groop L, Wollheim CB, Nitert MD, Ling C. *Insulin promoter DNA methylation correlates negatively with insulin gene expression and positively with HbA(1c) levels in human pancreatic islets*. Diabetologia 2011;54:360-367

168. Fisher MM, Watkins RA, Blum J, Evans-Molina C, Chalasani N, DiMeglio LA, Mather KJ, Tersey SA, Mirmira RG. *Elevations in Circulating Methylated and Unmethylated Preproinsulin DNA in New-Onset Type 1 Diabetes*. Diabetes 2015;64:3867-3872

169. Fisher MM, Perez Chumbiauca CN, Mather KJ, Mirmira RG, Tersey SA. *Detection of islet beta-cell death in vivo by multiplex PCR analysis of differentially methylated DNA*. Endocrinology 2013;154:3476-3481

170. Usmani-Brown S, Lebastchi J, Steck AK, Beam C, Herold KC, Ledizet M. *Analysis of beta-cell death in type 1 diabetes by droplet digital PCR*. Endocrinology 2014;155:3694-3698

171. Akirav EM, Lebastchi J, Galvan EM, Henegariu O, Akirav M, Ablamunits V, Lizardi PM, Herold KC. *Detection of beta cell death in diabetes using differentially methylated circulating DNA*. Proc Natl Acad Sci U S A 2011;108:19018-19023

172. Lehmann-Werman R, Neiman D, Zemmour H, Moss J, Magenheim J, Vaknin-Dembinsky A, Rubertsson S, Nellgard B, Blennow K, Zetterberg H, Spalding K, Haller MJ, Wasserfall CH, Schatz DA, Greenbaum CJ, Dorrell C, Grompe M, Zick A, Hubert A, Maoz M, Fendrich V, Bartsch DK, Golan T, Ben Sasson SA, Zamir G, Razin A, Cedar H, Shapiro AM, Glaser B, Shemer R, Dor

Y. *Identification of tissue-specific cell death using methylation patterns of circulating DNA*. Proc Natl Acad Sci U S A 2016;113:E1826-1834

173. Makino S, Kunimoto K, Muraoka Y, Mizushima Y, Katagiri K, Tochino Y. *Breeding of a non-obese, diabetic strain of mice*. Jikken dobutsu Experimental animals 1980;29:1-13

174. Liao X, Xue H, Wang YC, Nazor KL, Guo S, Trivedi N, Peterson SE, Liu Y, Loring JF, Laurent LC. *Matched miRNA and mRNA signatures from an hESC-based in vitro model of pancreatic differentiation reveal novel regulatory interactions*. Journal of cell science 2013;126:3848-3861

175. Klein D, Misawa R, Bravo-Egana V, Vargas N, Rosero S, Piroso J, Ichii H, Umland O, Zhijie J, Tsinoremas N, Ricordi C, Inverardi L, Dominguez-Bendala J, Pastori RL. *MicroRNA expression in alpha and beta cells of human pancreatic islets*. PLoS One 2013;8:e55064

176. Figliolini F, Cantaluppi V, De Lena M, Beltramo S, Romagnoli R, Salizzoni M, Melzi R, Nano R, Piemonti L, Tetta C, Biancone L, Camussi G. *Isolation, characterization and potential role in beta cell-endothelium cross-talk of extracellular vesicles released from human pancreatic islets*. PLoS One 2014;9:e102521

177. Bolmeson C, Esguerra JL, Salehi A, Speidel D, Eliasson L, Cilio CM. *Differences in islet-enriched miRNAs in healthy and glucose intolerant human subjects*. Biochem Biophys Res Commun 2011;404:16-22

178. Kang MH, Zhang LH, Wijesekara N, de Haan W, Butland S, Bhattacharjee A, Hayden MR. *Regulation of ABCA1 protein expression and function in hepatic and pancreatic islet cells by miR-145*. Arteriosclerosis, thrombosis, and vascular biology 2013;33:2724-2732

179. Melkman-Zehavi T, Oren R, Kredo-Russo S, Shapira T, Mandelbaum AD, Rivkin N, Nir T, Lennox KA, Behlke MA, Dor Y, Hornstein E. *miRNAs control insulin content in pancreatic beta-cells via downregulation of transcriptional repressors*. EMBO J 2011;30:835-845

180. Joglekar MV, Parekh VS, Mehta S, Bhonde RR, Hardikar AA. *MicroRNA profiling of developing and regenerating pancreas reveal post-transcriptional regulation of neurogenin3*. Dev Biol 2007;311:603-612

181. Chen BZ, Yu SL, Singh S, Kao LP, Tsai ZY, Yang PC, Chen BH, Shoei-Lung Li S. *Identification of microRNAs expressed highly in pancreatic islet-like cell clusters differentiated from human embryonic stem cells*. Cell biology international 2011;35:29-37

182. Mu C, Wang T, Wang X, Tian H, Liu Y. *Identification of microRNAs regulating Hlxb9 gene expression during the induction of insulin-producing cells*. Cell biology international 2016;40:515-523

183. Tsukita S, Yamada T, Takahashi K, Munakata Y, Hosaka S, Takahashi H, Gao J, Shirai Y, Kodama S, Asai Y, Sugisawa T, Chiba Y, Kaneko K, Uno K, Sawada S, Imai J, Katagiri H. *MicroRNAs 106b and 222 Improve Hyperglycemia in a Mouse Model of Insulin-Deficient Diabetes via Pancreatic beta-Cell Proliferation*. EBioMedicine 2017;15:163-172

184. van de Bunt M, Gaulton KJ, Parts L, Moran I, Johnson PR, Lindgren CM, Ferrer J, Gloyn AL, McCarthy MI. *The miRNA profile of human pancreatic islets and beta-cells and relationship to type 2 diabetes pathogenesis*. PLoS One 2013;8:e55272

185. Roggli E, Gattesco S, Caille D, Briet C, Boitard C, Meda P, Regazzi R. *Changes in microRNA expression contribute to pancreatic beta-cell dysfunction in prediabetic NOD mice*. Diabetes 2012;61:1742-1751

186. Joglekar MV, Patil D, Joglekar VM, Rao GV, Reddy DN, Mitnala S, Shouche Y, Hardikar AA. *The miR-30 family microRNAs confer epithelial phenotype to human pancreatic cells*. Islets 2009;1:137-147

187. Marchand L, Jalabert A, Meugnier E, Van den Hende K, Fabien N, Nicolino M, Madec AM, Thivolet C, Rome S. *miRNA-375 a Sensor of Glucotoxicity Is Altered in the Serum of Children with Newly Diagnosed Type 1 Diabetes*. Journal of diabetes research 2016;2016:1869082

188. Wong W, Farr R, Joglekar M, Januszewski A, Hardikar A. *Probe-based Real-time PCR Approaches for Quantitative Measurement of microRNAs*. J Vis Exp 2015;

189. Taylor CJ, Satoor SN, Ranjan AK, Pereira e Cotta MV, Joglekar MV. *A protocol for measurement of noncoding RNA in human serum*. Experimental diabetes research 2012;2012:168368

190. Hardikar AA, Farr RJ, Joglekar MV. *Circulating microRNAs: Understanding the Limits for Quantitative Measurement by Real-Time PCR*. Journal of the American Heart Association 2014;3:e000792

191. Fedick A, Su J, Jalas C, Northrop L, Devkota B, Ekstein J, Treff NR. *High-throughput carrier screening using TaqMan allelic discrimination*. PLoS One 2013;8:e59722

192. Kaneto H, Fujii J, Seo HG, Suzuki K, Matsuoka T, Nakamura M, Tatsumi H, Yamasaki Y, Kamada T, Taniguchi N. *Apoptotic cell death triggered by nitric oxide in pancreatic beta-cells*. Diabetes 1995;44:733-738

193. Yamada M, Momose K, Richelson E, Yamada M. *Sodium nitroprusside-induced apoptotic cellular death via production of hydrogen peroxide in murine neuroblastoma N1E-115 cells*. Journal of pharmacological and toxicological methods 1996;35:11-17

194. Thomas HE, Graham KL, Loudovaris T, Kay TW. Regenerative Medicine: Clinical Islet Transplantation- *In* Hardikar AA (Ed) Pancreatic Islet Biology, Stem Cell Biology and Regenerative Medicine Series. In *Pancreatic Islet Biology*, 2016, p. 257-284

195. Turk J, Corbett JA, Ramanadham S, Bohrer A, McDaniel ML. *Biochemical evidence for nitric oxide formation from streptozotocin in isolated pancreatic islets*. Biochem Biophys Res Commun 1993;197:1458-1464

196. Hanafusa T, Imagawa A. *Insulitis in human type 1 diabetes*. Annals of the New York Academy of Sciences 2008;1150:297-299

197. Vives-Pi M, Somoza N, Vargas F, Armengol P, Sarri Y, Wu JY, Pujol-Borrell R. *Expression of glutamic acid decarboxylase (GAD) in the alpha, beta and delta cells of normal and diabetic pancreas: implications for the pathogenesis of type I diabetes*. Clinical and experimental immunology 1993;92:391-396

198. De Vos A, Heimberg H, Quartier E, Huypens P, Bouwens L, Pipeleers D, Schuit F. *Human and rat beta cells differ in glucose transporter but not in glucokinase gene expression*. The Journal of clinical investigation 1995;96:2489-2495

199. Yang H, Wright JR, Jr. *Human beta cells are exceedingly resistant to streptozotocin in vivo*. Endocrinology 2002;143:2491-2495

200. Wen L, Ley RE, Volchkov PY, Stranges PB, Avanesyan L, Stonebraker AC, Hu C, Wong FS, Szot GL, Bluestone JA, Gordon JI, Chervonsky AV. *Innate immunity and intestinal microbiota in the development of Type 1 diabetes*. Nature 2008;455:1109-1113

201. Williams AJ, Krug J, Lampeter EF, Mansfield K, Beales PE, Signore A, Gale EA, Pozzilli P. *Raised temperature reduces the incidence of diabetes in the NOD mouse*. Diabetologia 1990;33:635-637

202. Funda DP, Kaas A, Bock T, Tlaskalova-Hogenova H, Buschard K. *Gluten-free diet prevents diabetes in NOD mice*. Diabetes/metabolism research and reviews 1999;15:323-327

203. Ruiz FS, Andersen ML, Zager A, Martins RC, Tufik S. *Sleep deprivation reduces the lymphocyte count in a non-obese mouse model of type 1 diabetes mellitus*. Brazilian journal of

medical and biological research = Revista brasileira de pesquisas medicas e biologicas 2007;40:633-637

204. Ibanez-Ventoso C, Vora M, Driscoll M. *Sequence relationships among C. elegans, D. melanogaster and human microRNAs highlight the extensive conservation of microRNAs in biology*. PLoS One 2008;3:e2818

205. Ameling S, Kacprowski T, Chilukoti RK, Malsch C, Liebscher V, Suhre K, Pietzner M, Friedrich N, Homuth G, Hammer E, Volker U. *Associations of circulating plasma microRNAs with age, body mass index and sex in a population-based study*. BMC Med Genomics 2015;8:61

206. Nathan DM, Group DER. *The diabetes control and complications trial/epidemiology of diabetes interventions and complications study at 30 years: overview*. Diabetes care 2014;37:9-16

207. *The relationship of glycemic exposure (HbA1c) to the risk of development and progression of retinopathy in the diabetes control and complications trial*. Diabetes 1995;44:968-983

208. Monnier L, Mas E, Ginet C, Michel F, Villon L, Cristol JP, Colette C. *Activation of oxidative stress by acute glucose fluctuations compared with sustained chronic hyperglycemia in patients with type 2 diabetes*. Jama 2006;295:1681-1687

209. Mestdagh P, Van Vlierberghe P, De Weer A, Muth D, Westermann F, Speleman F, Vandesompele J. *A novel and universal method for microRNA RT-qPCR data normalization*. Genome biology 2009;10:R64

210. Maciejak A, Kiliszek M, Opolski G, Segiet A, Matlak K, Dobrzycki S, Tulacz D, Sygitowicz G, Burzynska B, Gora M. *miR-22-5p revealed as a potential biomarker involved in the acute phase of myocardial infarction via profiling of circulating microRNAs*. Molecular medicine reports 2016;14:2867-2875

211. Zampetaki A, Willeit P, Burr S, Yin X, Langley SR, Kiechl S, Klein R, Rossing P, Chaturvedi N, Mayr M. *Angiogenic microRNAs Linked to Incidence and Progression of Diabetic Retinopathy in Type 1 Diabetes*. Diabetes 2016;65:216-227

212. Wu JH, Gao Y, Ren AJ, Zhao SH, Zhong M, Peng YJ, Shen W, Jing M, Liu L. *Altered microRNA expression profiles in retinas with diabetic retinopathy*. Ophthalmic Res 2012;47:195-201

213. Oh HJ, Kato M, Deshpande S, Zhang E, Sadhan D, Lanting L, Wang M, Natarajan R. *Inhibition of the processing of miR-25 by HIPK2-Phosphorylated-MeCP2 induces NOX4 in early diabetic nephropathy*. Sci Rep 2016;6:38789

214. Jha JC, Thallas-Bonke V, Banal C, Gray SP, Chow BS, Ramm G, Quaggin SE, Cooper ME, Schmidt HH, Jandeleit-Dahm KA. *Podocyte-specific Nox4 deletion affords renoprotection in a mouse model of diabetic nephropathy*. Diabetologia 2016;59:379-389

215. Sarkar G, Alattar M, Brown RJ, Quon MJ, Harlan DM, Rother KI. *Exenatide Treatment for 6 Months Improves Insulin Sensitivity in Adults With Type 1 Diabetes*. Diabetes care 2014;37:666-670

216. Sebastiani G, Spagnuolo I, Patti A, Grieco FA, Cataldo D, Ferretti E, Tiberti C, Dotta F. MicroRNA expression fingerprint in serum of type 1 diabetic patients. In *The 47th General Assembly Of The European Association For The Study Of Diabetes* Lisbon, Portugal, Diabetologia., 2012

217. Aly H, Gottlieb P. *The honeymoon phase: intersection of metabolism and immunology*. Current opinion in endocrinology, diabetes, and obesity 2009;16:286-292

218. Abdul-Rasoul M, Habib H, Al-Khouly M. *'The honeymoon phase' in children with type 1 diabetes mellitus: frequency, duration, and influential factors*. Pediatric diabetes 2006;7:101-107

219. Ehehalt S, Gauger N, Blumenstock G, Feldhahn L, Scheffner T, Schweizer R, Neu A, Baden-Wuerttemberg DI-G. *Hemoglobin A1c is a reliable criterion for diagnosing type 1 diabetes in childhood and adolescence*. Pediatric diabetes 2010;11:446-449

220. Helminen O, Aspholm S, Pokka T, Hautakangas MR, Haatanen N, Lempainen J, Ilonen J, Simell O, Knip M, Veijola R. *HbA1c Predicts Time to Diagnosis of Type 1 Diabetes in Children at Risk*. Diabetes 2015;64:1719-1727

221. Dungan KM. *1,5-anhydroglucitol (GlycoMark™) as a marker of short-term glycemic control and glycemic excursions*. Expert Review of Molecular Diagnostics 2008;8:9-19

222. Brod SA, Atkinson M, Lavis VR, Brosnan PG, Hardin DS, Orlander PR, Nguyen M, Riley WJ. *Ingested IFN-alpha preserves residual beta cell function in type 1 diabetes*. Journal of interferon & cytokine research : the official journal of the International Society for Interferon and Cytokine Research 2001;21:1021-1030

223. Brod SA, Lindsey JW, Vriesendorp FS, Ahn C, Henninger E, Narayana PA, Wolinsky JS. *Ingested IFN-alpha: results of a pilot study in relapsing-remitting MS*. Neurology 2001;57:845-852

224. Erener S, Marwaha A, Tan R, Panagiotopoulos C, Kieffer TJ. *Profiling of circulating microRNAs in children with recent onset of type 1 diabetes*. JCI insight 2017;2:e89656

225. Boeri M, Verri C, Conte D, Roz L, Modena P, Facchinetti F, Calabro E, Croce CM, Pastorino U, Sozzi G. *MicroRNA signatures in tissues and plasma predict development and prognosis of computed tomography detected lung cancer*. Proc Natl Acad Sci U S A 2011;108:3713-3718

226. Zile MR, Mehurg SM, Arroyo JE, Stroud RE, DeSantis SM, Spinale FG. *Relationship between the temporal profile of plasma microRNA and left ventricular remodeling in patients after myocardial infarction*. Circ Cardiovasc Genet 2011;4:614-619

227. Shen J, Todd NW, Zhang H, Yu L, Lingxiao X, Mei Y, Guarnera M, Liao J, Chou A, Lu CL, Jiang Z, Fang H, Katz RL, Jiang F. *Plasma microRNAs as potential biomarkers for non-small-cell lung cancer*. Laboratory investigation; a journal of technical methods and pathology 2011;91:579-587

228. Turchinovich A, Weiz L, Langheinz A, Burwinkel B. *Characterization of extracellular circulating microRNA*. Nucleic Acids Res 2011;39:7223-7233

Appendix A: Cellular RNA Isolation SOP

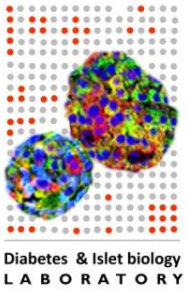

Reagents

1) 1.7 ml microcentrifuge tubes (Axygen, MCT-175-C)
2) TRIzol (Ambion, 15596018)
3) Chloroform (Sigma, 2432-500ml)
4) Isopropyl alcohol, IPA (Sigma, 59304-1L-F)
5) 100% ethanol (Sigma, E7023-500ml)
6) Fresh aliquot of nuclease-free water
7) P10, P20, P200 and P1000 filtered tips
8) RNase AWAY (highly preferred but not essential)

All plastic ware should be nuclease free. Never stick your hands into containers of nuclease-free plastic ware. Always pour out what is required.

Equipment

1) Refrigerated centrifuge for Eppendorf tubes set at 4°C
2) Vortex mixer
3) Well calibrated micropipettes designated for (pre-PCR) nucleic acid isolation

Reagent Setup

1) Allow samples to thaw thoroughly on ice prior to commencing.
    a. Due to the time involved in each stage of processing, a maximum of 8 samples should be processed at a time.
2) Set temperature on centrifuge to 4°C
    a. Run “Fast Temp” program if changing rotor or a quick cool down is required.
    b. Use a dedicated centrifuge with appropriate rotor
3) Clean gloves with RNase Away prior to commencing.

Procedure

1) **Lyse cells by adding 1 ml of Trizol to each sample in a 1.7 ml Eppendorf tube.** For this protocol use 1 ml of Trizol. If a different volume of Trizol is used, the volume of all other reagents must be altered accordingly to maintain the correct ratios.

2) **Add 200 µl of chloroform to each sample and shake vigorously for 1 min.** This ensures correct mixing. Do not vortex at this stage.

3) **Immediately centrifuge the tubes at 12,000 xg for 15 mins at 4°C.**

4) **Carefully remove the upper aqueous (clear) layer (400-500 µl) into a fresh 1.7 ml microcentrifuge tube.** Use a 200 µl pipette and tips to remove this gradually. **Note:** There will be a large amount of white precipitate at the interface between the organic and aqueous layers. **Do not disturb this layer.** After the removal of 400-500 µl there will still be some of the aqueous layer left; try to remove as much as possible without contamination.

5) **Add 500 µl of IPA.**

6) **Mix gently by inverting 7-10 times.** Do not vortex or shake tubes.

7) **Incubate for 10 mins at RT.**

8) **Centrifuge at 12,000 xg for 15 mins at 4°C.** A pellet may not always be visible at this stage, so **always** orient the tubes with the **hinge facing outwards** to allow estimation of the pellet location – in the bottom towards the hinge.

9) **Prepare a fresh volume of 75% ethanol while the samples are spinning.** For 8 samples, add 6.75 ml of 100% ethanol to 2.25 ml of nuclease-free water (9 ml in total).

10) **Carefully aspirate and discard the supernatant by placing the pipette tip along the wall of the tube opposite to the hinge.** When removing the supernatant, reduce the size of the pipette as you go to minimise disturbance to the pellet. Ideally, use a P200 initially, then a P20 when getting closer to the pellet.

11) **Add 1 ml of freshly prepared 75% ethanol to each tube and briefly vortex.**

12) **Centrifuge at 12,000 xg for 15 mins at 4°C.** As in #8, orient tubes with the hinge facing outwards.

13) **Carefully aspirate and discard the supernatant by placing the pipette tip along the wall of the tube opposite to the hinge.** As before (#10), reduce the size of the pipette when removing the supernatant. Ideally, use a P200 initially then a P10 to remove as much ethanol as possible.

14) **Allow the tubes to dry at RT for 5 minutes.** Lay the tubes flat with their lids open. If there are large droplets, gently twist the tube to spread out the liquid, allowing it to dry faster. **Note:** Do not over dry the samples as this will reduce the solubility of the RNA.

15) **Add 15 µl of nuclease-free water to each tube and resuspend.** Always store RNA on ice after this stage. The volume may vary depending on the pellet size.

16) **Measure concentration of RNA using Nanodrop.** If you are not going to proceed with downstream analysis immediately, skip this step and store your RNA. Always measure (Nanodrop, Qubit or Bioanalyzer) before downstream processing.

17) **Store RNA at -80°C.** Always log your sample details in the -80°C freezer log on the networked lab drive.

Appendix B: Biofluid RNA Isolation SOP

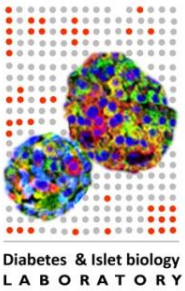

Reagents

1) Nuclease-free 2 ml microcentrifuge tubes (Axygen, MCT-200-C)
2) Glycogen (nuclease-free) 10 µg/µl (Sigma)
3) TRIzol (Ambion, 15596018)
4) Chloroform (Sigma, 2432-500ml)
5) Isopropyl alcohol, IPA (Sigma, 59304-1L-F)
6) 100% ethanol (Sigma E7023-500ml)
7) Fresh aliquot for nuclease-free water
8) P10, P20, P200 and P1000 filtered tips
9) RNase AWAY (highly preferred but not essential)

All plastic ware should be nuclease free. Never stick your hands into containers of nuclease-free plastic ware. Always pour out whatever is required.

Equipment

1) Refrigerated centrifuge for Eppendorf tubes set at 4°C
2) Vortex mixer
3) Well calibrated micropipettes designated for (pre-PCR) nucleic acid isolation

Reagent Setup

1) Allow samples to thaw thoroughly on ice prior to commencing.
   a. Due to the time involved in each stage of processing, a maximum of 8 samples should be processed at any time by a single user.
2) Set temperature on centrifuge to 4°C
   a. Run “Fast Temp” program if changing rotor or a quick cool down is required.
   b. Use a dedicated centrifuge with appropriate rotor.

3) Clean gloves with RNase Away prior to commencing.

Procedure

1) **Mix sample by gently pipetting up and down, then take out 200 µl* into a 2ml microcentrifuge tube.**
2) **Vortex and briefly spin glycogen (20 mg/ml stock) to mix, then add 1µl to each sample.**
3) **Add 1 ml of Trizol to each tube.** Yellow globules appear in the solution after adding TRIzol. These dissipate following vortexing and do not seem to affect downstream processing.
4) **Vortex each tube for 20 seconds.**
5) **Incubate at RT (22-24°C) for 10 minutes.**
6) **Add 5 µl of 50 nM ath-miR-172a spike in control to each tube, then vortex for 5 secs.**
7) **Add 200 µl of chloroform to each tube and shake vigorously for 40 seconds.** Place the tubes in a rack and ensure each tube is secured properly with your hand. This ensures proper mixing of Trizol and chloroform after addition. **Note: DO NOT vortex** the tubes at this stage.
8) **Incubate at RT for 15 minutes.**
9) **Centrifuge 12,000 xg for 15 minutes at 4°C.**
10) **Transfer 600-800 µl of the upper aqueous (clear) phase to a fresh 2 ml microcentrifuge tube.** Use a 200 µl pipette and tips to remove this gradually. **Note:** There will be a large amount of white precipitate at the interface between the aqueous and organic layer. **Do not disturb this layer**. After the removal of 800 µl there will still be some aqueous layer left; try to remove as much as aqueous layer that you can without any contamination.
11) **Add 1.1 ml of IPA to each tube in 2x 550 µl aliquots. Note:** It is normal that the tubes will be very full at this stage. Be careful to label tops and have clean (dry) fingers to avoid accidental erasure of labels.
12) **Vortex each tube for 5 seconds.**

13) **Incubate at RT for 10 minutes.**

14) **Centrifuge at 12,000 xg for 8 minutes at 4°C.** A pellet may not be visible at this stage, so **always** orient the tubes with the **hinge facing outwards** to allow estimation of the pellet location - in the bottom towards the hinge.

15) **Prepare a fresh volume of 75% ethanol while the samples are spinning.** For 8 samples, add 6.75 ml of 100% ethanol to 2.25 ml of nuclease-free water (9 ml in total)

16) **Carefully aspirate and discard the supernatant by placing the pipette tip along the wall of the tube opposite to the hinge.** When removing the supernatant, reduce the size of the pipette as you go to minimise disturbance to the pellet.

17) **Add 1 ml of freshly-prepared 75% ethanol to each tube and invert 5 times.** If a pellet is visible, you will see it floating after inversion.

18) **Centrifuge at 7,500 xg for 5 minutes at 4°C.**

19) **Carefully remove and discard supernatant.** As before (step 16), reduce the volume of the pipette when removing the supernatant.

20) **Allow the tubes to dry at RT for 5 minutes.** Do not over dry the samples as this will reduce the solubility of the RNA. If you have left excess ethanol and are not confident in removing it without disturbing the pellet, you may need to incubate tubes at 37°C for **maximum** of 3 minutes. Any longer can damage RNA quality.

21) **Add 10 – 15 µl of nuclease-free water to each tube and resuspend.** Always store RNA on ice after this stage. The volume may vary depending on the pellet size.

22) **Measure concentration of RNA using Nanodrop.** The 260/280 ratio may be as low as 1.3 but this does not affect downstream processing. If you are not going to proceed for downstream analysis immediately, then skip this step and proceed to store your RNA. Always measure (Nanodrop, Qubit or Bioanalyzer) before downstream processing.

23) **Store RNA at -80°C.** Always log your sample details in the -80°C freezer log on the networked lab drive.

Appendix C: Automated RNA Isolation SOP

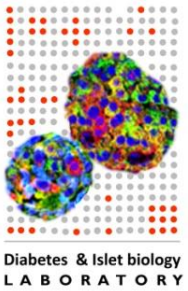

Reagents

1) Collection microtubes (Qiagen, 19560)
2) Lids for collection microtubes (Qiagen, 19566)
3) Glycogen (nuclease-free) 10 µg/µl (Sigma)
4) TRIzol (Ambion, 15596018)
5) Chloroform (Sigma, 2432-500ml)
6) Isopropyl alcohol, IPA (Sigma, 59304-1L-F)
7) 50 nM ath-miR-172a (8-well strips, stored in -80°C freezer)
8) RNeasy 96 QIAcube HT kit (Qiagen, CAT 74171)
9) QIAcube HT Plasticware (Qiagen, CAT 950067)
10) Tip disposal box (Qiagen, CAT 990550)
11) Reagent trough with lid, 70 ml (Qiagen, CAT 990554)
12) Reagent trough with lid, 170 ml (Qiagen, CAT 990556)
13) Filter tips, OnCor C, 200 µl (Qiagen, CAT 990610)
14) P10, P20, P200 and P1000 filtered tips
15) RNase AWAY (highly preferred but not essential)

All plastic ware should be nuclease free. Never stick your hands into containers of nuclease-free plastic ware. Always pour out whatever is required.

Equipment

1) QIAcube HT
2) Refrigerated centrifuge for plates set at 4°C
3) Vortex mixer
4) Well calibrated micropipettes designated for (pre-PCR) nucleic acid isolation

Reagent Setup

1) Allow samples to thaw thoroughly on ice prior to commencing.
2) Clean gloves with RNase Away prior to commencing.

Procedure

1) **Mix sample by gently pipetting up and down, then aliquot 100µl into one collection microtube (96 racked).**
2) **Vortex and briefly spin glycogen (10 µg/µl stock) to mix, then add 1µl to each sample.**
3) **Add 500 µl of Trizol to each tube.** Yellow globules appear in the solution after adding Trizol. These dissipate following vortexing and do not seem to affect downstream processing. Wear appropriate PPE and be careful when vortexing or shaking tubes containing Trizol.
4) **Vortex the microtubes for 40 secs or until the yellow globules disappear.**
5) **Incubate at RT (22-24°C) for 10 minutes.**
6) **Briefly centrifuge (1 min, 1500 rpm) the racked microtubes at 4°C to remove Trizol from the caps.**
7) **Add 2.5 µl of 50 nM ath-miR-172a spike in control to each tube.** One 8-well strip contains enough for an entire 96-well plate.
8) **Add 100 µl of chloroform to each tube and shake vigorously for 40 seconds.** Secure the caps using an upside down plastic lid and elastic bands as shown below.

   Note: DO NOT vortex the tubes at this stage.

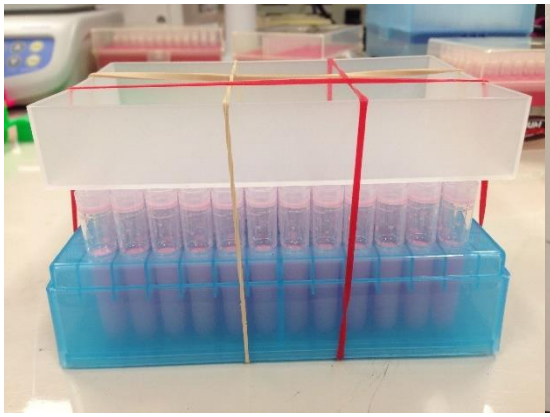

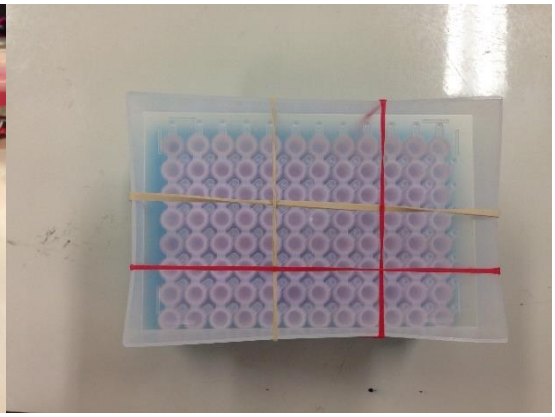

9) **Incubate at RT for 15 minutes.**

10) **Centrifuge 3,200 x g for 25 minutes at 4°C.**

11) **Turn on QIAcube HT system. Remove tip eject cover (red). Open the pre-treatment run file.**

12) **Place microtubes into position C1 of the QIAcube HT.** The trough holder in this position must be removed first.

13) **Load an empty S-block into position B1. Load tips.**

14) **Begin the run.** This program will transfer 300 µl of aqueous phase into the S-block.

15) **Remove the microtubes.** For protein/DNA analysis, store these samples at -80°C. Place the trough holder back into this position.

16) **Open the purification run file.**

17) **Load the appropriate reagents in their respective troughs.** See software for specific volumes. Ensure there is a little excess volume to avoid running out mid-cycle.

18) **Load RNeasy plate and Elution plate in A1 (left/right respectively).** Ensure that A1 is top left. The left section of A1 is for waste, while the right is for elution.

19) **Load tips (2x96). Start the run and complete the pre-run checklist.**

20) **Remove the Elution plate.** Cap these tubes and then store at -80°C. Always log your sample details on the networked database.

21) **Remove the reagent troughs and discard remaining liquid.** All troughs, except the Top Elute, may be rinsed with nuclease-free water and left to dry. The Top Elute trough must be wiped out with a Kim wipe. Reagent troughs can be used for a maximum of **one month or one full RNeasy kit** before being discarded.

22) **Remove channel block (three pieces) and pour 20 ml of RO water down the waste chute. Replace the tip eject cover (red).** Ensure that the rubber gasket is removed from the filter carriage for cleaning.

23) **Soak channel block in 1% Trigene for 15 – 30 mins. Rinse with RO water. Dry.**

24) **Run cleaning cycle, including UV if this is the last run of the day.** Select to turn off after the cleaning cycle is completed.

Appendix D: OpenArray Low Sample Input SOP

Reagents

1) Custom OpenArray Slides (Applied Biosystems, 4470813)
2) Custom RT primers (included with custom slides)
3) Custom PreAmp primers (Applied Biosystems, 4441856)
4) TaqMan microRNA reverse transcription kit (Applied Biosystems, 200 rxn 4366596, 1000 rxn 4366597)
5) 15 nM ath-miR-159a synthetic miRNA (Sigma)
6) OpenArray 384-well sample plate (Applied Biosystems, 4406947)
7) Aluminium Seal (Beckman-Coulter, 538619)
8) TaqMan PreAmp mastermix (Applied Biosystems, 1 ml 4391128, 5 ml 4488593)
9) TE Buffer (Invitrogen, 12090015)
10) OpenArray accessories kit (Applied Biosystems, 4453975)
11) TaqMan OpenArray real-time PCR mastermix (Applied Biosystems, 1.5 ml 4462159, 5 ml 4462164)
12) AccuFill tips (Applied Biosystems, 1 box 4457246, 10 boxes 4458107)
13) Filtered pipette tips
14) Nuclease-free water (Qiagen, 129117)
15) 0.2 ml 96-well plates (Axygen, PCR-96M2-HS-C)

All plastic ware should be nuclease free. Never stick your hands into containers of nuclease-free plastic ware. Always pour out whatever is required.

Equipment

1) Thermocycler
2) QuantStudio™ 12K Flex Accufill System
3) QuantStudio™ 12K Flex Real-Time PCR System
4) Vortex
5) Centrifuge

6) Axymat Silicon Seals (Axygen, AM-96-PCR-RD)

Reagent Setup

1) Download the relevant run file/s (.tpf) from the Life Technologies website (https://www.thermofisher.com/au/en/home/products-and-services/product-types/download-openarray-tpf-and-spf-plate-files.html) using the lot and serial number of the slide.
2) Thaw all reagents on ice, except for the RT enzyme, which must remain at -20°C until use.

Procedure

Reverse Transcription

1. **Dilute the RNA samples to <10 ng/µl.** This protocol is designed for samples with low RNA concentrations. Diluting to <10 ng/µl (around 8.5 ng/µl is sufficient) allows for >1µl to be taken in the next step, increasing accuracy.
2. **Add 10 ng of RNA to the respective well of a 96-well plate and then bring the volume to 3 ul.**
3. **Create an RT mastermix using the components from the reverse transcription kit, as detailed below.** It is recommended to add 5% excess to account for pipette error.

Component	**Per reaction (µl)**
Custom RT Primers	0.75
dNTPs with dTTp (100 mM)	0.15
RT Buffer (10X)	0.75
$MgCl_2$ (25 mM)	0.9
RNase Inhibitor (20 U/µl)	0.09
Nuclease-free Water	0.25
ath-miR-159a Spike In (15 nM)	0.10
Multiscribe Reverse Transcriptase (50 U/µl)	1.5
Total	**4.5**

4. **Pipette to mix and then centrifuge briefly at 10,000 x g for 10 sec (quick spin).**
5. **Aliquot 4.5 µl of the mastermix into each well. Seal with a silicon seal.**
6. **Invert to mix and then quick spin.**
7. **Incubate on ice for 5 min.**
8. **Place into the thermocycler and run the following program:** 40 cycles (16 °C for 2 min, 42 °C for 1 min, 50 °C for 1 sec), 85 °C for 5 min, hold at 4 °C.
9. **cDNA can be stored at -20°C or used immediately.**

Preamplification

10. **Create a preamp mastermix using the components listed below.** Swirl the PreAmp mastermix prior to use. It is recommended to add 5% excess to account for pipette error.

Component	**Per reaction (µl)**
TaqMan PreAmp Mastermix (2X)	20
Custom PreAmp Primers (10X)	4
Nuclease-free water	8.5
Total	**32.5**

11. **Invert to mix, and then quick spin.**
12. **Aliquot 32.5 µl of the mastermix into each well.**
13. **Invert to mix, and then quick spin.**
14. **Incubate on ice for 5 mins.**
15. **Place into thermocycler and run the following program:** 95°C for 10 mins, 55°C for 2 mins, 72°C for 2 mins, 16 cycles (95°C for 15 secs, 60 °C for 4 mins), 99°C for 10 mins, hold at 4°C.
16. **Invert preamplified cDNA and then quick spin.**
17. **Dilute 1:20 by adding 4 µl of preamplified cDNA to 76 µl of 0.1X TE buffer.**
18. **Both diluted and undiluted preamplified cDNA can be stored at -20°C for up to 1 week or used immediately.**

Loading OpenArray Slides and Performing qPCR

19. **Combine 5 µl of diluted, preamplified cDNA to 5 µl of TaqMan OpenArray real-time PCR mastermix in a new 96-well plate. Seal with a silicon seal.**

20. **Vortex and quick spin.**

21. **Aliquot 5 µl of each sample into 1 well of the 384-well sample plate.** The position of each sample will depend on the configuration of the custom slide. Each well of the sample plate corresponds to one subarray of the OpenArray slide. **An entire slide will take 48 wells (4 rows, 12 columns, see figure below).**

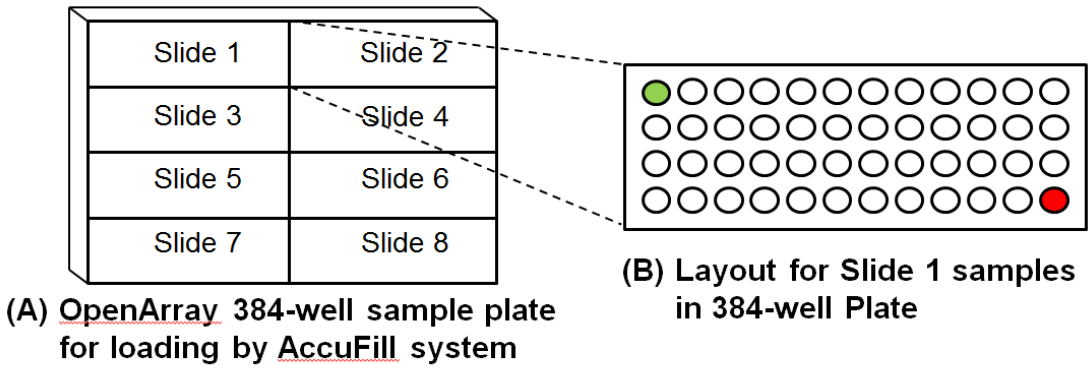

(A) OpenArray 384-well sample plate for loading by AccuFill system

(B) Layout for Slide 1 samples in 384-well Plate

(C) OpenArray Slide

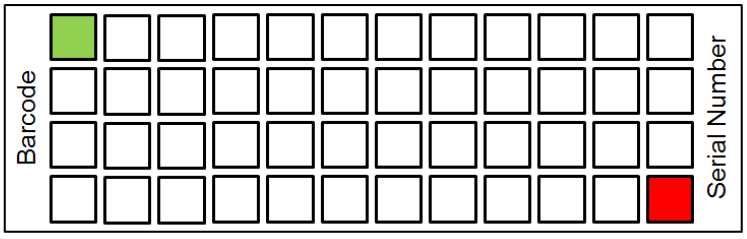

22. **Seal the samples plate.** It is advisable to **pre-cut the seal** into the required sections, so the sections may be sealed/unsealed individually to reduce evaporation. Alternatively, the plate may be sealed with an intact seal, and then sections can be individually cut out when loading.

23. **Centrifuge the sample plate at 490 xg for 1 min at 4°C.** Load the OpenArray slides within 1 hr.

24. **Remove the required slides from the freezer and allow them to come to room temperature (~15 mins).** As these slides work on hydrophobic/hydrophilic interactions, condensation should be avoided.

25. **Set up consumables from the accessory kit.**

    25.1. Gently pull on the plunger of the immersion fluid syringe to loosen. Remove cap, place tip on and flush air from the tip.

    25.2. Removed slide lid and plug from packaging.

    25.3. Place the loading system tips within the machine and remove lid.

    25.4. Place sample plate within PCR system.

    25.5. Put gloves on. Use a size lower than normal to minimise the risk of accidentally marking the slide lid.

    25.6. Carefully open slide packaging. Slowly tip slide into hand. Do not touch the top of the slide. Place slide into the AccuFill, with the barcode on the left.

    25.7. Remove seal from the portion of the sample plate intended for loading. Use the loading system software to enter the slide barcode, slide position, sample position and tip configuration.

26. **When all relevant checks are completed, press load slide. While the PCR system is loading the slide, remove the clear and red plastic from the bottom of the slide lid. When finished loading, carefully remove and seal the slide within 90 sec.**

    26.1. Place the slide within the plate clamp. Place the slide lid onto the slide. Clamp for 30 sec. Ensure the lid is positioned so that barcode is correctly displayed. Remove the assembly from the plate clamp.

    26.2. Position immersion fluid syringe within the slide so that the tip is pressing against the lid. Slowly fill slide with immersion fluid, ensuring the fluid runs along the lid. Once full, seal the slide with the plug, turning the screw until the handle breaks off.

26.3. Remove the plastic cover on the top of the slide lid, and then carefully place into the slide carrier of the real-time PCR system. Ensure there is support on the bottom of the slide as it is being lowered, so it does not drop suddenly, and do not touch the top of the slide. It is OK to touch the sides of the slide/cassette.

27. Initialise the QuantStudio 12K Flex and start the qPCR run.

27.1. Select “OpenArray” within the PCR-system software. Press “Find Slide IDs”. This will take a few mins. If the software cannot find the plate ID, it will ask for it to be entered manually.

27.2. Press “Confirm Plate Centres”. Again, this will take a few mins. Check that the red dot is within the centre and that there are no fingerprints/marks on the top of the slide. Load the respective tpf file for each slide and specify a result file name and location. Press “Start Run”. The program will take approximately 2 hr to complete.

Appendix E: Cell-free DNA Isolation SOP

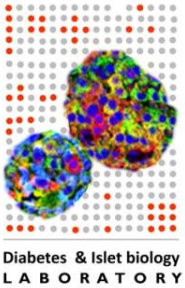

Reagents

1) 1.7 ml microcentrifuge tubes (Axygen, MCT-175-C)
2) QIAmp DNA Blood Mini Kit (Qiagen, 50 rxns 51104, 250 rxns 51106)
3) Poly(A) (10mg/ml) (Sigma 9403)
4) Dulbecco's Phosphate Buffered Saline, DPBS (Gibco, 14190-250)
5) 100% Ethanol (Sigma, E7023-500ml)
6) Fresh aliquot for nuclease-free water
7) 15 ml tubes (Falcon, FAL352096)
8) P10, P20, P200 and P1000 filtered tips

All plastic ware should be nuclease free. Never stick your hands into containers of nuclease-free plastic ware. Always pour out whatever is required.

Equipment

1) Centrifuge for Eppendorf tubes.
2) Vortex mixer
3) Well calibrated micropipettes designated for (pre-PCR) nucleic acid isolation
4) Thermomixer or convection oven set at 56°C.

Reagent Setup

1) Allow samples to thaw thoroughly on ice prior to commencing.
2) Set temperature on thermomixer or convection oven to 56°C.
3) Prepare buffers as per Qiagen manual.

Procedure

1. **Bring sample volume[1] to 200 µl total, using DPBS.**
2. **Add 20 µl Qiagen protease.**
3. **Add 200 µl Buffer AL.**
4. **Add 1 µl poly(A).**
5. **Vortex for 8 sec.**
6. **Incubate at 56°C for 10 min.**
7. **Briefly centrifuge for 7 sec.**
8. **Add 230 µl of 96-100% Ethanol.**
9. **Vortex for 8 secs and then briefly centrifuge.**
10. **Add the sample mixture (~630 ul) to QIAamp Mini Spin column.**
11. **Centrifuge at 6,000 xg for 1 min.**
12. **Place column in a clean tube and discard flow-through.**
13. **Add 500 µl Buffer AW1 to column.**
14. **Centrifuge at 6,000 xg for 1 min and discard flow-through.**
15. **Add 500 µl Buffer AW2 to column.**
16. **Centrifuge at full speed (20,000 xg) for 3 min.**
17. **Put column in a new 2 ml collection tube.**
18. **Centrifuge at full speed (20,000 xg) for 1 min.**
19. **Put column in a 1.7 ml microcentrifuge tube.**
20. **Put 60 µl Buffer AE directly on the filter.** Switch tips between samples to avoid cross-contamination.

[1] It is recommended to use 50 µl, however this protocol works with volumes between 20-200 µl.

21. Incubate at room temperature for 5 min.

22. Centrifuge at 6,000 xg for 1 min. **Discard filters.**

23. Measure concentration of cfDNA, go straight to bisulfite conversion, or store cfDNA at -20°C. Due to the addition of poly(A), the Nanodrop will not provide accurate quantitation of the DNA. Qubit or Bioanalyzer must be used for DNA quantitation. For long-term storage, place the DNA in -80°C. For high sensitivity applications, store in aliquots to avoid multiple freeze-thawing.

Appendix F: Human Islet Cell Death Assay SOP

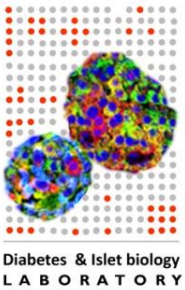

Reagents

1) Sterile 1.7 ml microcentrifuge tubes (Axygen, MCT-175-C)
2) Sterile 15 ml tubes (Falcon, FAL352096)
3) Ethanol (70%) for disinfection
4) Sodium Nitroprusside (SNP) (Sigma, 71778)
5) CMRL media (no glutamine) (Gibco, 11530037)
6) CMRL media + 2% bovine serum albumin, BSA (Roche, 10775835001) + 2X GlutaMAX* (Gibco, 35050-061)
7) Dulbecco's phosphate buffered saline, DPBS (Gibco, 14190-250)
8) P10, P20, P200 and P1000 autoclaved tips
9) P1000 autoclaved tips with the end cut off
10) 10 ml serology pipette tips
11) 24 well cell suspension plates
12) 0.2 µm syringe filter
13) 2 ml syringe

Equipment

1) Water bath set at 37°C
2) Centrifuge with 15ml swing-bucket rotor
3) Microcentrifuge
4) Well calibrated micropipettes designated for cell culture
5) Electronic serological pipette

Reagent Setup

1) Set water bath to 37°C
    a. Place PBS and CMRL + 2% BSA + 2X GlutaMAX into the water bath for >15 mins

2) Label 1.7ml Eppendorf tubes
    a. One per well for the islet cell pellet
    b. Three per well for the supernatant aliquots
3) Clean gloves, and anything else entering the biosafety cabinet, with 70% ethanol prior to use

Procedure

Plate Setup

1) **Prepare a <u>fresh</u> stock solution of 40 mM SNP by dissolving the SNP crystals in PBS.** 0.0596 g SNP in 5 ml PBS. Vortex to dissolve crystals.
2) **Dilute SNP to 20 mM in CMRL (nothing added).**
3) **Sterilise 20 mM SNP solution by passing it through a 0.2 um syringe filter.** Remove plunger from syringe, attach filter, pour in 20 mM SNP solution, and then push liquid through using the plunger. Ensure there is a sterile tube to collect the sterilised solution. It is also recommended to pre-wet the syringe filter by passing through a small amount of CMRL media to avoid binding SNP to the filter.
4) **Serially dilute the SNP solution in sterile CMRL (nothing added).** This should be completed as 1:10 dilutions to make 2 mM, 200 uM, 20 uM and 2 uM SNP.
5) **Aliquot 500 ul of each SNP dilution into the respective well of a 24-well suspension plate.** It is recommended to perform three technical replicates. If you are intending to perform staining or FACS on these cells, create additional replicates.
6) **Place the plate into an incubator at 37°C with 5% CO_2.** This will warm the media prior to the addition of the islets.

Islet Addition

7) **Place islets into a 15 ml Falcon tube and centrifuge at 1500 rpm for 2 min. Discard supernatant.**
8) **Resuspend islets in 10 ml warm PBS.**
9) **Centrifuge at 1500 rpm for 2 mins. Discard supernatant.**

10) **Repeat steps 8 and 9.**
11) **Resuspend islets in CMRL + 2% BSA + 2X GlutaMAX.** Add an appropriate volume of media so 200 IEQs will be added in 500 ul of media, with 5-10% extra to account for pipette error.
12) **Gently mix islets and then add 500 ul of the islet suspension to each well of the SNP plate.** Use the **P1000 pipette tips with the end cut off** to avoid shearing the islets. It is very important to mix the islets between **every** aliquot. It is also recommended to add the islets across the SNP dilutions rather than adding to all replicates of one condition before moving on to the next. This will evenly spread out any variation among all of the conditions.
13) **Place the plate into the incubator at 37°C with 5% CO_2 for 24 hours.** Take note of the time when the plate was placed into the incubator.

Islet and Supernatant Harvest

14) **Gently mix the islets and media, and then transfer to a sterile 1.7 ml Eppendorf tube.** Use the **P1000 pipette tips with the end cut off** to avoid shearing the islets.
15) **Centrifuge at 2000 rpm for 2 mins.** Always orient the tubes with the **hinge facing outwards** to allow estimation of the pellet location - in the bottom towards the hinge.
16) **Carefully aspirate 900 ul of the supernatant into a fresh 1.7 ml Eppendorf tube by placing the pipette tip along the wall of the tube opposite to the hinge.** Place the supernatant on ice at this stage.
17) **Mix supernatant by pipetting 5 times, and then aliquot 300 ul in two additional 1.7 ml Eppendorf tubes.**
18) **Centrifuge the tubes containing the islets at 2000 rpm for 2 mins.** Always orient the tubes with the **hinge facing outwards** to allow estimation of the pellet location - in the bottom towards the hinge
19) **Carefully aspirate and discard the remaining supernatant by placing the pipette tip along the wall of the tube opposite to the hinge.**
20) **Store the supernatant aliquots and islet pellets at -80°C.** Always log your sample details in the -80°C freezer log on the networked lab drive.

Appendix G: Mouse Terminal Blood Collection and Dissection SOP

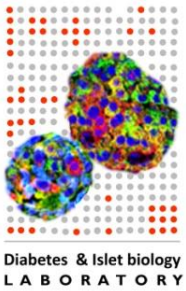

Reagents[1]

1) 1.7 ml microcentrifuge tubes (Axygen, MCT-175-C)
2) 0.1 M EDTA, pH 7.5-8
3) Dulbecco's Phosphate Buffered Saline, DPBS (Gibco, 14190-250)
4) 4% paraformaldehyde, PFA
5) 21G needles
6) 2ml syringes
7) Liquid nitrogen or dry ice
8) Wet ice
9) 70% Ethanol for disinfection
10) Isofluorane
11) Blood glucose testing strips

Equipment

1) Isofluorane anaesthetising equipment
2) Secured nose cone
3) Calibrated blood glucose testing meter
4) Sterilised dissection equipment (160 °C overnight/200 °C for ≥2 hours)
5) Working area with absorbent mat

Setup

1) Mice should be fasted for 12-14 hours overnight prior to this procedure.
2) Weigh and record the tubes containing DPBS.
3) Attach a needle to a syringe for each mouse to be processed.

[1] Reagents required will depend on the downstream applications.

4) Ensure there is a different set of scissors and forceps for each tissue, kept in separate, labelled positions.
5) Aliquot the following reagent into separate 1.7 ml tubes as necessary:
    a. 10 µl 0.1M EDTA pH7.5-8 (1 per mouse)
    b. 500 µl DPBS (1 per mouse)
    c. 500 µl 4% PFA (1 per tissue)

Procedure

1. **Weigh mouse.** Record their weight on the Record Sheet.
2. **Anaesthetise the mouse using 3% isofluorane with 0.5 L/min oxygen.** Ensure that reflexes are absent before moving to the next step.
3. **Transfer mouse to the working area (laying it on its back) and continue to anaesthetise using 1.5-2% isofluorane administered through the nose cone.**
4. **Disinfect the abdomen with 70% ethanol.**
5. **Collect blood via cardiac puncture.** Insert a 21 G needle under the ziphoid process (base of the sternum), parallel to the mouse's body, angled slightly to the right (mouse's left). Once blood is seen in the syringe, gently pull back on the plunger.
6. **Euthanise the mouse via cervical dislocation.** Turn off the isofluorane.
7. **Remove the needle from the syringe and then slowly dispense the blood into the tube containing 0.1M EDTA (pH7.5-8).** Place used needle in the appropriate sharps container.
8. **Invert to mix and then place on ice.**
9. **Measure the blood glucose using the small amount of blood left in the syringe.**
10. **Disinfect the abdomen again using 70% ethanol.**
11. **Using scissors, cut away the skin to expose the peritoneum.** Use forceps to pinch the skin away from the peritoneum, create a small incision, and then separate the skin from the peritoneal membrane. This minimises fur contamination.
12. **Open the peritoneum, being careful not to cut any of the underlying organs.**

13. **Identify the pancreas and carefully remove the organ.** The pancreas is located on the right side (left side of the mouse) and is easily located by gently pulling on the dark red spleen. The pancreas is attached to several points of the spleen, stomach and duodenum; these points must be carefully cut away to release the pancreas.

14. **Place the pancreas into the tube containing DPBS, weigh the tube, and then record this measurement.** This will allow measurement of the pancreas weight.

15. **Remove the pancreas from the DPBS, gently remove excess liquid by dabbing it onto some tissue paper and then store appropriately.** If the pancreas is needed for RNA/DNA isolation, place into an empty tube and snap freeze using dry ice or liquid nitrogen. If it is required for staining, store in 4% paraformaldehyde and place on wet ice. If both are required, use a sterile scalpel to cut the pancreas **lengthwise** prior to storage.

16. **Remove any other tissues that are required and store appropriately.**

17. **Discard the carcass by placing it into the provided plastic bag and store it in the animal house freezer for disposal.**

18. **Centrifuge the blood at 2000 xg for 20 mins at 4°C.**

19. **Aliquot the plasma into fresh 1.7 ml tubes.**

20. **You may isolate RNA directly from the fresh plasma, or store the aliquots at -80°C.** Always log your sample details in the -80°C freezer log on the networked lab drive.

21. **Store snap-frozen tissues at -80°C.** Always log your sample details in the -80°C freezer log on the networked lab drive.

22. **Store tissues in 4% PFA at 4°C.**

Appendix H: Plasmid Transformation SOP

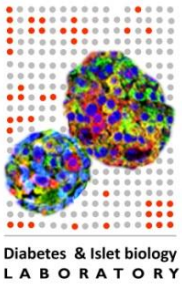

Reagents:

1) MAX Efficiency® DH5α™ Competent Cells (Invitrogen, CAT 18258-012)
2) S.O.C media (included with the cells, stored in the fridge)
3) Luria-Bertani (LB) agar plates with 50 µg/ml ampicillin
4) LB broth with 50 µg/ml ampicillin (100 ml per plasmid of interest)
5) Filtered pipette tips
6) Wet ice
7) 1.7 ml Eppendorf tubes
8) 75% ethanol
9) ZymoPURE Plasmid Midi Prep DNA Isolation Kit (Zymo D4200)

All plastic ware should be nuclease free. Never stick your hands into containers of nuclease-free plastic ware. Always pour out whatever is required.

Equipment

1) Culture spreader (glass pasteur pipette moulded using a bunsen burner)
2) Bunsen burner
3) Bacterial incubator set at 37°C
4) Water bath or thermoblock set at 42°C
5) Bacterial shaking incubator set at 37°C

Reagent Setup

1) Allow plasmids to thaw thoroughly on ice prior to commencing
2) Place the required number of Eppendorf tubes on ice (number of plasmids to be transformed plus one control)
3) Bring the S.O.C media to room temperature

Procedure

1. **Thaw cells on wet ice.** It is recommended not to freeze-thaw the cells often as it reduces the transformation efficiency.
2. **Gently mix the cells and then aliquot 100 µl into each of the pre-chilled Eppendorf tubes.** Refreeze any unused cells in a dry ice/ethanol bath for 5 minutes before returning to the -70°C freezer. Do not use liquid nitrogen.
3. **Add 5 µl (50 pg) of pUC19 control plasmid DNA to one tube of cells.** Move the pipette through the cells while dispensing. Tap the cells to mix.
4. **Add 1 µl (1-10 ng) of your plasmid of interest into their respective tubes of cells.** Move the pipette through the cells while dispensing. Tap the cells to mix.
5. **Incubate cells on ice for 30 mins.**
6. **Add cells to the waterbath or thermoblock at 42°C for 45 secs.** Do not shake.
7. **Place on ice for 2 mins.**
8. **Add 900 µl of room temperature S.O.C. medium.**
9. **Incubate at 37 °C shaking at 225 rpm for 1 hour.**
10. **Dilute the control 1:100 with S.O.C. medium and then spread 100 µl onto one LB agar plate.** This step should always be done next to a lit Bunsen burner to minimise contamination. The spreader should be sterilised by soaking it in 75% ethanol and then using the burner flame to burn away the alcohol. This should be done before spreading and between each plate.
11. **Spread 200 µl of the cells transformed with your plasmid of interest onto an LB agar plate.** To increase your chances of growing a viable colony, you may plate the full 1 ml onto five (5) separate plates.
12. **Place the plates upside down in the 37°C bacterial incubator overnight.**

13. **Count the colonies on the control pUC19 plate, and then use the following equation to determine the transformation efficiency:**

$$\frac{CFU}{\mu g} = \frac{colonies}{50\ pg} \times (1 \times 10^6 pg/\mu g) \times \frac{1\ ml}{0.1\ plated} \times 10^2$$

14. **Identify any colonies growing on the other plates.**

15. **Transfer a colony to a 4 ml of LB broth with 50 µg/ml ampicillin.** Use a sterilised wire loop or pasteur pipette to pick up the colony.

16. **Cover the flask with parafilm and then place the LB broth in the bacterial shaking incubator at 37°C for 3 hours, shaking at 300 rpm.**

17. **Transfer this 4 ml into the remaining 96 ml in a flat-bottom flask.**

18. **Incubate overnight in the shaking incubator at 37°C, shaking at 200 rpm.**

19. **If the media looks turbid, use 50 ml of the liquid to isolate the plasmid.** Plasmid isolation is done using the Zymo Plasmid DNA Isolation Kit as per the manufacturers protocol.

Appendix I: Bisulfite Conversion SOP

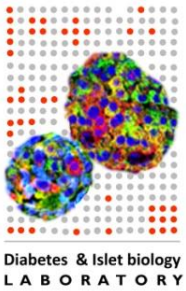

Reagents:

1) Nuclease-free 1.7 ml microcentrifuge tubes (Axygen, MCT-175-C)
2) EZ DNA Methylation-Lightning Kit (Zymo Research 50 rxns D5030, 200 rxns D5031)
3) Filtered pipette tips

All plastic ware should be nuclease free. Never stick your hands into containers of nuclease-free plastic ware. Always pour out whatever is required.

Equipment

1) Centrifuge designed for 2 ml tubes
2) Vortex mixer
3) Well calibrated micropipettes designated for (pre-PCR) nucleic acid isolation
4) Thermocycler

Reagent Setup

1) Allow samples to thaw thoroughly on ice prior to commencing.

Procedure

1) **Add 130 µl of Lightning Conversion Reagent to 20 µl[1] of DNA sample.** If <20 µl of DNA is to be used, make up the additional volume with nuclease-free water.
2) **Mix thoroughly by pipetting 20 times. Briefly centrifuge.**
3) **Place samples into a thermocycler and run the following program:**

[1] A maximum of 20 µl of isolated DNA may be used in this kit. If a greater input is required, concentrate your sample or complete the bisulfite conversion in multiple 20 µl aliquots.

a. 98˚C for 8 min

b. 54˚C for 60 min

c. Hold at 4˚C for up to 20 hours

4) **Place a Zymo-Spin IC Column for each sample into a collection tube.**

5) **Add 600 µl of M-Binding Buffer to each column.**

6) **Load sample into the respective column. Mix by pipetting 10 times.**

7) **Centrifuge at full speed (20,000 xg) for 30 sec. Discard flow-through.**

8) **Add 100 µl of M-Wash Buffer to column.**

9) **Centrifuge at full speed (20,000 xg) for 30 sec.**

10) **Add 200 µl of L-Desulphonation Buffer to the column.**

11) **Incubate at RT for 20 min.**

12) **Centrifuge at full speed (20,000 xg) for 30 sec.**

13) **Add 200 µl of M-Wash Buffer to the column.**

14) **Centrifuge at full speed (20,000 xg) for 30 sec.**

15) **Repeat steps 13 and 14.**

16) **Place the column into a fresh 1.7 ml tube.**

17) **Add 10 µl of the Elution Buffer directly onto the column filter.**

18) **Incubate at RT for 1 min.**

19) **Centrifuge at full speed (20,000 xg) for 30 sec.**

20) **Store eluent at -20°C or -80°C for long term storage.** Always log your sample details in the -80°C freezer log on the networked lab drive.

Appendix J: Digital Droplet PCR – Automated Droplet Generation SOP

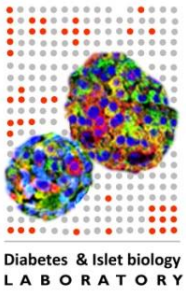

Reagents:

1) Custom TaqMan Assay AH21BH1 (Applied Biosystems)
2) ddPCR Supermix for Probes, no dUTP (Bio-Rad, 186-3024)
3) Semi-Skirted 96-well plate (Eppendorf, 951020346)
4) 20 U/µl EcoR1 (New-England Biolabs, R0101L)
5) 96-well aluminium foil plate seal (Beckman-Coulter, 538619)
6) Automated droplet generator oil (Bio-Rad, 186-4110)
7) Automated droplet generator tips (Bio-Rad, 186-4121)
8) Automated droplet generator cartridges (Bio-Rad, 186-4109)
9) Pierceable foil heat seal (Bio-Rad, 1814040)
10) Filtered pipette tips

All plastic ware should be nuclease free. Never stick your hands into containers of nuclease-free plastic ware. Always pour out whatever is required.

Equipment

1) Automated droplet generator
2) Heat sealer
3) QX200 Droplet Reader
4) Vortex mixer
5) Well calibrated micropipettes designated for pre- and post-PCR
6) C1000 thermocycler with deep 96-well block
7) Automated droplet generator cold block (stored at -20˚C)

Reagent Setup

1) Allow samples to thaw thoroughly on ice prior to commencing.

2) Thaw supermix on ice.
3) Turn on the QX200 droplet reader 30 mins before use.

Procedure

1) **Create the ddPCR mastermix.** Below is the volume (µl) of each reagent per reaction. It is recommended to add 5% extra to account for pipetting error.

a.	Supermix	12.5
b.	AH21BH1 Primer/Probe	1.25
c.	Water[1]	8.25
d.	EcoR1	0.5
e.	Total	22.5

2) **Briefly vortex and centrifuge the mastermix.**
3) **Add 22.5 µl of the mastermix to the respective wells in the Eppendorf 96-well plate.** Ensure that the samples are configured in groups of eight (8), positioned in the columns of the plate. If you do not have samples in multiples of eight, place the appropriate number of NTC controls to fill the remaining wells.
4) **Briefly vortex and spin the samples and then add 2.5 µl[1] of the bisulfite converted (bc)DNA to the respective well. Mix by pipetting twenty (20) times.**
5) **Seal the plate with an aluminium plate seal and centrifuge at 1500 rpm for 1 min at room temperature.**
6) **Allow the plate to sit at room temperature for 10 mins.** It is important to let the samples come to room temperature for optimal droplet generation.
7) **Set up the automatic droplet generator.** Load consumables from the back to the front of the machine to minimise contamination.
    a. Configure the sample plate.

[1] If a different volume / amount of DNA is required, please adjust the water accordingly.

b. Insert the required droplet generation cartridges and tips (**two tips per sample** are required) within the machine. Completely remove the lid of the tip boxes.

c. Check the tip waste.

d. Place the cool block into the machine with an Eppendorf 96-well plate.

8) **Place the sample plate into the machine and remove the foil seal.**

9) **Run the droplet generation program.** The cycle will take ~45 mins for a full 96-well plate. Remove the droplet plate within two (2) hours.

10) **Seal the droplet plate with the pierceable heat seal (180°C, 5 secs).** Make sure the red stripe on the seal is visible. Be careful when placing the block into the heat sealer; support the base to minimise damage to the rails. Remove the block after sealing. Turn on the heat sealer a few minutes before use to allow it to reach to 180°C.

11) **Thermocycle the sealed plate using the following cycling protocol.** Ensure that the ramp rate is set to **2°C/sec**.

a. 95°C for 10 mins, 40 cycles (94°C for 3 mins, 57.5°C for 1 min), 98°C for 10 mins, 12°C hold.

12) **Place the plate into the droplet reader.**

13) **Input the sample details.** Ensure that the experiment type is **rare even detection (RED)**, the supermix is **Probes (no dUTP)**, channel 1 (FAM) is **unmethylated** and channel 2 (VIC) is **methylated**.

14) **Check if all lights are solid green on the QX200.** If they are flashing or yellow, either the waste is too full or the oil is low. Empty the waste into the liquid waste bottle, wipe out excess oil and store upside down to drain. Replace with the secondary waste bottle. Top up or replace reader oil.

15) **Press Run.** Choose if you want the reader to go by columns or rows, and ensure it is set to FAM/VIC.

Appendix K: Immunofluorescent Staining of Paraffin Embedded Tissues SOP

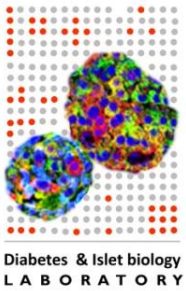

Reagents:

1) Normal donkey serum (Thermo Fisher, 14190250)
2) 100% ethanol (Sigma, E7023-500ml)
3) Distilled (or MilliQ) water
4) Tissue paper or Kimwipes
5) Xylene (Thermo Fisher, AJA2342-5L)
6) Primary antibody/ies
7) Dulbecco's phosphate buffered saline, DPBS (Gibco, 14190-250)
8) Secondary antibody/ies
9) Vectashield (Vector Laboratories, H-1000)
10) Hoechst 33342 nuclear stain (10 mg/ml)
11) Coverslips
12) Nail polish

All plastic ware should be nuclease free. Never stick your hands into containers of nuclease-free plastic ware. Always pour out whatever is required.

Equipment

1) Convection oven set at 85-90°C.
2) Coplin Jars
3) Forceps
4) Hydrophobic marker
5) Moist chamber

Reagent Setup

1) Fill two Coplin jars with Xylene.
2) Fill four Coplin jars decreasing concentrations of ethanol in this order: 100%, 90%, 70% and 50% (50 ml in distilled water).
3) Fill one Coplin Jar with distilled water.
4) Dilute normal donkey serum (NDS) with dPBS to 4% NDS
5) Dilute primary antibodies to a working stock in 4% NDS. The actual dilution factor with depend on the antibody used [for example the Guinea Pig anti-insulin polyclonal (from DAKO, catalogue number-A0564(01)) insulin is usually 1:100]. Multiple antibodies can be combined into one stock **ONLY if they were raised in different animals**.
6) Dilute secondary antibodies 1:100 to a working stock in 4% NDS. Ensure the antibodies target the animal in which the primary antibody was raised
7) Set up moist chamber by placing moist paper towel within the chamber.
8) Create the mounting solution by adding 10 µl of Hoechst to 1 ml of Vectashield.

Procedure

Primary Antibody

1. **Place slide at 85–90°C for 2-5 mins or until the paraffin wax becomes translucent (check every minute after the first 2 minutes).** The tissue will still be opaque.
2. **Immediately place slide into the first xylene Coplin jar for 2-3 mins.** When adding the slide to a Coplin jar, gently wash the slide by dipping into the liquid 3-4 times.
3. **Transfer slide to the second xylene Coplin jar for 5 mins.** When transferring the slide between jars, gently dab the edge of the slide onto tissue paper or Kimwipes to remove excess liquid.
4. **Transfer the slide to 100% ethanol for 5 mins.**
5. **Transfer the slide to 90% ethanol for 5 mins.**

6. **Transfer the slide to 70% ethanol for 5 mins.**
7. **Transfer the slide to 50% ethanol for 5 mins.**
8. **Transfer the slide to distilled water for 5 mins.**
9. **Remove slide and dab off excess liquid.**
10. **Using the hydrophobic marker, draw around your tissue section.** Ensure that the line is close to your sample **without touching it**.
11. **Add enough 4% NDS to cover the section.**
12. **Place slide into moist chamber and incubate at room temperature for 20 mins.**
13. **Tilt the slide and use a pipette to remove and discard the liquid.** Do not remove the slides from the moist chamber.
14. **Add enough of the selected primary antibody (working stock in 4% NDS) to cover the tissue.**
15. **Seal the moist chamber with parafilm and incubate at 4°C overnight.**

Secondary Antibody

16. **Tilt the slide and use a pipette to remove and discard the primary antibody.**
17. **Add DPBS and incubate at room temperature for 3-5 mins.** Add as much PBS as possible within the confines of the hydrophobic marker. This will create a large bubble of fluid over the tissue section.
18. **Remove liquid.**
19. **Repeat steps 17 and 18 at least 4 more times.**
20. **Add enough secondary antibody (working stock diluted in 4% NDS) to cover the tissue.** This step, and all subsequent steps, **MUST be completed in the dark** to ensure that the reporter dyes to not degrade.
21. **Seal the moist chamber with parafilm and incubate at 37°C for 1 hour.** Ensure there is ample liquid in the tissue paper used in the moist chamber.

22. **Remove the secondary antibody and then repeat steps 17 and 18 at least five times to remove any unbound secondary antibodies.**
23. **Tilting the slide and place folded tissue or Kimwipe at the bottom of the sample to soak up the remaining PBS.** It is important not to touch the tissue section or wipe the liquid.
24. **Add 20 µl of the mounting solution (Vectashield + Hoechst).**
25. **Add a coverslip and seal using nail polish.** Place one edge of the coverslip to the side of the sample, in contact with the mounting solution. Slowly lower the other edge using a scalpel blade (or another suitable thin, flat utensil), allowing the solution to spread along the coverslip. This method minimises the introduction of bubbles.
26. **Store slide(s) at RT in the dark until the slide is dry (~30 minutes).**
27. **Examine slide(s) using a fluorescent microscope.**
28. **Place the slide(s) at 4°C for long-term storage.**

Appendix L: Flow Cytometry Cell Death Analysis SOP

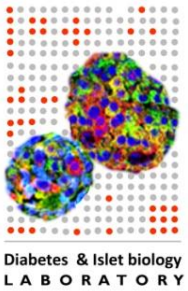

Reagents:

1) Sterile 15 ml Falcon tubes
2) Ethanol (70%) for disinfection
3) Accutase (Merk Millipore)
4) CMRL media + 10% FCS (Gibco)
5) Dulbecco's phosphate buffered saline (DPBS) (Gibco)
6) P10, P20, P200 and P1000 autoclaved tips
7) P1000 autoclaved tips with the end cut off (to transfer islets only)
8) 10 ml serology pipette tips
9) FACS tubes
10) Cell strainer (70 µm)
11) Hypotonic buffer – see step 1.

Equipment

1) Water bath set at 37°C
2) Centrifuge with 15ml swing-bucket rotor
3) Well calibrated micropipettes designated for cell culture
4) Electronic serological pipette
5) Flow-cytometer (turned on >20 mins before use)

Reagent Setup

1) Set water bath to 37°C
    a. Place PBS and CMRL + 10% FCS into the water bath for >15 mins
2) Clean gloves, and anything else entering the biosafety cabinet, with 70% ethanol prior to use

Procedure

1. **Create the hypotonic buffer.**

Reagent	Original Conc.	Final Conc.	Amount (for 2ml)
Sodium Citrate	1%	0.1%	200 ul
Triton-X 100	10%	0.1%	20 ul
Propidium Idodide	1 mg/ml	500 ug/ml	100 ul
Nuclease-free Water	-	-	1680 ul

2. **Transfer cells and media into a 15 ml tube.** It is recommended to gently mix the cells prior to transfer.
3. **Centrifuge at 1500 rpm for 2 mins.**
4. **Remove media.**
5. **Resuspend islets in 5 ml warm DPBS.**
6. **Repeat washing steps 3-4.**
7. **Remove DPBS.**
8. **Add 200 µl of Accutase and incubate in a 37°C water bath for 10 mins.**
9. **Gently pipette to break the cells apart.**
10. **Add 5 ml of CMRL + 10% FCS**
11. **Centrifuge at 1500 rpm for 2 mins.**
12. **Remove supernatant.**
13. **Add 5 ml of CMRL + 10% FCS.**
14. **Incubate for 30-60 mins at 37°C with 5% CO_2.** This will allow the cells to recover
15. **Centrifuge at 1500 rpm for 2 mins.**
16. **Remove media**
17. **Add 250 µl of hypotonic buffer.**

18. **Add to FACS tubes.** If any clumps can still be seen, pass the liquid through a cell filter as it is added to the FACS tubes.

19. **Set up and run FACSCalibur.** Read at least 10,000 events.